Sleep as an Essential Modulator for Plasticity and Cognition During Atypical Neurodevelopment

by

Jessy Martinez

A dissertation submitted in partial fulfillment
of the requirements for the degree of
Doctor of Philosophy
(Molecular, Cellular, and Developmental Biology)
in the University of Michigan
2023

Doctoral Committee:

Associate Professor Sara J. Aton, Chair
Assistant Professor Eleanor Josephine Clowney
Professor Richard I. Hume
Associate Professor Kenneth Kwan
Assistant Professor Sung Eun Kwon

Jessy D. Martinez

jessydm@umich.edu

ORCID ID: 0000-0001-9811-7626

© Jessy D. Martinez 2023

Dedication

For everyone who has accompanied me on my journey.

Acknowledgements

As I write this dissertation, I realized that I have been in the research game for ten years! That's quite a long time to be doing the same thing over and over, but also not quite doing the same thing over and over. Who would have thought that a flyer posted on the door of my introductory biology lab class at my community college, announcing a UCLA rep was coming to talk about biology research, would have landed me here writing my dissertation for my PhD ten years later. It just goes to show you how life has a way of getting you where you need to be at the right time. That is how I approached my research and science career journey, always believing I was in the right place at the right time (for the most part). However, I didn't embark on this journey alone. This journey was only made possible with the help of so many people in my life who stood by me through it all.

I must thank first and foremost, my PhD advisor, Sara Aton. Words cannot express how lucky I am to have you as my PhD advisor. I won't forget your detailed email to find the lab space for our first meeting so I wouldn't get lost in Kraus. The past six years have been adventurous so to speak. We have been through a lab relocation move, a lab lockdown via a pandemic, countless battles with reviewer #2 and we got through it all together. I cannot thank you enough for your endless support in both my professional and personal growth. Thank you for allowing me to do all the crazy science I could muster and yet never asking more from me than I could give. Thank you for always encouraging me to take time off so I could recharge and see my family back in California. You always

made sure I had the opportunity to go see them, especially after I moved to Ann Arbor, and I knew virtually nobody. Thank you for taking care of me as graduate student, it's all most of us ask of our PhD advisors.

This dissertation would not exist without the help of all my wonderful undergraduate students. I'm serious, half of this dissertation would NOT exist without all of you helping me with even the simplest of tasks. Thanks for dealing with my crazy schedules, failed experiments, and always keeping a positive attitude. You all kept me going and gave me a reason to keep coming to lab every day. To Marcus, Donald, Daniel, Lydia, William, Kathryn, Stephany, and Roxanne, I know you are all going to do amazing things with your futures, and I am so proud of all of you. To the rest of the Aton lab, thanks for all the support throughout the years. Thank you, Jackie, Carlos, and James, for answering my random questions when I joined the lab and offering advice when I needed it. To Sha, for being a wonderful lab manager and someone who always knew how to make me smile when I was having the worst of days. Your attitude and wonderful food could always brighten my day. I must give a special shoutout to Brittany Swift (née Clawson). I owe you everything!! Thank you for taking the time to teach "ephys" to someone who knew virtually nothing about it and being the best senior grad student mentor, one could ever ask for. I would not have survived in this lab without you and thanks for all the support even after you graduated. To the members who came after me, Lijing, Frank, Alexis, Vinodh, Delaney, Marcel and Zhongying, thanks for dealing with my sudden transition to senior grad student of the lab and always being a supportive system, especially as I write this dissertation. You all have wonderful futures ahead of you. Lastly, a thank you to Valentina. As I write this dissertation, I hope you had a good rotation

experience under my mentorship and thanks for all the last-minute help on getting these last pieces of data for the final data chapter. You are going to do amazing things in graduate school in whatever lab you decide to stay choose for your own thesis.

Next, I need to thank my cohort. I was lucky that all of you were welcoming, friendly, and full of advice on how to survive Michigan winter. A special shout out though to Bahaar Chawla. I cannot even begin to describe how much our friendship means to me and how you have been there for me even through the most difficult times of this PhD. From helping me proofread my emails to taking me to the hospital when I broke my ankle, you showed up. I cannot wait for the bright future ahead of you, because you are going to be amazing at it. Thanks for being an amazing friend and someone I can finally talk to about Little Mix's amazing discography. TJ, Hannah, Lotte, and Maria thanks for being a source of constant laughter, support, memes, and random Pokémon knowledge. All of you and Bahaar always knew how to make me smile and laugh at the world when I needed it most especially as we got through MCDB 615 and Checkpoint #2. I can't wait to see all of move forward and enjoy the bright futures you all have ahead. Other members of MCDB, especially Mary, thank you all for always answering me questions and providing me with support when I needed it. Lastly, thanks to Dr. Cathy Collins for switching my PhD application to MCDB and Dr. Anuj Kumar for helping me get involved in DEI work. Both of you really helped set a nice foundation for me to work with as I started the program. To non-MCDB and non-science friends, Luis Miguel, Luis E, Griff, Steven, and Trevor, thanks for the trips to Buffalo Wild Wings, Mario Party/Kart tournaments, and movie hang outs. Thanks for reminding me life exists outside the PhD, it was super needed.

My PhD journey would not have even started without all the help I got beforehand. To my UCLA advisor, Dr. Art Arnold, thank you for encouraging me to leave CA for my PhD. You were right, I did a lot of growing here and I met wonderful friends and people that I cannot imagine my life without. To Haley, Shayn, and Maureen, thanks for being so supportive of someone who knew nothing about neuroscience research, but always encouraged me to continue pursuing research. To Dr. Diana Azurdia and Dr. Tama Hasson, thank you both for introducing me to the world of research. Your presence at my community college changed my life and set me on this journey. I owe a debt of gratitude for all the support during my undergraduate years and helping me achieve this dream of a PhD. To my Cal State LA advisor, Dr. Laura Cocas, thank you introducing me the wonderful world of neurodevelopment and being a fantastic Master's thesis advisor. It was an honor being your first Master's student and I hope I did you proud. To Priscilla, Isabel, Aigbe, Jess, Alex, and Jeanine, thank you for being amazing lab members as we founded the Cocas Lab together and navigated this route to the PhD together. Lastly, thank you to my UCLA SACNAS family. Nancy, Benni, and Sandra. I could not have gotten through undergrad without all of you and I am happy to finally be joining the "adult" world with all of you. Thanks for always making time for me when I came back to visit and was in dire need of a good taco. You all instinctively knew what I needed when even I didn't know, so thank you for all the trips to WeHo and encouraging me to be adventurous and try new foods all around Los Angeles.

This next set of names are affiliated with a form of entertainment that was a constant source of joy and laughter while I wrote grants, sectioned brain tissue, analyzed data, and especially sleep deprive mice. So, thank you to this partial list of people and

characters: Sam, Dean, Louise, Tina, Gene, Linda, Bob, Paulina, Elena, Julian, Quentin, Eliot, Margo, Oscar, Alvaro, Ricardo, Tini, Danna, Ricky, Perrie, Jade, Leigh-Ann, Paty, Manuel, Becky, James, Kendall, Shady, Kelsey, Brandon, Alanda, Trixie, Katya, Red, Link, Cereza, and Shakira. I'll leave you to decipher who I'm talking about.

Lastly, I must thank my supporters from day 1: my family. To my mom (Alicia) and dad (Jose): I can only hope I have made you proud given all the sacrifices you made for me to pursue my education. You were always my biggest champions in everything, and I could not succeed without you both. Thank you for supporting me in leaving for Michigan. I know it was a scary thought having your only son moving 3,000 miles away, but you knew how important it was for me to be the first in our family to achieve this level of education. I reached this milestone thanks to you both. Los quiero mucho. To my sister, Patty, thank you for holding down the fort back home as I pursued this degree. I don't have the words to begin saying how much I appreciate you as my older sister. Thank you for the late-night phone calls, thank you for the Disneyland trips, thank you just for everything. I would not have the strength to pursue this PhD without your support as my sister. Thank you for always looking out for me my whole life. To my dog, T-Bone. I miss you buddy. Your conditional love for everyone (including me) always made everything feel better. You brought nothing but joy when I needed it most throughout my entire college life, especially when I visited home during the winters. To the newest doggy member of the family, Coco. Thanks for being biggest goofball ever and being a bundle of happiness. The videos of you learning all about the world always brought a smile to my face, especially during these past couple of months. In the end, thank you all for being an essential part of my journey.

Table of Contents

List of Figures

List of Abbreviations

ASD	Autism Spectrum Disorder
BLA	Basolateral Amygdala
BR	Binocular Recovery
bV1	binocular Primary Visual Cortex
CA1	cornu Ammonis 1
CA3	cornu Ammonis 3
CFC	Contextual Fear Conditioning
CFM	Contextual Fear Memory
DE	Deprived Eye
DG	Dentate Gyrus
EEG	Electroencephalogram
FMRP	Fragile X Messenger Ribonucleoprotein
FS	Fast Spiking
FXS	Fragile X Syndrome
GIRK	G-protein Inward Rectifying Potassium
IEG	Immediate Early Gene
IHC	Immunohistochemistry
LA	Lateral Amygdala

LTD	Long-Term Depression
LTP	Long-Term Potentiation
MD	Monocular Deprivation
MT	Melatonin
NDD	Neurodevelopmental Disorder
NR	Normally Reared
NREM	Non-Rapid Eye Movement
ODP	Ocular Dominance Plasticity
OF	Open Field
OLM	Object Location Memory
PFC	Prefrontal Cortex
PNN	Perineuronal Net
PV	Parvalbumin
REM	Rapid Eye Movement
RO	Reverse Occlusion
RS	Regular Spiking
SD	Sleep Deprivation
SE	Spared Eye
SWS	Slow Wave Sleep
TRN	Thalamic Reticular Nucleus
V1	Primary Visual Cortex
ZT	Zeitgeber Time

Abstract

Sleep is thought to be a critical regulator of neural circuitry during neurodevelopment. Under conditions where postnatal neurodevelopment is modified - either by altered sensory experience, or in the context of genetically-mediated neurodevelopmental disorders - sleep is commonly altered or disrupted. However, the precise role sleep plays in promoting brain plasticity is still unknown, and it is unclear whether normalizing sleep could help normalize brain functions in atypical neurodevelopment. My dissertation work addresses this gap, by measuring how sleep loss affects recovery of disrupted visual cortex function in a mouse model of amblyopia (a form of vision loss caused by altered experience during postnatal development) and testing how normalizing sleep behavior affects memory disruptions in a model of Fragile X syndrome (FXS; a genetic disorder). My electrophysiological, behavioral, and molecular data suggest that sleep not only is critical for recovery mechanisms in disrupted neurodevelopment, but is also a useful target for therapeutic intervention.

The first part of this dissertation (**Chapter 2**) examines the relationship between sleep and recovery of disrupted cortical dynamics in early neurodevelopment. Here, I examined the relative impacts of visual experience and sleep on recovery of cortical visual responses in a mouse model of amblyopia. Using monocular deprivation (MD) to disrupt vision for one eye during early postnatal development, we used *in vivo* single-unit recordings and immunohistochemistry (IHC) to measure how binocular and monocular

visual experience influenced recovery of deprived eye responses after MD. We found that binocular experience during recovery from MD vastly improved restoration of visual responses to the deprived eye. Furthermore, this recovery was dependent on sleep. Together, both binocular visual experience and subsequent sleep could be important factors mediating recovery of visual cortical responses in amblyopia.

The second part of this dissertation assesses the intersection of sleep and recovery of hippocampal-cognitive dysfunction in neurodevelopmental disorders. Here, I tested how a novel hypnotic, ML297, which acts via activation of G-protein inward rectifying potassium (GIRK) channels can rescue sleep loss and subsequent memory consolidation in a mouse model of FXS. First (**Chapter 3**), using C57BL/6 mice, we determined how ML297 affects memory consolidation using EEG/EMG recordings, contextual fear conditioning and IHC. We found that ML297 reversed reductions in NREM and REM spectral power, along with REM sleep amount and led to improved contextual fear memory. In a second study using *Fmr1*$^{-/y}$ mice (**Chapter 4**), we characterized sleep architecture and oscillatory activity for the first time in the FXS mouse model. We found deficits in NREM sleep architecture, spectral power, and inter-cortical coherence that were restored with ML297. Restoration of sleep via ML297 also showed improved cognition via fear learning and spatial memory tasks. Lastly, we found hippocampal activation patterns associated with memory formation change with ML297 to facilitate improved cognition. Overall, rescue of abnormal sleep could help with cognitive dysfunction in FXS and possibly other neurodevelopment disorders.

Together, these findings enlighten us on the contributions of sleep to cortical development and hippocampal cognition in the context of neurodevelopment. While both

have been extensively measured in past studies, the role of sleep remains vastly understudied. Further research into the underlying mechanisms by which sleep facilities recovery in these domains may lead to future and targeted therapeutic intervention for the diverse number of developmental and neurological disorders where sleep loss impacts plasticity and cognition.

Chapter 1 : Introduction

1.1 : Neurobiology of sleep

Sleep states are evolutionarily-conserved behaviors that can be seen in diverse organisms from invertebrates such as honeybees and cuttlefish to vertebrates such as fish, birds, and mammals. Sleep is a natural and reversible state, characterized by reduced responsiveness to external stimuli, increased arousal thresholds, and relative inactivity, with occurrence regulated by both circadian and homeostatic mechanisms [1-3]. These two regulatory processes controlling sleep timing are known as Process S (homeostatic) and Process C (circadian). Process S represents the homeostatic drive for sleep, where pressure to sleep accumulates over the course of extended wakefulness (across the light period in diurnal species such as humans), peaks before an individual's bedtime, and reduces over the course of the night during sleep [4-6]. Process C refers to mechanisms by which sleep is regulated by time cues such as environmental light, as well as an intrinsic, near-24-h timekeeping mechanism that promotes alertness and wakefulness. In diurnal mammals such as humans, arousal signals mediated by Process C counteract increased propensity to sleep over the course of the day caused by Process S. Cues such as light promote wakefulness across the day via the suprachiasmatic nuclei (SCN) of the hypothalamus, which sends projections to wake-promoting brain structures [7-10]. The study of sleep in vertebrate species expanded with the development of the electroencephalogram (EEG), which allows for differentiation of distinct sleep states.

Specific EEG oscillation patterns (along with phenomenological features like eye movements, muscular atonia, and vivid dreaming) can be used to classify sleep into two different distinct states: rapid eye movement (REM) sleep and non-REM (NREM) sleep [1,3], which alternate cyclically over a period of sleep (in mammals and a few other species). When EEG is coupled with electromyography (EMG, recording of skeletal muscle activity), EEG/EMG recordings can provide a basic understanding of sleep-wake cycles across a diverse number of animal species such as rodents and humans [11-13].

1.1.1 : Sleep states: NREM sleep

Humans sleep is typically composed of multiple, overnight cycles of NREM and REM stages, with each cycle lasting an average of 90 minutes. NREM sleep makes up the larger portion of the sleep cycle and is comprised of three stages: stages 1 and 2 (light and intermediate NREM sleep) and stage 3 (deep NREM sleep) (**Figure 1.1**) [1,2]. Stage 2 is characterized by the emergence of thalamocortical sleep spindles (waxing and waning 7-15 Hz oscillations) and K-complexes (high amplitude events) in the EEG. Stage 3 is also referred to as slow wave sleep (SWS), characterized by prominent, 0.5-4 Hz thalamocortical oscillations known as delta rhythms. These lower-frequency oscillations can coordinate other NREM EEG features including sleep spindles and hippocampal sharp-wave ripples (SWRs; which include both a high amplitude sharp wave and subsequent 150-250-Hz ripple oscillations) [14,15]. Neuromodulators such as acetylcholine (Ach), dopamine (DA), serotonin (5-HT), and norepinephrine (NE) are released at very low levels (compared with release levels during wake) across the central nervous system during NREM sleep [16-20].

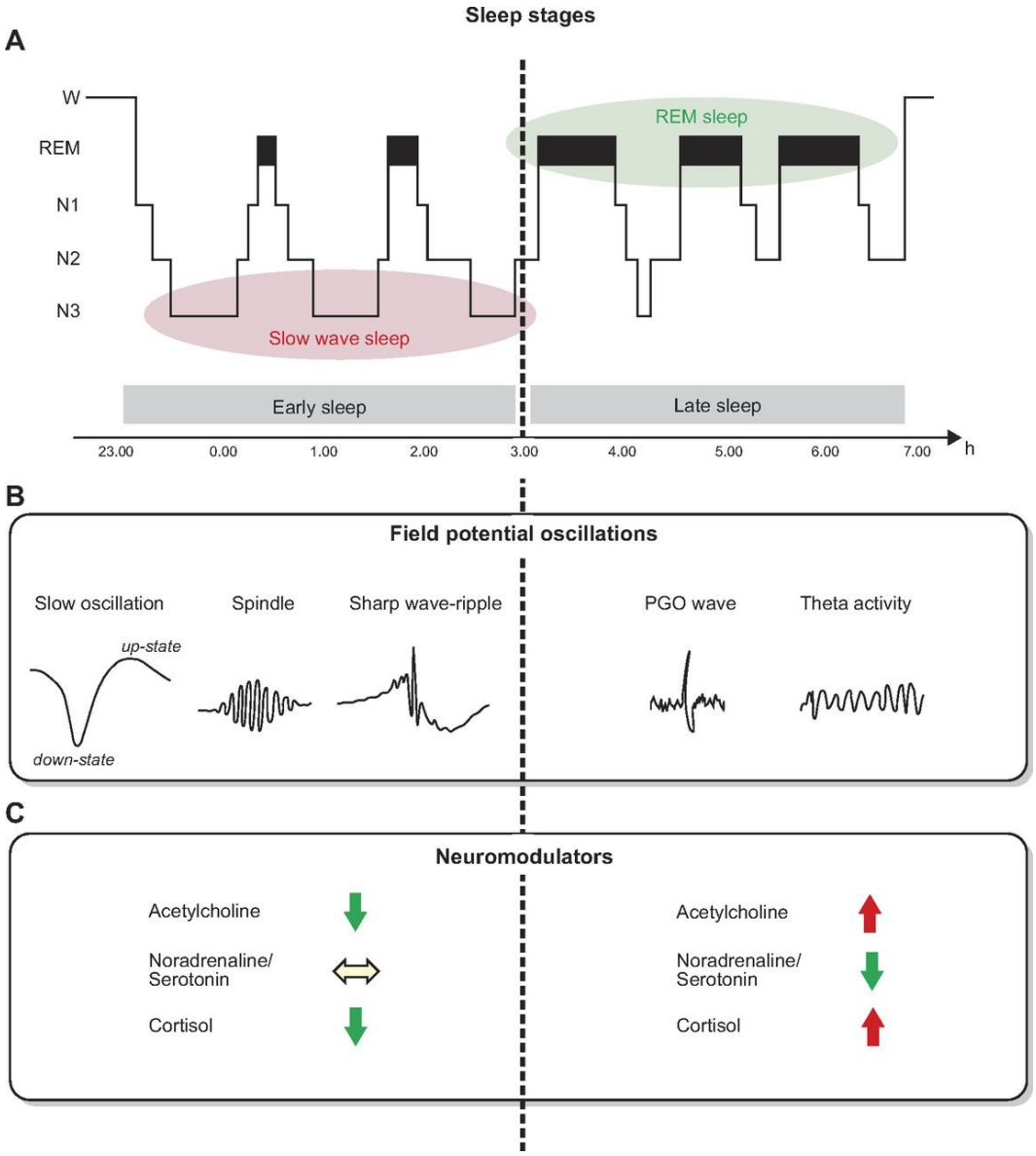

Figure 1.1: Typical human sleep profile and sleep-related neural oscillations patterns

(**A**) Sleep cycles characterized by the cyclic occurrence of rapid-eye-movement (REM) sleep and non-REM sleep. Non-REM sleep includes lighter sleep stages N1 and N2, followed by slow-wave sleep (SWS) corresponding to N3 or deep sleep. The first part of the night (early sleep) is dominated by SWS, whereas REM sleep prevails during the second half (late sleep). (**B**) Prominent electrical field potential oscillations during SWS are the neocortical slow oscillations (0.5-4 Hz), thalamocortical spindles (waxing and waning activity between 10–15 Hz), and the hippocampal sharp wave-ripples (SWR), i.e., fast depolarizing waves that are generated in CA3 and are superimposed by high-frequency (100–300 Hz) ripple oscillation. REM sleep is characterized by ponto-geniculooccipital (PGO) waves, which are associated with intense bursts of synchronized activity propagating from the pontine brain stem mainly to the lateral geniculate nucleus and visual cortex, and by theta (4–9 Hz) activity. (**C**) Sleep is accompanied by changes in levels of different neurotransmitters and neuromodulators. Compared with waking, cholinergic activity is low during SWS, whereas levels during REM sleep are similar or even higher than those during wakefulness. A similar pattern is observed for the stress hormone cortisol. Aminergic activity is high during waking, intermediate during SWS, and minimal during REM sleep. *Adapted and modified from Diekelmann and Born, 2010, Rash and Borne, 2013.*

Delta rhythms and NREM spindles represent coordinated activity between neurons in the neocortex and thalamus. Delta rhythms are generated in the thalamus, occur in a synchronized manner across the neocortex during NREM sleep, and are most pronounced in the EEG of frontal regions [14,21,22]. These oscillations are coupled with slower oscillations in other regions such as the cerebellum and parahippocampal gyrus [23]. Sleep spindles, which are most pronounced during Stage 2 sleep and at the transition between NREM and REM sleep, are characterized by waxing and waning bursts of sigma (7-15 Hz) frequency activity that are generated by the thalamic reticular nucleus (TRN) [24]. The TRN contains a dense population of parvalbumin-expressing GABAergic interneurons that is responsible for regulating communication between the neocortex and thalamus in wakefulness as well as during sleep oscillations [25-27]. Fast thalamocortical spindles generated by the TRN are temporally correlated with SWRs generated in the hippocampus during deep NREM sleep [28-31].

Multiple neurobiological features of NREM sleep are thought to promote memory storage in the brain. Current data regarding further roles for NREM sleep highlight that both the occurrence of, and the correspondence between, spindles and SWRs are associated with memory processing [28-31]. The coordination of these rhythms together is proposed to underlie the transfer of information between hippocampus and neocortical circuits during declarative memory consolidation [32]. Hippocampal SWRs and thalamocortical spindles synchronize spike timing between the two circuits, which is thought to promote long-term potentiation (LTP) of glutamatergic synapses between the structures. Over time, this synaptic strengthening mechanism may mediate transfer of memories from hippocampal circuits to long-term neocortical storage – a process referred

to as “systems consolidation” [33-35]. Lastly, reduced Ach levels during NREM sleep are thought to promote memory consolidation, again by increasing coordinated neuronal firing dynamics between the hippocampus and neocortex [36-38].

1.1.2 : Sleep states: REM sleep

In contrast to the EEG patterns associated with NREM sleep, REM sleep is characterized by faster neocortical activity, and hippocampal-generated rhythms in the 4-9 Hz (theta) frequency band (**Figure 1.1**). These oscillations are similar to oscillatory patterns found in neocortex and hippocampus during wakefulness [39-41]. Other signature features of REM sleep include the rapid eye movements (i.e. saccades) that give REM sleep its name, muscular atonia (reduction in muscle tone), muscle twitches, and vivid dreaming [1,42-44]. The regulation of REM sleep is not well understood, but current data suggest that brain and environmental temperatures as well as stress levels have critical roles in regulating total REM sleep amounts [45-47].

In contrast to NREM sleep, Ach levels are high during REM sleep, with release levels in hippocampus and neocortex even surpassing levels seen during wakefulness. These changes in Ach levels have the capacity to reduce hippocampal-neocortical communication established during NREM sleep, instead promoting cortico-cortical communication [36,37,48]. Similar to NREM sleep, REM sleep is thought to have critical roles in memory storage. Increased neuronal activity during post-learning REM sleep in the hippocampus and amygdala suggest a role in emotional learning [49-52]. In human subjects, occurrence of REM sleep is associated with retention of emotional aspects of learned information and is associated with more emotional content in dreams [53-59].

1.1.3 : Animal models and experimental sleep deprivation (SD) reveal functions of sleep

From an evolutionary perspective, sleep represents an exceptionally dangerous behavior to engage in - i.e., an extensive period of reduced responsiveness to potential threats, which displaces beneficial behaviors such as foraging for food. However, the conservation of sleep among animal species strongly suggests that it must play an adaptive role, increasing the overall fitness of organisms [3,60]. Several possible functional roles for sleep have been proposed, based on data from studies of sleep in model organisms [61]. Rodents, for example, have been a pioneer model for studying the neural circuitry involved in sleep and its possible related functions. Unlike humans, who tend to constrain sleep to a single overnight period consisting of ~90-minute cycles (i.e. monophasic sleep), rodents have polyphasic sleep, where a typical NREM -REM cycle lasts around 10-15 minutes [62,63]. Data from rodent studies implicated sleep in numerous biological processes including the removal of cellular waste from brain tissue, metabolism regulation, and cell/tissue repair and/or growth [64-66]. Based on data from studies using experimental sleep deprivation (SD) in rodents, sleep also appears to affect synaptic plasticity and various cognitive domains such as executive function, attention, and memory [1,67].

SD has also served as a classic experimental strategy to test the role of sleep on memory. A landmark study by Jenkins and Dallenbach in the 1920s showed that human subjects memorizing lists of nonsense syllables performed better at retention testing when allowed to sleep over subsequent hours, compared with those kept awake [1,68]. Over the ensuing decades, human studies using SD showed that sleep has critical roles in storing a diverse range of memory subtypes including visual, verbal, social, and spatial

[1,69,70]. Similarly, consolidation of fear memories in visually-cued and contextual fear conditioning tasks are disrupted by sleep deprivation following initial learning in mice [71,72]. Disturbed sleep is frequently seen among individuals with disorders such as schizophrenia, autism, anxiety disorders, and depression. The fact that these disorders are associated with cognitive disruptions present in healthy subjects in the context of SD (such as disrupted executive function, hallucinations, delusions, catatonia, paranoia, and negative affect) suggests that sleep recovery could be impactful in treating these conditions [12,27,73-76].

1.2 : Sleep and developmentally-regulated visual cortex plasticity

During neurodevelopment, sensory experiences shape neural circuits in a way that informs subsequent sensory processing – this represents a fundamental function of the neocortex. These processes are initially guided by a combination of intracellular signaling cascades, genetically-regulated programs, and spontaneous activity, as well as by exposure to external sensory stimuli in early postnatal life. A well-studied example of this is ocular dominance plasticity (ODP) in the visual system during a period of heightened plasticity (or critical period) in early postnatal development [77-84].

1.2.1 : Ocular dominance plasticity (ODP)

ODP is a well-established model of sensory cortex plasticity first studied in the kitten visual system during a period of early postnatal development – i.e., the critical period. Here, extracellular neuronal recordings demonstrated that visual experience influences the response properties within primary visual cortex (V1). In kittens and other species with a wide field of binocular vision, the majority of V1 neurons have equal firing

responses for stimuli presented to either eye (i.e., a completely binocular response). However, if vision in one eye was occluded during the critical period, a process known as monocular deprivation (MD), neurons in V1 eventually will respond exclusively to visual stimuli presented to spared eye [83]. Synaptic and molecular mechanisms of ODP have been evaluated in much greater detail in other model organisms including rodents, which possess binocular zones in V1 (bV1) where neurons undergo ODP after a period of MD during the critical period (**Figure 1.2**) [85,86]. ODP follows a series of distinct stages in response to MD. First, there is a depression of deprived eye (DE) responses, followed by potentiation of spared eye (SE) responses [87]. Depression of DE responses is mediated by NMDA receptor activation, internalization of AMPA receptors, activation of protein kinase A, and expression of immediate early genes such as *Arc* that regulate AMPA receptor internalization [88-91]. Similar to studies in cats and primates, over time, bV1 neurons in mice and rats lose responsiveness to DE stimuli and become responsive only to visual stimuli presented to the SE [83,92-94]. Various well-established molecular mechanisms of LTP are required for ODP, including activation of protein kinase A (PKA), CaMK2a activation, and extracellular signal-regulated kinase (ERK) phosphorylation [94-97]. These mechanisms mediate the second phase of changes in bV1, involving potentiation of responses to SE stimuli.

Changes in DE and SE responses are associated with changes in the bV1 inhibitory network. For example, the loss of DE responsiveness is associated with a transient decrease in cortical inhibition, mediated in part by reduced activity in parvalbumin-expressing (PV+) interneurons, which may be essential for subsequent changes in SE responses in bV1 [98,99].

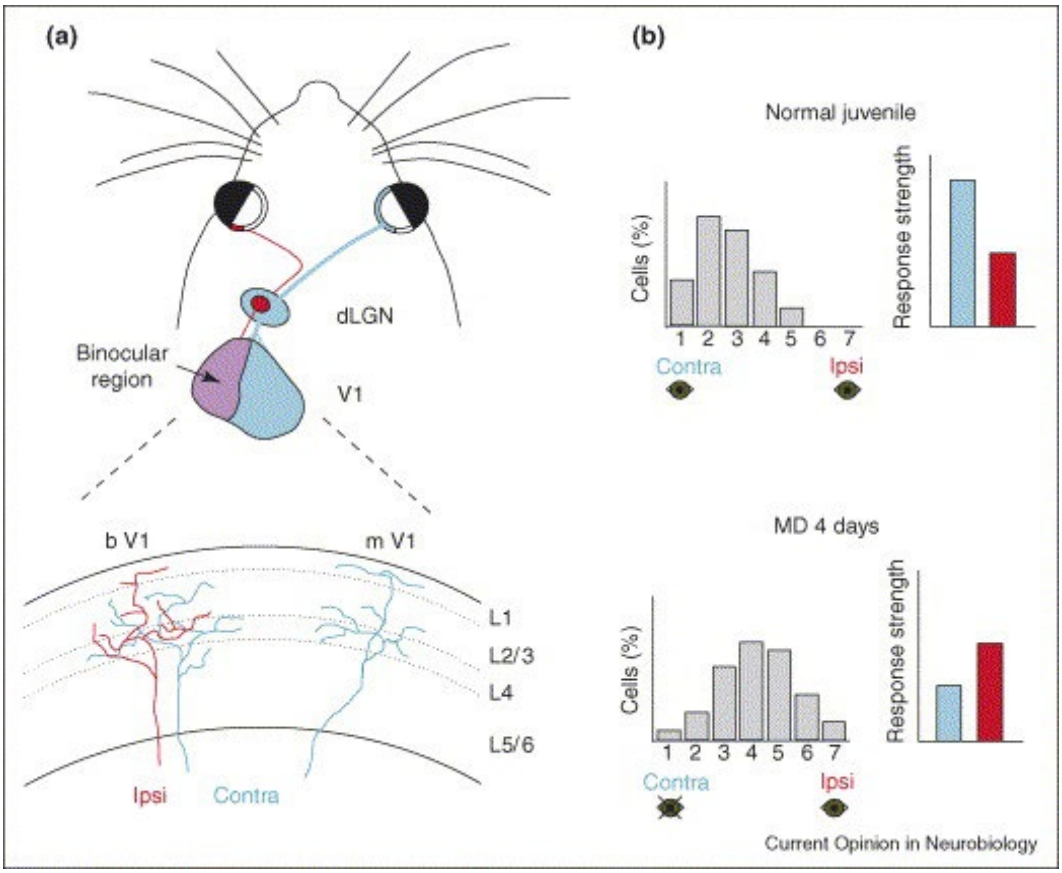

Figure 1.2: Ocular dominance plasticity in juvenile mouse visual cortex

(**A**) An illustration of the mouse visual system. Major areas of the primary visual cortex (V1) receive input only from the contralateral retina (turquoise projections). The lateral third of V1 is innervated additionally by ipsilateral projections (red). Although neurons in the binocular region are dominated by contralateral eye input, most neurons respond to both eyes. Thalamocortical axons from the dorsal lateral geniculate nucleus (dLGN) arborise not only within layer 4 (L4) but also in superficial layers (L1-3). (**B**) Four days of MD in juvenile mice (around P28) lead to strong changes in binocular cortical responses. The OD distribution of cortical neurons shifts towards the eye that remained open (ipsilateral eye), as can be seen when comparing the two histograms (grey). Ocular dominance classes from 1–7 indicate relative responsiveness of neurons to contralateral and ipsilateral eye stimulation (1 or 7, cells respond only to the contralateral or ipsilateral eye, respectively; 4, equal response to both eyes). The OD shifts are caused by a strong weakening of deprived eye responsiveness (compare turquoise bars) and a partial strengthening of non-deprived eye responsiveness (compare red bars), as indicated by measurements of population response strength with visually-evoked potentials and intrinsic signal imaging. *Adapted from Hofer et al., 2006.*

The maturation of the PV+ interneuron network is thought to gate both the opening and closure of the critical period [100-102]. Immediate early gene products such as neuronal pentraxin 2 (*Nptx2*) maintain excitatory synaptic connections to PV+ interneurons to initiate the window for critical period plasticity including ODP [103,104]. Lastly, neuromodulator inputs that activate downstream intracellular signaling cascades also communicate with molecular pathways that can alter neuronal activity patterns involved in ODP [105].

1.2.2 : Sleep-associated mechanisms of ocular dominance plasticity

Many of the network-level and molecular mechanisms that promote ODP are governed by changes that occur in the visual system during sleep-wake cycles. Studies using kittens show a period of MD (6 hours) during the critical period causes a small but measurable shift in ocular dominance that is enhanced following a period of *ad lib* sleep. Recordings of V1 neurons' firing responses in this context show that the depression of DE responses occurs during the waking hours of MD and are sustained following subsequent sleep. Furthermore, potentiation of SE responses occurs selectively during subsequent sleep. Sleep deprivation following MD disrupts ODP, suggesting sleep has critical roles in V1 plasticity [106,107]. Several mechanisms required for LTP are activated in V1 during post-MD sleep, and these pathways seem to be essential for sleep promotion of ODP. For example, pharmacological disruption of activity-dependent kinases such as PKA and ERK, and protein synthesis via the mTOR pathway, in V1 during post-MD sleep eliminated ODP consolidation [107-109].

1.2.3 : ODP as a model of amblyopia and amblyopia treatments

Amblyopia is a visual disorder which is frequently caused by disrupted vision in one eye (or loss of proper binocular input) in childhood. This disruption leads to long-lasting poor binocular vision and loss of visual acuity (in one or both eyes) in adulthood [110,111]. Common causes of amblyopia include MD-like deprivation caused from injuries such as cataracts, occlusion, misalignment of one of the eyes (strabismus) or even congenital defects that occlude vision in one eye [112,113].

Early studies of ODP in cats and primates suggested that if MD ceased (i.e., the DE was re-opened) outside of the critical period, long-lasting disruptions of visual persisted which reflected vision loss in patients with amblyopia. These early studies showed that “reverse occlusion” – i.e., occluding the original SE – led to some recovery of DE vision [114-117]. These findings informed the current standard of care for affected children, which is dominant eye patching and visual therapy to force use of the weaker eye. However, results are mixed on the effectiveness of dominant eye patching therapy, which is poorly tolerated by young children [118-120]. It is estimated that 54% of children still display residual amblyopia after patching treatment. In response to efficacy concerns, alternative treatments are under development, including binocular therapies such as iPad-based dichoptic training. However, these interventions, like dominant eye patching, show a low compliance rate among children treated [121-125].

Conclusions from animal model studies on post-MD recovery mechanisms involved in re-establishing binocular vision are mixed. Hypothetical models of ODP based on competition between synaptic inputs do not predict recovery of lost DE responses from simply re-opening of the eye, but studies have shown possible recovery of binocular vision in various species [85,126-129]. In addition, there is very little research on the role of

sleep in recovery mechanisms after loss of DE responses due to MD. A single study in kittens during the critical period showed that a period of sleep following a period of vision with occlusion of the dominant eye (analogous to dominant eye patching) impaired recovery of V1 responses, a juxtaposition of the enhancement in ODP by sleep seen after initial MD [130].

Critically, the relative efficacy of visual therapy providing binocular vs. monocular (dominant eye-only) visual input in promoting binocular vision has not been fully tested. Studies examining the roles of visual experience and sleep in cellular mechanisms involved in post-MD recovery could help in developing optimal treatments for individuals affected by amblyopia.

1.3 : Sleep and hippocampal memory consolidation

The ability to acquire, consolidate, and recall information from experiences in our surroundings is vital for survival. Translating these transient sensory experiences into short and long-term memories is a fundamental function of a brain structure called the hippocampus [19,131,132]. Landmark studies involving patient H.M., who underwent bilateral temporal lobe resection showed severe episodic memory impairments, i.e., an inability to commit new life events to long-term memory, despite retaining other cognitive faculties [133]. The case of patient H.M. launched the modern era of learning and memory research, characterizing how the neural circuits in the hippocampus mediate the consolidation of episodic memory.

1.3.1 : Hippocampal memory consolidation

The hippocampal circuits mediating memory consolidation have been studied intensively over the past few decades. The excitatory neurons in the hippocampus form a tri-synaptic circuit (**Figure 1.3**). The granule cells in the dentate gyrus (DG) receive sensory and non-sensory information via excitatory input from the entorhinal cortex [66,134]. DG granule cells project to pyramidal neurons in area CA3 (mossy fibers), which in turn project to pyramidal neurons within CA1 (Schaffer collaterals), these neurons form the major output from the hippocampus to neocortex [66,135,136]. Within this tri-synaptic excitatory circuit, molecular mechanisms required for LTP and LTD have been extensively studied [131,137-140]. The hippocampus also contains a diverse array of neighboring GABAergic interneurons. Recent studies have indicated that interneuron subpopulations in various subregions of the hippocampus contribute to mechanisms involved in the acquisition and consolidation of new memories [136,141-143].

Hippocampus-dependent learning and memory consolidation can be studied in rodent models using a diverse number of behavioral paradigms. One well-established example is contextual fear conditioning (CFC), here rodents learn to associate a neutral context (or environment) with an aversive stimulus (e.g. a foot shock) and subsequently display fear responses in the form of freezing when re-introduced to the shock-paired context [144,145]. The cellular and circuit-level mechanisms involved in the encoding and recall of contextual fear memory (CFM) have been revealed by recent work involving chemogenetic or optogenetic manipulations of hippocampal activity. For example, when CFM “engram ensembles”, i.e., the population of DG neurons activated during CFC, are reactivated, this is sufficient to induce a freezing response [143,146]. CFC also requires coordination of neuron populations’ activity between the hippocampus and amygdala,

specifically through vCA1 monosynaptic projections to the amygdala [147,148]. Furthermore, disruption of hippocampal network activity in areas such as CA3 lead to impairment of CFM consolidation [149,150]. Another form of hippocampus-dependent learning is object location memory (OLM), a spatial memory that can be measured based on the natural tendency of rodents to explore novel stimuli in their environment. During training on this task, rodents are exposed to two or more identical objects in set locations. When they are later returned to explore in a context where one of the objects is moved to a novel location, OLM can be measured based on selective exploration of the displaced object – i.e., exploration of the displaced object for longer periods of time. The hippocampal network has been shown to be essential for proper consolidation of OLM and related special memory paradigms [151-153]. Studies have used OLM tests to study spatial cognition without the need for traditional re-enforcers, and without the potential for causing distress, present in tasks such as the Morris water maze [154,155].

1.3.2 : Sleep-dependent mechanisms of hippocampal memory consolidation

Behavioral studies have shown that sleep has a vital role in memory consolidation, and an emerging hypothesis is that this is due to changes in hippocampal-cortical activity during sleep [156,157]. In mice, 5 hours of SD immediately following CFC training impairs CFM recall 24 hours later [71,158]. This suggests that the first few hours following CFC are critical for sleep-associated hippocampal mechanisms that consolidate CFM.

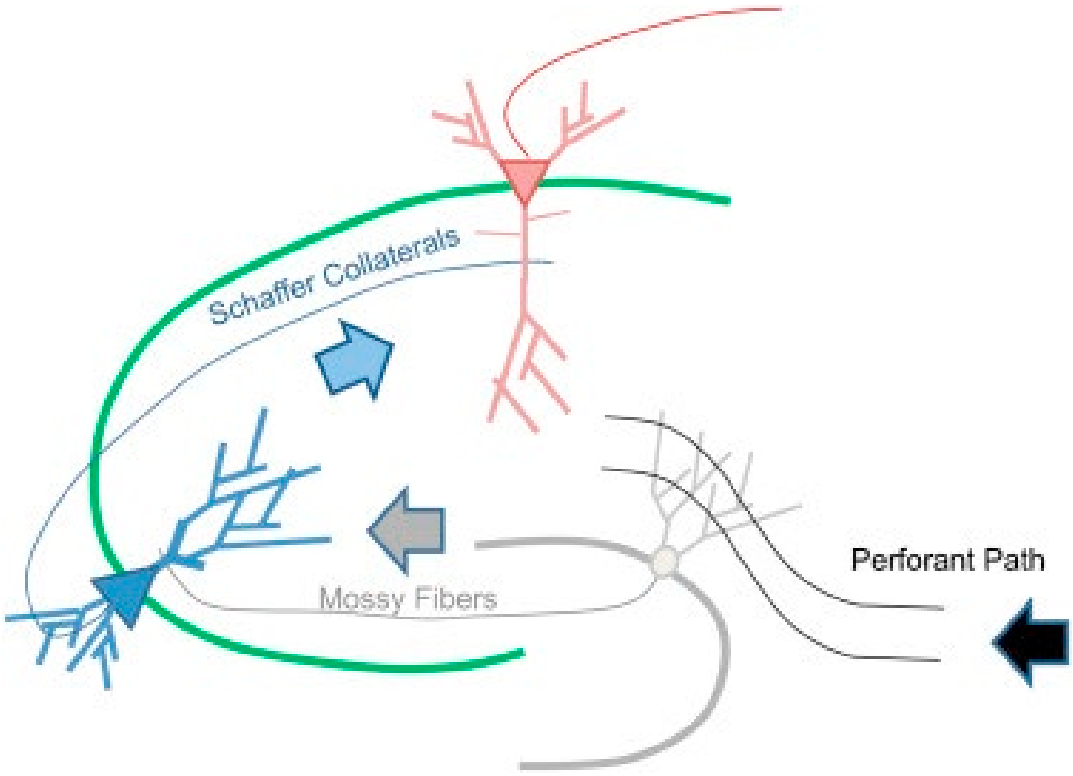

Figure 1.3: Hippocampal trisynaptic circuit

The hippocampal circuit is classically described as a trisynaptic loop. However, nowadays, it is assumed that information does not only flow serially in the hippocampus but that there is also parallel processing. For instance, the entorhinal cortex sends projections as well to CA3 and CA1 areas, several associational/commissural connections among CA3 pyramidal cells have been identified and it has even been suggested that CA3 cells project back to the dentate gyrus. Nonetheless, although the concept of the trisynaptic loop is an oversimplification of functional activity of the hippocampus it captures many important hippocampal features. *Modified from Lopez-Rojas and Kreutz, 2016*

How does post-CFC sleep change hippocampal function? Subsequent work from the Abel lab demonstrated that cAMP levels in the hippocampus were decreased during SD, and that this change (mediated by changes in phosphodiesterase activity) impaired CFM, suggesting maintenance of cAMP levels as a key mechanism in sleep-dependent memory consolidation [159]. Furthermore, there is evidence of increased expression of activity-dependent phosphorylation of ribosomal subunit S6 (pS6) across the dorsal hippocampus following CFC training. This expression is altered with 6 hours of SD following training and disrupts CFM. In addition, hippocampal somatostatin-expressing (SST+) interneuron activity is modulated by cholinergic inputs during SD. SD leads to heightened SST+ interneuron activity through this mechanism, leading to inhibition of surrounding pyramidal neurons and disrupted CFM consolidation [160]. In conjunction with molecular changes, there are many changes to hippocampal network dynamics, which occur in a sleep-dependent manner following CFC. For example, there are increases in CA1 neuronal firing, alongside changes in hippocampal delta and theta oscillations, during post-CFC NREM sleep [161]. Subsequent studies found that chemogenetically inhibiting fast-spiking PV+ interneuron activity following CFC impaired CFM consolidation and reduced post-CFC delta, theta, and SWR network activity. On the other hand, rhythmic optogenetic activation of PV+ interneurons within CA1 is sufficient to rescue CFM deficits caused by SD [28,29]. Lastly, evidience of altering specific sleep such as REM sleep, which is reduced following CFC training and pharmacologically increased immediately after training can improve CFM consolidation. [162-164].

Similar to CFC, the consolidation of object location memory (OLM) is also sleep-dependent. OLM is based on the mouse's ability to identify familiar objects that have been

moved to a new location within a familiar context. Mice that undergo 6 hours of SD immediately following OLM training show impairments in OLM consolidation. Intriguingly, 6 hours of SD is also sufficient to disrupt subsequent OLM encoding, and 6 hours of SD prior to OLM testing is sufficient to disrupt its recall [165]. These findings support the role of sleep in promoting memory for spatial tasks such as temporal object recognition tasks (which measures mice engagement with objects they previously interacted with at different points in time), Morris water maze, and spatial recognition tasks such as OLM [166-170], in addition to associative (contextual) tasks like CFM. Interestingly, hippocampus-dependent cognitive processes such as these are disrupted in mouse models of neurodevelopmental and neurodegenerative disorders. This begs the question of whether restoring healthy sleep can act as a therapeutic strategy to rescue cognitive abilities disrupted by such disorders.

1.4 : Sleep and Neurodevelopment

Over the course of human post-natal development, the amount of time spent in sleep each day changes dramatically. Human infants spend an average of 16-17 hours asleep per day (approximately 65% of their average day) and sleep time declines steadily as they reach adulthood [12,171]. These changes in sleep states are also found in rodent models. In mice and rats, EEG-defined NREM and REM sleep states are measurable around postnatal day 14 (P14), while infants show defined states at around 3 months [171-174]. Both humans and rodents display an increased proportion of total sleep time in REM sleep during early postnatal development; the proportion of time spent in REM sharply declines before reaching adulthood. In contrast, NREM sleep has a small steady increase in duration across infancy, but remains comparatively stable throughout one's lifespan

[12,171,173,175]. The overall temporal structure of sleep also changes across development. Circadian regulation of sleep is not present at birth and gradually matures in coordination with the decline of daily REM sleep amounts [176]. These drastic differences in sleep regulation and sleep time across the early development of the nervous system suggest that there may be a critical role for sleep in proper brain development.

1.4.1 : Sleep and brain development

Numerous studies have demonstrated that sleep can modulate developmentally-regulated synaptic plasticity. For example, REM sleep has been found to have roles in promoting critical period ODP. REM is necessary for alterations in cell sizes in the LGN layers representing the DE and SE after prolonged MD, and promotes ODP in V1 after very brief MD in kittens [109,177]. Additionally, REM sleep promotes spine elimination in V1 neurons following MD (as well as synaptic pruning in motor cortex after motor learning) [178,179]. While targeted disruption of NREM is more difficult to achieve than REM-specific sleep deprivation, available data suggest that NREM is also important for brain development. For example, chronic NREM sleep disruption in adolescent rats decreases hippocampal volume and impairs social bonding in adulthood [67,106,180,181]. Together, these data suggest that loss of sleep during early brain development can have long-lasting effects on both hippocampal and cortical functions, and suggests a strong relationship between sleep loss and atypical neurodevelopment.

1.4.2 : Autism spectrum disorders

Neurodevelopmental disorders (NDDs) are a heterogeneous group of early changes to brain development that result in atypical cognitive, neurological, and/or

psychiatric function. These disorders, including intellectual disability, epilepsy, bipolar disorder, cerebral palsy, Angelman syndrome, and autism spectrum disorder (ASD) can result from disruptions to neurodevelopmental processes such as neurogenesis, neuronal migration, synaptogenesis, and dendritic spine growth. [73,182-184]. ASDs are one of the more prevalent forms of NDD and are characterized by core phenotypes such as persistent, atypical social interactions and restricted, repetitive patterns of behavior. Currently, the Center for Disease Control reports that 1 in 44 children are diagnosed with ASD in the United States [185-188]. ASD is linked to many risk factors including prenatal, environmental, and genetic mutations. Several gene groups associated with processes such as axon guidance, synapse formation, and cell-type differentiation are tied to ASD diagnosed individuals [188-190].

Disrupted sleep has been reported in as many as 86% of children diagnosed with ASD. These phenotypes include forms of longer latency to sleep, sleep fragmentation, and insomnia. Insomnia is 2-3 times more prevalent in children with ASD than in children with typical development [191-194]. Studies from EEG/EMG recordings in children with ASD showed shorter sleep times, longer sleep latency, and decreased sleep efficiency [195,196]. Furthermore, affected individuals with ASD also demonstrate circadian cycle abnormalities including low melatonin production towards the end of the light phase (close to bedtime) that correlates with poor sleep and typical autistic behaviors [197,198]. Since sleep is critical for overall health including promoting synaptic plasticity and memory processes, it is unknown if sleep loss in ASD affected individuals is linked to behavioral phenotypes such as cognitive dysfunction. Rodent models of syndromic ASD such as Rett's syndrome, Angelman's syndrome, and Fragile X syndrome all display measurable

cognitive deficits [199-203], but there is little known about their sleep phenotypes and relationship of altered sleep to altered cognition.

1.4.3 : Fragile X syndrome

Fragile X syndrome (FXS) is an X-linked disorder that is a leading cause of both heritable intellectual disability and syndromic ASD [204,205]. It is estimated that 1 in 7000 males and 1 in 11000 females are diagnosed with FXS within the United States [206]. FXS develops due to mutations in the X chromosome Xq27.3 region where expansion of trinucleotide CGG repeats leads to transcriptional silencing of the Fragile X messenger ribonucleoprotein 1 (*FMR1*) gene via heterochromatin formation. Typical individuals have 5-50 CGG repeats within this 5'UTR region. Individuals with expansion of 55-200 CGG repeats are considered premutation carriers; this premutation increases mRNA transcription of *FMR1*, but reduces production of protein product Fragile X Messenger Ribonucleoprotein (FMRP). Expansion to over 200 CGG repeats leads to hypermethylation of cytosine bases and chromatin condensation and causes complete silencing of transcription of *FMR1* and loss of FMRP, resulting in FXS (**Figure 1.4**). FMRP is an RNA binding translational repressor protein that regulates transcription, translation, and transport of several mRNAs associated with synaptic plasticity and structure [203,207-213].

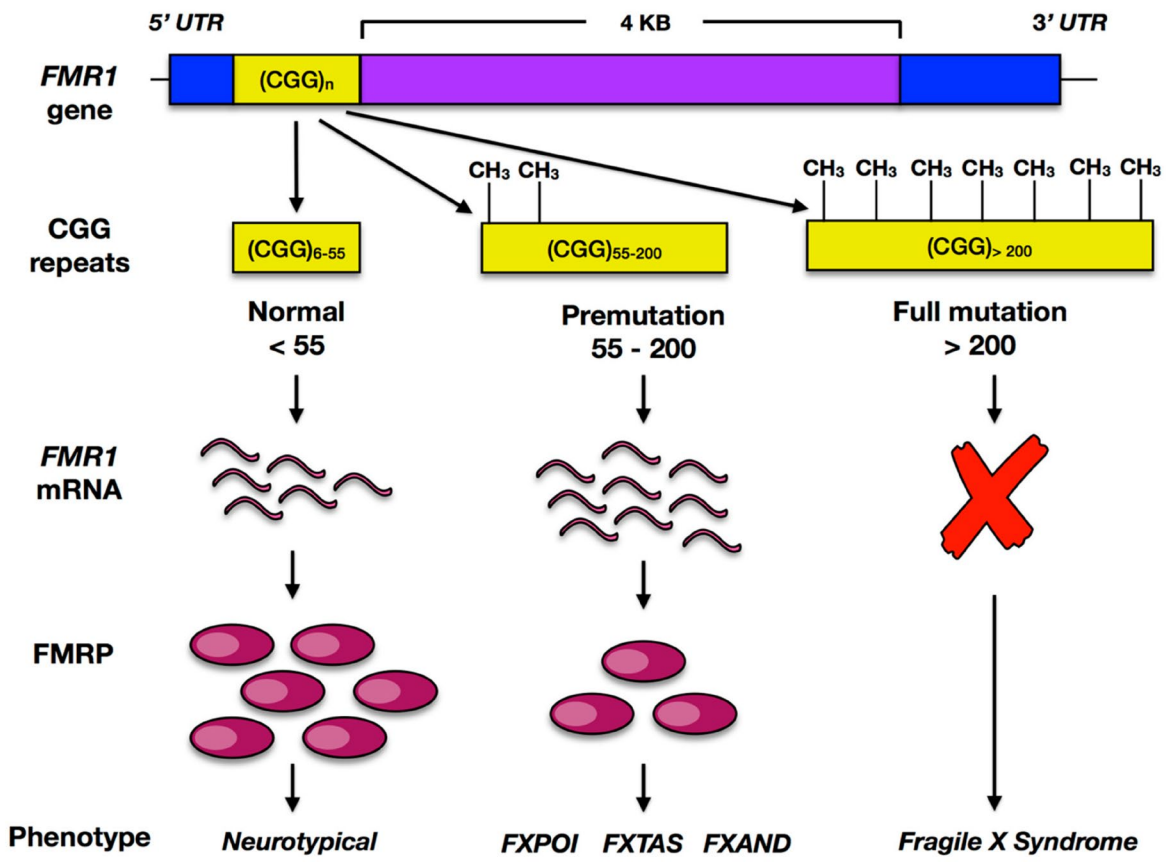

Figure 1.4: FMR1 gene and Fragile X pathology

CGG repeats (yellow) in the promoter region. <55 repeats are typical. Repeat expansion resulting in the premutation (55–200) is found in 1/130–250 females and 1/260–800 males. The premutation expansion increases mRNA transcription and is associated with Fragile X primary ovarian insufficiency (FXPOI), Fragile X-associated tremor and ataxia syndrome (FXTAS), and Fragile X-associated neuropsychiatric disorder (FXAND). Repeats greater than 200 results in the methylation of the promoter region and gene silencing that leads to complete loss of FMRP and subsequent Fragile X syndrome. *Modified from Fyke and Velinov, 2021.*

Individuals affected by FXS typically have anatomical, physiological, and cognitive phenotypes. Recognizable physical features of FXS include long faces, prominent ears, hyperflexible joints, and (in males) increased testicular volume during puberty (i.e., macroorchidism) [214,215]. Behavioral features include hyperactivity and atypical social engagement, ASD, anxiety, seizures, and learning impairments [216-221]. FXS-diagnosed individuals are reported to experience severe sleep problems. Large-scale studies based on questionnaire data from parents found that FXS children experience more frequent night awakenings and difficulty falling asleep at bedtime [222]. Additional studies using EEG/EMG recording demonstrated that FXS individuals show fragmented sleep, decreased sleep duration, and decreased NREM and REM sleep throughout the night [196,220,223-225]. Disrupted sleep phenotypes among FXS individuals are a growing concern with the need for better therapeutic approaches, including behavioral training and pharmacological intervention.

1.4.4 : Insights into Fragile X syndrome from FXS rodent models

Several animal models have been developed for the study of FXS including zebrafish, fruit flies, and rodents. The first mouse model for FXS, characterized by the knockout of the *Fmr1* gene (males: *Fmr1*$^{-/y}$, females: *Fmr1*$^{-/-}$), was created by the Dutch-Belgian Fragile X Consortium. This mouse line does not produce FMRP and has physiological attributes seen in those of FXS male patients such as macroorchidism [226]. The development of this mouse model has provided insight into the functional role of FMRP in neural development, cognition, and synaptic plasticity. Both FXS patients and *Fmr1*$^{-/y}$ mice show increased dendritic spine density in neocortical and hippocampal principal neurons, and immature dendritic spine morphology, which suggests improper

neurotransmission and synaptic plasticity. Studies using *Fmr1*$^{-/y}$ mice show FMRP localizes in dendritic spines, where it interacts with mRNAs and suppresses protein synthesis. FMRP also binds with other synaptic proteins, such as AMPA subunits GluR1 and GluR2, which are involved in dendritic spine structure. Loss of FMRP causes alterations of synaptic neurotransmission and metabotropic glutamate receptor-mediated (mGluR)-dependent LTD [227-229], related to its function in regulating protein synthesis from mRNAs in dendrites. FMRP is thought to suppress translation of mRNAs into proteins that negatively regulate internalization of AMPA receptors in the context of LTD. This translation is normally upregulated downstream of activation of mGluR. Loss of FMRP leads to persistent activation of mGluR-driven pathways and excessive productions of LTD-mediating proteins, which leads to exaggerated LTD. This LTD phenotype is associated with many of the cognitive impairments seen in both mice and FXS-affected individuals [205,230-233].

Behavioral deficits analogous to those found in humans have been extensively studied in *Fmr1*$^{-/y}$ mice, which show abnormalities in social discrimination tasks, increased hyperactivity and locomotion, and increased susceptibility to seizures [203,234,235]. Hippocampus-dependent memory consolidation is also impaired in *Fmr1*$^{-/y}$ mice, with *Fmr1*$^{-/y}$ mice showing reduced freezing responses 24 hours later after CFC compared to wild-type counterparts [236-238]. *Fmr1*$^{-/y}$ mice also show deficits in hippocampus-dependent visuo-spatial memory, including novel object recognition memory and OLM tasks, although spaced training can rescue OLM performance in *Fmr1*$^{-/y}$ mice, via activation of ERK signaling and LTP in the dorsal hippocampus [239-241]. While these hippocampus-

dependent tasks require sleep for their consolidation, the relationship of sleep and tasks such as OLM and CFC have not been extensively studied in *Fmr1*$^{-/y}$ mice.

There are few studies on how FXS and loss of FMRP affect sleep/wake architecture and circadian rhythms. Research done on other models of FXS such as *Drosophila* (*dFmr1* mutants) has revealed a loss of circadian rhythms and altered sleep bout durations [242-244]. Short-term EEG recordings on *Fmr1*$^{-/y}$ rats during wakefulness found increased gamma frequency power compared to wild-type controls [245]. With respect to *Fmr1*$^{-/y}$ mice, home-cage observational studies of locomotor activity suggest sleep changes across development. Young *Fmr1*$^{-/y}$ mice (postnatal day 17) show no differences in total sleep time compared WT controls. However, reaching adulthood ages (postnatal day 70 and 180), *Fmr1*$^{-/y}$ mice show reduced percentages of sleep compared to controls [246,247]. Lastly, only a single study using local field potential recording in CA1 has measured sleep states in *Fmr1*$^{-/y}$ mice. Here, they showed that *Fmr1*$^{-/y}$ mice exhibit reduced REM sleep and fewer bouts of REM sleep. They also provided further evidence of increased excitatory activity in CA1 during REM sleep [248]. However, this study only measured 120-minute durations, and at an undisclosed circadian phase. Further studies into a 24-hour sleep-wake cycle of *Fmr1*$^{-/y}$ mice are still needed to assess if they are representative of sleep deficits seen in FXS affected individuals.

1.5 : Hypnotic Targets for Treating Disrupted Sleep

Sleep disorders such as insomnia, sleep-related breathing disorders (e.g., sleep apnea), parasomnia, etc. have major negative effects on the quality of health and cognitive ability in humans [249]. Insomnia is the most widely recognized and diagnosed sleep disorder among individuals. It is characterized by features that include difficulty

falling or remaining asleep and coincide with other negative behavioral symptoms such as fatigue and brain fog. In individuals with ASD or other NDDs, these sleep disturbances are more prevalent [249-253]. The need for treatment of sleep disorders in both healthy and ASD populations is clearly shown by the fact that the loss of sleep not only negative impacts cognition (e.g., memory processing), but also early brain development and maturation [12,192,254,255]. The most widely-studied intervention is pharmacological treatment that promotes sleep. However, the use of these treatments to promote sleep and benefit deficits in cognitive ability in ASD-affected individuals (such as those with FXS) is less understood.

1.5.1 : Insomnia

An estimated 30-40% of the population experiences insomnia, with prevalence increasing with age. Consequences of insomnia include impaired work performance, deficiencies in cognitive ability, incidences of depression, and overall poor quality of life [253,256-258]. Chronic insomnia leads to health complications such as chronic pain, cardiovascular disease, gastrointestinal disorders, and other neurological disorders [250,254]. Since sleep is critical for brain developmental maturation, recurring sleep impairments over development could negatively impact developmental processes related to cognition such as decision-making, executive function, and memory processing. For children and adolescents, particularly those with ASD, it can also impact or exacerbate specific phenotypes related to hyperactivity, social interactions, and anxiety [259-262]. Lastly, other sleep disruptions that occur in both typical children and those with ASD include circadian rhythm disruptions, sleep apnea, hypersomnia, and restless leg syndrome that can also have negative impacts on the quality of life many can carry into adulthood [196,263].

1.5.2 : Treatments for insomnia and related sleep disorders

Pharmacological intervention is the primary therapeutic approach to treat insomnia. One class of sleep-promoting (hypnotic) drugs for patients with insomnia are benzodiazepines, which act as positive allosteric modulators of $GABA_A$ and $GABA_B$ receptors and promote inhibitory neurotransmission. While effective at promoting sleep (specifically NREM sleep), they can cause unwarranted side effects including oversedation, spike-wave discharges and other aberrant oscillatory patterns, and cognitive deficits [264-269]. Another widely prescribed class includes zolpidem (Ambien), zopiclone, and zaleplon- collectively known as "Z-drugs". Z hypnotics promote a more natural sleep pattern and possess shorter half-lives than benzodiazepines. Some act via the alpha-1 subunit of GABAA receptors to cause rapid sleep onset. However, there are still side effects from Z-drugs such as daytime drowsiness, impairments on cognition, and abuse potential in individuals who use more than the recommended dosage [270-272]. The similarities between benzodiazepines and Z-drugs, with regard to both efficacy and secondary side effects in patients, stem from shared GABAergic mechanisms. Additional hypnotic treatments include antihistamines, sedating antidepressants, tricyclic antidepressants, and atypical antipsychotics – these drugs all promote sleep, and also can cause impaired cognition, plasticity, and behavioral deficits [225,268,269,273-275]. The need for improved pharmacological interventions to promote physiologically normal sleep without adversely affecting typical neural development and function is vastly needed.

One emerging treatment for a set of sleep deficits is exogenous melatonin (MT) to help with impaired sleep onset and improve overall sleep quality in users [276-279]. The suprachiasmatic nucleus (SCN), that intakes circadian timing cues, regulates synthesis

of MT hormone via the pineal gland. MT targets two G-protein coupled receptors (MT1 and MT2) to induce sleep in accordance with circadian times such as dusk. MT1 receptors are widely expressed in orexin neurons within the hypothalamus and the SCN to influence REM sleep, while MT2 receptors are abundant in the thalamic reticular nucleus and other structures implicated NREM sleep. Due to limited side effects of exogenous MT in other studies and efficacy in promotion both NREM and REM sleep via dual receptors, MT has been suggested as a promising option for treating sleep disorders such as insomnia and poor sleep [280-282]. Lastly, MT treatment in children with ASDs causes some restoration of circadian rhythms and improved sleep. However some ASD patients do not respond to MT treatment - again suggesting new therapeutic targets are needed for this population [197,283].

1.5.3 : Novel target for treatment of sleep disorders: GIRK channels

One prospective novel hypnotic target is G-protein inward rectifying potassium (GIRK) channels involved in inhibitory neurotransmission. GIRK channels are coupled with G-protein coupled receptors (GPCRs) and widely found within the nervous and cardiovascular systems. Four distinct subunits (GIRK1-4) form both homo- or heterotetrametric combinations in several brain regions and cardiac tissue with combinations of GIRK1 and GIRK2 being most common in regions such as the hippocampus, neocortex, and cerebellum [284-287]. GIRK channels are activated using the Gi-dependent signaling pathway activated via GPCR activation of numerous ligands such as GABA, serotonin, and dopamine. Here, dissociation of the α-GTP and Gβγ subunit leads the Gβγ subunit to bind to GIRK channels to allow channel opening and results in

K+ ion flow (**Figure 1.5**). Opening of GIRK channels typically leads to hyperpolarization of neurons and decrease neuronal excitability [285,288-290].

GIRK channels provide critical modulation of neuronal excitation and membrane potential within the nervous system. Dysfunction of GIRK channels in areas such as the hippocampus can disrupt LTP and other forms of synaptic plasticity. Knockout of GIRK2 increases seizure susceptibility in mice, and causes chronic depolarization and neurodegeneration of dopaminergic neurons. Disruptions like these are implicated in various disorders such as Alzheimer's disease, Parkinson's disease, schizophrenia, and anxiety [291-294]. Lastly, GIRK channels have roles in circadian sleep regulation. Loss of GIRK2 shows disruption of MT-induced hyperpolarization within the SCN and disrupting SCN sleep-promoting mechanisms [295,296]. This suggests that GIRK channels may be a potential target for inducing sleep with hypnotics.

Few agonists have been developed to activate GIRK channels within the nervous system. One of the more potent agonists is ML297, which is selective for the GIRK1 subunit and upon binding causes channel opening and subsequent K+ conductance. ML297 binds to amino acids (phenylalanine and aspartate) on the GIRK1 subunit and can act independently of GPCR activity. This direct activation hyperpolarizes the cell and reduces excitability [297,298]. Research on ML297 initially focused on studying its function as a possible antiepileptic. Studies comparing ML297 and sodium valproate (a standard antiepileptic drug) in mice of epilepsy, found activation of GIRK channels via ML297 to be superior or equal in delaying seizures and increasing survival after seizure onset [297]. Further studies examined ML297 as a possible anxiolytic where administration to rats showed increased time in the open arms of the elevated plus maze [298].

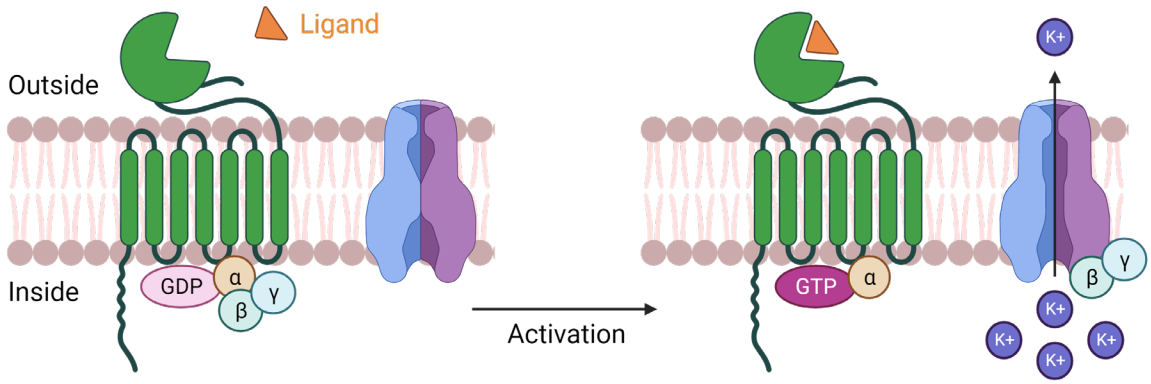

Figure 1.5: GIRK channel activation via Gi signaling pathway

G protein-activated inwardly rectifying potassium channels (GIRK channels) are activated by direct interaction with the βγ subunits of G protein (Gi signaling). Ligands of various types bind to the G protein-coupled receptor with seven transmembrane segments. The βγ subunits tag to GIRK channel to cause channel opening and subsequent flow of K+ ions to lead to hyperpolarization and inhibitory neurotransmission. *Adapted and modified from Lüscher and Slesinger, 2010 using BioRender© 2022.*

Lastly, more recent work has studied ML297 as a hypnotic agent. Studies have found that direct activation of GIRK1 via ML297 promotes NREM sleep. Excitatory hippocampal pyramidal and hypothalamic hypocretin neurons showed hyperpolarizing effects when exposed to ML297 using in vitro slice recordings. Using mice, administration of ML297 promoted NREM sleep during the dark phase without affecting memory retrieval in tasks such as CFC and novel object recognition memory [299]. GIRK channel activation via ML297 may be a potential hypnotic to treat sleep loss without negatively impacting cognition and could be helpful in treating children with ASDs and the general population.

1.6 : Outline of the dissertation

Sleep is critical for brain development. The shaping of synaptic circuits during neurodevelopment can be disrupted by genetic mutations or inadequate sensory stimuli early in life. The role of sleep as a mitigating factor for these deficits is not well understood, though many developmental disorders are characterized by sleep disruption. It remains unknown whether properly timed sleep could promote functional recovery of cognition and synaptic plasticity in neurodevelopmental disorders. We hypothesize that sleep can promote recovery of cortical and memory functions in the context of atypical neurodevelopmental conditions. The aim of this dissertation is to examine this hypothesis by 1) measuring how sleep and sleep loss affect recovery of visual cortex function in a mouse model of amblyopia and 2) assessing whether restoring normal sleep improves cognition in a mouse model of Fragile X syndrome (FXS).

In **Chapter 2**, I assess how sleep loss affects the recovery of visual responses in V1 in a mouse model of amblyopia. ODP is disrupted with subsequent sleep loss suggesting that ODP-associated synaptic changes caused by MD occur within sleep. I

test how reversal of these changes - through restoration of visual input to the DE using both binocular and monocular visual experience - were affected by subsequent sleep or sleep loss. Using *in vivo* electrophysiology and biochemical assays, I find that binocular visual experience was far more efficacious at reversing ODP changes caused by MD. In addition, we also show that if sleep was disrupted following a period of binocular recovery, it delays the cortical ocular dominance changes that restore DE function. Together, this suggests that the timing of sleep relative to visual experience during amblyopia treatment may be critical for restoring normal visual cortex function.

In **Chapter 3**, I examine how GIRK activating hypnotic agonist ML297 affects sleep-dependent memory consolidation. ML297 promotes NREM sleep without disrupting memory recall in hippocampal-dependent tasks. I test how GIRK channel activation affected sleep architecture following training of CFC and how it impacted hippocampal activation patterns during CFM recall. Using EEG/EMG recordings and biochemical assays, I find that REM sleep was increased immediately following CFC training, which lead to improved CFM consolidation. cFos expression in hippocampal subregions correlates with improvements in CFM recall driven by ML297. Together, this suggests that ML297 can also serve to improve sleep-dependent memory consolidation via increased REM sleep.

In **Chapter 4**, I examine sleep deficits found in *Fmr1*$^{-/y}$ mice and test whether normalizing sleep with ML297 reverses memory consolidation deficits associated with loss of *Fmr1* function. Currently, it is unclear how sleep disruption common to ASD and FXS contributes or exacerbates memory dysfunction in these disorders. I test how administration of ML297 to induce sleep improved sleep architectural and spectral power

alterations and subsequently led to improvements in fear memory consolidation. Using EEG/EMG recordings, behavioral assays, and biochemical techniques, I find that acute administration of ML297 improves NREM sleep architectural differences and delta spectral power changes found in *Fmr1*$^{-/y}$ mice. Sleep-dependent fear memory consolidation is also rescued with ML297 along with cFos driven hippocampal activation patterns correlating to improvements in CFM recall in *Fmr1*$^{-/y}$ mice. Together, this suggests that improving sleep via hypnotic treatments can have therapeutic potential in aid sleep deficits and the improvement of cognitive function in individuals with NDDs.

1.6.1 : Acknowledgements

I would like to thank my undergraduates Donald Popke, William Brancaleone, and Kathryn Peterson who each completed a Senior Honors Thesis as part of their major requirements for the Bachelor of Science in Neuroscience under the Undergraduate Program in Neuroscience. The literature search, review, and writing of the introductory portions of their honors theses helped make important contributions to the crafting and writing of this chapter of my dissertation.

1.7 : References

1. Rasch, B., and Born, J. (2013). About sleep's role in memory. Physiol Rev *93*, 681-766. 10.1152/physrev.00032.2012.
2. Vorster, A.P., and Born, J. (2015). Sleep and memory in mammals, birds and invertebrates. Neurosci Biobehav Rev *50*, 103-119. 10.1016/j.neubiorev.2014.09.020.
3. Siegel, J.M. (2005). Clues to the functions of mammalian sleep. Nature. Nature Publishing Group.
4. Porkka-Heiskanen, T. (2014). Sleep regulatory factors. Arch Ital Biol *152*, 57-65. 10.12871/000298292014231.
5. Borbely, A.A., and Achermann, P. (1999). Sleep homeostasis and models of sleep regulation. J Biol Rhythms *14*, 557-568. 10.1177/074873099129000894.
6. Murillo-Rodríguez, E., Yamamoto, T., Monteiro, D., Budde, H., Rocha, N.B., Cid, L., Teixeira, D.S., Telles-Correia, D., Veras, A.B., Machado, S., et al. (2020). Assessing the Management of Excessive Daytime Sleepiness by Napping Benefits. Sleep and Vigilance *4*, 117-123. 10.1007/S41782-020-00090-9/FIGURES/3.
7. Mistlberger, R.E. (2005). Circadian regulation of sleep in mammals: role of the suprachiasmatic nucleus. Brain Res Brain Res Rev *49*, 429-454. 10.1016/j.brainresrev.2005.01.005.
8. Stiller, J.W., and Postolache, T.T. (2005). Sleep-wake and other biological rhythms: functional neuroanatomy. Clin Sports Med *24*, 205-235, vii. 10.1016/j.csm.2004.12.008.
9. Meyer, N., Harvey, A.G., Lockley, S.W., and Dijk, D.J. (2022). Circadian rhythms and disorders of the timing of sleep. Lancet *400*, 1061-1078. 10.1016/S0140-6736(22)00877-7.
10. Perez-Carbonell, L., Mignot, E., Leschziner, G., and Dauvilliers, Y. (2022). Understanding and approaching excessive daytime sleepiness. Lancet *400*, 1033-1046. 10.1016/S0140-6736(22)01018-2.
11. Frank, M.G. (2015). Sleep, Neuronal Plasticity and Brain Function. Current topics in behavioral neurosciences *25*, 123-149.
12. Wintler, T., Schoch, H., Frank, M.G., and Peixoto, L. (2020). Sleep, brain development, and autism spectrum disorders: Insights from animal models. J Neurosci Res *98*, 1137-1149. 10.1002/jnr.24619.
13. Kreutzmann, J.C., Havekes, R., Abel, T., and Meerlo, P. (2015). Sleep deprivation and hippocampal vulnerability: changes in neuronal plasticity, neurogenesis and cognitive function. Neuroscience *309*, 173-190. 10.1016/j.neuroscience.2015.04.053.
14. Steriade, M., Timofeev, I., and Grenier, F. (2001). Natural waking and sleep states: a view from inside neocortical neurons. J Neurophysiol *85*, 1969-1985. 10.1152/jn.2001.85.5.1969.
15. Steriade, M. (2006). Grouping of brain rhythms in corticothalamic systems. Neuroscience *137*, 1087-1106. 10.1016/j.neuroscience.2005.10.029.

16. Watson, C.J., Baghdoyan, H.A., and Lydic, R. (2012). Neuropharmacology of Sleep and Wakefulness: 2012 Update. Sleep Med Clin *7*, 469-486. 10.1016/j.jsmc.2012.06.010.
17. Watson, C.J., Baghdoyan, H.A., and Lydic, R. (2010). Neuropharmacology of Sleep and Wakefulness. Sleep Med Clin *5*, 513-528. 10.1016/j.jsmc.2010.08.003.
18. Lyamin, O.I., Lapierre, J.L., Kosenko, P.O., Kodama, T., Bhagwandin, A., Korneva, S.M., Peever, J.H., Mukhametov, L.M., and Siegel, J.M. (2016). Monoamine Release during Unihemispheric Sleep and Unihemispheric Waking in the Fur Seal. Sleep *39*, 625-636. 10.5665/sleep.5540.
19. Puentes-Mestril, C., and Aton, S.J. (2017). Linking Network Activity to Synaptic Plasticity during Sleep: Hypotheses and Recent Data. Front Neural Circuits *11*, 61. 10.3389/fncir.2017.00061.
20. Puentes-Mestril, C., Roach, J., Niethard, N., Zochowski, M., and Aton, S.J. (2019). How rhythms of the sleeping brain tune memory and synaptic plasticity. Sleep *42*. 10.1093/sleep/zsz095.
21. Timofeev, I., Grenier, F., Bazhenov, M., Sejnowski, T.J., and Steriade, M. (2000). Origin of slow cortical oscillations in deafferented cortical slabs. Cereb Cortex *10*, 1185-1199. 10.1093/cercor/10.12.1185.
22. Steriade, M., and Timofeev, I. (2003). Neuronal plasticity in thalamocortical networks during sleep and waking oscillations. Neuron *37*, 563-576. 10.1016/s0896-6273(03)00065-5.
23. Dang-Vu, T.T., Schabus, M., Desseilles, M., Albouy, G., Boly, M., Darsaud, A., Gais, S., Rauchs, G., Sterpenich, V., Vandewalle, G., et al. (2008). Spontaneous neural activity during human slow wave sleep. Proc Natl Acad Sci U S A *105*, 15160-15165. 10.1073/pnas.0801819105.
24. Contreras, D., and Steriade, M. (1995). Cellular basis of EEG slow rhythms: a study of dynamic corticothalamic relationships. J Neurosci *15*, 604-622. 10.1523/JNEUROSCI.15-01-00604.1995.
25. Schabus, M., Hoedlmoser, K., Pecherstorfer, T., Anderer, P., Gruber, G., Parapatics, S., Sauter, C., Kloesch, G., Klimesch, W., Saletu, B., and Zeitlhofer, J. (2008). Interindividual sleep spindle differences and their relation to learning-related enhancements. Brain Res *1191*, 127-135. 10.1016/j.brainres.2007.10.106.
26. Bernardi, G., Betta, M., Ricciardi, E., Pietrini, P., Tononi, G., and Siclari, F. (2019). Regional Delta Waves In Human Rapid Eye Movement Sleep. J Neurosci *39*, 2686-2697. 10.1523/JNEUROSCI.2298-18.2019.
27. Thankachan, S., Katsuki, F., McKenna, J.T., Yang, C., Shukla, C., Deisseroth, K., Uygun, D.S., Strecker, R.E., Brown, R.E., McNally, J.M., and Basheer, R. (2019). Thalamic Reticular Nucleus Parvalbumin Neurons Regulate Sleep Spindles and Electrophysiological Aspects of Schizophrenia in Mice. Sci Rep *9*, 3607. 10.1038/s41598-019-40398-9.
28. Ognjanovski, N., Schaeffer, S., Wu, J., Mofakham, S., Maruyama, D., Zochowski, M., and Aton, S.J. (2017). Parvalbumin-expressing interneurons coordinate hippocampal network dynamics required for memory consolidation. Nat Commun *8*, 15039. 10.1038/ncomms15039.

29. Ognjanovski, N., Broussard, C., Zochowski, M., and Aton, S.J. (2018). Hippocampal Network Oscillations Rescue Memory Consolidation Deficits Caused by Sleep Loss. Cereb Cortex *28*, 3711-3723. 10.1093/cercor/bhy174.
30. Sirota, A., Csicsvari, J., Buhl, D., and Buzsaki, G. (2003). Communication between neocortex and hippocampus during sleep in rodents. Proceedings of the National Academy of Sciences of the United States of America *100*, 2065-2069. 10.1073/pnas.0437938100.
31. Clemens, Z., Molle, M., Eross, L., Jakus, R., Rasonyi, G., Halasz, P., and Born, J. (2011). Fine-tuned coupling between human parahippocampal ripples and sleep spindles. Eur J Neurosci *33*, 511-520. 10.1111/j.1460-9568.2010.07505.x.
32. Ji, D., and Wilson, M.A. (2007). Coordinated memory replay in the visual cortex and hippocampus during sleep. Nat Neurosci *10*, 100-107. 10.1038/nn1825.
33. Buzsaki, G. (1989). Two-stage model of memory trace formation: a role for "noisy" brain states. Neuroscience *31*, 551-570. 10.1016/0306-4522(89)90423-5.
34. Rosanova, M., and Ulrich, D. (2005). Pattern-specific associative long-term potentiation induced by a sleep spindle-related spike train. J Neurosci *25*, 9398-9405. 10.1523/JNEUROSCI.2149-05.2005.
35. Wierzynski, C.M., Lubenov, E.V., Gu, M., and Siapas, A.G. (2009). State-Dependent Spike-Timing Relationships between Hippocampal and Prefrontal Circuits during Sleep. Neuron *61*, 587-596. 10.1016/j.neuron.2009.01.011.
36. Hasselmo, M.E. (1999). Neuromodulation: acetylcholine and memory consolidation. Trends Cogn Sci *3*, 351-359. 10.1016/s1364-6613(99)01365-0.
37. Hasselmo, M.E., and Giocomo, L.M. (2006). Cholinergic modulation of cortical function. J Mol Neurosci *30*, 133-135. 10.1385/JMN:30:1:133.
38. Power, A.E. (2004). Slow-wave sleep, acetylcholine, and memory consolidation. Proc Natl Acad Sci U S A *101*, 1795-1796. 10.1073/pnas.0400237101.
39. Braun, A.R., Balkin, T.J., Wesenten, N.J., Carson, R.E., Varga, M., Baldwin, P., Selbie, S., Belenky, G., and Herscovitch, P. (1997). Regional cerebral blood flow throughout the sleep-wake cycle. An H2(15)O PET study. Brain *120 (Pt 7)*, 1173-1197. 10.1093/brain/120.7.1173.
40. Maquet, P., Peters, J., Aerts, J., Delfiore, G., Degueldre, C., Luxen, A., and Franck, G. (1996). Functional neuroanatomy of human rapid-eye-movement sleep and dreaming. Nature *383*, 163-166. 10.1038/383163a0.
41. Maquet, P., and Franck, G. (1997). REM sleep and amygdala. Mol Psychiatry *2*, 195-196. 10.1038/sj.mp.4000239.
42. Dement, W., and Kleitman, N. (1957). The relation of eye movements during sleep to dream activity: an objective method for the study of dreaming. J Exp Psychol *53*, 339-346. 10.1037/h0048189.
43. Staunton, H. (2005). Mammalian sleep. Naturwissenschaften.
44. Peever, J., and Fuller, P.M. (2016). Neuroscience: A Distributed Neural Network Controls REM Sleep. Curr Biol *26*, R34-35. 10.1016/j.cub.2015.11.011.
45. Deboer, T., and Tobler, I. (1996). Shortening of the photoperiod affects sleep distribution, EEG and cortical temperature in the Djungarian hamster. J Comp Physiol A *179*, 483-492. 10.1007/BF00192315.
46. Amici, R., Cerri, M., Ocampo-Garces, A., Baracchi, F., Dentico, D., Jones, C.A., Luppi, M., Perez, E., Parmeggiani, P.L., and Zamboni, G. (2008). Cold exposure

and sleep in the rat: REM sleep homeostasis and body size. Sleep *31*, 708-715. 10.1093/sleep/31.5.708.
47. Sanford, L.D., Yang, L., Wellman, L.L., Liu, X., and Tang, X. (2010). Differential effects of controllable and uncontrollable footshock stress on sleep in mice. Sleep *33*, 621-630. 10.1093/sleep/33.5.621.
48. Payne, J.D. (2011). Sleep on it!: stabilizing and transforming memories during sleep. Nat Neurosci *14*, 272-274. 10.1038/nn0311-272.
49. Ribeiro, S., Goyal, V., Mello, C.V., and Pavlides, C. (1999). Brain gene expression during REM sleep depends on prior waking experience. Learn Mem *6*, 500-508. 10.1101/lm.6.5.500.
50. Ribeiro, S., and Nicolelis, M.A. (2004). Reverberation, storage, and postsynaptic propagation of memories during sleep. Learn Mem *11*, 686-696. 10.1101/lm.75604.
51. Ribeiro, S., Gervasoni, D., Soares, E.S., Zhou, Y., Lin, S.C., Pantoja, J., Lavine, M., and Nicolelis, M.A. (2004). Long-lasting novelty-induced neuronal reverberation during slow-wave sleep in multiple forebrain areas. PLoS Biol *2*, E24. 10.1371/journal.pbio.0020024.
52. Ribeiro, S., Shi, X., Engelhard, M., Zhou, Y., Zhang, H., Gervasoni, D., Lin, S.C., Wada, K., Lemos, N.A., and Nicolelis, M.A. (2007). Novel experience induces persistent sleep-dependent plasticity in the cortex but not in the hippocampus. Front Neurosci *1*, 43-55. 10.3389/neuro.01.1.1.003.2007.
53. Smith, C., and Lapp, L. (1991). Increases in number of REMS and REM density in humans following an intensive learning period. Sleep *14*, 325-330. 10.1093/sleep/14.4.325.
54. Poe, G.R., Walsh, C.M., and Bjorness, T.E. (2010). Both duration and timing of sleep are important to memory consolidation. Sleep *33*, 1277-1278. 10.1093/sleep/33.10.1277.
55. Poe, G.R. (2017). Sleep Is for Forgetting. J Neurosci *37*, 464-473. 10.1523/JNEUROSCI.0820-16.2017.
56. Payne, J.D., Stickgold, R., Swanberg, K., and Kensinger, E.A. (2008). Sleep preferentially enhances memory for emotional components of scenes. Psychol Sci *19*, 781-788. 10.1111/j.1467-9280.2008.02157.x.
57. Fosse, R., Stickgold, R., and Hobson, J.A. (2001). Brain-mind states: reciprocal variation in thoughts and hallucinations. Psychol Sci *12*, 30-36. 10.1111/1467-9280.00306.
58. McNamara, P., Auerbach, S., Johnson, P., Harris, E., and Doros, G. (2010). Impact of REM sleep on distortions of self-concept, mood and memory in depressed/anxious participants. J Affect Disord *122*, 198-207. 10.1016/j.jad.2009.06.030.
59. McNamara, P., Johnson, P., McLaren, D., Harris, E., Beauharnais, C., and Auerbach, S. (2010). REM and NREM sleep mentation. Int Rev Neurobiol *92*, 69-86. 10.1016/S0074-7742(10)92004-7.
60. Brinkman, J.E., and Sharma, S. (2018). Physiology, Sleep (StatPearls Publishing).

61. Sulaman, B.A., Wang, S., Tyan, J., and Eban-Rothschild, A. (2023). Neuro-orchestration of sleep and wakefulness. Nat Neurosci *26*, 196-212. 10.1038/s41593-022-01236-w.
62. Trachsel, L., Tobler, I., Achermann, P., and Borbely, A.A. (1991). Sleep continuity and the REM-nonREM cycle in the rat under baseline conditions and after sleep deprivation. Physiol Behav *49*, 575-580. 10.1016/0031-9384(91)90283-t.
63. Trachsel, L., Tobler, I., and Borbely, A.A. (1988). Electroencephalogram analysis of non-rapid eye movement sleep in rats. Am J Physiol *255*, R27-37. 10.1152/ajpregu.1988.255.1.R27.
64. Adam, K., and Oswald, I. (1977). Sleep is for tissue restoration. J R Coll Physicians Lond *11*, 376-388.
65. Reimund, E. (1994). The free radical flux theory of sleep. Med Hypotheses *43*, 231-233. 10.1016/0306-9877(94)90071-x.
66. van Strien, N.M., Cappaert, N.L., and Witter, M.P. (2009). The anatomy of memory: an interactive overview of the parahippocampal-hippocampal network. Nat Rev Neurosci *10*, 272-282. 10.1038/nrn2614.
67. Killgore, W.D. (2010). Effects of sleep deprivation on cognition. Prog Brain Res *185*, 105-129. 10.1016/B978-0-444-53702-7.00007-5.
68. Jenkins, J.G., and Dallenbach, K.M. (1924). Obliviscence during sleep and waking. Am J Psychol *35*, 605-612. Doi 10.2307/1414040.
69. Diekelmann, S., and Born, J. (2010). The memory function of sleep. Nature Reviews Neuroscience.
70. Frankland, P.W., and Bontempi, B. (2005). The organization of recent and remote memories. Nature Reviews Neuroscience.
71. Graves, L.A., Heller, E.A., Pack, A.I., and Abel, T. (2003). Sleep deprivation selectively impairs memory consolidation for contextual fear conditioning. Learn Mem *10*, 168-176. 10.1101/lm.48803.
72. Clawson, B.C., Pickup, E.J., Ensing, A., Geneseo, L., Shaver, J., Gonzalez-Amoretti, J., Zhao, M., York, A.K., Kuhn, F.R., Swift, K., et al. (2021). Causal role for sleep-dependent reactivation of learning-activated sensory ensembles for fear memory consolidation. Nat Commun *12*, 1200. 10.1038/s41467-021-21471-2.
73. van Loo, K.M., and Martens, G.J. (2007). Genetic and environmental factors in complex neurodevelopmental disorders. Curr Genomics *8*, 429-444. 10.2174/138920207783591717.
74. Apa (2013). Diagnostic and statistical manual of mental disorders (DSM-5). American Psychiatric Publishing, 1-232.
75. Clawson, B.C., Durkin, J., and Aton, S.J. (2016). Form and Function of Sleep Spindles across the Lifespan. Neural Plast *2016*, 6936381. 10.1155/2016/6936381.
76. Morris-Rosendahl, D.J., and Crocq, M.A. (2020). Neurodevelopmental disorders-the history and future of a diagnostic concept. Dialogues Clin Neurosci *22*, 65-72. 10.31887/DCNS.2020.22.1/macrocq.
77. O'Leary, D.D., and Nakagawa, Y. (2002). Patterning centers, regulatory genes and extrinsic mechanisms controlling arealization of the neocortex. Curr Opin Neurobiol *12*, 14-25. 10.1016/s0959-4388(02)00285-4.

78. O'Leary, D.D.M., Chou, S.J., and Sahara, S. (2007). Area patterning of the mammalian cortex. Neuron. Cell Press.
79. Feldheim, D.A., and O'Leary, D.D.M. (2010). Visual map development: bidirectional signaling, bifunctional guidance molecules, and competition. Cold Spring Harbor perspectives in biology. Cold Spring Harbor Laboratory Press.
80. Hensch, T.K. (2004). Critical period regulation. Annu Rev Neurosci *27*, 549-579. 10.1146/annurev.neuro.27.070203.144327.
81. Levelt, C.N., and Hubener, M. (2012). Critical-period plasticity in the visual cortex. Annu Rev Neurosci *35*, 309-330. 10.1146/annurev-neuro-061010-113813.
82. Hubel, D.H., and Wiesel, T.N. (1962). Receptive fields, binocular interaction and functional architecture in the cat's visual cortex. J Physiol *160*, 106-154. 10.1113/jphysiol.1962.sp006837.
83. Wiesel, T.N., and Hubel, D.H. (1963). Single-Cell Responses in Striate Cortex of Kittens Deprived of Vision in One Eye. J Neurophysiol *26*, 1003-1017. 10.1152/jn.1963.26.6.1003.
84. Berardi, N., Pizzorusso, T., Ratto, G.M., and Maffei, L. (2003). Molecular basis of plasticity in the visual cortex. Trends Neurosci *26*, 369-378. 10.1016/S0166-2236(03)00168-1.
85. Hofer, S.B., Mrsic-Flogel, T.D., Bonhoeffer, T., and Hubener, M. (2006). Lifelong learning: ocular dominance plasticity in mouse visual cortex. Curr Opin Neurobiol *16*, 451-459. 10.1016/j.conb.2006.06.007.
86. Gordon, J.A., and Stryker, M.P. (1996). Experience-dependent plasticity of binocular responses in the primary visual cortex of the mouse. J Neurosci *16*, 3274-3286. 10.1523/JNEUROSCI.16-10-03274.1996.
87. Frenkel, M.Y., and Bear, M.F. (2004). How monocular deprivation shifts ocular dominance in visual cortex of young mice. Neuron *44*, 917-923. 10.1016/j.neuron.2004.12.003.
88. Bear, M.F., Kleinschmidt, A., Gu, Q.A., and Singer, W. (1990). Disruption of experience-dependent synaptic modifications in striate cortex by infusion of an NMDA receptor antagonist. J Neurosci *10*, 909-925. 10.1523/JNEUROSCI.10-03-00909.1990.
89. Chowdhury, S., Shepherd, J.D., Okuno, H., Lyford, G., Petralia, R.S., Plath, N., Kuhl, D., Huganir, R.L., and Worley, P.F. (2006). Arc/Arg3.1 interacts with the endocytic machinery to regulate AMPA receptor trafficking. Neuron *52*, 445-459. 10.1016/j.neuron.2006.08.033.
90. Bear, M.F., and Colman, H. (1990). Binocular competition in the control of geniculate cell size depends upon visual cortical N-methyl-D-aspartate receptor activation. Proc Natl Acad Sci U S A *87*, 9246-9249. 10.1073/pnas.87.23.9246.
91. McCurry, C.L., Shepherd, J.D., Tropea, D., Wang, K.H., Bear, M.F., and Sur, M. (2010). Loss of Arc renders the visual cortex impervious to the effects of sensory experience or deprivation. Nat Neurosci *13*, 450-457. 10.1038/nn.2508.
92. Wiesel, T.N., and Hubel, D.H. (1963). Effects of Visual Deprivation on Morphology and Physiology of Cells in the Cats Lateral Geniculate Body. J Neurophysiol *26*, 978-993. 10.1152/jn.1963.26.6.978.

93. Trachtenberg, J.T., Trepel, C., and Stryker, M.P. (2000). Rapid extragranular plasticity in the absence of thalamocortical plasticity in the developing primary visual cortex. Science *287*, 2029-2032. 10.1126/science.287.5460.2029.
94. Taha, S., and Stryker, M.P. (2002). Rapid ocular dominance plasticity requires cortical but not geniculate protein synthesis. Neuron *34*, 425-436. 10.1016/s0896-6273(02)00673-6.
95. Beaver, C.J., Ji, Q., Fischer, Q.S., and Daw, N.W. (2001). Cyclic AMP-dependent protein kinase mediates ocular dominance shifts in cat visual cortex. Nat Neurosci *4*, 159-163. 10.1038/83985.
96. Di Cristo, G., Berardi, N., Cancedda, L., Pizzorusso, T., Putignano, E., Ratto, G.M., and Maffei, L. (2001). Requirement of ERK activation for visual cortical plasticity. Science *292*, 2337-2340. 10.1126/science.1059075.
97. Cancedda, L., Putignano, E., Impey, S., Maffei, L., Ratto, G.M., and Pizzorusso, T. (2003). Patterned vision causes CRE-mediated gene expression in the visual cortex through PKA and ERK. J Neurosci *23*, 7012-7020. 10.1523/JNEUROSCI.23-18-07012.2003.
98. Kuhlman, S.J., Olivas, N.D., Tring, E., Ikrar, T., Xu, X., and Trachtenberg, J.T. (2013). A disinhibitory microcircuit initiates critical-period plasticity in the visual cortex. Nature *501*, 543-546. 10.1038/nature12485.
99. Harauzov, A., Spolidoro, M., DiCristo, G., De Pasquale, R., Cancedda, L., Pizzorusso, T., Viegi, A., Berardi, N., and Maffei, L. (2010). Reducing intracortical inhibition in the adult visual cortex promotes ocular dominance plasticity. J Neurosci *30*, 361-371. 10.1523/JNEUROSCI.2233-09.2010.
100. Huang, Z.J., Kirkwood, A., Pizzorusso, T., Porciatti, V., Morales, B., Bear, M.F., Maffei, L., and Tonegawa, S. (1999). BDNF regulates the maturation of inhibition and the critical period of plasticity in mouse visual cortex. Cell *98*, 739-755. 10.1016/s0092-8674(00)81509-3.
101. del Rio, J.A., de Lecea, L., Ferrer, I., and Soriano, E. (1994). The development of parvalbumin-immunoreactivity in the neocortex of the mouse. Brain Res Dev Brain Res *81*, 247-259. 10.1016/0165-3806(94)90311-5.
102. Hensch, T.K. (2005). Critical period plasticity in local cortical circuits. Nat Rev Neurosci *6*, 877-888. 10.1038/nrn1787.
103. Gu, Y., Huang, S., Chang, M.C., Worley, P., Kirkwood, A., and Quinlan, E.M. (2013). Obligatory role for the immediate early gene NARP in critical period plasticity. Neuron *79*, 335-346. 10.1016/j.neuron.2013.05.016.
104. Severin, D., Hong, S.Z., Roh, S.E., Huang, S., Zhou, J., Bridi, M.C.D., Hong, I., Murase, S., Robertson, S., Haberman, R.P., et al. (2021). All-or-none disconnection of pyramidal inputs onto parvalbumin-positive interneurons gates ocular dominance plasticity. Proc Natl Acad Sci U S A *118*. 10.1073/pnas.2105388118.
105. Gu, Q. (2002). Neuromodulatory transmitter systems in the cortex and their role in cortical plasticity. Neuroscience *111*, 815-835. 10.1016/s0306-4522(02)00026-x.
106. Frank, M.G., Issa, N.P., and Stryker, M.P. (2001). Sleep enhances plasticity in the developing visual cortex. Neuron *30*, 275-287. 10.1016/s0896-6273(01)00279-3.

107. Aton, S.J., Seibt, J., Dumoulin, M., Jha, S.K., Steinmetz, N., Coleman, T., Naidoo, N., and Frank, M.G. (2009). Mechanisms of sleep-dependent consolidation of cortical plasticity. Neuron *61*, 454-466. 10.1016/j.neuron.2009.01.007.
108. Seibt, J., Dumoulin, M.C., Aton, S.J., Coleman, T., Watson, A., Naidoo, N., and Frank, M.G. (2012). Protein synthesis during sleep consolidates cortical plasticity in vivo. Curr Biol *22*, 676-682. 10.1016/j.cub.2012.02.016.
109. Dumoulin Bridi, M.C., Aton, S.J., Seibt, J., Renouard, L., Coleman, T., and Frank, M.G. (2015). Rapid eye movement sleep promotes cortical plasticity in the developing brain. Sci Adv *1*, e1500105. 10.1126/sciadv.1500105.
110. Webber, A.L., and Wood, J. (2005). Amblyopia: prevalence, natural history, functional effects and treatment. Clin Exp Optom *88*, 365-375. 10.1111/j.1444-0938.2005.tb05102.x.
111. Levi, D.M., Knill, D.C., and Bavelier, D. (2015). Stereopsis and amblyopia: A mini-review. Vision Res *114*, 17-30. 10.1016/j.visres.2015.01.002.
112. Barrett, B.T., Bradley, A., and Candy, T.R. (2013). The relationship between anisometropia and amblyopia. Prog Retin Eye Res *36*, 120-158. 10.1016/j.preteyeres.2013.05.001.
113. Attebo, K., Mitchell, P., Cumming, R., Smith, W., Jolly, N., and Sparkes, R. (1998). Prevalence and causes of amblyopia in an adult population. Ophthalmology *105*, 154-159. 10.1016/s0161-6420(98)91862-0.
114. Fong, M.F., Mitchell, D.E., Duffy, K.R., and Bear, M.F. (2016). Rapid recovery from the effects of early monocular deprivation is enabled by temporary inactivation of the retinas. Proc Natl Acad Sci U S A *113*, 14139-14144. 10.1073/pnas.1613279113.
115. Fong, M.F., Duffy, K.R., Leet, M.P., Candler, C.T., and Bear, M.F. (2021). Correction of amblyopia in cats and mice after the critical period. Elife *10*. 10.7554/eLife.70023.
116. Resnick, H.H., Bear, M.F., and Gaier, E.D. (2022). Partial Recovery of Amblyopia After Fellow Eye Ischemic Optic Neuropathy. J Neuroophthalmol. 10.1097/WNO.0000000000001646.
117. Martinez, J.D., Donnelly, M.J., Popke, D.S., Torres, D., Wilson, L.G., Brancaleone, W.P., Clawson, B.C., Jiang, S., and Aton, S.J. (2022). Binocular visual experience and sleep promote visual cortex plasticity and restore binocular vision in a mouse model of amblyopia. bioRxiv, 2022.2001.2025.477697. 10.1101/2022.01.25.477697.
118. Pediatric Eye Disease Investigator, G., Wallace, D.K., Lazar, E.L., Holmes, J.M., Repka, M.X., Cotter, S.A., Chen, A.M., Kraker, R.T., Beck, R.W., Clarke, M.P., et al. (2013). A randomized trial of increasing patching for amblyopia. Ophthalmology *120*, 2270-2277. 10.1016/j.ophtha.2013.04.008.
119. Repka, M.X., Beck, R.W., Holmes, J.M., Birch, E.E., Chandler, D.L., Cotter, S.A., Hertle, R.W., Kraker, R.T., Moke, P.S., Quinn, G.E., et al. (2003). A randomized trial of patching regimens for treatment of moderate amblyopia in children. Arch Ophthalmol *121*, 603-611. 10.1001/archopht.121.5.603.

120. Khan, T. (2015). Is There a Critical Period for Amblyopia Therapy? Results of a Study on Older Anisometropic Amblyopes. J Clin Diagn Res *9*, NC01-04. 10.7860/JCDR/2015/13277.6288.
121. Kraus, C.L., and Culican, S.M. (2018). New advances in amblyopia therapy I: binocular therapies and pharmacologic augmentation. Br J Ophthalmol *102*, 1492-1496. 10.1136/bjophthalmol-2018-312172.
122. Kraus, C.L., and Culican, S.M. (2018). New advances in amblyopia therapy II: refractive therapies. Br J Ophthalmol *102*, 1611-1614. 10.1136/bjophthalmol-2018-312173.
123. Birch, E.E. (2013). Amblyopia and binocular vision. Progress in Retinal and Eye Research. Pergamon.
124. Holmes, J.M., Manh, V.M., Lazar, E.L., Beck, R.W., Birch, E.E., Kraker, R.T., Crouch, E.R., Erzurum, S.A., Khuddus, N., Summers, A.I., et al. (2016). Effect of a Binocular iPad Game vs Part-time Patching in Children Aged 5 to 12 Years With Amblyopia: A Randomized Clinical Trial. JAMA Ophthalmol *134*, 1391-1400. 10.1001/jamaophthalmol.2016.4262.
125. Kelly, K.R., Jost, R.M., Dao, L., Beauchamp, C.L., Leffler, J.N., and Birch, E.E. (2016). Binocular iPad Game vs Patching for Treatment of Amblyopia in Children: A Randomized Clinical Trial. JAMA Ophthalmol *134*, 1402-1408. 10.1001/jamaophthalmol.2016.4224.
126. LeVay, S., Wiesel, T.N., and Hubel, D.H. (1980). The development of ocular dominance columns in normal and visually deprived monkeys. J Comp Neurol *191*, 1-51. 10.1002/cne.901910102.
127. Mitchell, D.E., Cynader, M., and Movshon, J.A. (1977). Recovery from the effects of monocular deprivation in kittens. J Comp Neurol *176*, 53-63. 10.1002/cne.901760104.
128. Mitchell, D.E., Gingras, G., and Kind, P.C. (2001). Initial recovery of vision after early monocular deprivation in kittens is faster when both eyes are open. Proc Natl Acad Sci U S A *98*, 11662-11667. 10.1073/pnas.201392698.
129. Faulkner, S.D., Vorobyov, V., and Sengpiel, F. (2006). Visual cortical recovery from reverse occlusion depends on concordant binocular experience. J Neurophysiol *95*, 1718-1726. 10.1152/jn.00912.2005.
130. Dadvand, L., Stryker, M.P., and Frank, M.G. (2006). Sleep does not enhance the recovery of deprived eye responses in developing visual cortex. Neuroscience *143*, 815-826. 10.1016/j.neuroscience.2006.08.029.
131. Squire, L.R., and Zola, S.M. (1996). Structure and function of declarative and nondeclarative memory systems. Proc Natl Acad Sci U S A *93*, 13515-13522. 10.1073/pnas.93.24.13515.
132. Squire, L.R. (2009). The Legacy of Patient H.M. for Neuroscience. Neuron. NIH Public Access.
133. Scoville, W.B., and Milner, B. (1957). Loss of recent memory after bilateral hippocampal lesions. J Neurol Neurosurg Psychiatry *20*, 11-21. 10.1136/jnnp.20.1.11.
134. Fyhn, M., Molden, S., Witter, M.P., Moser, E.I., and Moser, M.B. (2004). Spatial representation in the entorhinal cortex. Science *305*, 1258-1264. 10.1126/science.1099901.

135. van Groen, T., and Wyss, J.M. (1990). Extrinsic projections from area CA1 of the rat hippocampus: olfactory, cortical, subcortical, and bilateral hippocampal formation projections. J Comp Neurol *302*, 515-528. 10.1002/cne.903020308.
136. Lopez-Rojas, J., and Kreutz, M.R. (2016). Mature granule cells of the dentate gyrus--Passive bystanders or principal performers in hippocampal function? Neurosci Biobehav Rev *64*, 167-174. 10.1016/j.neubiorev.2016.02.021.
137. Collingridge, G.L., Kehl, S.J., and McLennan, H. (1983). Excitatory amino acids in synaptic transmission in the Schaffer collateral-commissural pathway of the rat hippocampus. J Physiol *334*, 33-46. 10.1113/jphysiol.1983.sp014478.
138. Dudek, S.M., and Bear, M.F. (1992). Homosynaptic long-term depression in area CA1 of hippocampus and effects of N-methyl-D-aspartate receptor blockade. Proc Natl Acad Sci U S A *89*, 4363-4367. 10.1073/pnas.89.10.4363.
139. Lynch, G., Larson, J., Kelso, S., Barrionuevo, G., and Schottler, F. (1983). Intracellular injections of EGTA block induction of hippocampal long-term potentiation. Nature *305*, 719-721. 10.1038/305719a0.
140. Mulkey, R.M., and Malenka, R.C. (1992). Mechanisms underlying induction of homosynaptic long-term depression in area CA1 of the hippocampus. Neuron *9*, 967-975. 10.1016/0896-6273(92)90248-c.
141. Raven, F., and Aton, S.J. (2021). The Engram's Dark Horse: How Interneurons Regulate State-Dependent Memory Processing and Plasticity. Front Neural Circuits *15*, 750541. 10.3389/fncir.2021.750541.
142. Ivashkina, O.I., Toropova, K.A., Ivanov, A.A., Chekhov, S.A., and Anokhin, K.V. (2016). Waves of c-Fos and Arc Proteins Expression in Neuronal Populations of the Hippocampus in Response to a Single Episode of New Experience. Bull Exp Biol Med *160*, 729-732. 10.1007/s10517-016-3296-3.
143. Liu, X., Ramirez, S., Pang, P.T., Puryear, C.B., Govindarajan, A., Deisseroth, K., and Tonegawa, S. (2012). Optogenetic stimulation of a hippocampal engram activates fear memory recall. Nature *484*, 381-385. 10.1038/nature11028.
144. Rustay, N., Browman, K., and Curzon, P. (2008). Cued and Contextual Fear Conditioning for Rodents. In Methods of Behavior Analysis in Neuroscience, Second Edition, (CRC Press/Taylor & Francis), pp. 19-37. 10.1201/NOE1420052343.ch2.
145. Curzon, P., Rustay, N.R., and Browman, K.E. (2009). Cued and Contextual Fear Conditioning for Rodents. In Methods of Behavior Analysis in Neuroscience, J.J. Buccafusco, ed.
146. Ramirez, S., Liu, X., Lin, P.A., Suh, J., Pignatelli, M., Redondo, R.L., Ryan, T.J., and Tonegawa, S. (2013). Creating a false memory in the hippocampus. Science *341*, 387-391. 10.1126/science.1239073.
147. McGaugh, J.L. (2004). The amygdala modulates the consolidation of memories of emotionally arousing experiences. Annu Rev Neurosci *27*, 1-28. 10.1146/annurev.neuro.27.070203.144157.
148. Kim, W.B., and Cho, J.H. (2020). Encoding of contextual fear memory in hippocampal-amygdala circuit. Nat Commun *11*, 1382. 10.1038/s41467-020-15121-2.

149. Daumas, S., Halley, H., and Lassalle, J.M. (2004). Disruption of hippocampal CA3 network: effects on episodic-like memory processing in C57BL/6J mice. Eur J Neurosci *20*, 597-600. 10.1111/j.1460-9568.2004.03484.x.
150. Daumas, S., Halley, H., Frances, B., and Lassalle, J.M. (2005). Encoding, consolidation, and retrieval of contextual memory: differential involvement of dorsal CA3 and CA1 hippocampal subregions. Learn Mem *12*, 375-382. 10.1101/lm.81905.
151. Bruno, O., Fedele, E., Prickaerts, J., Parker, L.A., Canepa, E., Brullo, C., Cavallero, A., Gardella, E., Balbi, A., Domenicotti, C., et al. (2011). GEBR-7b, a novel PDE4D selective inhibitor that improves memory in rodents at non-emetic doses. Brit J Pharmacol *164*, 2054-2063. 10.1111/j.1476-5381.2011.01524.x.
152. Oliveira, A.M., Hawk, J.D., Abel, T., and Havekes, R. (2010). Post-training reversible inactivation of the hippocampus enhances novel object recognition memory. Learn Mem *17*, 155-160. 10.1101/lm.1625310.
153. Vanmierlo, T., Rutten, K., Dederen, J., Bloks, V.W., van Vark-van der Zee, L.C., Kuipers, F., Kiliaan, A., Blokland, A., Sijbrands, E.J., Steinbusch, H., et al. (2011). Liver X receptor activation restores memory in aged AD mice without reducing amyloid. Neurobiol Aging *32*, 1262-1272. 10.1016/j.neurobiolaging.2009.07.005.
154. Murai, T., Okuda, S., Tanaka, T., and Ohta, H. (2007). Characteristics of object location memory in mice: Behavioral and pharmacological studies. Physiol Behav *90*, 116-124. 10.1016/j.physbeh.2006.09.013.
155. Assini, F.L., Duzzioni, M., and Takahashi, R.N. (2009). Object location memory in mice: pharmacological validation and further evidence of hippocampal CA1 participation. Behav Brain Res *204*, 206-211. 10.1016/j.bbr.2009.06.005.
156. Stickgold, R., and Walker, M.P. (2005). Memory consolidation and reconsolidation: what is the role of sleep? Trends Neurosci *28*, 408-415. 10.1016/j.tins.2005.06.004.
157. Walker, M.P., and Stickgold, R. (2009). Sleep and Memory Consolidation. In Sleep Disorders Medicine, pp. 112-126. 10.1016/b978-0-7506-7584-0.00009-4.
158. Hellman, K., and Abel, T. (2007). Fear conditioning increases NREM sleep. Behav Neurosci *121*, 310-323. 10.1037/0735-7044.121.2.310.
159. Vecsey, C.G., Baillie, G.S., Jaganath, D., Havekes, R., Daniels, A., Wimmer, M., Huang, T., Brown, K.M., Li, X.Y., Descalzi, G., et al. (2009). Sleep deprivation impairs cAMP signalling in the hippocampus. Nature *461*, 1122-1125. 10.1038/nature08488.
160. Delorme, J., Wang, L., Kuhn, F.R., Kodoth, V., Ma, J., Martinez, J.D., Raven, F., Toth, B.A., Balendran, V., Vega Medina, A., et al. (2021). Sleep loss drives acetylcholine- and somatostatin interneuron-mediated gating of hippocampal activity to inhibit memory consolidation. Proc Natl Acad Sci U S A *118*. 10.1073/pnas.2019318118.
161. Ognjanovski, N., Maruyama, D., Lashner, N., Zochowski, M., and Aton, S.J. (2014). CA1 hippocampal network activity changes during sleep-dependent memory consolidation. Front Syst Neurosci *8*, 61. 10.3389/fnsys.2014.00061.
162. Qureshi, M.F., and Jha, S.K. (2017). Short-Term Total Sleep-Deprivation Impairs Contextual Fear Memory, and Contextual Fear-Conditioning Reduces REM

Sleep in Moderately Anxious Swiss Mice. Front Behav Neurosci *11*, 239. 10.3389/fnbeh.2017.00239.
163. Kumar, T., and Jha, S.K. (2017). Influence of cued-fear conditioning and its impairment on NREM sleep. Neurobiol Learn Mem *144*, 155-165. 10.1016/j.nlm.2017.07.008.
164. Martinez, J.D., Brancaleone, W.P., Peterson, K.G., Wilson, L.G., and Aton, S.J. (2022). Atypical hypnotic compound ML297 restores sleep architecture immediately following emotionally-valenced learning, to promote memory consolidation and hippocampal network activation during recall. Sleep. 10.1093/sleep/zsac301.
165. Heckman, P.R.A., Roig Kuhn, F., Meerlo, P., and Havekes, R. (2020). A brief period of sleep deprivation negatively impacts the acquisition, consolidation, and retrieval of object-location memories. Neurobiol Learn Mem *175*, 107326. 10.1016/j.nlm.2020.107326.
166. Habib, D., and Dringenberg, H.C. (2010). Surprising similarity between mechanisms mediating low (1 Hz)-and high (100 Hz)-induced long-lasting synaptic potentiation in CA1 of the intact hippocampus. Neuroscience *170*, 489-496. 10.1016/j.neuroscience.2010.06.074.
167. Habib, D., Tsui, C.K., Rosen, L.G., and Dringenberg, H.C. (2014). Occlusion of low-frequency-induced, heterosynaptic long-term potentiation in the rat hippocampus in vivo following spatial training. Cereb Cortex *24*, 3090-3096. 10.1093/cercor/bht174.
168. Binder, S., Baier, P.C., Molle, M., Inostroza, M., Born, J., and Marshall, L. (2012). Sleep enhances memory consolidation in the hippocampus-dependent object-place recognition task in rats. Neurobiol Learn Mem *97*, 213-219. 10.1016/j.nlm.2011.12.004.
169. Inostroza, M., Binder, S., and Born, J. (2013). Sleep-dependency of episodic-like memory consolidation in rats. Behav Brain Res *237*, 15-22. 10.1016/j.bbr.2012.09.011.
170. Mitchell, J.B., and Laiacona, J. (1998). The medial frontal cortex and temporal memory: tests using spontaneous exploratory behaviour in the rat. Behav Brain Res *97*, 107-113. 10.1016/s0166-4328(98)00032-1.
171. Roffwarg, H.P., Muzio, J.N., and Dement, W.C. (1966). Ontogenetic development of the human sleep-dream cycle. Science *152*, 604-619. 10.1126/science.152.3722.604.
172. Frank, M.G. (2011). Sleep and developmental plasticity not just for kids. Prog Brain Res *193*, 221-232. 10.1016/B978-0-444-53839-0.00014-4.
173. Frank, M.G., and Heller, H.C. (1997). Development of REM and slow wave sleep in the rat. Am J Physiol *272*, R1792-1799. 10.1152/ajpregu.1997.272.6.R1792.
174. Chen, H.L., Gao, J.X., Chen, Y.N., Xie, J.F., Xie, Y.P., Spruyt, K., Lin, J.S., Shao, Y.F., and Hou, Y.P. (2022). Rapid Eye Movement Sleep during Early Life: A Comprehensive Narrative Review. Int J Environ Res Public Health *19*. 10.3390/ijerph192013101.
175. Iglowstein, I., Jenni, O.G., Molinari, L., and Largo, R.H. (2003). Sleep duration from infancy to adolescence: reference values and generational trends. Pediatrics *111*, 302-307. 10.1542/peds.111.2.302.

176. Frank, M.G., Ruby, N.F., Heller, H.C., and Franken, P. (2017). Development of Circadian Sleep Regulation in the Rat: A Longitudinal Study Under Constant Conditions. Sleep *40*. 10.1093/sleep/zsw077.
177. Shaffery, J.P., Sinton, C.M., Bissette, G., Roffwarg, H.P., and Marks, G.A. (2002). Rapid eye movement sleep deprivation modifies expression of long-term potentiation in visual cortex of immature rats. Neuroscience *110*, 431-443. 10.1016/s0306-4522(01)00589-9.
178. Zhou, Y., Lai, C.S.W., Bai, Y., Li, W., Zhao, R., Yang, G., Frank, M.G., and Gan, W.B. (2020). REM sleep promotes experience-dependent dendritic spine elimination in the mouse cortex. Nat Commun *11*, 4819. 10.1038/s41467-020-18592-5.
179. Li, W., Ma, L., Yang, G., and Gan, W.B. (2017). REM sleep selectively prunes and maintains new synapses in development and learning. Nat Neurosci *20*, 427-437. 10.1038/nn.4479.
180. Jones, C.E., Opel, R.A., Kaiser, M.E., Chau, A.Q., Quintana, J.R., Nipper, M.A., Finn, D.A., Hammock, E.A.D., and Lim, M.M. (2019). Early-life sleep disruption increases parvalbumin in primary somatosensory cortex and impairs social bonding in prairie voles. Sci Adv *5*, eaav5188. 10.1126/sciadv.aav5188.
181. Novati, A., Hulshof, H.J., Koolhaas, J.M., Lucassen, P.J., and Meerlo, P. (2011). Chronic sleep restriction causes a decrease in hippocampal volume in adolescent rats, which is not explained by changes in glucocorticoid levels or neurogenesis. Neuroscience *190*, 145-155. 10.1016/j.neuroscience.2011.06.027.
182. Knudsen, E.I. (2004). Sensitive periods in the development of the brain and behavior. J Cogn Neurosci *16*, 1412-1425. 10.1162/0898929042304796.
183. Forrest, M.P., Parnell, E., and Penzes, P. (2018). Dendritic structural plasticity and neuropsychiatric disease. Nat Rev Neurosci *19*, 215-234. 10.1038/nrn.2018.16.
184. Gilbert, J., and Man, H.Y. (2017). Fundamental Elements in Autism: From Neurogenesis and Neurite Growth to Synaptic Plasticity. Front Cell Neurosci *11*, 359. 10.3389/fncel.2017.00359.
185. Johnson, C.P., Myers, S.M., and American Academy of Pediatrics Council on Children With, D. (2007). Identification and evaluation of children with autism spectrum disorders. Pediatrics *120*, 1183-1215. 10.1542/peds.2007-2361.
186. Hyman, S.L., Levy, S.E., Myers, S.M., Council On Children With Disabilities, S.O.D., and Behavioral, P. (2020). Identification, Evaluation, and Management of Children With Autism Spectrum Disorder. Pediatrics *145*. 10.1542/peds.2019-3447.
187. Maenner, M.J., Shaw, K.A., Bakian, A.V., Bilder, D.A., Durkin, M.S., Esler, A., Furnier, S.M., Hallas, L., Hall-Lande, J., Hudson, A., et al. (2021). Prevalence and Characteristics of Autism Spectrum Disorder Among Children Aged 8 Years - Autism and Developmental Disabilities Monitoring Network, 11 Sites, United States, 2018. MMWR Surveill Summ *70*, 1-16. 10.15585/mmwr.ss7011a1.
188. Abrahams, B.S., and Geschwind, D.H. (2008). Advances in autism genetics: on the threshold of a new neurobiology. Nat Rev Genet *9*, 341-355. 10.1038/nrg2346.

189. Warrier, V., Zhang, X., Reed, P., Havdahl, A., Moore, T.M., Cliquet, F., Leblond, C.S., Rolland, T., Rosengren, A., Eu-Aims, L., et al. (2022). Genetic correlates of phenotypic heterogeneity in autism. Nat Genet *54*, 1293-1304. 10.1038/s41588-022-01072-5.
190. Penagarikano, O., Abrahams, B.S., Herman, E.I., Winden, K.D., Gdalyahu, A., Dong, H., Sonnenblick, L.I., Gruver, R., Almajano, J., Bragin, A., et al. (2011). Absence of CNTNAP2 leads to epilepsy, neuronal migration abnormalities, and core autism-related deficits. Cell *147*, 235-246. 10.1016/j.cell.2011.08.040.
191. Sadeh, A., Mindell, J.A., and Owens, J. (2011). Why care about sleep of infants and their parents? Sleep Med Rev *15*, 335-337. 10.1016/j.smrv.2011.03.001.
192. Owens, J.A., and Mindell, J.A. (2011). Pediatric insomnia. Pediatr Clin North Am *58*, 555-569. 10.1016/j.pcl.2011.03.011.
193. Veatch, O.J., Maxwell-Horn, A.C., and Malow, B.A. (2015). Sleep in Autism Spectrum Disorders. Curr Sleep Med Rep *1*, 131-140. 10.1007/s40675-015-0012-1.
194. Maxwell-Horn, A., and Malow, B.A. (2017). Sleep in Autism. Semin Neurol *37*, 413-418. 10.1055/s-0037-1604353.
195. Elrod, M.G., and Hood, B.S. (2015). Sleep differences among children with autism spectrum disorders and typically developing peers: a meta-analysis. J Dev Behav Pediatr *36*, 166-177. 10.1097/DBP.0000000000000140.
196. Blackmer, A.B., and Feinstein, J.A. (2016). Management of Sleep Disorders in Children With Neurodevelopmental Disorders: A Review. Pharmacotherapy *36*, 84-98. 10.1002/phar.1686.
197. Rossignol, D.A., and Frye, R.E. (2011). Melatonin in autism spectrum disorders: a systematic review and meta-analysis. Dev Med Child Neurol *53*, 783-792. 10.1111/j.1469-8749.2011.03980.x.
198. Tordjman, S., Anderson, G.M., Botbol, M., Toutain, A., Sarda, P., Carlier, M., Saugier-Veber, P., Baumann, C., Cohen, D., Lagneaux, C., et al. (2012). Autistic disorder in patients with Williams-Beuren syndrome: a reconsideration of the Williams-Beuren syndrome phenotype. PLoS One *7*, e30778. 10.1371/journal.pone.0030778.
199. Kaufmann, W.E., Johnston, M.V., and Blue, M.E. (2005). MeCP2 expression and function during brain development: Implications for Rett syndrome's pathogenesis and clinical evolution.
200. Moretti, P., Bouwknecht, J.A., Teague, R., Paylor, R., and Zoghbi, H.Y. (2005). Abnormalities of social interactions and home-cage behavior in a mouse model of Rett syndrome. Hum Mol Genet *14*, 205-220. 10.1093/hmg/ddi016.
201. Jiang, Y.H., Armstrong, D., Albrecht, U., Atkins, C.M., Noebels, J.L., Eichele, G., Sweatt, J.D., and Beaudet, A.L. (1998). Mutation of the Angelman ubiquitin ligase in mice causes increased cytoplasmic p53 and deficits of contextual learning and long-term potentiation. Neuron *21*, 799-811. 10.1016/s0896-6273(00)80596-6.
202. Kaphzan, H., Hernandez, P., Jung, J.I., Cowansage, K.K., Deinhardt, K., Chao, M.V., Abel, T., and Klann, E. (2012). Reversal of impaired hippocampal long-term potentiation and contextual fear memory deficits in Angelman syndrome model mice by ErbB inhibitors. Biol Psychiatry *72*, 182-190. 10.1016/j.biopsych.2012.01.021.

203. Penagarikano, O., Mulle, J.G., and Warren, S.T. (2007). The pathophysiology of fragile x syndrome. Annu Rev Genomics Hum Genet *8*, 109-129. 10.1146/annurev.genom.8.080706.092249.
204. Rogers, S.J., Wehner, D.E., and Hagerman, R. (2001). The behavioral phenotype in fragile X: symptoms of autism in very young children with fragile X syndrome, idiopathic autism, and other developmental disorders. J Dev Behav Pediatr *22*, 409-417. 10.1097/00004703-200112000-00008.
205. Dahlhaus, R. (2018). Of men and mice: modeling the fragile X syndrome. Frontiers in Molecular Neuroscience. Frontiers Media S.A.
206. Hunter, J., Rivero-Arias, O., Angelov, A., Kim, E., Fotheringham, I., and Leal, J. (2014). Epidemiology of fragile X syndrome: a systematic review and meta-analysis. Am J Med Genet A *164A*, 1648-1658. 10.1002/ajmg.a.36511.
207. Fyke, W., and Velinov, M. (2021). FMR1 and Autism, an Intriguing Connection Revisited. Genes (Basel) *12*, 1218-1218. 10.3390/genes12081218.
208. Zafeiriou, D.I., Ververi, A., and Vargiami, E. (2007). Childhood autism and associated comorbidities. Brain Dev *29*, 257-272. 10.1016/j.braindev.2006.09.003.
209. Fu, Y.H., Kuhl, D.P., Pizzuti, A., Pieretti, M., Sutcliffe, J.S., Richards, S., Verkerk, A.J., Holden, J.J., Fenwick, R.G., Jr., Warren, S.T., and et al. (1991). Variation of the CGG repeat at the fragile X site results in genetic instability: resolution of the Sherman paradox. Cell *67*, 1047-1058. 10.1016/0092-8674(91)90283-5.
210. Verkerk, A.J., Pieretti, M., Sutcliffe, J.S., Fu, Y.H., Kuhl, D.P., Pizzuti, A., Reiner, O., Richards, S., Victoria, M.F., Zhang, F.P., and et al. (1991). Identification of a gene (FMR-1) containing a CGG repeat coincident with a breakpoint cluster region exhibiting length variation in fragile X syndrome. Cell *65*, 905-914. 10.1016/0092-8674(91)90397-h.
211. Pieretti, M., Zhang, F.P., Fu, Y.H., Warren, S.T., Oostra, B.A., Caskey, C.T., and Nelson, D.L. (1991). Absence of expression of the FMR-1 gene in fragile X syndrome. Cell *66*, 817-822. 10.1016/0092-8674(91)90125-i.
212. Richter, J.D., and Zhao, X. (2021). The molecular biology of FMRP: new insights into fragile X syndrome. Nat Rev Neurosci *22*, 209-222. 10.1038/s41583-021-00432-0.
213. Khandjian, E.W., Robert, C., and Davidovic, L. (2022). FMRP, a multifunctional RNA-binding protein in quest of a new identity. Front Genet *13*, 976480. 10.3389/fgene.2022.976480.
214. Heulens, I., Suttie, M., Postnov, A., De Clerck, N., Perrotta, C.S., Mattina, T., Faravelli, F., Forzano, F., Kooy, R.F., and Hammond, P. (2013). Craniofacial characteristics of fragile X syndrome in mouse and man. Eur J Hum Genet *21*, 816-823. 10.1038/ejhg.2012.265.
215. Kidd, S.A., Lachiewicz, A., Barbouth, D., Blitz, R.K., Delahunty, C., McBrien, D., Visootsak, J., and Berry-Kravis, E. (2014). Fragile X syndrome: a review of associated medical problems. Pediatrics *134*, 995-1005. 10.1542/peds.2013-4301.
216. Garber, K.B., Visootsak, J., and Warren, S.T. (2008). Fragile X syndrome. Eur J Hum Genet *16*, 666-672. 10.1038/ejhg.2008.61.

217. Darnell, J.C., Van Driesche, S.J., Zhang, C., Hung, K.Y., Mele, A., Fraser, C.E., Stone, E.F., Chen, C., Fak, J.J., Chi, S.W., et al. (2011). FMRP stalls ribosomal translocation on mRNAs linked to synaptic function and autism. Cell *146*, 247-261. 10.1016/j.cell.2011.06.013.
218. Hartley, S.L., Seltzer, M.M., Raspa, M., Olmstead, M., Bishop, E., and Bailey, D.B. (2011). Exploring the adult life of men and women with fragile X syndrome: results from a national survey. Am J Intellect Dev Disabil *116*, 16-35. 10.1352/1944-7558-116.1.16.
219. de Vries, B.B., Jansen, C.C., Duits, A.A., Verheij, C., Willemsen, R., van Hemel, J.O., van den Ouweland, A.M., Niermeijer, M.F., Oostra, B.A., and Halley, D.J. (1996). Variable FMR1 gene methylation of large expansions leads to variable phenotype in three males from one fragile X family. J Med Genet *33*, 1007-1010. 10.1136/jmg.33.12.1007.
220. van der Molen, M.J., Stam, C.J., and van der Molen, M.W. (2014). Resting-state EEG oscillatory dynamics in fragile X syndrome: abnormal functional connectivity and brain network organization. PLoS One *9*, e88451. 10.1371/journal.pone.0088451.
221. Baumgardner, T.L., Reiss, A.L., Freund, L.S., and Abrams, M.T. (1995). Specification of the neurobehavioral phenotype in males with fragile X syndrome. Pediatrics *95*, 744-752.
222. Kronk, R., Bishop, E.E., Raspa, M., Bickel, J.O., Mandel, D.A., and Bailey, D.B., Jr. (2010). Prevalence, nature, and correlates of sleep problems among children with fragile X syndrome based on a large scale parent survey. Sleep *33*, 679-687. 10.1093/sleep/33.5.679.
223. Elia, M., Ferri, R., Musumeci, S.A., Del Gracco, S., Bottitta, M., Scuderi, C., Miano, G., Panerai, S., Bertrand, T., and Grubar, J.C. (2000). Sleep in subjects with autistic disorder: a neurophysiological and psychological study. Brain Dev *22*, 88-92. 10.1016/s0387-7604(99)00119-9.
224. Miano, S., Bruni, O., Elia, M., Scifo, L., Smerieri, A., Trovato, A., Verrillo, E., Terzano, M.G., and Ferri, R. (2008). Sleep phenotypes of intellectual disability: a polysomnographic evaluation in subjects with Down syndrome and Fragile-X syndrome. Clin Neurophysiol *119*, 1242-1247. 10.1016/j.clinph.2008.03.004.
225. Angriman, M., Caravale, B., Novelli, L., Ferri, R., and Bruni, O. (2015). Sleep in children with neurodevelopmental disabilities. Neuropediatrics *46*, 199-210. 10.1055/s-0035-1550151.
226. Thedutchbelgianfragilexconsor (1994). Fmr1 knockout mice: A model to study fragile X mental retardation. Cell *78*, 23-33. 10.1016/0092-8674(94)90569-x.
227. Miyashiro, K.Y., Beckel-Mitchener, A., Purk, T.P., Becker, K.G., Barret, T., Liu, L., Carbonetto, S., Weiler, I.J., Greenough, W.T., and Eberwine, J. (2003). RNA cargoes associating with FMRP reveal deficits in cellular functioning in Fmr1 null mice. Neuron *37*, 417-431. 10.1016/s0896-6273(03)00034-5.
228. Nimchinsky, E.A., Sabatini, B.L., and Svoboda, K. (2002). Structure and function of dendritic spines. Annu Rev Physiol *64*, 313-353. 10.1146/annurev.physiol.64.081501.160008.
229. Muddashetty, R.S., Kelic, S., Gross, C., Xu, M., and Bassell, G.J. (2007). Dysregulated metabotropic glutamate receptor-dependent translation of AMPA

receptor and postsynaptic density-95 mRNAs at synapses in a mouse model of fragile X syndrome. J Neurosci *27*, 5338-5348. 10.1523/JNEUROSCI.0937-07.2007.
230. Bear, M.F., Huber, K.M., and Warren, S.T. (2004). The mGluR theory of fragile X mental retardation. Trends Neurosci *27*, 370-377. 10.1016/j.tins.2004.04.009.
231. Dolen, G., Osterweil, E., Rao, B.S., Smith, G.B., Auerbach, B.D., Chattarji, S., and Bear, M.F. (2007). Correction of fragile X syndrome in mice. Neuron *56*, 955-962. 10.1016/j.neuron.2007.12.001.
232. Dölen, G., and Bear, M.F. (2008). Role for metabotropic glutamate receptor 5 (mGluR5) in the pathogenesis of fragile X syndrome. The Journal of Physiology *586*, 1503-1508. 10.1113/jphysiol.2008.150722.
233. Choi, C.H., Schoenfeld, B.P., Bell, A.J., Hinchey, P., Kollaros, M., Gertner, M.J., Woo, N.H., Tranfaglia, M.R., Bear, M.F., Zukin, R.S., et al. (2011). Pharmacological reversal of synaptic plasticity deficits in the mouse model of fragile X syndrome by group II mGluR antagonist or lithium treatment. Brain Res *1380*, 106-119. 10.1016/j.brainres.2010.11.032.
234. Sorensen, E.M., Bertelsen, F., Weikop, P., Skovborg, M.M., Banke, T., Drasbek, K.R., and Scheel-Kruger, J. (2015). Hyperactivity and lack of social discrimination in the adolescent Fmr1 knockout mouse. Behav Pharmacol *26*, 733-740. 10.1097/FBP.0000000000000152.
235. Pietropaolo, S., Guilleminot, A., Martin, B., D'Amato, F.R., and Crusio, W.E. (2011). Genetic-background modulation of core and variable autistic-like symptoms in Fmr1 knock-out mice. PLoS One *6*, e17073. 10.1371/journal.pone.0017073.
236. Dam, D.V., D 'hooge, R., Hauben, E., Reyniers, E., Gantois, I., Bakker, C.E., Oostra, B.A., Kooy, R.F., De Deyn, P.P., D'Hooge, R., et al. (2000). Spatial learning, contextual fear conditioning and conditioned emotional response in Fmr1 knockout mice. Behavioural Brain Research.
237. Ding, Q., Sethna, F., and Wang, H. (2014). Behavioral analysis of male and female Fmr1 knockout mice on C57BL/6 background. Behav Brain Res *271*, 72-78. 10.1016/j.bbr.2014.05.046.
238. Li, J., Jiang, R.Y., Arendt, K.L., Hsu, Y.T., Zhai, S.R., and Chen, L. (2020). Defective memory engram reactivation underlies impaired fear memory recall in Fragile X syndrome. Elife *9*. 10.7554/eLife.61882.
239. King, M.K., and Jope, R.S. (2013). Lithium treatment alleviates impaired cognition in a mouse model of fragile X syndrome. Genes Brain Behav *12*, 723-731. 10.1111/gbb.12071.
240. Seese, R.R., Wang, K., Yao, Y.Q., Lynch, G., and Gall, C.M. (2014). Spaced training rescues memory and ERK1/2 signaling in fragile X syndrome model mice. Proc Natl Acad Sci U S A *111*, 16907-16912. 10.1073/pnas.1413335111.
241. Ventura, R., Pascucci, T., Catania, M.V., Musumeci, S.A., and Puglisi-Allegra, S. (2004). Object recognition impairment in Fmr1 knockout mice is reversed by amphetamine: involvement of dopamine in the medial prefrontal cortex. Behav Pharmacol *15*, 433-442. 10.1097/00008877-200409000-00018.

242. Bushey, D., Tononi, G., and Cirelli, C. (2009). The Drosophila fragile X mental retardation gene regulates sleep need. J Neurosci *29*, 1948-1961. 10.1523/JNEUROSCI.4830-08.2009.
243. Donlea, J.M., Thimgan, M.S., Suzuki, Y., Gottschalk, L., and Shaw, P.J. (2011). Inducing sleep by remote control facilitates memory consolidation in Drosophila. Science *332*, 1571-1576. 10.1126/science.1202249.
244. Donlea, J.M., Pimentel, D., and Miesenbock, G. (2014). Neuronal machinery of sleep homeostasis in Drosophila. Neuron *81*, 860-872. 10.1016/j.neuron.2013.12.013.
245. Kozono, N., Okamura, A., Honda, S., Matsumoto, M., and Mihara, T. (2020). Gamma power abnormalities in a Fmr1-targeted transgenic rat model of fragile X syndrome. Sci Rep *10*, 18799. 10.1038/s41598-020-75893-x.
246. Sare, R.M., Harkless, L., Levine, M., Torossian, A., Sheeler, C.A., and Smith, C.B. (2017). Deficient Sleep in Mouse Models of Fragile X Syndrome. Front Mol Neurosci *10*, 280. 10.3389/fnmol.2017.00280.
247. Sare, R.M., Lemons, A., and Smith, C.B. (2022). Effects of Treatment With Hypnotics on Reduced Sleep Duration and Behavior Abnormalities in a Mouse Model of Fragile X Syndrome. Front Neurosci *16*, 811528. 10.3389/fnins.2022.811528.
248. Boone, C.E., Davoudi, H., Harrold, J.B., and Foster, D.J. (2018). Abnormal Sleep Architecture and Hippocampal Circuit Dysfunction in a Mouse Model of Fragile X Syndrome. Neuroscience *384*, 275-289. 10.1016/j.neuroscience.2018.05.012.
249. Sateia, M.J. (2014). International classification of sleep disorders-third edition: highlights and modifications. Chest *146*, 1387-1394. 10.1378/chest.14-0970.
250. Tan, T.L., Kales, J.D., Kales, A., Soldatos, C.R., and Bixler, E.O. (1984). Biopsychobehavioral correlates of insomnia. IV: Diagnosis based on DSM-III. Am J Psychiatry *141*, 357-362. 10.1176/ajp.141.3.357.
251. Liu, X., Hubbard, J.A., Fabes, R.A., and Adam, J.B. (2006). Sleep disturbances and correlates of children with autism spectrum disorders. Child Psychiatry Hum Dev *37*, 179-191. 10.1007/s10578-006-0028-3.
252. Colten, H.R., and Altevogt, B.M. (2006). Sleep disorders and sleep deprivation: An unmet public health problem (National Academies Press). 10.17226/11617.
253. Buysse, D.J. (2013). Insomnia. JAMA *309*, 706-716. 10.1001/jama.2013.193.
254. Basta, M., Chrousos, G.P., Vela-Bueno, A., and Vgontzas, A.N. (2007). Chronic Insomnia and Stress System. Sleep Med Clin *2*, 279-291. 10.1016/j.jsmc.2007.04.002.
255. Kotagal, S., and Broomall, E. (2012). Sleep in children with autism spectrum disorder. Pediatr Neurol *47*, 242-251. 10.1016/j.pediatrneurol.2012.05.007.
256. Bhaskar, S., Hemavathy, D., and Prasad, S. (2016). Prevalence of chronic insomnia in adult patients and its correlation with medical comorbidities. J Family Med Prim Care *5*, 780-784. 10.4103/2249-4863.201153.
257. Fietze, I., Laharnar, N., Koellner, V., and Penzel, T. (2021). The Different Faces of Insomnia. Front Psychiatry *12*, 683943. 10.3389/fpsyt.2021.683943.
258. Stelzer, F.G., Garcia, E., Schorr, F., Barea, L.M., and Barros, H.T. (2021). Prevalence of chronic insomnia in patients with obstructive sleep apnea. Braz J Psychiatry *43*, 370-375. 10.1590/1516-4446-2019-0814.

259. Chaput, J.P., Gray, C.E., Poitras, V.J., Carson, V., Gruber, R., Olds, T., Weiss, S.K., Gorber, S.C., Kho, M.E., Sampson, M., et al. (2016). Systematic review of the relationships between sleep duration and health indicators in school-aged children and youth. Applied Physiology Nutrition and Metabolism *41*, S266-S282. 10.1139/apnm-2015-0627.
260. Tamura, N., and Tanaka, H. (2016). Effects of a sleep education program with self-help treatment on sleeping patterns and daytime sleepiness in Japanese adolescents: A cluster randomized trial. Chronobiol Int *33*, 1073-1085. 10.1080/07420528.2016.1199561.
261. Owens, J., Adolescent Sleep Working, G., and Committee on, A. (2014). Insufficient sleep in adolescents and young adults: an update on causes and consequences. Pediatrics *134*, e921-932. 10.1542/peds.2014-1696.
262. Turnbull, K., Reid, G.J., and Morton, J.B. (2013). Behavioral Sleep Problems and their Potential Impact on Developing Executive Function in Children. Sleep *36*, 1077-1084. 10.5665/sleep.2814.
263. M, K.P., and Latreille, V. (2019). Sleep Disorders. Am J Med *132*, 292-299. 10.1016/j.amjmed.2018.09.021.
264. Snead, O.C., 3rd (1992). Evidence for GABAB-mediated mechanisms in experimental generalized absence seizures. Eur J Pharmacol *213*, 343-349. 10.1016/0014-2999(92)90623-c.
265. Black, S.W., Morairty, S.R., Chen, T.M., Leung, A.K., Wisor, J.P., Yamanaka, A., and Kilduff, T.S. (2014). GABAB agonism promotes sleep and reduces cataplexy in murine narcolepsy. J Neurosci *34*, 6485-6494. 10.1523/JNEUROSCI.0080-14.2014.
266. Carter, L.P., Pardi, D., Gorsline, J., and Griffiths, R.R. (2009). Illicit gamma-hydroxybutyrate (GHB) and pharmaceutical sodium oxybate (Xyrem): differences in characteristics and misuse. Drug Alcohol Depend *104*, 1-10. 10.1016/j.drugalcdep.2009.04.012.
267. Lader, M.H. (1999). Limitations on the use of benzodiazepines in anxiety and insomnia: are they justified? Eur Neuropsychopharmacol *9 Suppl 6*, S399-405. 10.1016/s0924-977x(99)00051-6.
268. Seibt, J., Aton, S.J., Jha, S.K., Coleman, T., Dumoulin, M.C., and Frank, M.G. (2008). The non-benzodiazepine hypnotic zolpidem impairs sleep-dependent cortical plasticity. Sleep *31*, 1381-1391. 10.5665/sleep/31.10.1381.
269. Aton, S.J., Seibt, J., Dumoulin, M.C., Coleman, T., Shiraishi, M., and Frank, M.G. (2009). The sedating antidepressant trazodone impairs sleep-dependent cortical plasticity. PLoS One *4*, e6078. 10.1371/journal.pone.0006078.
270. Treves, N., Perlman, A., Kolenberg Geron, L., Asaly, A., and Matok, I. (2018). Z-drugs and risk for falls and fractures in older adults-a systematic review and meta-analysis. Age Ageing *47*, 201-208. 10.1093/ageing/afx167.
271. Drover, D.R. (2004). Comparative pharmacokinetics and pharmacodynamics of short-acting hypnosedatives: zaleplon, zolpidem and zopiclone. Clin Pharmacokinet *43*, 227-238. 10.2165/00003088-200443040-00002.
272. Ford, J.A., and McCutcheon, J. (2012). The misuse of Ambien among adolescents: prevalence and correlates in a national sample. Addict Behav *37*, 1389-1394. 10.1016/j.addbeh.2012.06.015.

273. Mednick, S.C., McDevitt, E.A., Walsh, J.K., Wamsley, E., Paulus, M., Kanady, J.C., and Drummond, S.P. (2013). The critical role of sleep spindles in hippocampal-dependent memory: a pharmacology study. J Neurosci *33*, 4494-4504. 10.1523/JNEUROSCI.3127-12.2013.
274. Vienne, J., Bettler, B., Franken, P., and Tafti, M. (2010). Differential effects of GABAB receptor subtypes, gamma-hydroxybutyric Acid, and Baclofen on EEG activity and sleep regulation. J Neurosci *30*, 14194-14204. 10.1523/JNEUROSCI.3145-10.2010.
275. Vienne, J., Lecciso, G., Constantinescu, I., Schwartz, S., Franken, P., Heinzer, R., and Tafti, M. (2012). Differential effects of sodium oxybate and baclofen on EEG, sleep, neurobehavioral performance, and memory. Sleep *35*, 1071-1083. 10.5665/sleep.1992.
276. Waly, N.E., and Hallworth, R. (2015). Circadian Pattern of Melatonin MT1 and MT2 Receptor Localization in the Rat Suprachiasmatic Nucleus. J Circadian Rhythms *13*, 1. 10.5334/jcr.ab.
277. Bourne, R.S., Mills, G.H., and Minelli, C. (2008). Melatonin therapy to improve nocturnal sleep in critically ill patients: encouraging results from a small randomised controlled trial. Crit Care *12*, R52. 10.1186/cc6871.
278. Borazan, H., Tuncer, S., Yalcin, N., Erol, A., and Otelcioglu, S. (2010). Effects of preoperative oral melatonin medication on postoperative analgesia, sleep quality, and sedation in patients undergoing elective prostatectomy: a randomized clinical trial. J Anesth *24*, 155-160. 10.1007/s00540-010-0891-8.
279. Xie, Z., Chen, F., Li, W.A., Geng, X., Li, C., Meng, X., Feng, Y., Liu, W., and Yu, F. (2017). A review of sleep disorders and melatonin. Neurol Res *39*, 559-565. 10.1080/01616412.2017.1315864.
280. Gobbi, G., and Comai, S. (2019). Differential Function of Melatonin MT(1) and MT(2) Receptors in REM and NREM Sleep. Front Endocrinol (Lausanne) *10*, 87. 10.3389/fendo.2019.00087.
281. Gobbi, G., and Comai, S. (2019). Sleep well. Untangling the role of melatonin MT1 and MT2 receptors in sleep. J Pineal Res *66*, e12544. 10.1111/jpi.12544.
282. Zhao, D., Yu, Y., Shen, Y., Liu, Q., Zhao, Z., Sharma, R., and Reiter, R.J. (2019). Melatonin Synthesis and Function: Evolutionary History in Animals and Plants. Front Endocrinol (Lausanne) *10*, 249. 10.3389/fendo.2019.00249.
283. Leger, D., Quera-Salva, M.A., Vecchierini, M.F., Ogrizek, P., Perry, C.A., and Dressman, M.A. (2015). Safety profile of tasimelteon, a melatonin MT1 and MT2 receptor agonist: pooled safety analyses from six clinical studies. Expert Opin Drug Saf *14*, 1673-1685. 10.1517/14740338.2015.1093112.
284. Hibino, H., Inanobe, A., Furutani, K., Murakami, S., Findlay, I., and Kurachi, Y. (2010). Inwardly rectifying potassium channels: Their structure, function, and physiological roles. Physiological Reviews. American Physiological Society Bethesda, MD.
285. Lüscher, C., and Slesinger, P.A. (2010). Emerging roles for G protein-gated inwardly rectifying potassium (GIRK) channels in health and disease. Nature Reviews Neuroscience. Nature Publishing Group.
286. Krapivinsky, G., Gordon, E.A., Wickman, K., Velimirovic, B., Krapivinsky, L., and Clapham, D.E. (1995). The G-protein-gated atrial K+ channel IKACh is a

heteromultimer of two inwardly rectifying K(+)-channel proteins. Nature *374*, 135-141. 10.1038/374135a0.
287. Luján, R., Marron Fernandez de Velasco, E., Aguado, C., and Wickman, K. (2014). New insights into the therapeutic potential of Girk channels. Trends in Neurosciences. Elsevier Ltd.
288. Signorini, S., Liao, Y.J., Duncan, S.A., Jan, L.Y., and Stoffel, M. (1997). Normal cerebellar development but susceptibility to seizures in mice lacking G protein-coupled, inwardly rectifying K+ channel GIRK2. Proc Natl Acad Sci U S A *94*, 923-927. 10.1073/pnas.94.3.923.
289. Newberry, N.R., and Nicoll, R.A. (1985). Comparison of the action of baclofen with gamma-aminobutyric acid on rat hippocampal pyramidal cells in vitro. J Physiol *360*, 161-185. 10.1113/jphysiol.1985.sp015610.
290. Luscher, C., Jan, L.Y., Stoffel, M., Malenka, R.C., and Nicoll, R.A. (1997). G protein-coupled inwardly rectifying K+ channels (GIRKs) mediate postsynaptic but not presynaptic transmitter actions in hippocampal neurons. Neuron *19*, 687-695. 10.1016/s0896-6273(00)80381-5.
291. Sanchez-Rodriguez, I., Temprano-Carazo, S., Najera, A., Djebari, S., Yajeya, J., Gruart, A., Delgado-Garcia, J.M., Jimenez-Diaz, L., and Navarro-Lopez, J.D. (2017). Activation of G-protein-gated inwardly rectifying potassium (Kir3/GirK) channels rescues hippocampal functions in a mouse model of early amyloid-beta pathology. Sci Rep *7*, 14658. 10.1038/s41598-017-15306-8.
292. Djebari, S., Iborra-Lazaro, G., Temprano-Carazo, S., Sanchez-Rodriguez, I., Nava-Mesa, M.O., Munera, A., Gruart, A., Delgado-Garcia, J.M., Jimenez-Diaz, L., and Navarro-Lopez, J.D. (2021). G-Protein-Gated Inwardly Rectifying Potassium (Kir3/GIRK) Channels Govern Synaptic Plasticity That Supports Hippocampal-Dependent Cognitive Functions in Male Mice. J Neurosci *41*, 7086-7102. 10.1523/JNEUROSCI.2849-20.2021.
293. Jeremic, D., Sanchez-Rodriguez, I., Jimenez-Diaz, L., and Navarro-Lopez, J.D. (2021). Therapeutic potential of targeting G protein-gated inwardly rectifying potassium (GIRK) channels in the central nervous system. Pharmacol Ther *223*, 107808. 10.1016/j.pharmthera.2021.107808.
294. Zhao, Y., Gameiro-Ros, I., Glaaser, I.W., and Slesinger, P.A. (2021). Advances in Targeting GIRK Channels in Disease. Trends Pharmacol Sci *42*, 203-215. 10.1016/j.tips.2020.12.002.
295. Hablitz, L.M., Molzof, H.E., Abrahamsson, K.E., Cooper, J.M., Prosser, R.A., and Gamble, K.L. (2015). GIRK Channels Mediate the Nonphotic Effects of Exogenous Melatonin. J Neurosci *35*, 14957-14965. 10.1523/JNEUROSCI.1597-15.2015.
296. van den Top, M., Buijs, R.M., Ruijter, J.M., Delagrange, P., Spanswick, D., and Hermes, M.L. (2001). Melatonin generates an outward potassium current in rat suprachiasmatic nucleus neurones in vitro independent of their circadian rhythm. Neuroscience *107*, 99-108. 10.1016/s0306-4522(01)00346-3.
297. Kaufmann, K., Romaine, I., Days, E., Pascual, C., Malik, A., Yang, L., Zou, B., Du, Y., Sliwoski, G., Morrison, R.D., et al. (2013). ML297 (VU0456810), the first potent and selective activator of the GIRK potassium channel, displays

antiepileptic properties in mice. ACS Chem Neurosci *4*, 1278-1286. 10.1021/cn400062a.
298. Wydeven, N., Marron Fernandez de Velasco, E., Du, Y., Benneyworth, M.A., Hearing, M.C., Fischer, R.A., Thomas, M.J., Weaver, C.D., and Wickman, K. (2014). Mechanisms underlying the activation of G-protein-gated inwardly rectifying K+ (GIRK) channels by the novel anxiolytic drug, ML297. Proc Natl Acad Sci U S A *111*, 10755-10760. 10.1073/pnas.1405190111.
299. Zou, B., Cao, W.S., Guan, Z., Xiao, K., Pascual, C., Xie, J., Zhang, J., Xie, J., Kayser, F., Lindsley, C.W., et al. (2019). Direct activation of G-protein-gated inward rectifying K+ channels promotes nonrapid eye movement sleep. Sleep *42*, 1-16. 10.1093/sleep/zsy244.

Chapter 2：Enriched Binocular Experience Followed by Sleep Optimally Restores Binocular Visual Cortical Response in a Mouse Model of Amblyopia

This chapter includes the manuscript currently in revision at Communications Biology: ***Martinez JD****, Donnelly MJ, Popke DS, Torres D, Wilson LG, Brancaleone WP, Clawson BC, Jiang S, & Aton SJ. (2023) Enriched binocular experience followed by sleep optimally restores binocular visual cortical response in a mouse model of amblyopia.*

2.1 : Abstract

Studies of developmental plasticity of the binocular zone of the primary visual cortex (bV1) have furthered our understanding of neural mechanisms underlying amblyopia, which arises from an altered balance of input from the two eyes to bV1 during childhood. Amblyopia causes long-lasting visual impairment and is commonly treated by patching the dominant eye. However, the relative impacts of monocular vs. binocular visual experiences on restoration of bV1 function remains unclear. Moreover, while sleep has been implicated in bV1 plasticity in response to vision loss, its role in recovery of visual function is unknown. We used monocular deprivation (MD) in juvenile male mice to model amblyopia in bV1. We compared recovery of visual responses for the two eyes among bV1 neurons after identical-duration, identical-quality binocular recovery (BR) or monocular, reverse occlusion (RO) experiences. Using this paradigm, we find that BR is quantitatively superior to RO with respect to restoring binocular responses in bV1

neurons. However, this recovery was seen only in freely-sleeping mice; post-BR sleep deprivation prevented functional recovery. Thus, both binocular visual experience and subsequent sleep help to optimally renormalize bV1 responses in a mouse model of amblyopia.

2.2 : Significance Statement

Amblyopia resulting from altered childhood vision is a leading cause of lifelong vision loss. Treatment typically involves patching of the dominant eye (forcing monocular visual experience) and produces only partial recovery of vision. Using a well-established mouse model of amblyopia, we directly compared the effects of binocular vs. monocular enriched visual experience on visual cortex function recovery and tested the contribution of sleep to this process. Our data suggest that clinical strategies for amblyopia treatment should include coordinated stimulation of both eyes, occurring prior to a period of sleep.

2.3 : Introduction

During early postnatal development, both experience-driven synaptic plasticity and sleep impact lifelong sensory and behavioral functions [1-3]. For example, MD (occlusion of one of the two eyes) early in life shifts responsiveness of bV1 neurons to favor the dominant eye [4,5] - a process known as ocular dominance plasticity (ODP). ODP results from depression of deprived eye (DE) responses, followed by potentiation of spared eye (SE) responses, in bV1 neurons [6,7]. Sleep plays an essential role in promoting ODP during the critical period, promoting both synaptic strengthening and weakening in V1 in the hours following monocular visual experience [8-11].

ODP is a model for the neural mechanisms underlying amblyopia, a visual disorder caused by imbalanced input to bV1 from the two eyes in early childhood, leading to long-term disruption of binocular vision and poor visual acuity [12-15]. Dominant eye patching is the standard clinical intervention to promote recovery in amblyopia. This strategy was established based on studies carried out in both cats and monkeys, in which occlusion of the previously-dominant eye (reverse occlusion; RO) was sufficient to drive a somewhat greater recovery of DE responses in bV1 than reopening the DE alone [16,17]. Critically, however, neither RO nor simply reopening the DE restored binocularity of bV1 neurons' visual responses [17], and numerous studies have found long-lasting visual deficits after RO, despite recovery of DE responses [18-20]. More recently, studies in developing cats and rodents have found that under certain conditions, binocular vision can serve to restore binocularity of responses in bV1 [21-24]. Across species and developmental stages, binocular presentation of high-contrast stimuli such as gratings that synchronously activate left and right eye pathways (leading to coincident activation of bV1 neurons) seems to be an optimal driver of recovery [24,25]. Thus, intensive binocular experience – aimed at promoting cooperative input from the two eyes to bV1 - has recently been explored as a therapeutic strategy for recovery in amblyopic patient [26-31]. It remains unclear whether binocular or monocular interventions are superior at restoring vision to amblyopic children – with randomized clinical trials using dichoptic iPad games to provide binocular stimulation yielding conflicting results [14,29,32]. It thus remains unclear: 1) whether differences in recovery are apparent when the duration and quality (e.g., with identical contrast, spatial frequency, and temporal features) of visual stimuli are carefully

controlled, and 2) what changes to the bV1 network (e.g., in visual responses of excitatory vs. inhibitory neurons) mediate these differences.

Sleep can benefit processes relying on synaptic plasticity, including ODP in bV1 [8-11,33-35]. In cat V1, initial shifts in ocular dominance following a brief period of MD are augmented by a few hours of subsequent sleep [9] and are disrupted by sleep deprivation (SD) [8]. This suggests that sleep immediately following either monocular (RO) or binocular (BR) recovery experiences could also promote recovery of bV1 function after a period of MD. However, in a single study in critical period cats, a period of sleep following a brief interval of post-MD RO actually impaired (rather than enhanced) recovery of normal V1 ocular dominance [36]. Thus, the function of appropriately-timed sleep in promoting (or disrupting) visual cortical responses in amblyopia - particularly after binocular visual recovery - remains to be determined.

To address these questions, we first directly compared how multi-day, post-MD BR and RO - of identical duration and visual stimulus content - affect recovery of function in mouse binocular V1 (bV1). Using single-neuron recordings, we find that bV1 ocular dominance shifts caused by 5-day MD are completely reversed by a period of visually-enriched BR experience (in a scenario where high-contrast, dynamic stimuli are delivered to the two eyes simultaneously), but are only partially reversed by RO of identical duration and quality. These differential effects were observed in both regular spiking (RS) neurons and fast spiking (FS; putative parvalbumin-expressing [PV+]) interneurons. BR, but not RO, reversed MD-induced depression of DE-driven firing rate responses in both RS neurons and FS interneurons, and increases in SE-driven responses in both populations. Recovery of bV1 visual function was confirmed by quantifying DE-driven cFos expression,

which was reduced in layers 2/3 after MD (across the population as a whole, and among PV+ interneurons), and recovered to control levels after BR, but not RO. Critically, BR-driven recovery of ocular dominance, bV1 visual response changes, and DE-driven cFos expression were all disrupted by SD in the hours immediately following periods of visual experience. Together, these results suggest that optimal recovery of bV1 function after a period of MD is promoted by enriched binocular visual experience and subsequent, undisturbed sleep. These data add to a growing body of literature that suggests potential alternative strategies for amblyopia treatment that may improve upon the current standard for clinical care (dominant eye patching, with no emphasis on relative sleep timing).

2.4 : Materials and Methods

2.4.1 : Animal housing and husbandry

All mouse husbandry and experimental/surgical procedures were reviewed and approved by the University of Michigan Internal Animal Care and Use Committee. C57BL6/J mice were housed in a vivarium under 12h:12h light/dark cycles (lights on at 9AM) unless otherwise noted and had *ad lib* access to food and water. After eyelid suture surgeries, mice were single housed in standard cages with beneficial environmental enrichment. For studies comparing the effects of sleep on BR visual experience, mice were housed with a 4h:20h light:dark cycle (lights on from 9AM-1PM during visual enrichment experience, dim red light outside of visual enrichment) and had *ad lib* access to food and water.

2.4.2 : Monocular deprivation, recovery, visual enrichment, and sleep deprivation

For all experiments, male littermates were randomly assigned to treatment groups. monocular deprivation (MD), mice were anesthetized at P28 using 1-1.5% isoflurane. Nylon non-absorbable sutures (Henry Schein) were used to occlude the left eye. Sutures were checked twice daily to verify continuous MD; during this time, they were handled 5 min/day. After MD (at P33), mice were anesthetized with 1-1.5% isoflurane a second time and left eyelid sutures were removed. Mice that underwent binocular recovery (BR) were then housed over the next 5 days with both eyes open; during this time, they were handled daily for 5 min/day. Mice that underwent reverse occlusion (RO) had the right (previously spared; SE) eye sutured for the next 5 days; these mice were also handled 5 min/day during this period. Mice that lost sutures during the MD or recovery periods or developed eye abnormalities were excluded from the study. BR and RO mice underwent a 5-day period of identical daily enriched visual experience from P34-38. This regimen consisted of a daily placement in a 15” × 15” Plexiglas chamber surrounded by 4 high-contrast LED monitors, from ZT0 (lights on) to ZT4. Phase-reversing oriented grating stimuli (100% contrast, 1 Hz reversal frequency) of 8 orientations were presented repeatedly on the 4 monitors in a random, interleaved fashion. Spatial frequencies for grating stimuli varied from 0.0025-0.1 cycles/deg during this period, depending on the mouse’s position within the arena. During this 4-h period of daily visual enrichment, mice were encouraged to remain awake and explore the chamber via presentation of a variety of enrichment toys (novel objects, transparent tubes, and a running wheel) and palatable treats. For sleep deprivation (SD) studies on BR experience, immediately following the 4-h visual enrichment period, mice were placed in their home cage within a sound-attenuated behavioral chamber (Med Associates) under dim red light (**Figure 2.4B**). BR+Sleep and

BR+SD mice were housed under the same conditions, with BR+SD undergoing SD by gentle handling for the first 4 h post-enrichment [37,38]. Ambient red-light levels (measured at 530-980 nm) during this period were sufficiently low (≤ 3.68×10^9 photons/cm2/s) that mice would have negligible additional visual experience (i.e., form vision) during SD, based on published psychometric data [39]. Briefly, gentle handling procedures involved visually monitoring the mice for assumption of sleep posture - i.e., huddled in their nest with closed eyes. Upon detection of sleep posture, the cage was either tapped or (if necessary) shaken briefly (1-2 sec). If sleep posture was maintained after these interventions, the nesting material within the cage would be moved using a cotton-tipped applicator. No novel objects or additional sensory stimuli were provided, to limit sensory-based neocortical plasticity during sleep deprivation procedures [40]. To estimate the amount of sleep lost in BR+SD mice, BR+Sleep mice were visually monitored every 5 min over the first 4 h following visual enrichment for assumption of sleep postures, similar to previous studies [41-43]. As previously described, similar procedures used for sleep deprivation in adult mice [44] and critical period cats [11] either have no significant effect on serum cortisol, or increases it to a degree that is orders of magnitude lower than that capable of disrupting ODP [45].

2.4.3 : In vivo neurophysiology and single unit analysis

Mice underwent stereotaxic, anesthetized recordings using a combination of 0.5-1.0% isoflurane and 1 mg/kg chlorprothixene (Sigma). A small craniotomy (1 mm in diameter) was made over right-hemisphere bV1 (i.e., contralateral to the original DE) using stereotaxic coordinates 2.6-3.0 mm lateral to lambda. Recordings of neuronal firing responses were made using a 2-shank, linear silicon probe spanning the layers of bV1

(250 μm spacing between shanks, 32 electrodes/shank, 25 μm inter-electrode spacing; Cambridge Neurotech). The probe was slowly advanced into bV1 until stable, consistent spike waveforms were observed on multiple electrodes. Neural data acquisition using a 64-channel Omniplex recording system (Plexon) was carried out for individual mice across presentation of visual stimuli to each of the eyes, via a full field, high-contrast LED monitor positioned directly in front of the mouse. Recordings were made for the right and left eyes during randomly interleaved presentation of a series of phase-reversing oriented gratings (8 orientations + blank screen for quantifying spontaneous firing rates, reversing at 1 Hz, 0.05 cycles/degree, 100% contrast, 10 sec/stimulus; Matlab Psychtoolbox). Spike data for individual neurons was discriminated offline using previously-described PCA and MANOVA analysis [37,38,46-48] using Offline Sorter software (Plexon). Spike sorting and subsequent analysis of firing response properties was carried out by a scorer blinded to each animal's experimental group. To discriminate between pyramidal, regular spiking (RS) cells and putative, fast-spiking (FS) interneurons, evoked firing rates of each recorded unit were plotted as a function of the cell's spike half-width (**Supplemental Figure 2.5, Supplemental Figure 2.6).** This yield two distinct populations of cortical cells with RS and FS spiking dynamics seen in previously published studies [49].

For each neuron, a number of response parameters were calculated [9,10]. Firing rate-based comparisons were made using firing rate responses recorded for oriented grating stimulus (or blank screen presentation), for each eye, averaged across all presentations (i.e., 8 presentations for 10 sec each; 80 sec total). For analysis of DE and SE maximal firing rates (**Figure 2.2**, **Figure 2.5**), values were compared for mean firing rate across the 80 sec of presentation for each neuron's preferred stimulus orientation.

Comparisons of mean and spontaneous firing rates (**Supplemental Figure 2.1**, **Supplemental Figure 2.3**) were made on neuronal data averaged across all presentations of all oriented grating stimuli (i.e., preferred and non-preferred), or all blank screen presentations, respectively, for each of the two eyes. Visual responsiveness was assessed by comparing each neuron's spontaneous firing rates during blank screen presentations with evoked firing during grating presentations of the preferred orientation. Neurons with spontaneous firing higher than maximum evoked firing were considered non-visually-responsive. An ocular dominance index (ODI) was calculated for each visually-responsive unit as (C-I)/(C+I) where C represents the maximal visually-evoked firing rate for preferred-orientation stimuli presented to the contralateral (deprived) eye and I represents the maximal firing rate for stimuli presented to the ipsilateral (spared) eye. ODI values range from -1 to +1, where negative values indicate an ipsilateral (SE) bias, positive values indicate a contralateral (DE) bias, and values close to 0 indicate similar responses for stimuli presented to either eye. The contralateral bias index (CBI; a measure of dominance of input from the contralateral eye [or deprived eye in the case of MD and recovery mice]) and other visual measurements were made using previously published methods [50].

2.4.4 : Histology and immunohistochemistry

Following all electrophysiological recordings, mice were euthanized and perfused with ice cold PBS and 4% paraformaldehyde. Brains were dissected, post-fixed, cryoprotected in 30% sucrose solution, and frozen for sectioning. 50 µm coronal sections containing bV1 were stained with DAPI (Fluoromount-G with DAPI; Southern Biotech). DAPI staining provided contrast for identifying sites of electrode shank penetration into

the tissue, and for approximating stereotaxic coordinates of shank locations to verify placement within bV1 (**Figure 2.1B, Figure 2.4D**). Mice whose electrode placement could not be verified were excluded from further analyses.

For immunohistochemical quantification of PV and DE-driven cFos expression in bV1, mice from all groups underwent monocular eyelid suture of the original SE (i.e., the right eye) at ZT12 (lights off) the evening before visual stimulation. At ZT0 (next day), stimulation of the original DE (i.e., the left eye) was carried out in the LED-monitor-surrounded arena with treats and toys to maintain a high level of arousal (as described above) Mice from all groups were exposed to a 30-min period of oriented gratings (as described for visual enrichment above), after which they were returned to their home cage for 90 min (for maximal visually-driven cFos expression) prior to perfusion. Coronal sections of bV1 were collected as described above and immunostained using rabbit-anti-cFos (1:1000; Abcam, ab190289) and mouse-anti-PV (1:2000; Millipore, MAB1572) followed by secondary antibodies: Alexa Fluor 488 (1:200; Invitrogen, A11032) and Alexa Fluor 594 (1:200; Invitrogen, A11034). Stained sections were mounted using Prolong Gold antifade reagent (Invitrogen) and imaged using a Leica SP8 confocal microscope with a 10× objective, to obtain z-stack images (10 µm steps) for maximum projection of fluorescence signals. Identical image acquisition settings (e.g. exposure times, frame average, pixel size) were used for all sections. bV1 boundaries were estimated using comparisons to established stereotaxic coordinates. cFos+ and PV+ cell bodies were quantified in 3-4 sections (spanning the anterior-posterior extent of bV1) per mouse by a scorer blinded to the animal's experimental condition, and reported as approximate density, using previously established procedures. Co-labeling was quantified using the

Image J JACoP plugin [51] and values for each mouse are averaged across 3-4 sections. As an added control (to ensure that observed changes in expression in bV1 were the result of visual manipulations; **Figure 2.3**, **Figure 2.6**), primary auditory cortex (A1) was identified in the same brain sections used for bV1 measurement. A1 boundaries were estimated using established stereotaxic coordinates. A1 layer-specific expression was quantified in each section as described above (**Supplemental Figure 2.2**, **Supplemental Figure 2.4**).

2.4.5 : Statistical analysis

Statistical analyses were carried out using GraphPad Prism software (Version 9.1). Comparisons of ocular dominance, firing rates, and visual response properties were made using stably recorded (i.e., with consistent waveforms present across the entire visual stimulation period), visually-responsive (visually-evoked firing rate > spontaneous firing rate) units in bV1. Nonparametric tests were used for non-normal data distributions. Specific statistical tests and p-values can be found within the results section and in corresponding figures and figure legends.

2.5 : Results

2.5.1 : Binocular recovery (BR) causes more complete reversal of MD-induced bV1 ocular dominance shifts than identical-duration reverse occlusion (RO)

We first directly compared the degree of bV1 response recovery induced by multi-day BR and RO in bV1 neurons following a 5-day period of MD (**Figure 2.1A**). The duration and timing of MD (P28-33; during the peak of the critical period for ODP) was chosen with the aim of inducing a robust ocular dominance shift, with changes to both DE

and SE responses in bV1 [7]. To ensure comparable quality and duration of visual experience between BR and RO recovery groups, and to optimize potential for recovery of binocular responses, from P33-38, these mice were placed for 4 h/day (starting at lights-on) in a square chamber surrounded by four LED monitors presenting high-contrast, phase-reversing gratings (8 orientations, 0.05 cycles/deg, reversing at 1 Hz) in an interleaved manner. This type of visual stimulus was selected to mimic visual stimuli used experimentally to promote recovery in amblyopia patients [29-32,52,53], and is similar to stimuli that promote optimal recovery from MD in adult mice [24]. With binocular presentation, this visual enrichment would optimize for synchronous co-activation of inputs to V1 representing the two eyes, which is thought to be an important feature of visual response recovery. During this period of visual enrichment, mice had access to a running wheel, manipulanda, and treats in order to increase wake time, promote more consistent visual stimulation, and drive maximum recovery [24]. After the 5-day recovery period, we compared bV1 neurons' visual responses for stimuli presented to either the right or left eyes, for the hemisphere contralateral to the original DE (**Figure 2.1B**).

Consistent with previous reports, 5-day MD induced a large ocular dominance shift in favor of the SE compared to normally-reared (NR) control mice with binocular vision from birth (**Figure 2.1C-E**). 5 days of BR visual experience returned bV1 ocular dominance to a distribution similar to age-matched NR mice, completely reversing the effects of MD. After BR, ocular dominance index distributions (**Figure 2.1D**) and contralateral bias indices for each mouse (**Figure 2.1E**) matched those of NR mice, showing a preference for the DE (contralateral) eye. In contrast, ocular dominance distributions following 5-day RO visual experience were intermediate between MD mice

and age-matched NR mice (**Figure 2.1C-E**), suggesting only partial recovery. Visual responsiveness among neurons within bV1 was similar between the groups. The proportion of visually-responsive recorded neurons (i.e., those with higher firing rate responses to grating stimuli than to blank screen presentation) was 84.4% (222/263), 85.6% (238/278), 85.8% (230/268), and 82.8% (217/262) for NR, MD, BR, and RO groups, respectively.

MD is known to effect a change in the balance of activity between principal (RS; mainly glutamatergic) neurons and FS (mainly PV+, GABAergic) interneurons [10,54,55]. In our extracellular recordings, FS interneurons (identifiable based on distinctive spike waveform features ([10,48]) represented roughly 15-20% of all stably-recorded neurons (i.e., those with spiking present across the entire visual response testing period), across all treatment conditions (**Figure 2.1F**). We found that relative to neurons recorded from NR mice, MD led to similar ocular dominance shifts toward the SE in both RS neurons and FS interneurons (**Figure 2.1G-H**, respectively). These MD-induced changes were completely reversed in both RS and FS populations in BR mice, but were only partially reversed in RO mice (**Figure 2.1G-H**). We conclude that near the closure of the critical period for ODP, 5-day BR is quantitatively superior to 5-day RO at reversing effects of MD.

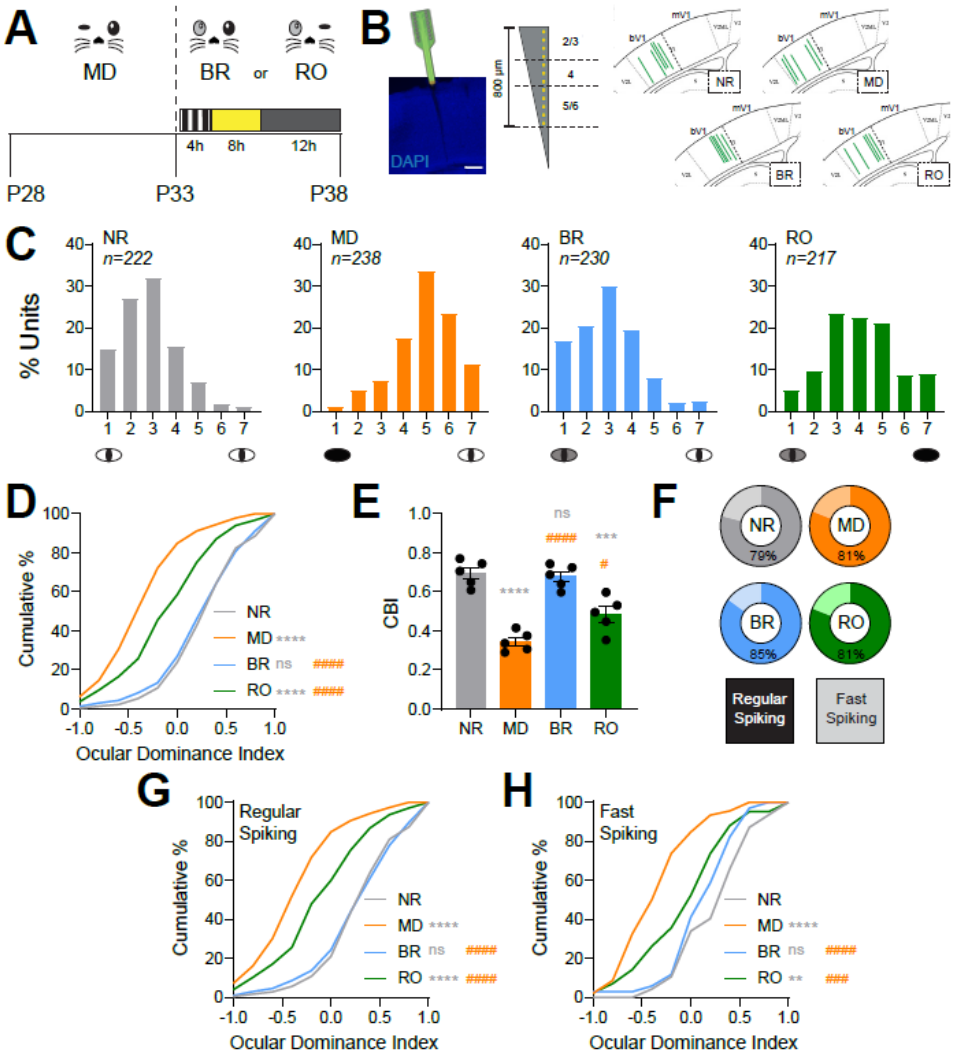

Figure 2.1: BR is more effective than RO at reversing MD-induced ocular dominance shifts.

(**A**) Experimental design. Mice underwent 5-day MD from P28-P33. MD mice were recorded at P33. Two recovery groups with either binocular recovery (BR) or reverse occlusion (RO) visual experience from P33-38 had daily 4-h periods of visual enrichment starting at lights on and were recorded at P38. Normally-reared (NR) mice were recorded at P38 without prior manipulation of vision. (**B**) Representative image of electrode probe placement in bV1 coronal section stained with DAPI (left), and enlarged view of electrode contacts, which spanned the layers of bV1 (center). Schematic of bV1 coordinates in coronal sections. Green lines represent probe placements in bV1 for all groups (right). (**C**) Ocular dominance histograms from bV1 neurons recorded contralateral to the original DE for all four groups, using a 7-point scale (1= neurons driven exclusively by contralateral eye; 7= neurons driven exclusively by ipsilateral eye, 4= neurons with binocular responses) n = 5 mice/group. (**D**) Cumulative distribution of ocular dominance indices for all neurons recorded in each group. **** (gray) indicates $p < 0.0001$, K-S test vs. NR; #### (orange) indicates $p < 0.0001$, K-S test vs MD; ns indicates not significant. (**E**) Contralateral bias indices for mice in each treatment group. One-way ANOVA: $F(3, 16) = 29.34$, $p < 0.0001$. Tukey's post hoc test vs NR – MD: $p < 0.0001$; BR: p = ns; RO: $p < 0.001$. Tukey's post hoc test vs MD – BR: $p < 0.0001$; RO: $p < 0.01$. Error bars indicate mean ± SEM. (**F**) The proportion of recorded neurons classified as regular spiking (RS) neurons and fast-spiking (FS) interneurons in each treatment group. RS neurons: NR (n = 175); MD (n = 192); BR (n = 196); RO (n = 175). FS interneurons: NR (n = 47); MD (n = 46); BR (n = 34); RO (n = 42). (**G-H**) Ocular dominance index cumulative distributions for RS neurons (**G**) and FS interneurons (**H**). Ocular dominance index values for both populations were significantly shifted in favor of the SE after MD, were comparable to those of NR mice after BR, and were intermediate – between NR and MD values – after RO. ** and **** (gray) indicate $p < 0.01$ and $p < 0.0001$, K-S test vs. NR; ### and #### (orange) indicate $p < 0.001$ and $p < 0.0001$, K-S test vs MD.

2.5.2 : BR and RO differentially restore bV1 RS neurons and FS interneuron firing rate responses after MD

MD leads to sequential changes in V1 neurons' maximal responses to DE and SE stimulation (which are depressed and potentiated, respectively) [6,7,9,10,56]. We next investigated which of these changes could be reversed in bV1 neurons as a function of post-MD BR or RO. To better characterize microcircuit-level changes due to MD, we examined how DE and SE visual response recovery varied between RS neuron and FS interneuron populations, and in different layers of bV1. DE responses were significantly depressed after 5-day MD as previously reported [6,7]; these changes were seen across cortical layers, in both RS neurons (**Figure 2.2A-B**) and FS interneurons (**Figure 2.2E-F**). In both populations, DE response depression was most pronounced in the extragranular layers. Both BR and RO both largely reversed DE response depression in RS neurons, although modest differences remained after RO (**Figure 2.2A**); recovery appeared most complete in RS neurons in layers 5/6 (**Figure 2.2B**). DE response depression in FS interneurons was fully reversed by 5-day BR (**Figure 2.2E**), with the most dramatic changes occurring in the extragranular layers (**Figure 2.2F**). In comparison, response depression reversal was more modest (though still significant) after RO (**Figure 2.2E**), with the largest changes occurring in layer 4 FS interneurons (**Figure 2.2F**).

MD strongly potentiated responses to SE stimulation, across both bV1 neuron populations, and across cortical layers (**Figure 2.2C-D, G-H**). BR and RO had differential effects with respect to reversing MD-potentiated responses. For both RS neurons and FS interneurons (**Figure 2.2C, G**), potentiation of SE responses was almost completely

reversed by BR. In contrast, in both neuron populations, RO led to only partial reversal of MD-induced SE response potentiation (**Figure 2.2C, G**). After BR, reversal of SE response potentiation was present in RS neurons across bV1 layers. In contrast, after RO, SE responses remained significantly potentiated in layer 4 and layers 5/6 (**Figure 2.2D**). Among FS interneurons, BR tended to reverse SE response potentiation more completely than RO across all layers of bV1, with the most complete reversal (leading to significant differences from MD alone) seen in layer 4 (**Figure 2.2H**). Together, these data suggest that 5-day BR is superior to RO with respect to reversing both synaptic depression and synaptic potentiation in bV1 caused by prior MD.

MD-driven changes in bV1 neurons' visually-evoked firing responses reflect a combination of Hebbian and homeostatic plasticity mechanisms [57-61]. While Hebbian plasticity mechanisms (i.e., LTP and LTD of glutamatergic synapses) have the potential to alter maximal firing rate responses to visual stimulation, homeostatic plasticity could also affect the spontaneous firing rate of bV1 neurons. To assess how MD and recovery experiences affect the overall firing of bV1 neurons, we also compared mean (across all visual stimulus presentations) and spontaneous (during blank screen presentation) firing rates in bV1 after MD and recovery experience (**Supplemental Figure 2.1**). Among RS neurons, mean (**Supplemental Figure 2.1A**) and spontaneous (**Supplemental Figure 2.1C)** responses for the DE were unaffected or augmented, respectively – effects which differed from the depression of DE maximal firing rate responses observed after MD (**Figure 2.2A**). This difference suggests that while peak DE visual responses are depressed after MD (via a Hebbian mechanism), this effect may be partially offset by homeostatic firing enhancement. While RO had no further effect on DE mean or

spontaneous firing rates, BR enhanced overall firing in RS neurons (i.e., beyond levels seen after MD). SE mean and spontaneous firing in RS neurons were enhanced by MD; these effects were not altered by RO and were only partially reversed after BR. Among bV1 FS interneurons, DE mean and spontaneous firing rate changes after MD, RO, and BR (**Supplemental Figure 2.1B, D**) followed the same pattern as changes in maximal firing rates (**Figure 2.2E**) – with suppression after MD which were reversed after both recovery experiences. SE mean and spontaneous firing was modestly, but significantly, enhanced in FS neurons after MD; this enhancement remained after RO, but not BR. Taken together, these data suggest that many, but not all, of the response changes observed in bV1 neurons' preferred-orientation responses after visual manipulations are also observed in their mean and spontaneous firing.

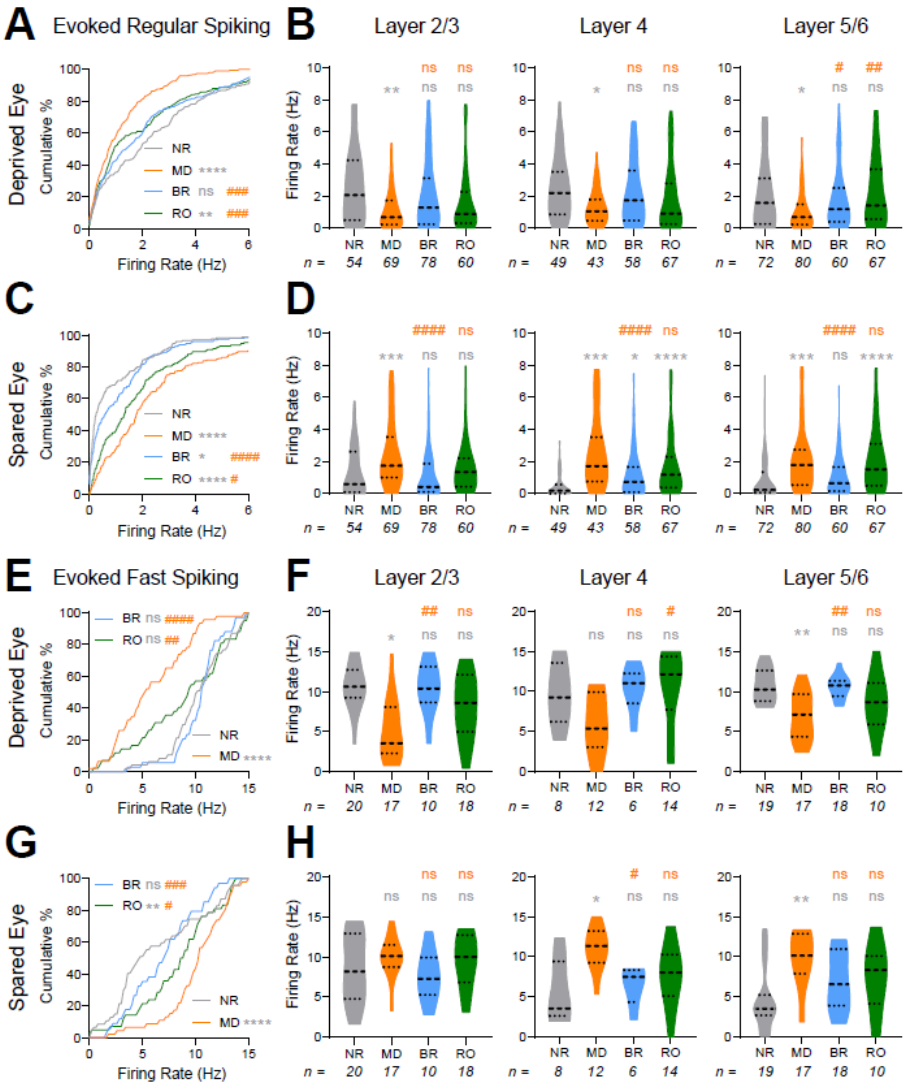

Figure 2.2: BR and RO differentially reverse MD-induced changes in DE and SE firing rate responses among RS neurons and FS interneurons.

(**A, C**) Cumulative distributions of preferred-stimulus (i.e. maximal) DE (**A**) and SE (**C**) visually-evoked firing rate responses for bV1 RS neurons. DE responses were significantly depressed after 5-day MD; this was reversed fully after BR and partially after RO. SE responses in RS neurons showed post-MD potentiation, which was maintained after RO, but largely reversed by BR. *, **, and **** (gray) indicate $p < 0.05$, $p < 0.01$, and $p < 0.0001$, K-S test vs. NR; #, ### and #### (orange) indicate $p < 0.05$, $p < 0.001$, and $p < 0.0001$, K-S test vs MD. (**B, D**) Violin plots of RS neurons' DE (**B**) and SE (**D**) visually-evoked responses recorded from neurons in bV1 layers 2/3, 4, or 5/6. Dashed lines represent the 25%, median, and 75% quartiles. *, **, ***, and **** (gray) indicate $p < 0.05$, $p < 0.01$, $p < 0.001$, and $p < 0.0001$, Dunn's post hoc test vs. NR; #, ##, and #### (orange) indicate $p < 0.05$, $p < 0.01$ and $p < 0.0001$, Dunn's post hoc test vs MD. $p < 0.01$, < 0.05, and < 0.01 for DE responses recorded in layers 2/3, 4, and 5/6, respectively; $p < 0.0001$ for SE responses recorded in all layers, Kruskal-Wallis test. (**E, G**) Cumulative distributions of maximal DE (**E**) and SE (**G**) visually-evoked firing rate responses for FS interneurons. DE and SE responses were depressed and potentiated, respectively, after MD. These response changes were partially reversed by RO, and fully reversed by BR. ** and **** (gray) indicate $p < 0.01$ and $p < 0.0001$, K-S test vs. NR; #, ##, ###, and #### (orange) indicate $p < 0.05$, $p < 0.01$, $p < 0.01$, and $p < 0.0001$, K-S test vs MD. (**F, H**) Violin plots of FS interneurons' DE (**F**) and SE (**H**) visually-evoked responses recorded from neurons in each bV1 layer. * and ** (gray) indicate $p < 0.05$ and $p < 0.01$, Dunn's post hoc test vs. NR; # and ## (orange) indicate $p < 0.05$ and $p < 0.01$, Dunn's post hoc test vs MD. $p < 0.001$, < 0.05, < 0.001 for DE responses recorded in layers 2/3, 4, and 5/6, respectively; p = ns, < 0.01, and < 0.01 for SE responses recorded in layers 2/3, 4, and 5/6 respectively, Kruskal-Wallis test.

2.5.3 : BR, but not RO, fully restore DE-driven cFos expression in bV1 layers 2/3

To further characterize how MD, BR, and RO affect visual responses throughout bV1, we used immunohistochemistry to quantify DE-driven cFos expression in PV+ interneurons and non-PV+ neurons. Mice were treated as shown in **Figure 2.1**, after which they were returned to the visual enrichment arena for 30 min of visual stimulation of the DE only, then were perfused 90 min later. Visually-driven expression of cFos and PV expression were quantified across the layers of bV1 contralateral to the DE (**Figure 2.3A-D**). Consistent with previous reports [62,63], DE-driven cFos expression was significantly reduced across bV1 after MD (**Figure 2.3B**). Both total density of cFos+ neurons and the density of cFos+ PV+ interneurons decreased after MD. BR reversed these changes, restoring DE-driven cFos expression to levels seen in NR control mice (**Figure 2.3B, C**). In contrast, and consistent with data shown in **Figure 2.3A, D,** both total DE-driven cFos expression and density of cFos+ PV+ interneurons remained significantly reduced after RO. Quantification of cFos and PV by layer showed that the largest differential effects of visual experience were seen in layers 2/3. Following MD, DE-driven cFos expression was reduced across all layers (**Figure 2.3B**), and cFos+ PV+ interneuron density was dramatically reduced in layers 2/3 (and to a lesser extent, layer 4) (**Figure 2.3D**). RO restored DE-driven cFos expression in layer 4 and layers 5/6, but not layers 2/3 (**Figure 2.3B**). After BR, total and PV+ interneuron cFos expression was renormalized across all layers, including layer 2/3, where cFos+ neuron density was restored to levels seen in NR mice (**Figure 2.3D**). As an additional control, to verify that changes in expression were driven by alterations of visual input, the same analysis was applied to adjacent segments of primary auditory cortex (A1) within the same

immunolabeled brain sections used for bV1 measurements. As shown in **Supplemental Figure 2.2**, no differences in cFos or PV expression were observed between the four experimental groups. Together, these data suggest that activity-driven plasticity in layer 2/3, especially in layer 2/3 PV+ interneurons, differs dramatically during monocular vs. binocular recovery from MD.

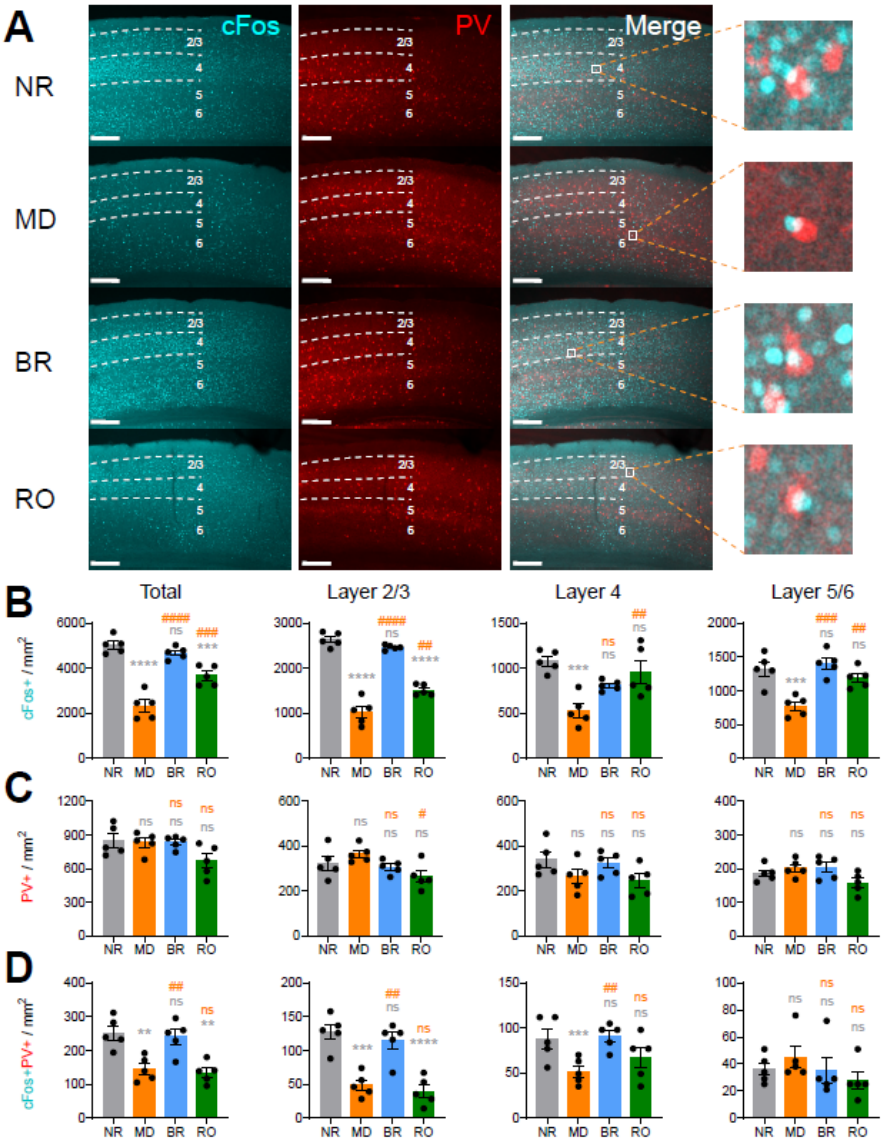

Figure 2.3: DE-driven cFos expression is reduced after MD and restored after BR, but not RO.

(**A**) Representative images of bV1 cFos (cyan), parvalbumin (PV) [red], and overlap across treatment groups following DE stimulation. Mice (n = 5/treatment group) received DE-only visual stimulation for 30 min, then were returned to their home cages for 90 min prior to perfusion. Dashed lines represent cortical layer distribution used in cell counting analysis. Scale bar = 100 µm. (**B**) DE-driven cFos+ neuron density was decreased in bV1 after MD. cFos expression was fully rescued after BR and partially rescued after RO. One-way ANOVA: F (3, 16) = 39.65, p < 0.0001; *** and **** (gray) indicate p < 0.001 and p < 0.0001, Tukey test vs. NR; ### and #### (orange) indicate p < 0.001 and p < 0.0001, Tukey test vs MD. cFos+ neuron density in bV1 layers 2/3, 4, and 5/6. One-way ANOVA for layers 2/3, 4, or 5/6, respectively: F (3, 16) = 95.41, p < 0.0001, F (3, 16) = 9.093, p = 0.001, and F (3, 16) = 12.35, p = 0.0002. (**C**) Density of PV+ bV1 interneurons was similar between groups. One-way ANOVA: F (3, 16) = 2.99, p = 0.062. PV+ interneuron density in bV1 layers 2/3, 4, and 5/6. One-way ANOVA for layers 2/3, 4, or 5/6, respectively: F (3, 16) = 3.40, p = 0.044, ns, and ns. (**D**) cFos+ PV+ interneuron density decreased with MD and recovered with BR, but not RO. One-way ANOVA: F (3, 16) = 11.40, p = 0.0003; ** (gray) indicates p < 0.01, Tukey test vs. NR; ## (orange) indicates p < 0.01, Tukey test vs MD. cFos+PV+ interneuron density in bV1 layers 2/3, 4, and 5/6. One-way ANOVA for layers 2/3, 4, or 5/6, respectively: F (3, 16) = 18.88, p < 0.0001, F (3, 16) = 4.25, p = 0.022, and ns. *, ***, and **** (gray) indicate p < 0.05, p < 0.001, and p < 0.0001, Tukey test vs. NR; #, ##, ### and #### (orange) indicate p < 0.05, p < 0.01, p < 0.001, and p < 0.0001, Tukey test vs MD. Error bars indicate mean ± SEM.

2.5.4 : Sleep in the hours following BR visual experience is necessary for ocular dominance recovery

Initial shifts in ocular dominance in favor of the SE are promoted by periods of sleep following monocular visual experience [8-10,64]. However, it is unclear whether, or how, sleep contributes to bV1 functional recovery after MD. Because 5-day BR (with 4 h of binocular visual enrichment per day) was effective at reversing many of the effects of prior MD, we tested whether post-visual enrichment sleep plays an essential role in this recovery. Mice underwent the same 5-day MD and 5-day BR periods shown in **Figure 2.1**. Following each daily visual enrichment period, mice were returned to their home cage, and over the next 4 h were either sleep deprived (SD) under dim red light (to prevent additional visual input to V1) or allowed *ad lib* sleep (BR+SD and BR+Sleep, respectively; **Figure 2.4A-B**). BR+Sleep mice spent (on average) just over 70% of the first 4 h post-enrichment period (corresponding to SD in BR+SD mice) in a behavioral sleep posture (crouched, immobile, nested and with closed eyes) (**Figure 2.4C**). We then compared bV1 neurons' visual responses for stimuli presented to either the right or left eyes, for the hemisphere contralateral to the original DE, between BR+Sleep and BR+SD mice (**Figure 2.4D**). In contrast to prior reports on the effects of SD following RO in critical period cats (Dadvand et al., 2006), we found that SD in the hours following daily BR visual experience reduced post-MD recovery of ocular dominance in favor of the original DE (**Figure 2.4E**). Ocular dominance index and contralateral bias index values for bV1 neurons recorded from BR+SD mice were significantly reduced compared to those of BR+Sleep mice, indicating reduced DE preference similar to that seen after MD alone (**Figure 2.4F-G**). These effects of SD on ocular dominance recovery across BR were present in both RS

neurons and FS interneurons in bV1 (**Figure 2.4H-J**). The proportion of visually responsive neurons recorded in BR+Sleep and BR+SD mice was also similar (88.3% and 84.5%, respectively). Thus, in the context of BR-mediated recovery from MD, post-experience sleep plays an essential role in recovery of ocular dominance in bV1.

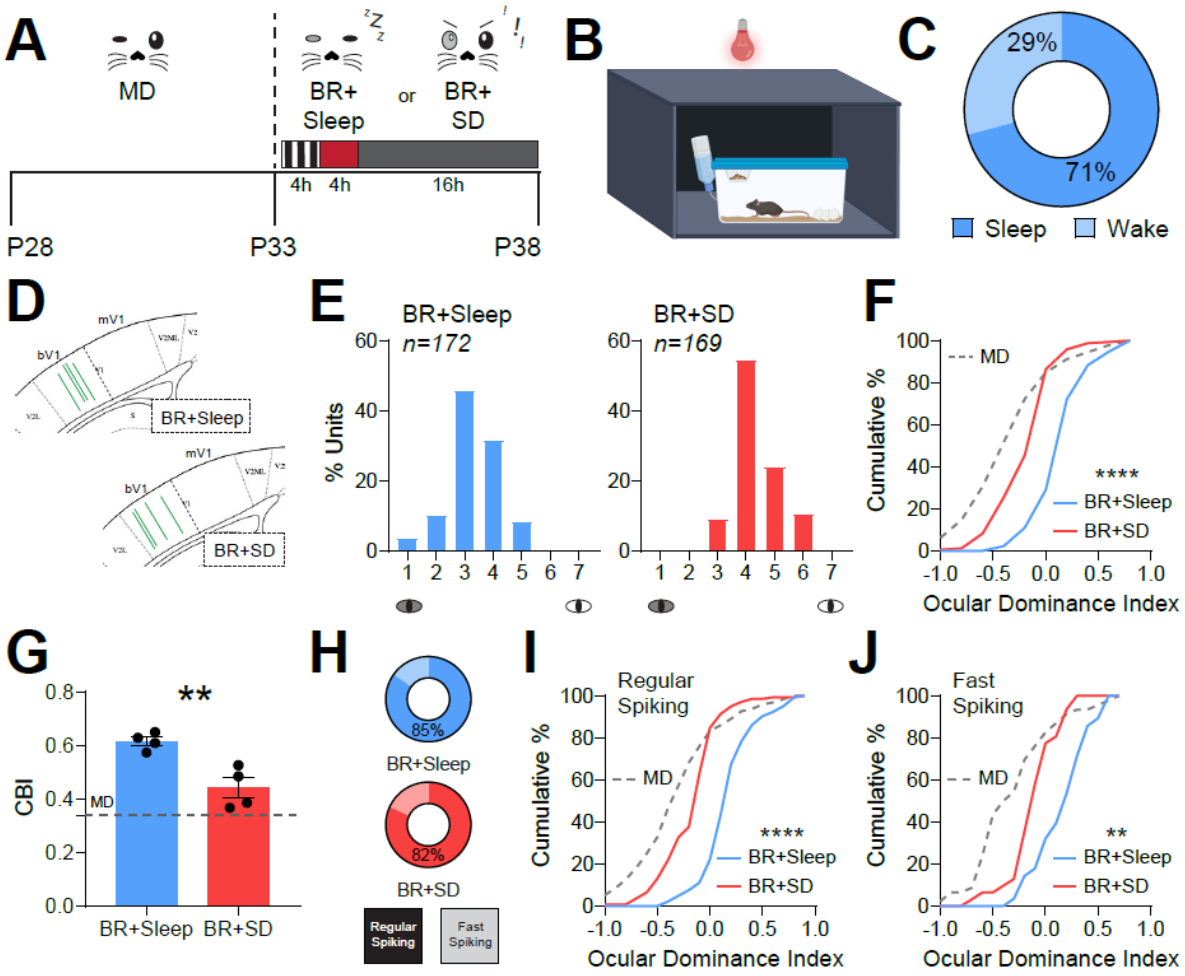

Figure 2.4: Sleep loss following BR visual experience prevents ocular dominance shifts

(**A**) Experimental design. Mice underwent 5-day MD and 5-day BR; each day after 4-hr BR, BR+Sleep mice were returned to their home cage and allowed ad lib sleep under dim red light, BR mice underwent 4 hours of sleep deprivation (BR+SD) through gentle handling under dim red light. (**B**) Schematic of experimental setup for animal observation under dim red light. (**C**) On average, BR+Sleep mice spent 71% of the 4 h period following visual enrichment (n = 5) in sleep, based on visual confirmation of immobility, stereotyped (crouched) sleep postures, nesting, and closed eyes, consistent with prior studies (Delorme et al 2021, Puentes-Mestril et al 2021). (**D**) Schematic of bV1 coordinates in coronal sections. Green lines indicate probe placements in bV1 for BR+Sleep and BR+SD groups. (**E**) Ocular dominance histograms for bV1 neurons recorded from BR+Sleep and BR+SD groups (4 mice/group). (**F**) Cumulative distribution of ocular dominance index values for bV1 neurons recorded from BR+Sleep and BR+SD mice. **** indicates $p < 0.0001$, K-S test for BR+Sleep vs. BR+SD. Values from neurons recorded in MD-only mice from Fig. 1 are shown (dashed gray lines) for comparison. (**G**) Contralateral bias index values were reduced for bV1 neurons recorded from BR+SD mice. Unpaired t-test: $p = 0.0059$. Error bars indicate mean ± SEM. (**H**) Proportion of recorded neurons identified as RS neurons or FS interneurons for the two groups. RS neurons: BR+Sleep (n = 144); BR+SD (n = 138). FS interneurons: BR+Sleep (n = 28); BR+SD (n = 31). (**I-J**) Ocular dominance index values for recorded RS neurons (**I**) and FS interneurons (**J**) were reduced in BR+SD mice. ** and **** indicate $p < 0.01$ and $p < 0.0001$, K-S test.

2.5.5 : BR-mediated renormalization of DE and SE responses are reversed by sleep loss

To determine how SD affects visual responsiveness in DE and SE pathways, we assessed how maximal visually-evoked firing rates (at each neuron's preferred stimulus orientation) were affected by post-BR sleep vs. SD. In both RS neurons and FS interneurons, post-BR SD led to a significant reduction of DE firing rate responses compared with those recorded from freely-sleeping mice (**Figure 2.5A-B, E-F**). When DE responses were compared across bV1, as a whole, those recorded from BR+SD mice were significantly lower than those recorded from BR+Sleep mice, similar to those recorded from mice after MD alone. Among RS neurons, we found that this effect was most pronounced in layers 2/3, where DE-driven firing rates in BR+SD mice were similar to those recorded from MD mice (**Figure 2.5B**). Among FS interneurons, SD effects were most pronounced in layer 4, where depressed DE responses were similar to those of MD-only mice (**Figure 2.5F**).

Across bV1, as a whole, RS neurons' SE responses were not significantly different between BR+Sleep and BR+SD mice (**Figure 2.5C**). SE responses were significantly elevated in RS neurons recorded in layer 4 and layers 5/6 from BR+SD mice, where median response rates were similar to those recorded in MD-only mice (**Figure 2.5D**). Across the bV1 FS interneuron population, SD interfered with BR-driven normalization of SE responses, which remained elevated, similar to those recorded from mice following MD alone (**Figure 2.5G**). FS interneurons' SE responses in BR+SD mice were significantly elevated relative to BR+Sleep mice in layers 5/6, with median firing rate responses similar to those seen in MD mice (**Figure 2.5H**). Together, these data suggest

that eye-specific response renormalization due to BR in both RS neurons and FS interneurons is suppressed by post-BR SD.

As with MD, BR, and RO groups (**Supplemental Figure 2.1**), we also compared mean (i.e., across all visual stimulus orientations) and spontaneous (blank screen) firing between BR+Sleep and BR+SD groups (**Supplemental Figure 2.3**), to identify sleep-dependent changes that might be mediated by homeostatic, rather than Hebbian, mechanisms. As shown in **Supplemental Figure 2.3A and C**, both DE and SE mean and spontaneous firing followed a similar pattern to maximal visually-evoked firing (**Figure 2.5A, C**). Because both SE mean and spontaneous firing differed between the two groups, with SE firing being reduced overall in BR+Sleep mice (and this was most pronounced for spontaneous firing (**Supplemental Figure 2.3C**), one possibility is that this difference is driven by homeostatic synaptic downscaling occurring in a sleep-dependent manner in bV1 [65]. FS interneurons' mean and spontaneous firing rates generally did not differ significantly between BR+Sleep and BR+SD mice (**Supplemental Figure 2.3B, D**), although SE mean firing rates were lower in BR+Sleep mice, similar to maximal visually-evoked firing (**Figure 2.5G**).

To further characterize layer- and cell type-specific changes in visual responses after post-BR sleep vs. SD**,** we quantified DE-driven cFos and PV+ interneuron expression in bV1 of BR+Sleep and BR+SD mice (**Figure 2.6A-D**), using the same DE visual stimulation strategy described for **Figure 2.3**. Across bV1, as a whole, overall DE-driven cFos expression was significantly reduced in BR+SD mice compared to BR+Sleep mice (**Figure 2.6A-B**). This reduction was most dramatic in layers 2/3 and 5/6 (**Figure 2.6B**), where cFos levels in BR+SD mice were intermediate between those of BR+Sleep

and MD-only mice. The density of cFos+ PV+ interneurons was likewise significantly decreased after DE stimulation in BR+SD mice (**Figure 2.6D**), with dramatic reductions in layers 2/3 and 4 (**Figure 2.6D**). As an additional control, to verify that changes in expression were driven by alterations of visual input, the same analysis was applied to adjacent segments of primary auditory cortex (A1) within the same immunolabeled brain sections used for bV1 measurements. As shown in **Supplemental Figure 2.4**, no differences in cFos or PV expression were observed between BR+Sleep and BR+SD groups. Taken together, our data suggests that most of the changes to DE and SE responses initiated in bV1 by MD are sustained when BR is followed by SD. Conversely, BR-mediated recovery of binocular function in bV1 RS neurons and FS interneurons relies on post-BR sleep.

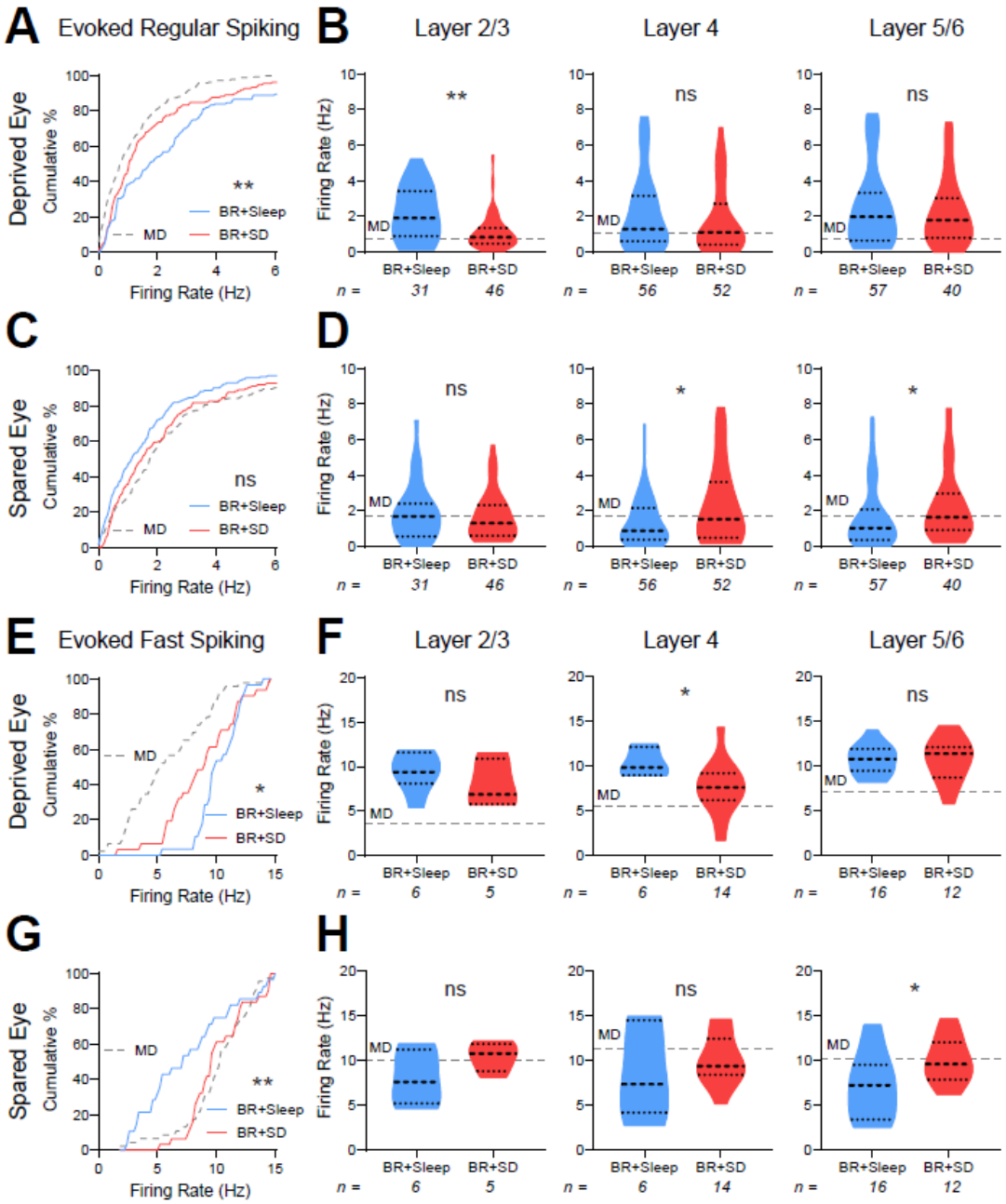

Figure 2.5: Post-BR SD prevents recovery of DE and SE responses after MD

(**A, C**) Cumulative distributions of preferred-stimulus DE (**A**) and SE (**C**) visually-evoked firing rate responses for bV1 RS neurons. DE firing rate responses were significantly decreased in BR+SD mice relative to BR+Sleep mice. ** indicates p < 0.01, K-S test. (**B, D**) Violin plots of RS neurons' DE (**B**) and SE (**D**) visually-evoked responses recorded from neurons in bV1 layers 2/3, 4, or 5/6. Dashed lines represent the 25%, median, and 75% quartiles; * and ** indicate p < 0.05 and p < 0.01, Mann-Whitney test. (**E, G**) Cumulative distributions of maximal DE (**E**) and SE (**G**) visually-evoked firing rate responses for bV1 FS interneurons. Firing rate responses for DE and SE stimulation were significantly decreased and increased, respectively, in BR+SD mice. * and ** indicate $p < 0.05$ and $p < 0.01$, K-S test. (**F, H**) Violin plots of FS interneurons' DE (**F**) and SE (**H**) visually-evoked responses recorded from neurons in bV1 layers 2/3, 4, or 5/6. * indicates $p < 0.05$, Mann-Whitney test. Values for the MD-only condition (gray dashed lines) from **Fig. 2** are shown for comparison.

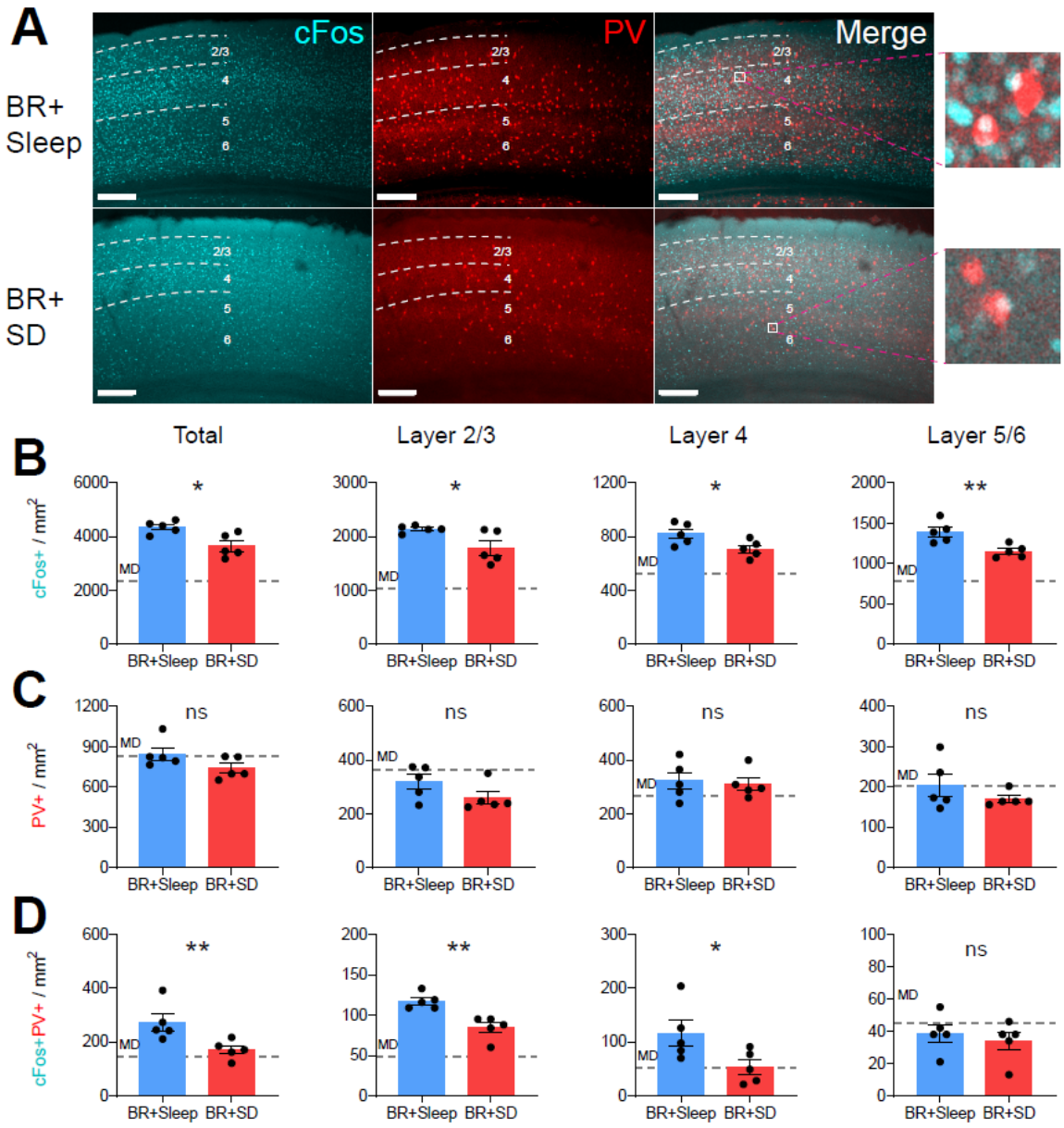

Figure 2.6: Post-BR SD prevents recovery of DE-driven cFos expression in bV1

(**A**) bV1 cFos (cyan) and PV (red) expression after DE stimulation in BR+Sleep and BR+SD mice. Mice (n = 5/treatment group) received DE-only visual stimulation for 30 min, then were returned to their home cages for 90 min prior to perfusion. Scale bar = 100 µm. (**B**) DE-driven cFos+ neuron density was reduced in BR+SD mice relative to BR+Sleep mice. Unpaired t-test: * indicates $p < 0.05$. cFos+ neuron density was reduced in bV1 layers 2/3, 4, and 5/6 after BR+SD relative to BR+Sleep. Unpaired t-test: * and ** indicate $p < 0.05$, and $p < 0.01$, respectively. (**C**) PV immunostaining was similar between groups. PV+ interneuron density in bV1 layers 2/3, 4, and 5/6 was similar between groups. (**D**) cFos+ PV+ interneuron density was decreased in BR+SD mice relative to BR+Sleep mice. Unpaired t-test: ** indicates $p < 0.01$. cFos+ PV+ interneuron density was reduced in bV1 layers 2/3 and 4 in BR+SD mice relative to BR+Sleep mice. Unpaired t-test: * and ** indicate $p < 0.05$ and $p < 0.01$, respectively. Values for the MD-only condition (gray dashed lines) from Fig. 3 are shown for comparison.

2.6 : Discussion

In this study, we compared how different recovery experiences and subsequent sleep affect recovery of visual cortical responses following MD. We first compared the effects of equal-duration, qualitatively-similar binocular vs. monocular visual experience on recovery of bV1 responses following MD, using single-unit electrophysiology and immunohistochemistry. It is important to note that our BR intervention did not involve simply re-opening the original DE – an intervention used in early studies using primates and cats as an amblyopia model [16,17]. Rather, we attempted to create an experimental scenario for BR where cooperative input from the two eyes might be expected to reach bV1 simultaneously, and that mice would be encouraged to use the eyes together. We chose to optimize visual stimulation during recovery experiences with high-contrast gratings, which have been shown to optimize recovery of visual function in adult mice after MD [24,25], and which would optimize coincident activation of the two eyes during binocular viewing. Moreover, we place BR and RO mice in a behavioral scenario where: 1) the stimuli were novel, and 2) as BR mice moved through the environment, binocular disparity cues (i.e., spatial frequency of stimuli presented to the eyes) would be constantly changing. Critically, a side-by-side comparison of equal-duration BR and RO clearly showed that bV1 ocular dominance shifts in favor of the SE are reversed after 5-day BR, but not 5-day RO (**Figure 2.1**). This reversal is present in both RS neurons and FS interneurons, and is associated with reversal of both MD-driven DE response depression and SE response potentiation (**Figure 2.2, Supplemental Figure 2.1**). Insofar as MD serves as a model for amblyopia caused by disruption of vision in one of the two eyes during childhood, these data add to a body of growing evidence that suggests that

enriched binocular visual experience may offer advantages over and above the standard of care for amblyopia. We also characterized the effects of post-experience sleep and sleep loss on recovery processes. When daily BR experience is followed by SD, recovery of normal binocular vision in bV1 is nearly completely blocked (**Figure 2.4, Figure 2.5, Figure 2.6**). This suggests that the relative timing of sleep relative to recovery experience is potentially a critical – but overlooked - consideration for the treatment of amblyopia.

How do BR and RO differ in their effects in bV1? Here we find that 5-day MD causes significant DE response depression among both RS neurons and FS interneurons in bV1 – with the most dramatic depression observed among FS interneurons in layers 2/3. These findings are consistent with results of longitudinal calcium imaging studies in mouse V1 [55] and both acute and longitudinal electrophysiological recordings in cat V1 [9,10]. These changes not only reduce FS interneuron firing rates, but also strongly reduce DE-driven cFos expression among PV+ and PV- neuron populations in layers 2/3 (**Figure 2.3**). Thus, our data are consistent with the interpretation that MD leads to a transient decrease in cortical inhibition through effects of PV+ interneurons [10,55]. Importantly, closure of the critical period for ODP is thought to involve restoration of “mature” levels of cortical inhibition, which disrupts subsequent competitive plasticity of excitatory inputs [1,66-68]. We find that while this response depression is almost completely reversed by 5-day BR, only partial recovery of DE responses is achieved with RO. Differential recovery between BR and RO is evident both at the level of firing rates (**Figure 2.2**) and DE-driven cFos expression (**Figure 2.3**). Across the initial 5-day MD period, both FS interneurons and RS neurons also show widespread potentiation of SE firing rate responses, across all layers of bV1. These SE response changes (which are thought to occur only after DE

response depression has already take place) [7,9,10] appear to be almost fully reversed after 5-day BR visual experience. In contrast, SE response enhancement is minimally altered after 5-day subsequent RO. In general, these findings are consistent with intrinsic signal imaging studies in binocular mouse V1, which indicated that a single day of BR is superior to RO at restoring binocularity [23]. Future studies will be needed to determine the precise role of FS interneurons' response properties in mediating recovery, the extent to which initial eye-specific response changes during MD are mediated by Hebbian vs. homeostatic plasticity mechanisms [58,60,61,69-72], and how differential outcomes with BR vs. RO themselves reflect Hebbian vs. homeostatic changes within bV1.

How does post-experience sleep or sleep loss affect bV1 during recovery? Our data clearly demonstrate that following periods of BR experience, subsequent sleep is essential for recovery of MD-driven changes in ocular dominance (**Figure 2.4**), DE and SE firing rate responses (**Figure 2.5**), and DE-driven cFos expression (**Figure 2.6**). These are the first data demonstrating that following MD, sleep plays a critical role in restoring normal visual function. Prior work has shown that post-MD sleep is essential for initial ocular dominance shifts in favor of the spared eye [8-11,33] and for MD-induced structural plasticity in V1 neurons [64]. In comparison, the role of sleep in promoting recovery of bV1 function following amblyopia onset is understudied. Prior work done in critical period cats after brief RO indicated that post-RO SD had little impact – and even tended to reduce recovery of binocular vision [36]. However, virtually nothing is known about interactions between BR visual experience and subsequent sleep. While post-BR sleep has been suggested to promote homeostatic downscaling of firing rates in rodent monocular zone [65], no prior work has addressed how it affects bV1 ODP. The present

work characterizes how sleep contributes to experience-driven recovery of binocular vision in bV1. We find that post-BR sleep is required for reversal of both DE response depression and SE response potentiation, in both RS neurons and FS interneurons. As with changes driven by initial MD (**Figure 2.2, Figure 2.3**), changes driven by post-BR sleep appear to be most dramatic in layers 2/3 (**Figure 2.5, Figure 2.6**).

Why might sleep be essential for these changes? Available data suggests that both Hebbian synaptic potentiation and weakening can occur in bV1 during post-MD sleep [9,10,33,73,74] through sleep-dependent activation of specific molecular pathways [9,11,33] or sleep-specific activity patterns [10]. It is plausible that similar mechanisms are involved in the reversal of MD-driven synaptic changes during post-BR sleep. For example, specific oscillatory patterning of neuronal firing in the V1-LGN network during sleep may be essential for spike timing-dependent plasticity between synaptically-connected neurons [34,35,37,75-77]. Alternatively, sleep may promote permissive changes in biosynthetic pathways that are essential for consolidating some forms of plasticity *in vivo* [41,78]. In V1, sleep plays a role in increasing inhibition within layers 2/3, reducing E/I ratios across the rest phase [79]; this may play a role in reversing ocular dominance changes driven by suppression of FS interneurons in the context of MD [10,55]. Finally, sleep also contributes to homeostatic changes in V1 neurons' firing rates [38,65]; thus sleep-dependent homeostatic plasticity may also contribute to bV1 changes observed in BR+Sleep, but not BR+SD, mice. Indeed, spontaneous and mean neuronal firing rate data from these mice (**Supplemental Figure 2.3**) support this idea.

Many factors affect the degree of ODP initiated by MD in animal models of amblyopia, including behavioral state [8,9,11] and neuropharmacology [67,80-82]. Emerging data

suggests that these factors may also affect recovery from amblyopia [80,83,84]. However, findings from both patients and animal models have raised debate about whether dominant-eye (SE) patching provides the optimal sensory stimulus for promoting recovery of vision [26,29,85,86]. Here, in side-by-side comparison of the effects of brief binocular vs. monocular recovery experiences in mice, we show the two have strikingly different effects on bV1 ocular dominance and network activation in bV1. These data reflect findings using comparisons of 24-h binocular vs. monocular recovery [23], where simply re-opening the DE in mice was found to be more efficacious for restoring binocular vision than RO. One possibility is that plasticity mechanisms in mouse bV1 differ from those in operation in primate bV1 when the DE is reopened [17]. In support of this argument, simply reversing occlusion of the weaker eye is insufficient to correct amblyopia in patients. On the other hand, our present data suggests that features of the binocular visual stimulation used in our BR condition may be useful for developing experimental therapeutics for amblyopia recovery. Critically, our data also provide the first demonstration that the timing of sleep relative to visual experience during amblyopia treatment may be an important consideration for restoring normal bV1 function. This finding may have important implications for treating amblyopia later in life, after the critical period, and future studies should address whether similar or different mechanisms are in operation when recovery occurs long after the critical period has closed. We hope that the present data will inform future strategies for optimizing amblyopia treatment in children.

2.6.1 Acknowledgements

We thank Abbey Roelofs (LSA Informational Technology Services) for software programming assistance. This work was supported by a University of Michigan Rackham

Graduate School Candidate Grant and Merit Fellowship to JDM, National Institutes of Health R01NS104776, and a Research to Prevent Blindness Walt and Lilly Disney Award for Amblyopia Research to SJA.

2.7 : References

1. Hensch, T.K. (2004). Critical period regulation. Annu Rev Neurosci *27*, 549-579. 10.1146/annurev.neuro.27.070203.144327.
2. Knudsen, E.I. (2004). Sensitive periods in the development of the brain and behavior. J Cogn Neurosci *16*, 1412-1425. 10.1162/0898929042304796.
3. Blumberg, M.S. (2015). Developing Sensorimotor Systems in Our Sleep. Curr Dir Psychol Sci *24*, 32-37. 10.1177/0963721414551362.
4. Wiesel, T.N., and Hubel, D.H. (1963). Single-Cell Responses in Striate Cortex of Kittens Deprived of Vision in One Eye. J Neurophysiol *26*, 1003-1017. 10.1152/jn.1963.26.6.1003.
5. Gordon, J.A., and Stryker, M.P. (1996). Experience-dependent plasticity of binocular responses in the primary visual cortex of the mouse. J Neurosci *16*, 3274-3286. 10.1523/JNEUROSCI.16-10-03274.1996.
6. Mioche, L., and Singer, W. (1989). Chronic recordings from single sites of kitten striate cortex during experience-dependent modifications of receptive-field properties. J Neurophysiol *62*, 185-197. 10.1152/jn.1989.62.1.185.
7. Frenkel, M.Y., and Bear, M.F. (2004). How monocular deprivation shifts ocular dominance in visual cortex of young mice. Neuron *44*, 917-923. 10.1016/j.neuron.2004.12.003.
8. Frank, M.G., Issa, N.P., and Stryker, M.P. (2001). Sleep enhances plasticity in the developing visual cortex. Neuron *30*, 275-287. 10.1016/s0896-6273(01)00279-3.
9. Aton, S.J., Seibt, J., Dumoulin, M., Jha, S.K., Steinmetz, N., Coleman, T., Naidoo, N., and Frank, M.G. (2009). Mechanisms of sleep-dependent consolidation of cortical plasticity. Neuron *61*, 454-466. 10.1016/j.neuron.2009.01.007.
10. Aton, S.J., Broussard, C., Dumoulin, M., Seibt, J., Watson, A., Coleman, T., and Frank, M.G. (2013). Visual experience and subsequent sleep induce sequential plastic changes in putative inhibitory and excitatory cortical neurons. Proc Natl Acad Sci U S A *110*, 3101-3106. 10.1073/pnas.1208093110.
11. Dumoulin Bridi, M.C., Aton, S.J., Seibt, J., Renouard, L., Coleman, T., and Frank, M.G. (2015). Rapid eye movement sleep promotes cortical plasticity in the developing brain. Sci Adv *1*, e1500105. 10.1126/sciadv.1500105.
12. Attebo, K., Mitchell, P., Cumming, R., Smith, W., Jolly, N., and Sparkes, R. (1998). Prevalence and causes of amblyopia in an adult population. Ophthalmology *105*, 154-159. 10.1016/s0161-6420(98)91862-0.
13. Webber, A.L., and Wood, J. (2005). Amblyopia: prevalence, natural history, functional effects and treatment. Clin Exp Optom *88*, 365-375. 10.1111/j.1444-0938.2005.tb05102.x.
14. Levi, D.M., Knill, D.C., and Bavelier, D. (2015). Stereopsis and amblyopia: A mini-review. Vision Res *114*, 17-30. 10.1016/j.visres.2015.01.002.
15. Birch, E.E. (2013). Amblyopia and binocular vision. Progress in Retinal and Eye Research. Pergamon.

16. Mitchell, D.E., Cynader, M., and Movshon, J.A. (1977). Recovery from the effects of monocular deprivation in kittens. J Comp Neurol *176*, 53-63. 10.1002/cne.901760104.
17. LeVay, S., Wiesel, T.N., and Hubel, D.H. (1980). The development of ocular dominance columns in normal and visually deprived monkeys. J Comp Neurol *191*, 1-51. 10.1002/cne.901910102.
18. Movshon, J.A. (1976). Reversal of the physiological effects of monocular deprivation in the kitten's visual cortex. J Physiol *261*, 125-174. 10.1113/jphysiol.1976.sp011551.
19. Mitchell, D.E., Murphy, K.M., and Kaye, M.G. (1984). Labile nature of the visual recovery promoted by reverse occlusion in monocularly deprived kittens. Proc Natl Acad Sci U S A *81*, 286-288. 10.1073/pnas.81.1.286.
20. Murphy, K.M., and Mitchell, D.E. (1986). Bilateral amblyopia after a short period of reverse occlusion in kittens. Nature *323*, 536-538. 10.1038/323536a0.
21. Iny, K., Heynen, A.J., Sklar, E., and Bear, M.F. (2006). Bidirectional modifications of visual acuity induced by monocular deprivation in juvenile and adult rats. J Neurosci *26*, 7368-7374. 10.1523/JNEUROSCI.0124-06.2006.
22. Fischer, Q.S., Aleem, S., Zhou, H., and Pham, T.A. (2007). Adult visual experience promotes recovery of primary visual cortex from long-term monocular deprivation. Learn Mem *14*, 573-580. 10.1101/lm.676707.
23. Kaneko, M., Cheetham, C.E., Lee, Y.S., Silva, A.J., Stryker, M.P., and Fox, K. (2010). Constitutively active H-ras accelerates multiple forms of plasticity in developing visual cortex. Proc Natl Acad Sci U S A *107*, 19026-19031. 10.1073/pnas.1013866107.
24. Kaneko, M., and Stryker, M.P. (2014). Sensory experience during locomotion promotes recovery of function in adult visual cortex. Elife *3*, e02798. 10.7554/eLife.02798.
25. Kind, P.C., Mitchell, D.E., Ahmed, B., Blakemore, C., Bonhoeffer, T., and Sengpiel, F. (2002). Correlated binocular activity guides recovery from monocular deprivation. Nature *416*, 430-433. 10.1038/416430a.
26. Repka, M.X., Beck, R.W., Holmes, J.M., Birch, E.E., Chandler, D.L., Cotter, S.A., Hertle, R.W., Kraker, R.T., Moke, P.S., Quinn, G.E., et al. (2003). A randomized trial of patching regimens for treatment of moderate amblyopia in children. Arch Ophthalmol *121*, 603-611. 10.1001/archopht.121.5.603.
27. Pediatric Eye Disease Investigator, G., Wallace, D.K., Lazar, E.L., Holmes, J.M., Repka, M.X., Cotter, S.A., Chen, A.M., Kraker, R.T., Beck, R.W., Clarke, M.P., et al. (2013). A randomized trial of increasing patching for amblyopia. Ophthalmology *120*, 2270-2277. 10.1016/j.ophtha.2013.04.008.
28. Khan, T. (2015). Is There a Critical Period for Amblyopia Therapy? Results of a Study on Older Anisometropic Amblyopes. J Clin Diagn Res *9*, NC01-04. 10.7860/JCDR/2015/13277.6288.
29. Kelly, K.R., Jost, R.M., Dao, L., Beauchamp, C.L., Leffler, J.N., and Birch, E.E. (2016). Binocular iPad Game vs Patching for Treatment of Amblyopia in Children: A Randomized Clinical Trial. JAMA Ophthalmol *134*, 1402-1408. 10.1001/jamaophthalmol.2016.4224.

30. Kraus, C.L., and Culican, S.M. (2018). New advances in amblyopia therapy I: binocular therapies and pharmacologic augmentation. Br J Ophthalmol *102*, 1492-1496. 10.1136/bjophthalmol-2018-312172.
31. Kraus, C.L., and Culican, S.M. (2018). New advances in amblyopia therapy II: refractive therapies. Br J Ophthalmol *102*, 1611-1614. 10.1136/bjophthalmol-2018-312173.
32. Holmes, J.M., Manh, V.M., Lazar, E.L., Beck, R.W., Birch, E.E., Kraker, R.T., Crouch, E.R., Erzurum, S.A., Khuddus, N., Summers, A.I., et al. (2016). Effect of a Binocular iPad Game vs Part-time Patching in Children Aged 5 to 12 Years With Amblyopia: A Randomized Clinical Trial. JAMA Ophthalmol *134*, 1391-1400. 10.1001/jamaophthalmol.2016.4262.
33. Seibt, J., Dumoulin, M.C., Aton, S.J., Coleman, T., Watson, A., Naidoo, N., and Frank, M.G. (2012). Protein synthesis during sleep consolidates cortical plasticity in vivo. Curr Biol *22*, 676-682. 10.1016/j.cub.2012.02.016.
34. Puentes-Mestril, C., and Aton, S.J. (2017). Linking Network Activity to Synaptic Plasticity during Sleep: Hypotheses and Recent Data. Front Neural Circuits *11*, 61. 10.3389/fncir.2017.00061.
35. Puentes-Mestril, C., Roach, J., Niethard, N., Zochowski, M., and Aton, S.J. (2019). How rhythms of the sleeping brain tune memory and synaptic plasticity. Sleep *42*. 10.1093/sleep/zsz095.
36. Dadvand, L., Stryker, M.P., and Frank, M.G. (2006). Sleep does not enhance the recovery of deprived eye responses in developing visual cortex. Neuroscience *143*, 815-826. 10.1016/j.neuroscience.2006.08.029.
37. Durkin, J., Suresh, A.K., Colbath, J., Broussard, C., Wu, J., Zochowski, M., and Aton, S.J. (2017). Cortically coordinated NREM thalamocortical oscillations play an essential, instructive role in visual system plasticity. Proc Natl Acad Sci U S A *114*, 10485-10490. 10.1073/pnas.1710613114.
38. Clawson, B.C., Durkin, J., Suresh, A.K., Pickup, E.J., Broussard, C.G., and Aton, S.J. (2018). Sleep Promotes, and Sleep Loss Inhibits, Selective Changes in Firing Rate, Response Properties and Functional Connectivity of Primary Visual Cortex Neurons. Front Syst Neurosci *12*, 40. 10.3389/fnsys.2018.00040.
39. Nikbakht, N., and Diamond, M.E. (2021). Conserved visual capacity of rats under red light. Elife *10*. 10.7554/eLife.66429.
40. Havekes, R., and Aton, S.J. (2020). Impacts of Sleep Loss versus Waking Experience on Brain Plasticity: Parallel or Orthogonal? Trends Neurosci *43*, 385-393. 10.1016/j.tins.2020.03.010.
41. Delorme, J., Wang, L., Kuhn, F.R., Kodoth, V., Ma, J., Martinez, J.D., Raven, F., Toth, B.A., Balendran, V., Vega Medina, A., et al. (2021). Sleep loss drives acetylcholine- and somatostatin interneuron-mediated gating of hippocampal activity to inhibit memory consolidation. Proc Natl Acad Sci U S A *118*. 10.1073/pnas.2019318118.
42. Puentes-Mestril, C., Delorme, J., Wang, L., Donnelly, M., Popke, D., Jiang, S., and Aton, S.J. (2021). Sleep Loss Drives Brain Region-Specific and Cell Type-Specific Alterations in Ribosome-Associated Transcripts Involved in Synaptic Plasticity and Cellular Timekeeping. J Neurosci *41*, 5386-5398. 10.1523/JNEUROSCI.1883-20.2021.

43. Martinez, J.D., Brancaleone, W.P., Peterson, K.G., Wilson, L.G., and Aton, S.J. (2022). Atypical hypnotic compound ML297 restores sleep architecture immediately following emotionally-valenced learning, to promote memory consolidation and hippocampal network activation during recall. Sleep. 10.1093/sleep/zsac301.
44. Raven, F., Heckman, P.R.A., Havekes, R., and Meerlo, P. (2020). Sleep deprivation-induced impairment of memory consolidation is not mediated by glucocorticoid stress hormones. J Sleep Res *29*, e12972. 10.1111/jsr.12972.
45. Daw, N.W., Sato, H., Fox, K., Carmichael, T., and Gingerich, R. (1991). Cortisol reduces plasticity in the kitten visual cortex. J Neurobiol *22*, 158-168. 10.1002/neu.480220206.
46. Durkin, J., and Aton, S.J. (2016). Sleep-Dependent Potentiation in the Visual System Is at Odds with the Synaptic Homeostasis Hypothesis. Sleep *39*, 155-159. 10.5665/sleep.5338.
47. Ognjanovski, N., Schaeffer, S., Wu, J., Mofakham, S., Maruyama, D., Zochowski, M., and Aton, S.J. (2017). Parvalbumin-expressing interneurons coordinate hippocampal network dynamics required for memory consolidation. Nat Commun *8*, 15039. 10.1038/ncomms15039.
48. Ognjanovski, N., Maruyama, D., Lashner, N., Zochowski, M., and Aton, S.J. (2014). CA1 hippocampal network activity changes during sleep-dependent memory consolidation. Front Syst Neurosci *8*, 61. 10.3389/fnsys.2014.00061.
49. Quirk, M.C., Sosulski, D.L., Feierstein, C.E., Uchida, N., and Mainen, Z.F. (2009). A defined network of fast-spiking interneurons in orbitofrontal cortex: responses to behavioral contingencies and ketamine administration. Front Syst Neurosci *3*, 13. 10.3389/neuro.06.013.2009.
50. Issa, N.P., Trachtenberg, J.T., Chapman, B., Zahs, K.R., and Stryker, M.P. (1999). The critical period for ocular dominance plasticity in the Ferret's visual cortex. J Neurosci *19*, 6965-6978. 10.1523/JNEUROSCI.19-16-06965.1999.
51. Bolte, S., and Cordelieres, F.P. (2006). A guided tour into subcellular colocalization analysis in light microscopy. J Microsc *224*, 213-232. 10.1111/j.1365-2818.2006.01706.x.
52. Bossi, M., Tailor, V.K., Anderson, E.J., Bex, P.J., Greenwood, J.A., Dahlmann-Noor, A., and Dakin, S.C. (2017). Binocular Therapy for Childhood Amblyopia Improves Vision Without Breaking Interocular Suppression. Invest Ophthalmol Vis Sci *58*, 3031-3043. 10.1167/iovs.16-20913.
53. Pineles, S.L., Aakalu, V.K., Hutchinson, A.K., Galvin, J.A., Heidary, G., Binenbaum, G., VanderVeen, D.K., and Lambert, S.R. (2020). Binocular Treatment of Amblyopia: A Report by the American Academy of Ophthalmology. Ophthalmology *127*, 261-272. 10.1016/j.ophtha.2019.08.024.
54. Yazaki-Sugiyama, Y., Kang, S., Cateau, H., Fukai, T., and Hensch, T.K. (2009). Bidirectional plasticity in fast-spiking GABA circuits by visual experience. Nature *462*, 218-221. 10.1038/nature08485.
55. Kuhlman, S.J., Olivas, N.D., Tring, E., Ikrar, T., Xu, X., and Trachtenberg, J.T. (2013). A disinhibitory microcircuit initiates critical-period plasticity in the visual cortex. Nature *501*, 543-546. 10.1038/nature12485.

56. Hooks, B.M., and Chen, C. (2020). Circuitry Underlying Experience-Dependent Plasticity in the Mouse Visual System. Neuron *107*, 986-987. 10.1016/j.neuron.2020.08.004.
57. Hofer, S.B., Mrsic-Flogel, T.D., Bonhoeffer, T., and Hubener, M. (2006). Lifelong learning: ocular dominance plasticity in mouse visual cortex. Curr Opin Neurobiol *16*, 451-459. 10.1016/j.conb.2006.06.007.
58. Mrsic-Flogel, T.D., Hofer, S.B., Ohki, K., Reid, R.C., Bonhoeffer, T., and Hubener, M. (2007). Homeostatic regulation of eye-specific responses in visual cortex during ocular dominance plasticity. Neuron *54*, 961-972. 10.1016/j.neuron.2007.05.028.
59. Smith, G.B., Heynen, A.J., and Bear, M.F. (2009). Bidirectional synaptic mechanisms of ocular dominance plasticity in visual cortex. Philos Trans R Soc Lond B Biol Sci *364*, 357-367. 10.1098/rstb.2008.0198.
60. Ranson, A., Cheetham, C.E., Fox, K., and Sengpiel, F. (2012). Homeostatic plasticity mechanisms are required for juvenile, but not adult, ocular dominance plasticity. Proc Natl Acad Sci U S A *109*, 1311-1316. 10.1073/pnas.1112204109.
61. Kaneko, M., and Stryker, M.P. (2017). Homeostatic plasticity mechanisms in mouse V1. Philos Trans R Soc Lond B Biol Sci *372*. 10.1098/rstb.2016.0504.
62. Mainardi, M., Landi, S., Berardi, N., Maffei, L., and Pizzorusso, T. (2009). Reduced responsiveness to long-term monocular deprivation of parvalbumin neurons assessed by c-Fos staining in rat visual cortex. PLoS One *4*, e4342. 10.1371/journal.pone.0004342.
63. Nakadate, K., Imamura, K., and Watanabe, Y. (2012). Effects of monocular deprivation on the spatial pattern of visually induced expression of c-Fos protein. Neuroscience *202*, 17-28. 10.1016/j.neuroscience.2011.12.004.
64. Zhou, Y., Lai, C.S.W., Bai, Y., Li, W., Zhao, R., Yang, G., Frank, M.G., and Gan, W.B. (2020). REM sleep promotes experience-dependent dendritic spine elimination in the mouse cortex. Nat Commun *11*, 4819. 10.1038/s41467-020-18592-5.
65. Torrado Pacheco, A., Bottorff, J., Gao, Y., and Turrigiano, G.G. (2021). Sleep Promotes Downward Firing Rate Homeostasis. Neuron *109*, 530-544 e536. 10.1016/j.neuron.2020.11.001.
66. Hensch, T.K., and Fagiolini, M. (2005). Excitatory-inhibitory balance and critical period plasticity in developing visual cortex. Prog Brain Res *147*, 115-124. 10.1016/S0079-6123(04)47009-5.
67. Hensch, T.K., and Quinlan, E.M. (2018). Critical periods in amblyopia. Vis Neurosci *35*, E014. 10.1017/S0952523817000219.
68. Harauzov, A., Spolidoro, M., DiCristo, G., De Pasquale, R., Cancedda, L., Pizzorusso, T., Viegi, A., Berardi, N., and Maffei, L. (2010). Reducing intracortical inhibition in the adult visual cortex promotes ocular dominance plasticity. J Neurosci *30*, 361-371. 10.1523/JNEUROSCI.2233-09.2010.
69. Maffei, A., Nataraj, K., Nelson, S.B., and Turrigiano, G.G. (2006). Potentiation of cortical inhibition by visual deprivation. Nature *443*, 81-84. 10.1038/nature05079.
70. Cooke, S.F., and Bear, M.F. (2014). How the mechanisms of long-term synaptic potentiation and depression serve experience-dependent plasticity in primary

visual cortex. Philos Trans R Soc Lond B Biol Sci *369*, 20130284. 10.1098/rstb.2013.0284.
71. Guo, Y., Zhang, W., Chen, X., Fu, J., Cheng, W., Song, D., Qu, X., Yang, Z., and Zhao, K. (2017). Timing-dependent LTP and LTD in mouse primary visual cortex following different visual deprivation models. PLoS One *12*, e0176603. 10.1371/journal.pone.0176603.
72. Lambo, M.E., and Turrigiano, G.G. (2013). Synaptic and intrinsic homeostatic mechanisms cooperate to increase L2/3 pyramidal neuron excitability during a late phase of critical period plasticity. J Neurosci *33*, 8810-8819. 10.1523/JNEUROSCI.4502-12.2013.
73. Aton, S.J., Seibt, J., Dumoulin, M.C., Coleman, T., Shiraishi, M., and Frank, M.G. (2009). The sedating antidepressant trazodone impairs sleep-dependent cortical plasticity. PLoS One *4*, e6078. 10.1371/journal.pone.0006078.
74. Seibt, J., Aton, S.J., Jha, S.K., Coleman, T., Dumoulin, M.C., and Frank, M.G. (2008). The non-benzodiazepine hypnotic zolpidem impairs sleep-dependent cortical plasticity. Sleep *31*, 1381-1391. 10.5665/sleep/31.10.1381.
75. Clawson, B.C., Durkin, J., and Aton, S.J. (2016). Form and Function of Sleep Spindles across the Lifespan. Neural Plast *2016*, 6936381. 10.1155/2016/6936381.
76. Durkin, J.M., and Aton, S.J. (2019). How Sleep Shapes Thalamocortical Circuit Function in the Visual System. Annu Rev Vis Sci *5*, 295-315. 10.1146/annurev-vision-091718-014715.
77. Clawson, B.C., Pickup, E.J., Ensing, A., Geneseo, L., Shaver, J., Gonzalez-Amoretti, J., Zhao, M., York, A.K., Kuhn, F.R., Swift, K., et al. (2021). Causal role for sleep-dependent reactivation of learning-activated sensory ensembles for fear memory consolidation. Nat Commun *12*, 1200. 10.1038/s41467-021-21471-2.
78. Seibt, J., and Frank, M.G. (2019). Primed to Sleep: The Dynamics of Synaptic Plasticity Across Brain States. Front Syst Neurosci *13*, 2. 10.3389/fnsys.2019.00002.
79. Bridi, M.C.D., Zong, F.J., Min, X., Luo, N., Tran, T., Qiu, J., Severin, D., Zhang, X.T., Wang, G., Zhu, Z.J., et al. (2020). Daily Oscillation of the Excitation-Inhibition Balance in Visual Cortical Circuits. Neuron *105*, 621-629 e624. 10.1016/j.neuron.2019.11.011.
80. Maya Vetencourt, J.F., Sale, A., Viegi, A., Baroncelli, L., De Pasquale, R., O'Leary, O.F., Castren, E., and Maffei, L. (2008). The antidepressant fluoxetine restores plasticity in the adult visual cortex. Science *320*, 385-388. 10.1126/science.1150516.
81. Heimel, J.A., van Versendaal, D., and Levelt, C.N. (2011). The role of GABAergic inhibition in ocular dominance plasticity. Neural Plast *2011*, 391763. 10.1155/2011/391763.
82. Steinzeig, A., Cannarozzo, C., and Castren, E. (2019). Fluoxetine-induced plasticity in the visual cortex outlasts the duration of the naturally occurring critical period. Eur J Neurosci *50*, 3663-3673. 10.1111/ejn.14512.
83. Baroncelli, L., Bonaccorsi, J., Milanese, M., Bonifacino, T., Giribaldi, F., Manno, I., Cenni, M.C., Berardi, N., Bonanno, G., Maffei, L., and Sale, A. (2012). Enriched experience and recovery from amblyopia in adult rats: impact of motor,

social and sensory components. Neuropharmacology *62*, 2388-2397. 10.1016/j.neuropharm.2012.02.010.
84. Sansevero, G., Torelli, C., Mazziotti, R., Consorti, A., Pizzorusso, T., Berardi, N., and Sale, A. (2020). Running towards amblyopia recovery. Sci Rep *10*, 12661. 10.1038/s41598-020-69630-7.
85. Faulkner, S.D., Vorobyov, V., and Sengpiel, F. (2006). Visual cortical recovery from reverse occlusion depends on concordant binocular experience. J Neurophysiol *95*, 1718-1726. 10.1152/jn.00912.2005.
86. Lunghi, C., Sframeli, A.T., Lepri, A., Lepri, M., Lisi, D., Sale, A., and Morrone, M.C. (2019). A new counterintuitive training for adult amblyopia. Ann Clin Transl Neurol *6*, 274-284. 10.1002/acn3.698.

2.8 : Chapter 2 Supplementary Information Figures

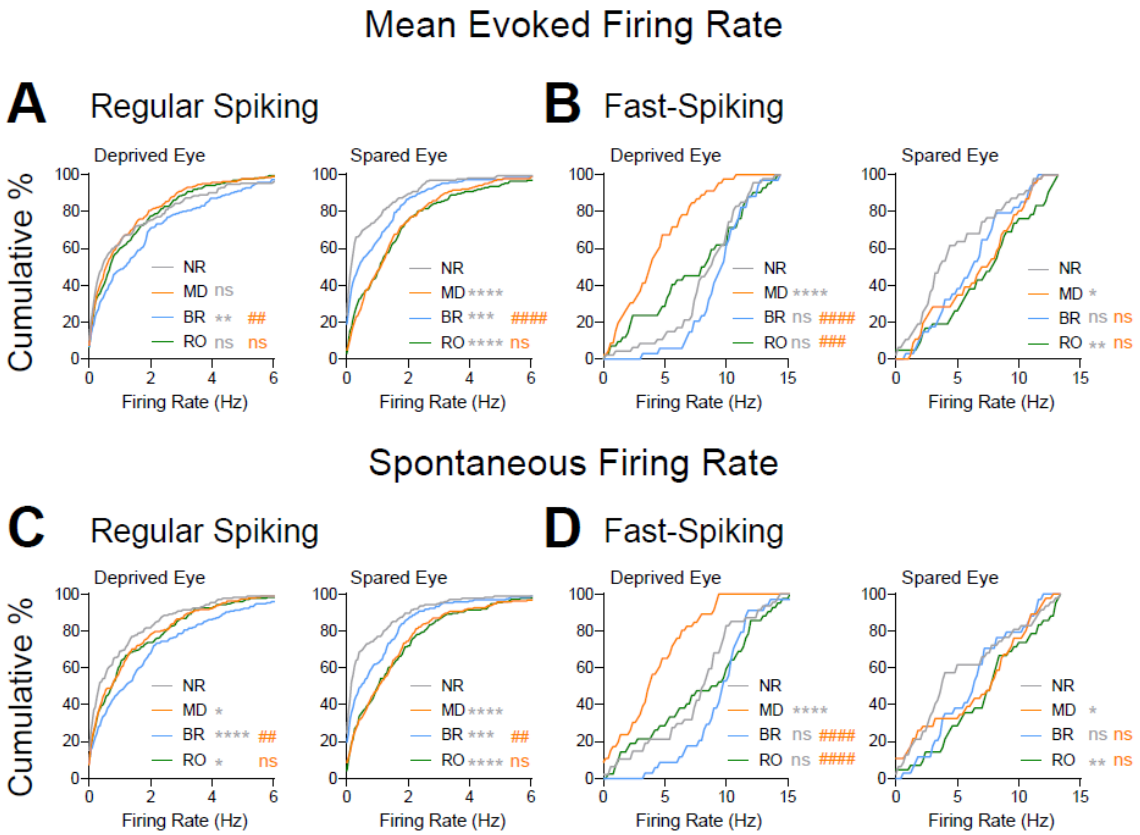

Supplemental Figure 2.1: Mean and spontaneous firing rate changes associated with MD, BR, and RO.

(**A**) Cumulative distributions of DE (left) and SE (right) mean visually-evoked firing rate responses (i.e. across all stimulus orientations) for bV1 RS neurons. DE mean firing responses were unchanged after MD and RO, but increased after BR. MD enhanced SE mean firing responses. This enhancement was unaffected by RO and only partially reversed by BR. **, ***, and **** (gray) indicate $p < 0.01$, $p < 0.001$, and $p < 0.0001$, K-S test vs. NR; ## and #### (orange) indicate $p < 0.01$ and $p < 0.0001$, K-S test vs. MD. (**B**) Cumulative distributions of DE (left) and SE (right) mean visually-evoked firing rates for FS interneurons. DE responses were depressed after MD; this was effect was reversed by both BR and RO. SE responses were enhanced after MD; this effect was partially reversed by BR, but not RO. *, **, and **** (gray) indicate $p < 0.05$, $p < 0.01$, and $p < 0.0001$, K-S test vs. NR; ### and #### (orange) indicate $p < 0.001$ and $p < 0.0001$, K-S test vs. MD. (**C**) Cumulative distributions of RS neurons' DE (left) and SE (right) spontaneous firing rates (during presentation of a blank screen). MD enhanced DE spontaneous firing, and which was further enhanced by BR. *, ***, and *** (gray) indicate $p < 0.05$, $p < 0.001$, and $p < 0.0001$, respectively, K-S test vs. NR; ## (orange) indicates $p < 0.01$, K-S test vs. MD. (**D**) Cumulative distributions of FS neurons' DE (left) and SE (right) spontaneous firing rates. *, **, and *** (gray) indicate $p < 0.05$, $p < 0.01$, and $p < 0.0001$, respectively, K-S test vs. NR; #### (orange) indicates $p < 0.0001$, K-S test vs. MD.

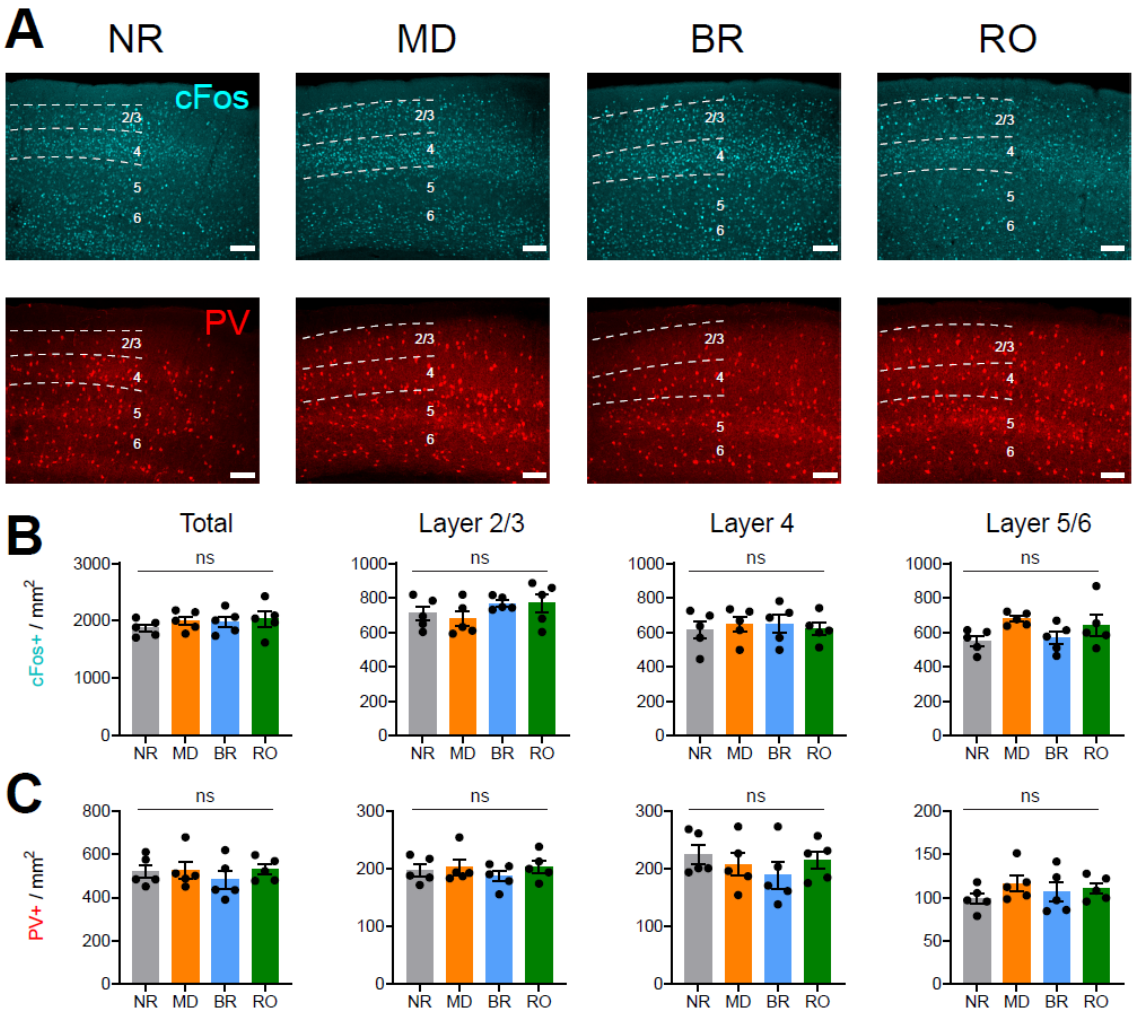

Supplemental Figure 2.2: cFos and PV expression are unchanged in primary auditory cortex (A1) after manipulations of visual experience.

(**A**) Representative images of cFos (cyan) and parvalbumin (PV) [red] expression in A1 for the main treatment groups (n = 5/treatment group). A1 regions were measured in the same brain sections, ipsilateral to bV1 measures (**Figure 4**). (**B**) No changes in cFos expression across NR, MD, and both visual experience groups were observed in total or across cortical layers. One-way ANOVA: F (3, 16) = 0.527, p = 0.669 for total cFos expression. cFos in bV1 layers 2/3, 4, and 5/6. One-way ANOVA for layers 2/3, 4, or 5/6, respectively: F (3, 16) = 1.17, p = 0.349, F (3, 16) = 0.153, p = 0.925, and F (3, 16) = 2.356, p = 0.110. (**C**) No changes in PV+ interneuron density groups were observed in total or across cortical layers. One-way ANOVA: F (3, 16) = 0.3867, p = 0.7641 for total PV+ density. PV+ interneuron density in bV1 layers 2/3, 4, and 5/6. One-way ANOVA for layers 2/3, 4, or 5/6, respectively: F (3, 16) = 0.456, p = 0.716, F (3, 16) = 0.631, p = 0.605, and F (3, 16) = 0.743, p = 0.541. Scale bar = 100 µm.

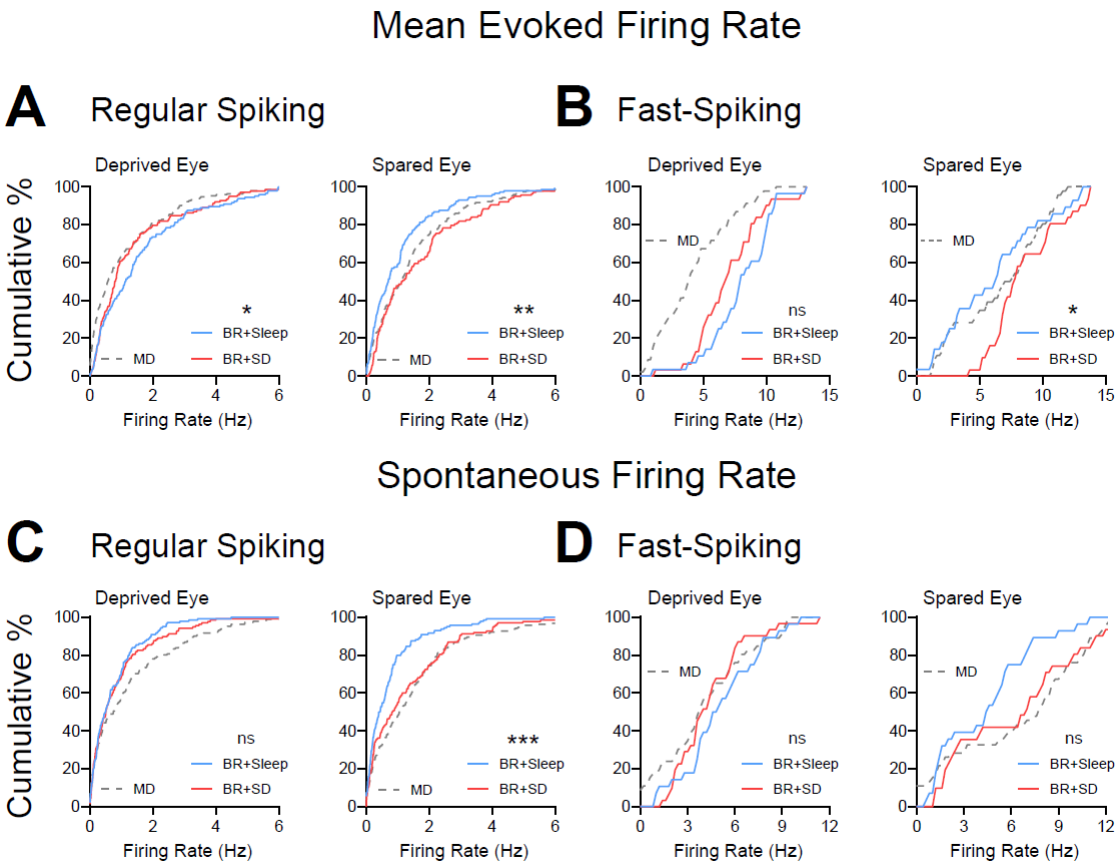

Supplemental Figure 2.3: Mean and spontaneous firing rate comparisons for BR+Sleep and BR+SD groups.

(**A**) Cumulative distributions of DE (left) and SE (right) mean visually-evoked firing rate responses (i.e. across all stimulus orientations) for bV1 RS neurons. Similar to maximal visually-evoked firing at the preferred stimulus orientation (**Fig. 5**) mean DE responses were significantly decreased and SE responses were significantly increased in BR+SD mice, relative to responses recorded from BR+Sleep mice. * and ** indicate $p < 0.05$, and $p < 0.01$, K-S test. (**B**) Cumulative distributions of DE (left) and SE (right) mean visually-evoked firing rate responses (i.e. across all stimulus orientations) for bV1 FS interneurons. No changes in DE responses were observed. SE responses were significantly higher BR+SD mice compared to BR+Sleep counterparts. * indicates $p < 0.05$, K-S test. (**C**) Cumulative distributions of RS neurons' DE (left) and SE (right) spontaneous firing rates (during presentation of a blank screen). While DE spontaneous activity was unaffected, SE spontaneous activity was significantly lower in BR+Sleep mice. *** indicates $p < 0.001$, K-S test. (**D**) FS interneurons' DE (left) and SE (right) spontaneous firing rates (during presentation of a blank screen) did not differ between BR+Sleep and BR+SD condition. Values for the MD-only condition (gray dashed lines) from **Fig. 2** are shown for comparison.

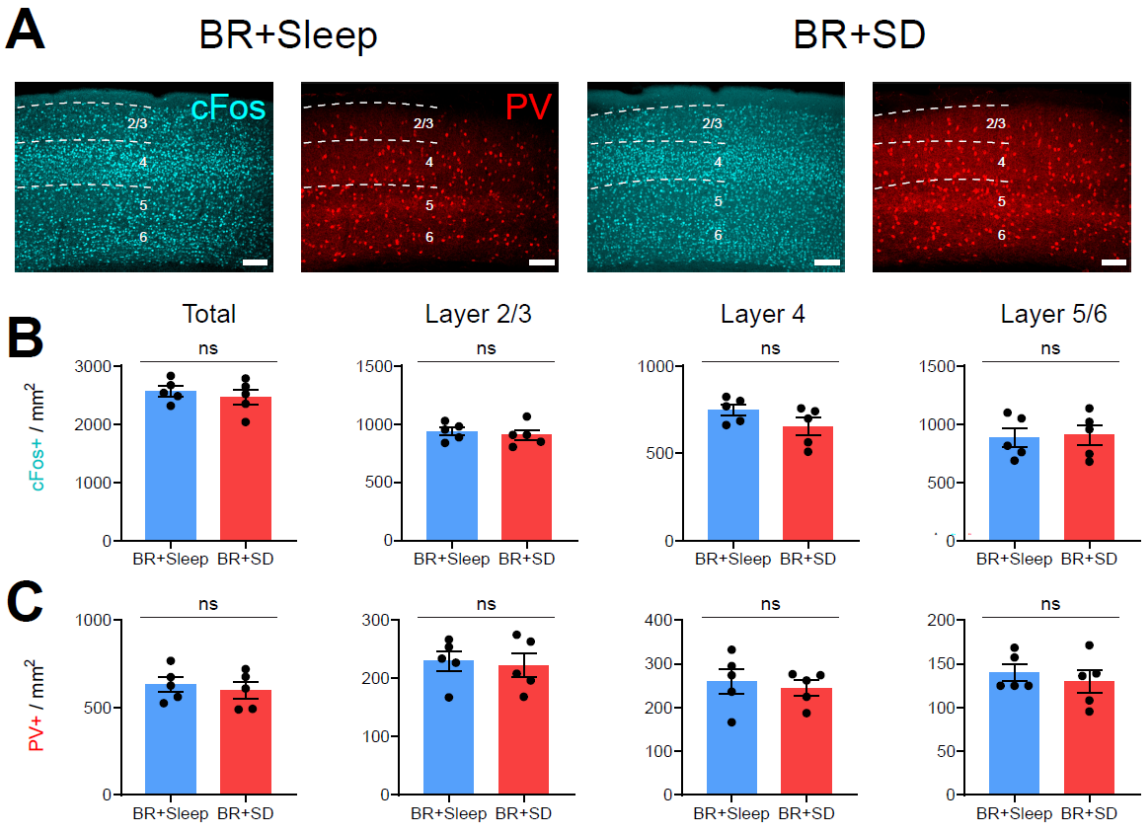

Supplemental Figure 2.4: cFos and PV expression in A1 do not differ between BR+Sleep and BR+SD mice

(**A**) Representative images of A1 cFos (cyan) and parvalbumin (PV) [red] expression in BR+Sleep and BR+SD mice (n = 5/treatment group), from the same brain sections shown in **Fig. 6**, and ipsilateral to measured DE expression in bV1. (**B-C**) No changes in cFos expression or PV+ interneuron density were observed between the groups. cFos expression: p = 0.55 (total), p = 0.59 (layer 2/3), p = 0.15 (layer 4), and p = 0.83 (layer 5/6). PV expression: p = 0.61 (total), p = 0.78 (layer 2/3), p = 0.64 (layer 4), and p = 0.55 (layer 5/6). Unpaired t-test. Scale bar = 100 µm.

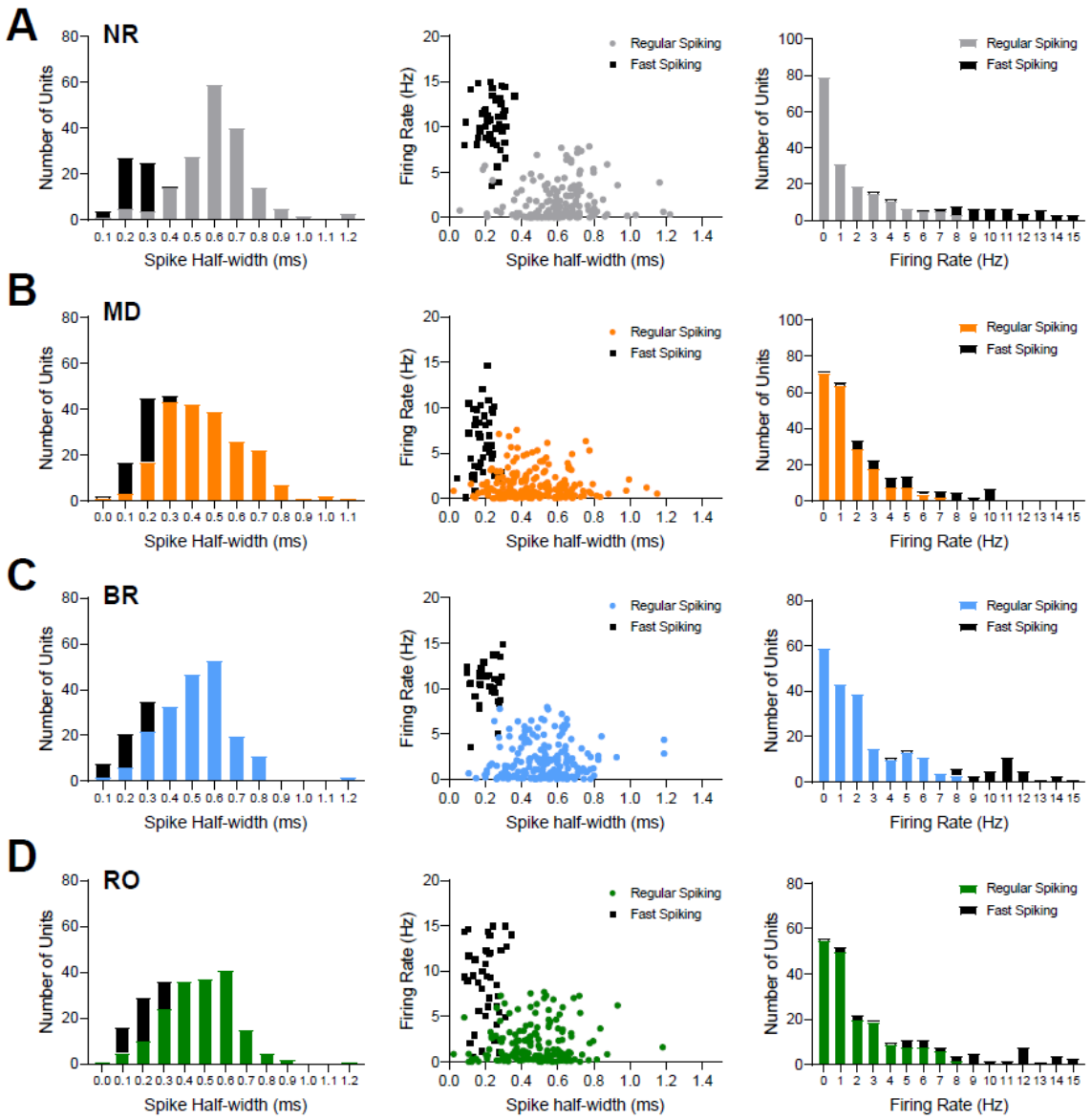

Supplemental Figure 2.5: Spike sorting half-widths for acute recorded mice.

(**A-D**) Left: Distribution of spike half-widths (ms) for all recorded units in Figs. 1-2. Middle: Evoked firing rate of a unit plotted as a function of the cell's spike half-width yielding two distinct populations of cortical cells corresponding to putative, fast-spiking interneurons (squares) and pyramidal, regular-spiking cells (circles). Right: Distribution of all evoked firing rates for all acute recorded units. Fast-spiking units: black for all groups. Regular-spiking units: NR (gray, **A**), MD (orange, **B**), BR (blue, **C**), and RO (green, **D**)

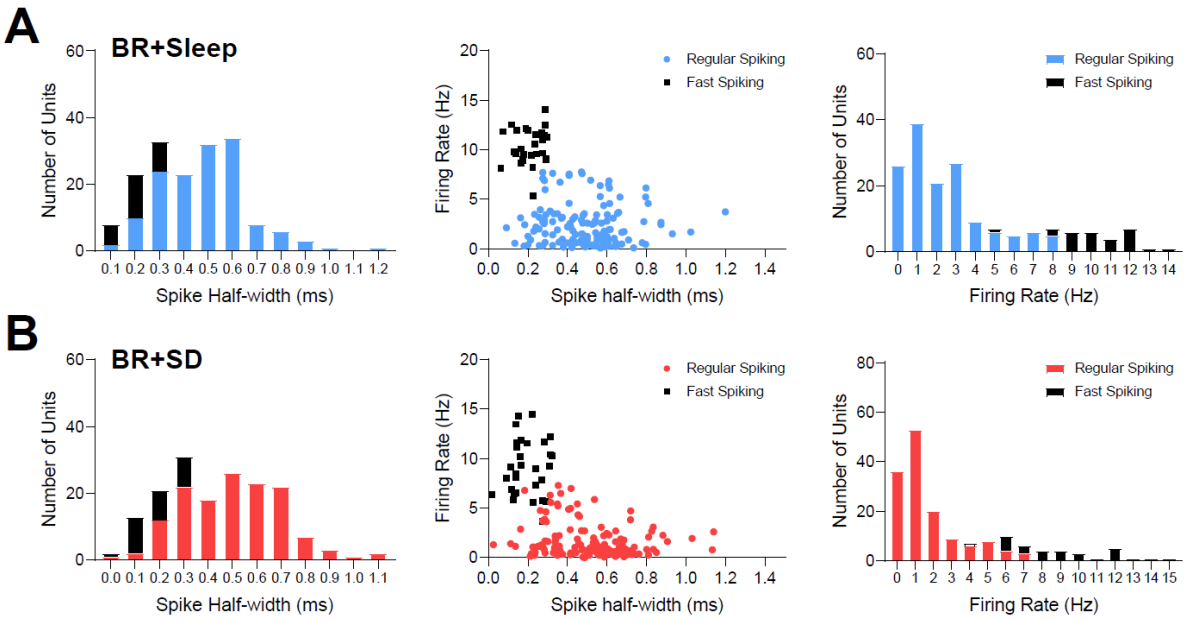

Supplemental Figure 2.6: Spike sorting half-widths for acute recorded mice in BR+sleep and BR+SD mice.

(**A-D**) Left: Distribution of spike half-widths (ms) for all recorded units in Figs. 4-5. Middle: Evoked firing rate of a unit plotted as a function of the cell's spike half-width yielding two distinct populations of cortical cells corresponding to putative, fast-spiking interneurons (squares) and pyramidal, regular-spiking cells (circles). Right: Distribution of all evoked firing rates for all acute recorded units. Fast-spiking units: black for all groups. Regular-spiking units: BR+sleep (blue, **A**), and BR+SD (red, **B**)

Chapter 3：Atypical Hypnotic Compound ML297 Restores Sleep Architecture Immediately Following Emotionally Valenced Learning to Promote Memory Consolidation and Hippocampal Network Activation During Recall

This chapter includes the publication: ***Martinez JD****, Brancaleone WB, Peterson KP, Wilson LG, & Aton SJ. (2022) Atypical hypnotic compound ML297 restores sleep architecture immediately following emotionally valenced learning to promote memory consolidation and hippocampal network activation during recall. Sleep. DOI:10.1093/sleep/zsac301*

3.1 : Abstract

Sleep plays a critical role in consolidating many forms of hippocampus-dependent memory. While various classes of hypnotic drugs have been developed in recent years, it remains unknown whether, or how, some of them affect sleep-dependent memory consolidation mechanisms. We find that ML297, a recently-developed candidate hypnotic agent targeting a new mechanism (activating GIRK1/2-subunit containing G-protein coupled inwardly rectifying potassium [GIRK] channels), alters sleep architecture in mice over the first 6 h following a single-trial learning event. Following contextual fear conditioning (CFC), ML297 reversed post-CFC reductions in NREM sleep spindle power and REM sleep amounts and architecture, renormalizing sleep features to what was observed at baseline, prior to CFC. Renormalization of post-CFC REM sleep latency,

REM sleep amounts, and NREM spindle power were all associated with improved contextual fear memory (CFM) consolidation. We find that improvements in CFM consolidation due to ML297 are sleep-dependent and are associated with increased numbers of highly-activated dentate gyrus (DG), CA1, and CA3 neurons during CFM recall. Together our findings suggest that GIRK1/2 channel activation restores normal sleep architecture - including REM sleep, which is normally suppressed following CFC - and increases the number of hippocampal neurons incorporated into the CFM engram during memory consolidation.

3.2 : Significance Statement

Both REM and NREM sleep are thought to be important for consolidating hippocampus-dependent memories. We find that GIRK1/2 activator ML297, administered after single-trial fear learning, restores REM sleep that is normally suppressed after learning fearful associations. This restoration is associated with improvements in fear memory storage, resulting in more robust hippocampus activation in the context of subsequent memory recall. Thus, this drug, which also has antiepileptic and anxiolytic properties, may be useful for promoting normal, restorative sleep that benefits memory storage.

3.3 : Introduction

Sleep plays an essential role in memory consolidation [1-3]. Available data from both human subjects and animal models have implicated both non-rapid eye movement (NREM) and REM sleep in the process of memory storage. While the underlying mechanisms are still under investigation, these states differ one another, and from wake,

with respect to neuromodulation, neural network oscillatory behavior, neuronal firing patterns, gene expression, and protein translation [2-12]

Sleep loss over the first few hours following training on many hippocampus-dependent tasks leads to long-term memory disruption [1,13,14]. Among these, one of the most well-studied is contextual fear memory (CFM), which is initiated by single-trial contextual fear conditioning (CFC) in mice, and is consolidated in a sleep-dependent manner over the next few hours [6,8,15-17]. During these first few hours following CFC, both NREM and REM sleep are altered [17-21]. Some of these changes, including enhancements in REM theta (4-12 Hz), NREM spindle (7-15 Hz) and NREM sharp wave-ripple oscillations, predict successful CFM consolidation and recall [17-21]. Both CFC and tone-cued fear conditioning also affect sleep architecture in mice, including transiently suppressing REM sleep [22,23]. How REM suppression affects CFM consolidation remains unknown. However, data from analogous studies with human subjects have suggested that post-conditioning REM sleep time, and limbic system brain activation during REM, predicts successful fear memory consolidation [24-26]. Moreover, in mice, theta oscillations present in the dorsal hippocampus during post-CFC REM sleep have been shown to play a causal role in promoting CFM consolidation [17,27]. Optogenetically-driven hippocampal theta activity can even rescue CFM consolidation from the deleterious effects of post-CFC sleep deprivation (SD) [17]. Thus, taken together, available data suggest that limbic system activity and oscillations associated with both NREM and REM sleep contribute to the long-term storage of recently-encoded fear memories.

Hypnotic drug interventions have recently been used as an experimental strategy to test the relationships between sleep, memory consolidation, and synaptic plasticity [28-

[34]. The majority of the hypnotics used in these studies - including benzodiazepines, non-benzodiazepine “z-drugs”, and sodium oxybate - act as positive allosteric modulators of GABAA receptors or as GABAB receptor agonists. These drugs, while effective at promoting NREM sleep, can have unwanted side effects, including over-sedation, electroencephalogram (EEG) anomalies including aberrant oscillations, and memory deficits [28-30,35-37]. Recent work has aimed to develop new classes of hypnotic drugs, including orexin receptor antagonists, melatonin receptor agonists, and most recently, activators of G-protein inward rectifying potassium (GIRK) channels [38-40]. GIRK channels consist of four subunits (1-4 or K_{ir}3.1-3.4), with homo- or hetero-tetrameric compositions that are specific to organs, brain regions, and cell types (e.g. GIRK1/2 channels are selectively expressed in hippocampal neurons, GIRK1/4 channels are present in cardiac myocytes, and GIRK2/3 channels are present in the midbrain) [41-46]. GIRK channel activation is typically associated with G_i-mediated intracellular signaling and itself causes neuronal hyperpolarization, leading to reduced neuronal activity [47,48]. Recent studies have found that the GIRK1/2 subunits can be directly activated independently of G_i signaling using a selective and potent compound known as ML297 [49,50]. Behavioral studies using ML297 in rodents have shown it suppresses seizures, reduces anxiety-like behaviors, and promotes NREM sleep during the circadian active phase (i.e., dark phase) [40,49,51]. However, it remains unclear whether, and how, ML297 affects sleep-dependent memory processing.

To characterize the effects of GIRK1/2 channel activation on post-learning sleep and sleep-dependent memory consolidation, we administered ML297 immediately following CFC and measured changes in post-conditioning sleep architecture. We found

that while post-CFC NREM sleep was unchanged, ML297 administration restored REM sleep in the hours following CFC (renormalizing it to levels seen at baseline), and significantly improved CFM consolidation. This effect was sleep-dependent - i.e., ML297 had no beneficial effect on CFM when administered during post-CFC SD. Finally, we found that post-CFC sleep, and particularly ML297-augmented post-CFC sleep, led to increased hippocampal cFos and Arc expression during CFM recall. Taken together, our data demonstrate that post-CFC REM sleep plays a critical role in CFM consolidation, leading to greater hippocampal activation during recall - and that restoration of normal post-CFC REM sleep by ML297 promotes this process.

3.4 : Materials and Methods

3.4.1 : Animal handling and husbandry

All mouse husbandry, experimental, and surgical procedures were reviewed and approved by the University of Michigan Internal Animal Care and Use Committee (PRO00010245). For all experiments, 4–5-month-old, male C57BL/6J mice (Stock No. 000664, Jackson Labs) were housed under a 12:12h light/dark cycle (lights on at 9 AM) and had *ad lib* access to food and water. Mice were housed with littermates until either EEG implantation surgery or (for non-implanted mice) daily habituation prior to behavioral procedures, at which point they were single housed in standard cages with beneficial environmental enrichment.

3.4.2 : Experimental design and statistical analyses

Male littermates were randomly assigned to treatment groups (n = 5-7 per group) at the time of single housing for EEG implantation or behavioral procedures. Data

analyses were carried out in a blinded manner; in some cases (e.g., for EEG recordings), data were consensus scored by 2 individuals in order to reduce variability. Statistical analyses were carried out using GraphPad Prism software (Version 9.1). For each specific data set, the statistical tests and p-values used are listed in the “Results” section and in corresponding figures and figure legends.

3.4.3 : Surgical procedures and EEG recording

For EEG experiments, mice underwent surgical procedures for implantation of electroencephalogram (EEG) and electromyogram (EMG) electrodes. Briefly, mice were anesthetized with 1-2% isoflurane. Stainless steel screw electrodes for EEG recording and referencing were positioned over primary visual cortex (2.9 mm posterior to Bregma, 2.7 mm lateral) bilaterally and cerebellum, respectively, and a braided stainless steel wire EMG electrode was placed in the nuchal muscle. After 11 days of postoperative recovery, each mouse underwent 3 days of habituation to daily handling (5 min/day) and tethering to recording cables in their home cage. Following habituation, 24-h baseline recordings were made from each mouse, starting at lights-on (ZT0). Subsequently, for studies of sleep-dependent memory consolidation, mice underwent CFC training at lights on (ZT0) the following day, and were recorded for an additional 24 h thereafter. EEG/EMG signals (0.5-300 Hz) were amplified at 20 ×, digitized, further digitally amplified at 20-100 ×, and continuously recorded (with a 60-Hz notch filter) using Plexon Omniplex software and hardware (Plexon Inc.) as previously described [17,19,52,53].

3.4.4 : Sleep state and power spectra analysis

Baseline and post-CFC recordings were scored in 10-second epochs as wake, NREM, or REM sleep using custom MATLAB software. EEG and EMG data were band-pass filtered at 0-90 Hz and 150-250 Hz, respectively, for viewing during scoring. Raw EEG data (0.5-300 Hz) were used for fast-Fourier transform and generation of power spectral density from 0.5 to 20 Hz using NeuroExplorer 5 software (Plexon Inc.). An automated spindle detection algorithm was used to identify sleep spindles in band-pass filtered EEG data (7-15 Hz), as intervals containing ≥ 6 successive deviations (i.e., peaks or troughs) of signal that surpassed mean signal amplitude by 1.5 standard deviations, lasting between 0.25-1.75 seconds [52].

3.4.5 : CFC, drug administration, sleep monitoring, and sleep deprivation

Mice underwent single-trial CFC as previously described [6,8,17-19]. Each mouse was placed in a novel cylindrical conditioning chamber made of clear Plexiglas with a metal grid floor and distal cues (Med Associates). Mice were allowed to freely explore for 2 min and 28 s, after which they received a 0.75 mA, 2-s foot shock through the grid floor, followed by an additional 30 s in the CFC chamber. Immediately following CFC, mice were returned to their home cage and given an i.p. injection of either ML297 (30 mg/kg; Tocris) or vehicle (2% DMSO in 0.5% hydrooxypropyl cellulose aqueous solution). Injections occurred within 5 min of removal from the CFC chamber. CFM tests were conducted 24 h later by returning mice to the CFC chamber for 5 min. Mice were video monitored continuously during both CFC training and CFM testing, and both freezing behavior and time-in-location (**Supplemental Figure 3.1, Supplemental Figure 3.8**) within the CFC chamber was quantified in a semi-automated manner using Ethovision XT 16 software (Noldus). Freezing was first scored based transient periods of immobility, as

described previously [54], and was verified offline based on assessment of characteristic freezing-associated posture [17,53]. CFM-associated freezing behavior was quantified by subtracting each mouse's % freezing time during pre-shock baseline from % freezing time across the entire CFM test, as described previously [6,17,19].

Following CFC, mice were either allowed *ad lib* sleep (Sleep) or were sleep-deprived (SD) via gentle handing over the next 6 h (ZT0-6). This method of SD was chosen based on prior work showing that stress response (e.g. glucocorticoid production) evoked by gentle handling SD is not sufficient to disrupt consolidation of fear memory (and in fact may enhance consolidation) [55-57]. Following SD, all mice were allowed ad lib recovery sleep over the next 18 h prior to CFM testing. For mice without EEG/EMG implants, sleep was quantified over the first 6 h post-CFC via visual monitoring. Every 5 min, individual mice were scored as awake or asleep, with sleep identification based on immobility, slow breathing, and presence of stereotyped (crouched) sleep postures, consistent with prior studies. For SD, gentle handling procedures included cage tapping or shaking, or nest disturbance [4,6,7,58]. EEG/EMG-based validation of both the visual sleep scoring method, and SD methodology, are shown in **Supplemental Figure 3.7**.

3.4.6 : Histology and immunohistochemistry

To quantify hippocampal activation patterns associated with recall, 90 min following the conclusion of CFM tests, mice were euthanized with an overdose of sodium pentobarbital and perfused with ice cold PBS, followed by ice cold 4% paraformaldehyde. Brains were dissected, post-fixed, and cryoprotected in a 30% sucrose solution. 50 µm coronal dorsal hippocampal sections were immunostained using rabbit-anti-cFos (1:1000; Abcam, ab190289) and guinea pig-anti-Arc (1:500; Synaptic Systems, 156004) as

markers of neuronal activation. Secondary antibodies used included Alexa Fluor 488 (1:200; Invitrogen, A11032) and Alexa Fluor 594 (1:200; Invitrogen, A11034). Stained sections were mounted using Prolong Gold antifade reagent with DAPI (Invitrogen, P36931) and imaged using a Leica SP8 confocal microscope with a 10X objective, to obtain z-stack images (10 μm steps) for maximum projection of fluorescence signals. Identical image acquisition settings (e.g. exposure times, frame average, pixel size) were used for all sections.

For analysis of hippocampal activation patterns, three images of dorsal hippocampus were taken per mouse and equally sized regions of interest (ROIs) for DG, CA1 and CA3 regions were obtained for each image. cFos+ and Arc+ neurons were identified and quantified in subregions of these ROIs (i.e., pyramidal or granule cell layers, DG hilus) by a scorer blinded to animal condition, using ImageJ software. For Arc expression in pyramidal cell layers of CA1 and CA3, mean fluorescent intensity (MFI) was measured by adaptive thresholding of fluorescent signals and subtracting the fluorescence intensity of each region from mean background fluorescence [4].

3.5 : Results

3.5.1 : GIRK channel activation renormalizes REM sleep architecture in the hours immediately following CFC and improves CFM consolidation

To test how GIRK1/2 channel activation affects post-CFC sleep and sleep-dependent CFM consolidation, we recorded ML297-induced changes in sleep architecture and EEG activity following CFC (**Figure 3.1, Figure 3.2**). 4-5 month old, male C57BL/6J mice underwent continuous 24-h baseline EEG/EMG recording starting at lights-on (ZT0), followed by single-trial CFC at ZT0 the following day. Immediately

following CFC, mice were administered either vehicle or ML297 (30 mg/kg, i.p.), and underwent EEG recording for an additional 24 h prior to CFM testing at ZT0 on the third day (**Figure 3.1A**). Automated scoring during CFC and CFM testing was used to quantify both CFC- and CFM-associated freezing behavior (**Figure 3.1B**). Representative heat maps showing time spent at different locations within the conditioning chamber during training and testing can be seen in **Supplemental Figure 3.1**. During initial training (prior to foot shock), vehicle and ML297 groups showed comparable, low levels of freezing behavior (two-tailed, unpaired t-test; $p = 0.2663$; t, df = 1.177, 10). During the post-shock period of CFC, freezing amounts were likewise comparable between vehicle and ML297 groups (two-tailed, unpaired t-test; $p = 0.8990$; t, df = 0.1419, 10), suggesting similar initial behavioral responses during encoding. However, during CFM testing (i.e., recall), both total freezing (two-tailed, unpaired t-test; $p = 0.0141$; t, df = 2.969, 10) and the change in freezing from pre-shock values (two-tailed, unpaired t-test; $p = 0.0101$; t, df = 3.162, 10), were higher in ML297-treated mice than vehicle-treated controls (**Figure 3.1B**). This suggests that CFM consolidation was improved by post-CFC administration of ML297.

To test whether enhanced CFM consolidation following ML297 administration correlated with differences in sleep architecture, we first compared baseline vs. post-CFC sleep amounts between vehicle and ML297 groups. Vehicle and ML297 groups showed similar NREM, REM, and wake amounts across the 24-hour baseline recording period (**Figure 3.1C-D, Supplemental Figure 3.2A-B, Supplemental Figure 3.3A, Supplemental Figure 3.4A,C**), as well as similar NREM sleep amounts over the next 24 h post-CFC (two-way repeated measures (RM) ANOVA; p(time of day x treatment) = 0.8121; $F(11, 110 = 0.6157)$; **Figure 3.1E**). Wake amounts post-CFC were similar as well

(two-way RM ANOVA; p(time of day x treatment) = 0.7915; F(1,110) = 0.6394; **Supplemental Figure 3.3B**). However, ML297 significantly altered the time course of REM sleep following CFC (two-way RM ANOVA; p(time of day x treatment) = <0.0001; F(11,110) = 4.209; **Figure 3.1F**). This was observed as increased REM sleep amounts over the first 6 h following CFC in ML297-treated mice (two-way RM ANOVA; p(time of day x treatment) = 0.0006; F(11,10 = 24.26); Sidak's *post hoc* test for vehicle vs. ML297, p = 0.0226; **Figure 3.1F**), and reduced REM sleep amount (relative to vehicle-treated controls) over the latter 6 h of the light phase (ZT6-12; Sidak's *post hoc* test for vehicle vs. ML297, p = 0.0045; **Figure 3.1F**). CFC reduced REM sleep during the first 6 h post-CFC (relative to baseline) in vehicle-treated mice (two-way RM ANOVA; p(time of day x treatment) = 0.0003; F(1,10 = 30.57)), consistent with previous findings [22,23]. ML297 reversed this effect over ZT0-6 by increasing REM sleep during this same time period (Sidak's *post hoc* test for vehicle vs. ML297, p = 0.0004; **Figure 3.1D, F-G**). ML297 did not affect the proportion of time spent in NREM at any timepoint compared with vehicle (two-way RM ANOVA; p(time of day x treatment) = 0.1657; F(1,10 = 2.236)), the change in NREM amounts from baseline following CFC (two-way RM ANOVA; p(time of day x treatment) = 0.0749; F(1,10 = 3.953); **Figure 3.1C, E, G**), or the proportion of time spent in NREM or REM during the dark phase following CFC (ZT12-24) (**Supplemental Figure 3.2C-D**). Critically, freezing behavior at CFM recall was positively correlated with the proportion of time spent in REM sleep over the first 6 h post-CFC (Pearson correlation coefficient, R = 0.6319; p = 0.0275), but negatively correlated with REM amounts over the subsequent 6 h (i.e., ZT6-12; Pearson correlation coefficient, R = -0.6550, p = 0.0208; **Figure 3.1H**).

We also quantified how CFC and ML297 affected other features of sleep architecture, including NREM and REM bout durations and bout numbers. These aspects of NREM and REM sleep were similar at baseline between the vehicle and ML297 groups (**Figure 3.2A-B, E-F**). Following CFC, both vehicle and ML297 groups had comparable NREM bout duration (two-way RM ANOVA; p(time of day x treatment) = 0.4974; F(11,110 = 0.9487); **Figure 3.2C**) and bout numbers (two-way RM ANOVA; p(time of day x treatment) = 0.6252; F(11,110 = 0.8149); **Figure 3.2D**). In contrast, over the first 6 h post-CFC, ML297-treated mice showed significantly increased REM sleep bout durations compared to vehicle-treated counterparts (two-way RM ANOVA; p(time of day x treatment) = 0.0245; F(1,10 = 6.994); Sidak's *post hoc* test for vehicle vs. ML297, p = 0.0003; **Figure 3.2G**) and bout numbers (two-way RM ANOVA; p(time of day x treatment) = 0.0016; F(1,10 = 18.39); Sidak's *post hoc* test, p = 0.0267; **Figure 3.2H**). Group differences in wake bout duration or number were not observed, either at baseline or post-CFC (**Supplemental Figure 3.4**). In the hours immediately following CFC, vehicle-treated mice showed both reduced REM bout duration and number (relative to baseline); ML297 restored REM bout numbers to baseline levels during this same period (Sidak's *post hoc* test for vehicle vs. ML297, p = 0.0019; **Figure 3.2I**). Finally, latency to the first bout of post-CFC REM sleep (but not NREM sleep) was significantly reduced in mice administered ML297 (two-way RM ANOVA; p(sleep state x treatment) = 0.0052; F(1,10 = 12.67); Sidak's *post hoc* test for vehicle vs. ML297, p = 0.0001; **Figure 3.2J**). Reduced latency to REM following CFC also predicted successful CFM recall the following day, with mice with the shortest latency to REM showing the highest levels of freezing (Pearson correlation coefficient, R = -0.7924, p = 0.0021; **Figure 3.2J**).

Taken together, these data suggest that ML297-mediated GIRK channel activation may improve CFM consolidation through a restorative increase in REM sleep over the first few hours following CFC. Thus, ML297 treatment has the effect of renormalizing REM sleep architecture, to offset suppression of REM that typically occurs after CFC and other fear-associated learning [59].

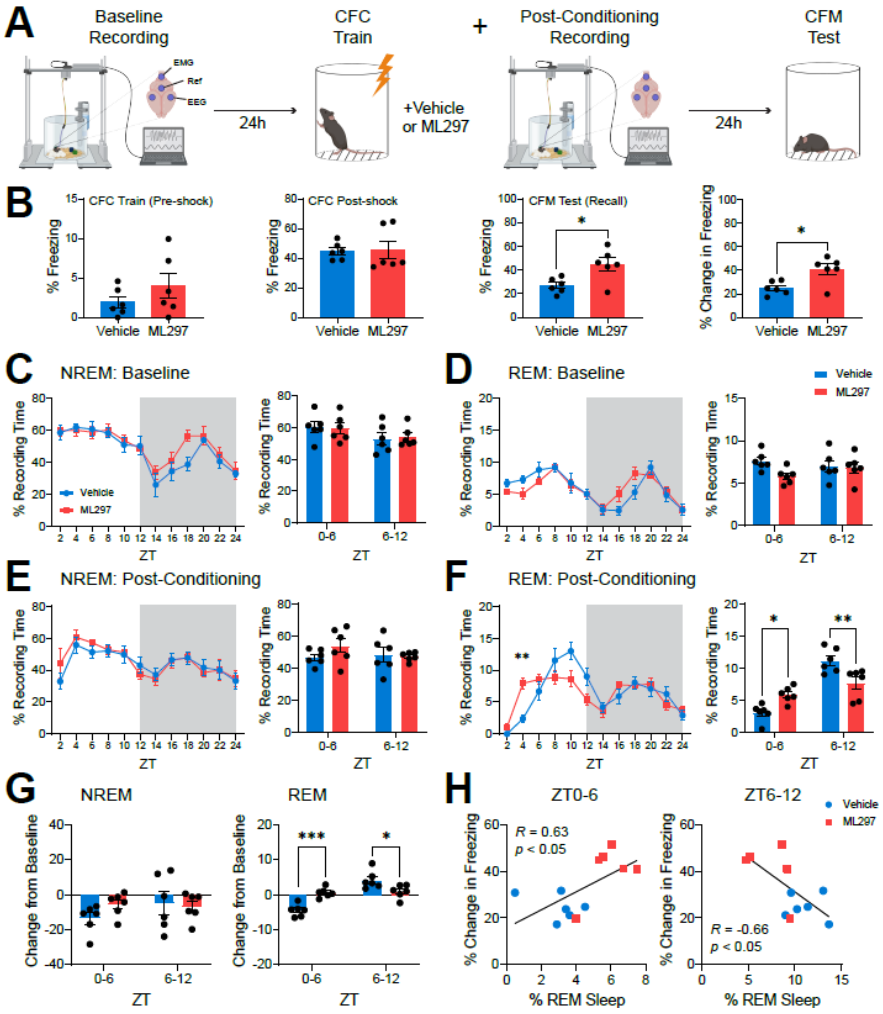

Figure 3.1: GIRK1/2 activation restores REM sleep amounts during the first few hours of fear memory consolidation and improves fear memory recall.

(**A**) Configuration of EEG electrodes for sleep recording and schematic of experimental design. Mice were recorded over a 24-h baseline starting at lights-on (ZT0), then underwent single-trial contextual fear conditioning (CFC) followed by an i.p. injection of vehicle or GIRK1/2 activator ML297 (30 mg/kg). Each mouse was recorded for an additional 24 h prior to being tested for contextual fear memory (CFM). (**B**) During CFC training mice in the two groups displayed similar freezing behavior. During CFM testing, freezing behavior was significantly greater in ML297-treated mice. Bars indicate mean ± SEM; n = 6 mice/group; * indicates p = 0.0141 (total freezing during recall), * indicates p = 0.0101 (change in freezing from pre-shock period during CFC), two-tailed, unpaired t-test. (**C**) NREM and (**D**) REM sleep behavior during baseline across the light:dark cycle for vehicle- and ML297-treated mice. Gray shaded areas represent lights off. No changes seen in time spent in NREM or REM sleep across the light:dark cycle nor in total NREM or REM sleep across 6 h quartiles. n = 6 mice/group. (**E-F**) Sleep behavior post-conditioning across the light:dark cycle for vehicle- and ML297-treated mice. Gray shaded areas represent lights off. No changes seen in time spent in NREM across the light:dark cycle. Time spent in REM sleep was significantly altered during the light cycle. REM sleep is significantly increased 3-4 hours post-treatment of ML297 compared to vehicle controls at this same time point. Values indicate mean ± SEM; n = 6 mice/group; ** indicates p = 0.0057, Sidak's post hoc test vs. vehicle. ML297 reorganized sleep to show significantly more total REM sleep during ZT0-6 and significantly less total REM sleep during ZT6-12. Sidak's post hoc test vs. vehicle. * indicates p = 0.0226 (ZT0-6) and p = 0.0045 (ZT6-12), Sidak's post hoc test vs. vehicle. (**G**) Compared to baseline, REM sleep in the first 6 h post-CFC was more suppressed in vehicle-treated vs. ML297-treated mice, while significantly promoted during the last 6 h post-CFC. *** and * indicates p = 0.0004 (ZT0-6) and p = 0.0169 (ZT6-12), respectively, Sidak's post hoc test vs. vehicle. (**H**) Correlation between freezing behavior and % time spent in REM sleep in the first 6 h post CFC and last 6 h post CFC of the light cycle. *R* and *p* values are shown for Pearson correlation.

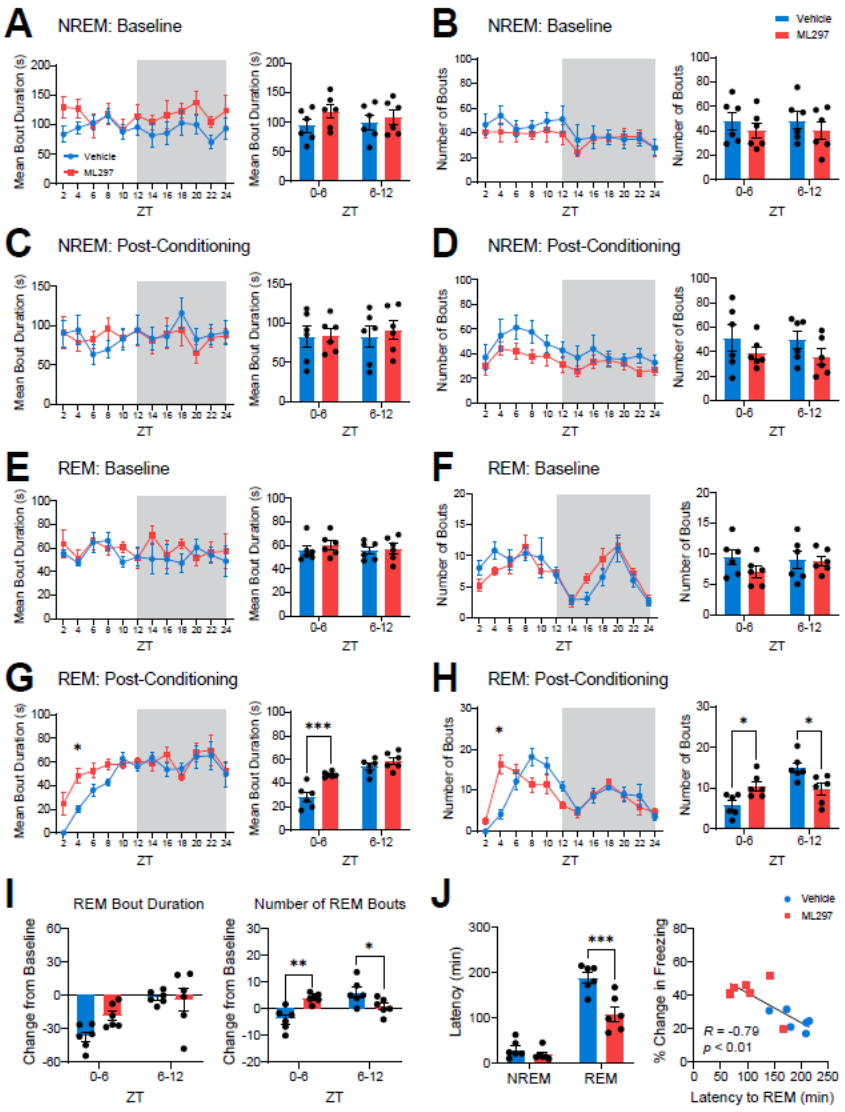

Figure 3.2: ML297 REM sleep architecture is promoted during post-conditioning with GIRK channel activation.

(**A**) Mean bout duration and (**B**) number of bouts for NREM sleep over the 24 h during baseline in vehicle and ML297 groups were similar. (**C**) Mean bout duration and (**D**) number of bouts for NREM sleep over the 24 h post-CFC in vehicle- and ML297-treated mice were similar. (**E**) Mean bout duration and (**F**) bout numbers for REM sleep over the 24 h during baseline in vehicle and ML297 groups were similar. (**G**) Mean bout duration and (**H**) bout numbers for REM sleep over the 24 h post-CFC in vehicle- and ML297 treated mice. * indicates $p = 0.0400$ (REM bout duration), $p = 0.0177$ (number of REM bouts), Sidak's *post hoc* test vs. vehicle. Values indicate mean ± SEM. (**G**) REM mean bout durations and (**H**) bout numbers are shown for hours 0-6 and 6-12 post-CFC. ML297-treated mice show longer REM bout durations during ZT0-6. ** indicates $p = 0.0003$, Sidak's *post hoc* test vs. vehicle. ML297-treated mice show a greater number of REM sleep bouts during ZT0-6 and a reduced number of REM sleep bouts during ZT6-12. * indicates $p = 0.0267$ (ZT0-6), $p = 0.0123$ (ZT6-12), Sidak's *post hoc* test vs. vehicle. (**I**) Post-CFC changes in REM mean bout duration (*left*) and number (*right*) from time-matched baseline values. ML297 administration led to a relative increase in the number of REM sleep bouts in the first 6 h post-CFC, and a decrease in bouts in the last half of the light cycle. ** indicates $p = 0.0019$ (ZT0-6) and * indicates $p = 0.0419$ (ZT6-12), Sidak's *post hoc* test vs. vehicle. (**J**) ML297-treated mice showed decreased latency to REM sleep (but unchanged latency to NREM sleep) after CFC (*** indicates $p = 0.0001$, Sidak's *post hoc* test vs. vehicle). Shorter REM latency predicted successful CFM consolidation. R and p values are shown for Pearson correlation. $n = 6$ mice/group

3.5.2 : ML297 administration alters NREM and REM EEG oscillations in a manner consistent with renormalizing sleep architecture

We next assessed how NREM- and REM-associated EEG oscillations are affected by ML297 administration. We found that at baseline, vehicle and ML297 groups showed no EEG spectral power differences in either NREM or REM sleep (**Figure 3.3A, C**). Following CFC, vehicle- and ML297-treated mice showed NREM spectral power differences (two-way RM ANOVA; p(frequency x treatment) < 0.0001; F(78, 1343 = 3.643)) with vehicle-treated mice having a greater proportion of total EEG power in the NREM delta (0.5-4 Hz) band (**Figure 3.3B**). Post-CFC REM EEG spectra also differed between groups, with ML297-treated mice having greater proportional spectral power in the theta (4-12 Hz) band (two-way RM ANOVA; p(frequency x treatment) < 0.0001; F(78, 869 = 2.349), Sidak's *post hoc* test for vehicle vs. ML297, p = 0.001; **Figure 3.3D**). We assessed the change in power from baseline in both vehicle and ML297 groups during post-CFC NREM and REM sleep. We found changes in NREM delta (two-way RM ANOVA; p(frequency x treatment) < 0.0001; F(78, 1343 = 5.290)) and REM theta (two-way RM ANOVA; p(frequency x treatment) < 0.0001; F(78, 869 = 4.082)), during ZT0-6 and ZT2-6, respectively (**Figure 3.3E-F**). No differences were observed for NREM- or REM-associated EEG oscillations between groups during the dark phase (**Supplemental Figure 3.5**).

Because ML297 promoted REM sleep during the first few hours post-CFC, and caused relative decrease in NREM delta power, we also assessed the effects of both CFC and ML297 on NREM sleep spindles - waxing-and-waning, discrete EEG oscillations with a peak frequency of 7-15 Hz. Spindles are: 1) inversely related to NREM delta power

[60-62], 2) implicated in CFM consolidation [21,63], and 3) critical for transitions between NREM and REM sleep [64,65]. To test whether alterations in REM sleep architecture after ML297 administration were associated with changes in NREM spindles, we next detected these events in a semi-automated manner [52] and compared post-CFC spindle characteristics between groups. Both at baseline, and following CFC, neither spindle density (two-way RM ANOVA; p(time of day x treatment) = 0.7795; F(5, 50 = 0.4935)) nor duration (two-way RM ANOVA; p(time of day x treatment) = 0.7784; F(5, 50 = 0.4951)) differed significantly between ML297- and vehicle-treated mice (**Figure 3.4A-B, D-E**). Spindle power during baseline NREM sleep was similar between the two groups and relatively invariant across the entire light phase (ZT0-12; **Figure 3.4C**). However, in the first few hours following CFC, the proportion of total NREM EEG spectral power in the spindle (i.e., sigma) band was significantly higher in ML297-treated vs. vehicle-treated mice (two-way RM ANOVA; p(time of day x treatment) = 0.0211; F(5, 50 = 2.938); **Figure 3.4E**). This difference appeared to reflect suppressed spindle power (relative to baseline) in vehicle-treated mice over the first 4 h of post-CFC NREM sleep, which was reversed by ML297 (Sidak's *post hoc* test for vehicle vs. ML297 at ZT0-2 and 2-4, p = 0.0223 and p = 0.0424). This difference in spindle power between the groups following CFC is consistent with both the relative increases in NREM EEG delta power, and the overall suppression of REM, following conditioning in vehicle-treated (but not ML297-treated) mice. Intriguingly, this difference in spindle power continued into the subsequent dark phase (ZT12-24) (two-way RM ANOVA; p(time of day x treatment) = 0.0300; F(5, 50 = 2.718); **Supplemental Figure 3.6**). Together, our EEG data suggest that administration of GIRK channel activator ML297 following CFC modestly augments REM theta, and renormalizes

NREM delta/spindle ratios, in a manner consistent with its renormalization of sleep architecture. Because these EEG oscillatory changes are similar to those known to be associated with successful sleep-dependent CFM consolidation [17,19,21], they are consistent with state-dependent hippocampal oscillations serving as a potential driver of memory enhancement by ML297 [2,3].

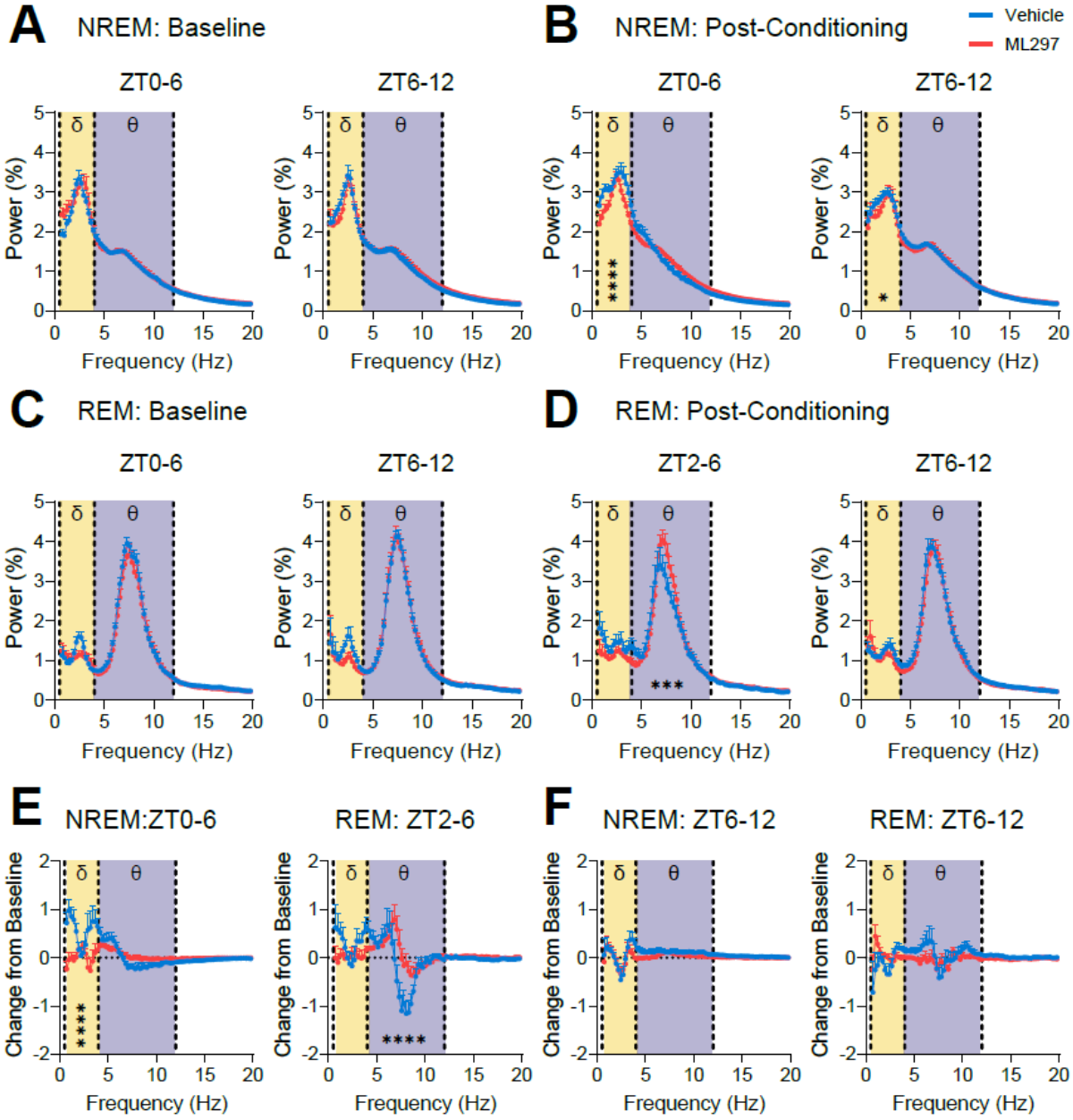

Figure 3.3: ML297 has modest effects on overall NREM and REM EEG spectral power.

EEG power spectra (recorded over visual cortex, bilaterally) are shown for vehicle- and ML297-treated mice during NREM baseline (**A**) and post-CFC (**B**), and during REM baseline (**C**) and post-CFC (**D**). Values indicate % of total spectral power at each frequency band, mean ± SEM; *n* = 6 mice/group. For (**B**), **** and * indicate post-CFC differences in NREM delta frequency bands at ZT0-6 and 6-12, respectively, $p \leq 0.0001$ for 2.9-3.9 Hz and $p < 0.05$ for 1.4-1.7 Hz, respectively, Sidak's *post hoc* test vs. vehicle. For (**D**), *** indicates post-CFC differences in REM at ZT2-6, $p < 0.001$ for 7.1-8.1 Hz, Sidak's *post hoc* test vs. vehicle. Values indicate mean ± SEM; *n* = 6 mice/group. (**E**) Comparisons of changes in spectral power from baseline showed significant differences in NREM delta frequency bands from 0.7-1.9 and 2.9-3.9 Hz ($p < 0.0001$, Sidak's *post hoc* test) at ZT0-6 and REM theta frequency bands 6.8-8.3 Hz ($p < 0.0001$, Sidak's *post hoc* test) at ZT2-6. (**F**) Over the following 6 h of the light phase (ZT6-12) no changes in spectral power from baseline were observed in either NREM or REM.
were observed in either NREM or REM.

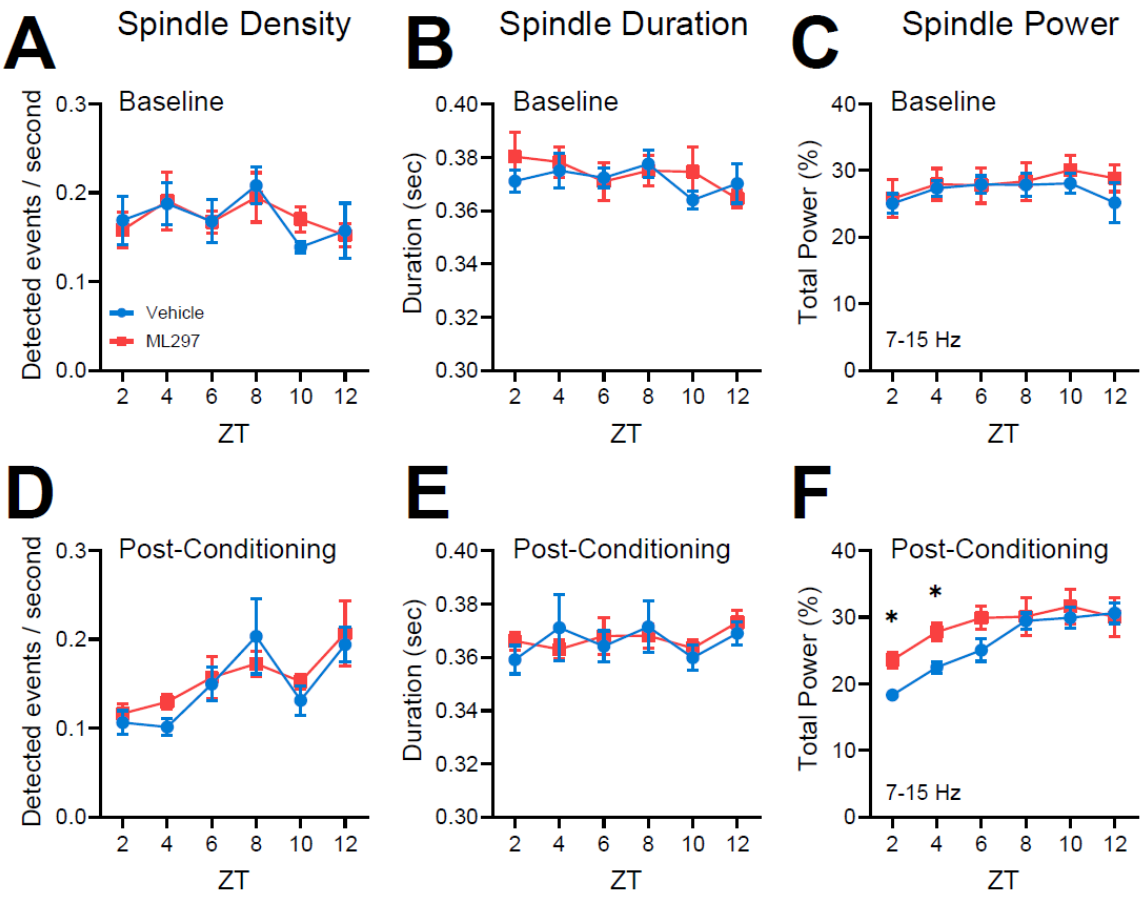

Figure 3.4: ML297 normalizes NREM sleep spindle power in the hours following CFC.

NREM spindle density (**A**) and mean duration (**B**) were similar between vehicle and ML297 groups for hours 0-12 during baseline. (**C**) NREM EEG spectral power within the spindle/sigma frequency band (7-15 Hz) was similar between groups at baseline. NREM spindle density (**D**) and mean duration (**E**) were similar between both vehicle- and ML297-treated mice following CFC. (**F**) Over the first 4 h following CFC, NREM spindle power was higher in ML297-treated mice relative to vehicle-treated mice. * indicates $p < 0.05$, Sidak's *post hoc* test. Values indicate mean ± SEM; $n = 6$ mice/group.

3.5.3 : ML297 effects on CFM consolidation are sleep-dependent

Because ML297 restores REM sleep architecture and NREM oscillations during a critical time window for CFM consolidation, we next tested whether ML297-mediated improvement in CFM was sleep-dependent, or due to other effects of GIRK activation. In a second cohort of non-instrumented mice, we tested whether post-CFC SD interfered with ML297-driven improvements in CFM consolidation. At lights-on, mice underwent single-trial CFC training and were immediately administered either vehicle or ML297. Over the next 6 h, mice in each treatment group were either allowed *ad lib* sleep (and visually monitored for changes in sleep amount) or underwent gentle-handling SD in their home cage (which is sufficient to disrupt CFM consolidation) [6,17]. To further validate this approach, we compared the sleep architecture based on EEG/EMG recordings and visual scoring in the same cohort of mice. We found no difference in total sleep time measured using EEG analysis vs. visual observations (**Supplemental Figure 3.7A-C**). EEG measurements in SD mice indicated that gentle handling led to 90% of the 6-h SD period spent in wake, with minimal NREM bouts and no REM sleep (**Supplemental Figure 3.7D**). Over the course of SD, mice underwent a progressively increasing number of experimenter interventions to prevent sleep, as predicted based on accumulating homeostatic sleep drive (**Supplemental Figure 3.7E**).

CFM recall was tested for all mice 24 h after training (**Figure 3.5A**). The total time spent asleep over the first 6 h following CFC was similar for the two freely-sleeping groups, with no significant effect of ML297 on total sleep time (two-tailed, unpaired t-test; $p = 0.4077$; t, df = 0.8684, 9) (**Figure 3.5B**). Mice were video monitored during both CFC and CFM recall testing; representative heat maps showing time-in-location within the CFC

chamber during training and testing can be seen in **Supplemental Figure 3.8**. As expected, during CFC training, freezing behavior was similar between groups during both pre-shock (two-way ANOVA; p(treatment) = 0.9848; F(1, 20 = 0.3134); p(sleep condition) = 0.0669; F(1, 20 = 3.754)) and post-shock (two-way ANOVA; p(treatment) = 0.4845; F(1, 20 = 0.5075); p(sleep condition) = 0.0803; F(1, 20 = 3.394)) intervals (**Figure 3.5C**). 24 h after CFC, mice were returned to the CFC chamber to test CFM recall. There were significant effects of both prior sleep condition and drug treatment on freezing during recall (two-way ANOVA; p(treatment) = 0.00213; F(1, 20 = 14.03); p(sleep condition) < 0.0001; F(1, 20 = 39.71)), and on the change in freezing between recall and training (two-way ANOVA; p(treatment) = 0.0022; F(1, 20 = 12.29); p(sleep condition) < 0.0001; F(1, 20 = 31.07), **Figure 3.5C**). As expected, freely-sleeping vehicle-treated mice had superior CFM comparted to vehicle-treated SD mice (Tukey's *post hoc* test, p = 0.0140) (**Figure 3.5C**). Freely-sleeping ML297-treated mice showed stronger CFM than all other groups tested (Tukey's *post hoc* test vs. Sleep+ML297: Sleep+Vehicle, p = 0.0423, SD+Vehicle, p < 0.0001, and SD+ML297, p = 0.0012). However, SD disrupted CFM consolidation regardless of ML297 treatment - i.e., there was no effect of ML297 when mice were sleep deprived (Tukey's *post hoc* test for vehicle vs. ML297 in the SD condition, *NS*). These findings support the conclusion that sleep is required for ML297-mediated improvements in CFM consolidation. Together, these data suggest that GIRK1/2 channel activation promotes memory consolidation via sleep-dependent mechanisms.

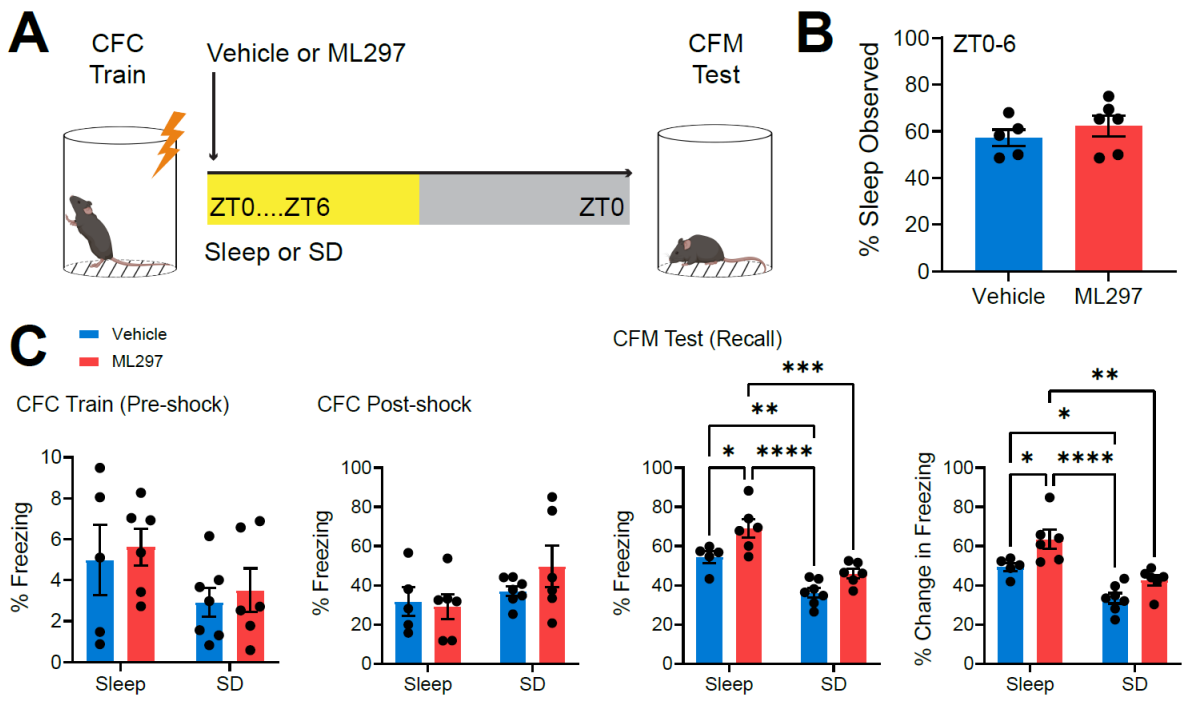

Figure 3.5: Post-CFC ML297 administration improves CFM consolidation in a sleep-dependent manner.

(**A**) Experimental design. Mice underwent single-trial CFC at lights on, were subsequentially administered vehicle or ML297 (30 mg/kg) via i.p. injection and returned to their home cage. Mice in the two drug treatment groups were then allowed *ad lib* sleep or were sleep deprived over the first 6 h post-CFC, after which all mice were allowed to sleep freely in their home cage until CFM testing the following day at lights on. (**B**) Total amounts of observed sleep during the first 6 h post-CFC were similar for the two *ad lib* sleep groups. Bars indicate mean ± SEM, n = 5 and 6 mice, respectively, for vehicle and ML297. (**C**) Vehicle and ML297 groups in both *ad lib* sleep and sleep deprivation (SD) conditions had similar freezing behavior during training (pre-shock and post-shock). n = 5 and 6 mice, respectively, for vehicle and ML297 groups with *ad lib* sleep, and n = 7 and 6 mice, respectively, for vehicle and ML297 groups with SD. Freezing behavior during recall, and changes in freezing from the CFC pre-shock period, were significantly greater in freely-sleeping ML297-treated mice compared with freely-sleeping vehicle-treated mice. SD reduced CFM-associated freezing behavior in both treatment groups, which did not differ from one another. n = 5 and 6 mice, respectively, for vehicle and ML297 with *ad lib* sleep, and n = 7 and 6 mice, respectively, for vehicle and ML297 with SD. *, **, *** and **** indicate $p < 0.05$, $p < 0.01$, $p < 0.001$, and $p < 0.0001$, respectively, Tukey's *post hoc* test.

3.5.4 : ML297-mediated improvement in CFM consolidation is associated with greater hippocampal activation during subsequent recall

The major input to hippocampus from the neocortex is relayed through the DG. Acting as a gateway to the rest of the hippocampus, the DG receives sensory and non-sensory information from the rest of the neocortex via entorhinal cortical input. Neuronal immediate early gene (IEG) expression increases among DG granule cells during both initial learning and memory retrieval, and granule cell activation plays a causal role in recall [66]. We tested whether changes in DG activity during CFM recall were associated with sleep- and ML297-mediated improvements in CFM consolidation, by quantifying cFos and Arc expression in hippocampus. After CFM recall, mice were returned to their home cages; 90 min later they were perfused to quantify protein products of IEG expression associated with recall. We found a significant effects of both sleep and ML297 treatment on cFos expression in the DG (two-way ANOVA; p(sleep condition) < 0.0001, F (1, 16) = 57.37; p(treatment) = 0.0003, F(1, 16 = 20.80); **Figure 3.6A-B**). ML297-treated mice allowed *ad lib* sleep had significantly increased cFos+ cell counts in DG during recall compared to both SD groups, and freely-sleeping vehicle-treated counterparts (Sidak's *post hoc* test vs. Sleep+ML297: Sleep+Vehicle, p = 0.0116; SD+Vehicle, p < 0.0001; SD+ML297, p = 0.0002; **Figure 3.6B-C**). SD also disrupted recall-associated DG cFos expression in vehicle-treated mice (Sidak's *post hoc* test, p = 0.0010; **Figure 3.6C**). Similar recall-associated patterns were observed for DG Arc expression (two-way ANOVA; p(sleep condition) = 0.0009; F(1, 16 = 16.49); p(treatment) = 0.0304; F(1, 16 = 5.641)) (**Figure 3.6B, D**), with reduced numbers of Arc+ neurons in SD mice (Sidak's *post hoc* test vs. Sleep+ML297: SD+Vehicle, p = 0.0020; SD+ML297, p = 0.0057) (**Figure**

3.6D). Overall expression of both IEGs in DG at recall was predictive of successful recall, with higher numbers of cFos+ and Arc+ neurons corresponding to increased freezing behavior during CFM testing (cFos: Pearson correlation coefficient, R = 0.7225, p = 0.0003; Arc: Pearson correlation coefficient, R = 0.5521, p = 0.0116) (**Figure 3.6E**).

We also quantified IEG expression within individual subregions of the DG to examine whether changes associated with recall in the four treatment groups were region-specific. As shown in **Figure 3.6C-D**, similar patterns of expression were observed in the granule cell body layer of both the superior and inferior blade of DG, and in the DG hilus. For cFos expression, we found significant effect of both sleep and treatment in both the superior and inferior blades (superior: two-way ANOVA; p(sleep condition) = 0.0005, F (1, 16) = 19.15; p(treatment) = 0.0127 F(1, 16 = 7.863); inferior: two-way ANOVA; p(sleep condition) = 0.0051, F (1, 16) = 10.53; p(treatment) = 0.0379; F(1, 16 = 5.123)), as well as in the hilus (two-way ANOVA; p(sleep condition) < 0.0001, F (1, 16) = 82.24; p(treatment) = 0.0002; F(1, 16 = 22.19); **Figure 3.6C**). Similarly, Arc expression patterns in superior and inferior blades after recall were similar to overall Arc+ neuron numbers (superior: two-way ANOVA; p(sleep condition) = 0.0021, F (1, 16) = 13.37; p(treatment) = 0.0584 F(1, 16 = 4.155); inferior: two-way ANOVA; p(sleep condition) = 0.0010, F (1, 16) = 16.03; p(treatment) = 0.0246; F(1, 16 = 6.154); **Figure 3.6D**).

To better understand how recall-associated neuronal activation is affected across the rest of the hippocampal circuit as a function of post-learning sleep and ML297, we also examined IEG expression within the pyramidal cell layers of CA1 and CA3 after CFM recall (**Figure 3.7A-B**). Recall-driven cFos+ neuron numbers in CA1 varied significantly as a function of prior sleep and drug treatment in CA1 (CA1: two-way ANOVA; p(sleep

condition) = 0.0060, F (1, 16) = 10.03; p(treatment) = 0.0011 F(1, 16 = 15.72); **Figure 3.7C**). Critically, however, cFos+ neuron numbers in CA1 were increased by ML297, even in SD mice (Sidak's *post hoc* test vs. SD+Vehicle, p = 0.0058). This suggests that CA1 cFos+ cell numbers are enhanced by ML297 administration even in a scenario where consolidation of CFM has been disrupted by SD. Nonetheless, higher numbers of cFos+ neurons in CA1 were associated with better CFM recall (i.e., higher levels of freezing; Pearson correlation coefficient, R = 0.6701, p = 0.0012; **Figure 3.7D**). cFos+ neuron numbers in CA3 showed a similar overall pattern, but varied significantly as a function of sleep only (two-way ANOVA; p(sleep condition) = 0.0030, F (1, 16) = 12.25; p(treatment) = 0.1914; F(1, 16 = 1.861); **Figure 3.7C**). cFos+ cell counts in CA3 also reflected freezing levels during recall for individual animals (Pearson correlation coefficient, R = 0.5719, p = 0.0084; **Figure 3.7D**).

Due to the widespread nature of Arc expression in CA1 and CA3, we quantified mean fluorescence intensity (MFI) of Arc immunostaining in these sections after recall, using previously described methods [4]. Using this strategy for quantification of Arc, no significant differences were observed across groups for any of the groups in either CA1 or CA3 (**Figure 3.7C**), and MFI values were not predictive of freezing behavior during recall (**Figure 3.7D**).

Taken together, these studies suggest that both post-CFC sleep (vs. SD), and post-CFC administration of ML297, can increase dorsal hippocampus neuronal activation during subsequent CFM recall. These effects on hippocampal activation (particularly on neuronal activation in DG) during recall mirror, and are positively correlated with freezing behavior during recall. These findings also support the idea that GIRK1/2 activation alters

hippocampal network-level processes involved in consolidation in a sleep-dependent manner, leading to sleep-dependent changes in activation during recall.

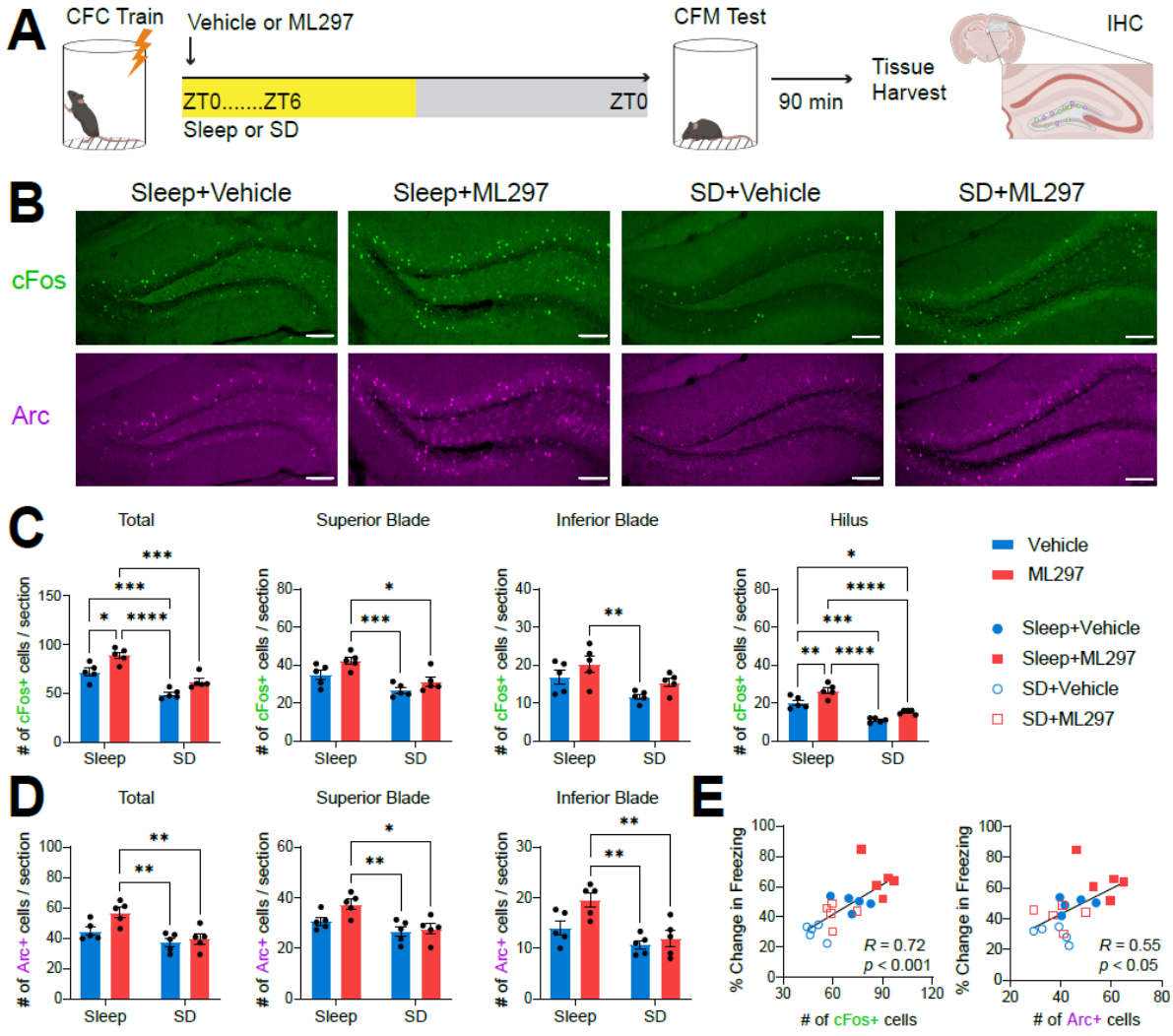

Figure 3.6: Post-CFC ML297 increases the number of active neurons in DG during subsequent CFM recall, in a sleep-dependent manner.

(**A**) Experimental paradigm. Mice underwent single-trial CFC, were administered vehicle or ML297 (30 mg/kg) following training, and then were either allowed *ad lib* sleep or underwent 6-h SD. 24 h after CFC, mice were tested for CFM, and perfused 90 min later to immunohistochemically quantify recall-associated cFos and Arc IEG expression in dorsal hippocampus. n = 5 mice/ group. (**B**) Representative images of cFos+ (green) and Arc+ (magenta) DG neurons following CFM recall in the four treatment groups. Scale bar = 100 µm. (**C**) Mice allowed *ad lib* sleep had significantly increased cFos+ neuron counts across DG compared to both SD groups. ML297 increased cFos+ neuron numbers further in freely-sleeping mice. Similar patterns were observed for the two DG granule cell blades, and for the DG hilus. (**D**) Arc+ neuron counts across DG were also reduced in both SD groups. ML297 administration led to a trend for higher overall Arc+ DG neurons relative to vehicle in freely-sleeping mice. *, **, ***, and **** indicate $p < 0.05$, $p < 0.01$, $p < 0.001$, and $p < 0.0001$, respectively, Sidak's *post hoc* test. (**E**) Higher numbers of cFos+ and Arc+ neurons across DG at recall reflected the success of CFM consolidation across individual mice. R and p values are shown for Pearson correlation.

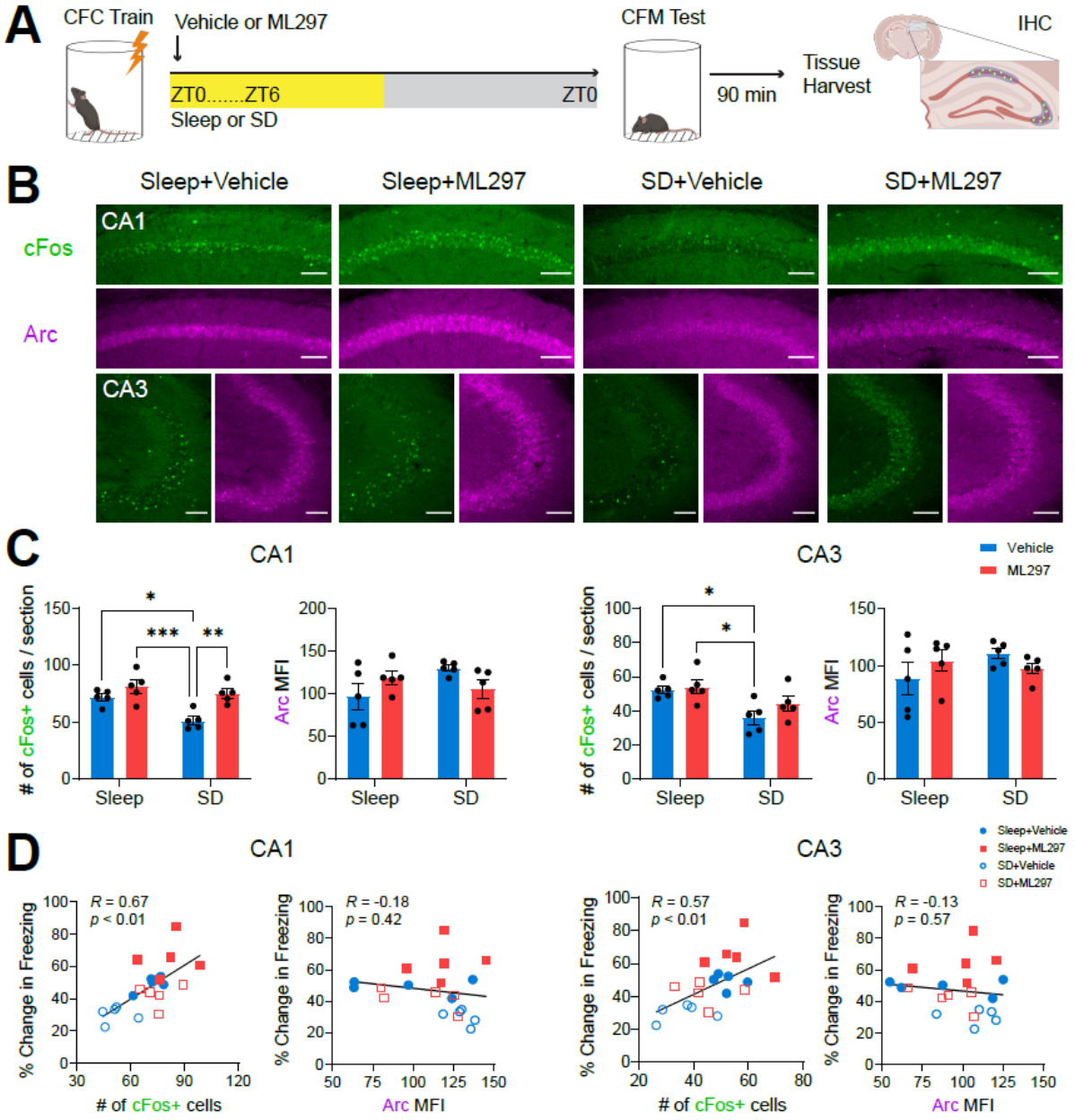

Figure 3.7: Post-CFC ML297 increases the number of active neurons in CA1 during subsequent CFM recall, in a sleep-independent manner.

(**A**) Experimental design, as in **Fig. 6A**. (**B**) Representative images of cFos+ neurons (green) and Arc+ mean fluorescence intensity (MFI) in the pyramidal layers (magenta) in CA1 and CA3 following CFM recall in the four groups. Scale bar = 100 µm. (**C**) Post-CFC SD significantly decreased the number of cFos+ neurons in CA1 and CA3 during recall in vehicle-treated mice. In CA1 only, ML297 increased cFos+ neuron numbers after recall in SD mice as well as freely-sleeping mice. No significant changes in Arc MFI were observed with SD or drug treatment in either CA1 or CA3. *, **, and *** indicate $p < 0.05$, $p < 0.01$, and $p < 0.001$, respectively, Sidak's *post hoc* test. (**D**) Numbers of cFos+ neurons in both CA1 and CA3 during recall correlated with CFM recall performance. No correlations were observed between freezing behavior and Arc MFI expression. *R* and *p* values are shown for Pearson correlation.

3.6 : Discussion

We find that in the hours immediately following CFC, direct GIRK1/2 channel activation can increase REM sleep, restoring REM sleep architecture (normally suppressed after fear learning) to baseline levels, and improving sleep-dependent consolidation of fear memory. We find that ML297-associated increases in overall REM sleep amounts, bout durations, and bout numbers (and reduced latency to REM sleep) co-occur with increased NREM spindle power over the first 6 h post-CFC (and higher spindle power continuing into the subsequent dark phase). It is likely that these changes are driven by the same underlying mechanism, due to the increasingly well-established causal relationship between spindle-rich NREM sleep and transitions from NREM into REM sleep [64,65]. In other words, it is likely that transitions into REM sleep after ML297 administration reflect the normal physiology of such transitions. Critically, all of the NREM and REM sleep changes caused by ML297 in the hours following CFC appear to be renormalizing sleep architecture to what is typically observed under baseline conditions (i.e., in the absence of fear learning). Two features of these findings are worth noting. First, the ML297-induced changes in sleep architecture that are correlated with successful CFM consolidation occur almost exclusively within a window of time (i.e., the first 6 h after CFC) where SD is sufficient to disrupt the consolidation process [6,8,15-17]. Second, post-CFC SD is sufficient to prevent the CFM consolidation benefits of ML297 administration.

It is worth noting that both spindle-rich NREM sleep (such as that present at the transition to REM) and REM sleep have been linked to memory storage, across species - from humans to rodent models [1,67,68]. NREM spindles have received a great deal of recent study due to their linkage to sleep-related improvements on a range of mnemonic

tasks, and to sleep-dependent synaptic plasticity in neocortex [3,21,31,52,69,70]. Within the hippocampus, spindles and other NREM-associated electrophysiological [19,21] and neuromodulatory [6,20] changes have been mechanistically linked to successful CFM consolidation. Our present data suggest that REM is at least equally vital for CFM, and support growing body of data indicating that REM-specific features of post-learning hippocampal activity [17,27] and gene expression [71-73] are essential for the consolidation process. Together, our findings support the notion that post-CFC REM sleep plays a causal role in promoting fear memory consolidation.

To better understand the link between our behavioral results and hippocampal network-level events underlying successful memory consolidation, we examined IEG expression within the hippocampus following CFM recall. We find that just as recall itself is suppressed after post-CFC SD, the number of cFos+ and Arc+ neurons in DG after recall, as well as the number of cFos+ neurons in downstream regions CA3 and CA1, is decreased in SD mice. This is consistent with the idea that hippocampal activation during recall is reduced overall after SD-disrupted consolidation. Because mice are given an adequate opportunity for recovery sleep between SD and recall (i.e., 18 h from ZT6 to ZT0 the following day), we believe that this alteration is due to a long-term change in the strength of the memory trace itself, rather than an acute effect of SD on hippocampal activation [4,6,74]. In other words, an increase in the number of neurons active at recall following *ad lib* sleep would reflect more neurons' inclusion into the hippocampal "engram", while decreases after SD would reflect a reduction in neuronal incorporation into the memory trace. Intriguingly, ML297 administration after CFC in freely-sleeping mice results in a further increase in the number of IEG+ neurons in DG, where recall-

activated neurons are generally sparser, but does not affect IEG+ numbers when administered in the context of SD. These sleep-dependent effects of ML297 on DG neurons' activity during recall closely reflect effects of ML297 on CFM consolidation. In contrast, in CA1, ML297 increases numbers of recall-activated cFos+ neurons, regardless of whether mice are freely-sleeping or sleep-deprived. This suggests additional, sleep-independent effects of ML297 within CA1, the region of hippocampus where GIRK1/2 channels are most abundant [41,44,49]. Overall, our data suggest that GIRK channel activation has sleep-dependent and sleep-independent effects on the dorsal hippocampal network in the context of consolidation, leading to incorporation of more neurons into the CFM engram, which is evident in the pattern of network activation during CFM recall.

While numerous genetic findings suggest that loss of GIRK channel activity disrupts hippocampal memory processing [75], their precise molecular role in this process remains unclear. *In vitro* studies have shown that in the hippocampus (e.g. CA1) GIRK channel activation induces hyperpolarization, reduce neuronal excitability, and suppresses LTP [47,48,51]. However, it is unknown how these effects translate to *in vivo* function, and particularly how these changes are modulated in different brain states (such as wake vs. NREM and REM sleep). Future studies will be needed to disentangle the relationship between direct cellular effects of ML297 administration, its behavioral effects (e.g., sleep-promoting, anxiolytic), and its mnemonic effects during the memory consolidation process.

It is also worth noting that GIRK1/2 is expressed in other brain regions, including the neocortex and the thalamus [76]. The effects of ML297 treatment on delta and spindle

oscillations may very well be mediated by activation of GIRK1/2 in these structures [2,3]. While our present findings are focused on drug effects on subsequent recall-associated activation in the hippocampus, it is very plausible that ML297 also affects other structures important for CFM, including thalamocortical circuits and the amygdala.

Recent data have implicated GIRK channels as a target for therapeutics in various neurological and psychiatric conditions including epilepsy, Alzheimer's disease, substance abuse, and anxiety disorders [49,75]. Our present data support the recent suggestion [40] that GIRK1/2 activation via ML297 could also be beneficial as a hypnotic. Beyond this, our data demonstrate that this hypnotic agent restores physiological REM sleep (whose disruption by fear learning is well-established [23] to promote sleep-dependent memory consolidation. These findings have important ramifications for treatment of disorders - including neurodevelopmental disorders, dementia, and anxiety disorders) where both sleep architecture and cognitive function are disrupted.

3.6.1 Acknowledgements

We thank the members of the Aton lab for useful feedback on these studies, and Gregg Sobocinski for microscopy support. This work was supported by a University of Michigan Rackham Graduate School Predoctoral Fellowship, Graduate Student Research Grant, and Merit Fellowship to JDM, a University of Michigan Kavli Neuroscience Innovators Magnificent Michigan Summer Fellowship to WPB, and NIH research grants R01 NS104776 and RF1 NS118440 to SJA.

3.7 : References

1. Rasch, B., and Born, J. (2013). About sleep's role in memory. Physiol Rev *93*, 681-766. 10.1152/physrev.00032.2012.
2. Puentes-Mestril, C., and Aton, S.J. (2017). Linking Network Activity to Synaptic Plasticity during Sleep: Hypotheses and Recent Data. Front Neural Circuits *11*, 61. 10.3389/fncir.2017.00061.
3. Puentes-Mestril, C., Roach, J., Niethard, N., Zochowski, M., and Aton, S.J. (2019). How rhythms of the sleeping brain tune memory and synaptic plasticity. Sleep *42*. 10.1093/sleep/zsz095.
4. Delorme, J.E., Kodoth, V., and Aton, S.J. (2019). Sleep loss disrupts Arc expression in dentate gyrus neurons. Neurobiol Learn Mem *160*, 73-82. 10.1016/j.nlm.2018.04.006.
5. Havekes, R., and Aton, S.J. (2020). Impacts of Sleep Loss versus Waking Experience on Brain Plasticity: Parallel or Orthogonal? Trends Neurosci *43*, 385-393. 10.1016/j.tins.2020.03.010.
6. Delorme, J., Wang, L., Kuhn, F.R., Kodoth, V., Ma, J., Martinez, J.D., Raven, F., Toth, B.A., Balendran, V., Vega Medina, A., et al. (2021). Sleep loss drives acetylcholine- and somatostatin interneuron-mediated gating of hippocampal activity to inhibit memory consolidation. Proc Natl Acad Sci U S A *118*. 10.1073/pnas.2019318118.
7. Puentes-Mestril, C., Delorme, J., Wang, L., Donnelly, M., Popke, D., Jiang, S., and Aton, S.J. (2021). Sleep Loss Drives Brain Region-Specific and Cell Type-Specific Alterations in Ribosome-Associated Transcripts Involved in Synaptic Plasticity and Cellular Timekeeping. J Neurosci *41*, 5386-5398. 10.1523/JNEUROSCI.1883-20.2021.
8. Delorme, J., Wang, L., Kodoth, V., Wang, Y., Ma, J., Jiang, S., and Aton, S.J. (2021). Hippocampal neurons' cytosolic and membrane-bound ribosomal transcript profiles are differentially regulated by learning and subsequent sleep. Proc Natl Acad Sci U S A *118*. 10.1073/pnas.2108534118.
9. Noya, S.B., Colameo, D., Bruning, F., Spinnler, A., Mircsof, D., Opitz, L., Mann, M., Tyagarajan, S.K., Robles, M.S., and Brown, S.A. (2019). The forebrain synaptic transcriptome is organized by clocks but its proteome is driven by sleep. Science *366*. 10.1126/science.aav2642.
10. Bruning, F., Noya, S.B., Bange, T., Koutsouli, S., Rudolph, J.D., Tyagarajan, S.K., Cox, J., Mann, M., Brown, S.A., and Robles, M.S. (2019). Sleep-wake cycles drive daily dynamics of synaptic phosphorylation. Science *366*. 10.1126/science.aav3617.
11. Hor, C.N., Yeung, J., Jan, M., Emmenegger, Y., Hubbard, J., Xenarios, I., Naef, F., and Franken, P. (2019). Sleep-wake-driven and circadian contributions to daily rhythms in gene expression and chromatin accessibility in the murine cortex. Proc Natl Acad Sci U S A *116*, 25773-25783. 10.1073/pnas.1910590116.
12. Klinzing, J.G., Niethard, N., and Born, J. (2019). Mechanisms of systems memory consolidation during sleep. Nat Neurosci *22*, 1598-1610. 10.1038/s41593-019-0467-3.

13. Prince, T.M., Wimmer, M., Choi, J., Havekes, R., Aton, S., and Abel, T. (2014). Sleep deprivation during a specific 3-hour time window post-training impairs hippocampal synaptic plasticity and memory. Neurobiol Learn Mem *109*, 122-130. 10.1016/j.nlm.2013.11.021.
14. Havekes, R., and Abel, T. (2017). The tired hippocampus: the molecular impact of sleep deprivation on hippocampal function. Curr Opin Neurobiol *44*, 13-19. 10.1016/j.conb.2017.02.005.
15. Graves, L.A., Heller, E.A., Pack, A.I., and Abel, T. (2003). Sleep deprivation selectively impairs memory consolidation for contextual fear conditioning. Learn Mem *10*, 168-176. 10.1101/lm.48803.
16. Vecsey, C.G., Baillie, G.S., Jaganath, D., Havekes, R., Daniels, A., Wimmer, M., Huang, T., Brown, K.M., Li, X.Y., Descalzi, G., et al. (2009). Sleep deprivation impairs cAMP signalling in the hippocampus. Nature *461*, 1122-1125. 10.1038/nature08488.
17. Ognjanovski, N., Broussard, C., Zochowski, M., and Aton, S.J. (2018). Hippocampal Network Oscillations Rescue Memory Consolidation Deficits Caused by Sleep Loss. Cereb Cortex *28*, 3711-3723. 10.1093/cercor/bhy174.
18. Ognjanovski, N., Maruyama, D., Lashner, N., Zochowski, M., and Aton, S.J. (2014). CA1 hippocampal network activity changes during sleep-dependent memory consolidation. Front Syst Neurosci *8*, 61. 10.3389/fnsys.2014.00061.
19. Ognjanovski, N., Schaeffer, S., Wu, J., Mofakham, S., Maruyama, D., Zochowski, M., and Aton, S.J. (2017). Parvalbumin-expressing interneurons coordinate hippocampal network dynamics required for memory consolidation. Nat Commun *8*, 15039. 10.1038/ncomms15039.
20. Skilling, Q.M., Eniwaye, B., Clawson, B.C., Shaver, J., Ognjanovski, N., Aton, S.J., and Zochowski, M. (2021). Acetylcholine-gated current translates wake neuronal firing rate information into a spike timing-based code in Non-REM sleep, stabilizing neural network dynamics during memory consolidation. PLoS Comput Biol *17*, e1009424. 10.1371/journal.pcbi.1009424.
21. Xia, F., Richards, B.A., Tran, M.M., Josselyn, S.A., Takehara-Nishiuchi, K., and Frankland, P.W. (2017). Parvalbumin-positive interneurons mediate neocortical-hippocampal interactions that are necessary for memory consolidation. Elife *6*. 10.7554/eLife.27868.
22. Sanford, L.D., Silvestri, A.J., Ross, R.J., and Morrison, A.R. (2001). Influence of fear conditioning on elicited ponto-geniculo-occipital waves and rapid eye movement sleep. Arch Ital Biol *139*, 169-183.
23. Tang, X., Yang, L., and Sanford, L.D. (2007). Interactions between brief restraint, novelty and footshock stress on subsequent sleep and EEG power in rats. Brain Res *1142*, 110-118. 10.1016/j.brainres.2007.01.029.
24. Menz, M.M., Rihm, J.S., Salari, N., Born, J., Kalisch, R., Pape, H.C., Marshall, L., and Buchel, C. (2013). The role of sleep and sleep deprivation in consolidating fear memories. Neuroimage *75*, 87-96. 10.1016/j.neuroimage.2013.03.001.
25. Spoormaker, V.I., Gvozdanovic, G.A., Samann, P.G., and Czisch, M. (2014). Ventromedial prefrontal cortex activity and rapid eye movement sleep are associated with subsequent fear expression in human subjects. Exp Brain Res *232*, 1547-1554. 10.1007/s00221-014-3831-2.

26. Pace-Schott, E.F., Germain, A., and Milad, M.R. (2015). Effects of sleep on memory for conditioned fear and fear extinction. Psychol Bull *141*, 835-857. 10.1037/bul0000014.
27. Boyce, R., Glasgow, S.D., Williams, S., and Adamantidis, A. (2016). Causal evidence for the role of REM sleep theta rhythm in contextual memory consolidation. Science *352*, 812-816. 10.1126/science.aad5252.
28. Seibt, J., Aton, S.J., Jha, S.K., Coleman, T., Dumoulin, M.C., and Frank, M.G. (2008). The non-benzodiazepine hypnotic zolpidem impairs sleep-dependent cortical plasticity. Sleep *31*, 1381-1391. 10.5665/sleep/31.10.1381.
29. Aton, S.J., Seibt, J., Dumoulin, M.C., Coleman, T., Shiraishi, M., and Frank, M.G. (2009). The sedating antidepressant trazodone impairs sleep-dependent cortical plasticity. PLoS One *4*, e6078. 10.1371/journal.pone.0006078.
30. Vienne, J., Lecciso, G., Constantinescu, I., Schwartz, S., Franken, P., Heinzer, R., and Tafti, M. (2012). Differential effects of sodium oxybate and baclofen on EEG, sleep, neurobehavioral performance, and memory. Sleep *35*, 1071-1083. 10.5665/sleep.1992.
31. Mednick, S.C., McDevitt, E.A., Walsh, J.K., Wamsley, E., Paulus, M., Kanady, J.C., and Drummond, S.P. (2013). The critical role of sleep spindles in hippocampal-dependent memory: a pharmacology study. J Neurosci *33*, 4494-4504. 10.1523/JNEUROSCI.3127-12.2013.
32. Leong, C.W.Y., Leow, J.W.S., Grunstein, R.R., Naismith, S.L., Teh, J.Z., D'Rozario, A.L., and Saini, B. (2022). A systematic scoping review of the effects of central nervous system active drugs on sleep spindles and sleep-dependent memory consolidation. Sleep Med Rev *62*, 101605. 10.1016/j.smrv.2022.101605.
33. Wamsley, E.J., Shinn, A.K., Tucker, M.A., Ono, K.E., McKinley, S.K., Ely, A.V., Goff, D.C., Stickgold, R., and Manoach, D.S. (2013). The effects of eszopiclone on sleep spindles and memory consolidation in schizophrenia: a randomized placebo-controlled trial. Sleep *36*, 1369-1376. 10.5665/sleep.2968.
34. Hall-Porter, J.M., Schweitzer, P.K., Eisenstein, R.D., Ahmed, H.A., and Walsh, J.K. (2014). The effect of two benzodiazepine receptor agonist hypnotics on sleep-dependent memory consolidation. J Clin Sleep Med *10*, 27-34. 10.5664/jcsm.3352.
35. Snead, O.C., 3rd (1992). Evidence for GABAB-mediated mechanisms in experimental generalized absence seizures. Eur J Pharmacol *213*, 343-349. 10.1016/0014-2999(92)90623-c.
36. Black, J., Pardi, D., Hornfeldt, C.S., and Inhaber, N. (2009). The nightly administration of sodium oxybate results in significant reduction in the nocturnal sleep disruption of patients with narcolepsy. Sleep Med *10*, 829-835. 10.1016/j.sleep.2009.05.004.
37. Roth, T., Dauvilliers, Y., Guinta, D., Alvarez-Horine, S., Dynin, E., and Black, J. (2017). Effect of sodium oxybate on disrupted nighttime sleep in patients with narcolepsy. J Sleep Res *26*, 407-414. 10.1111/jsr.12468.
38. Kuriyama, A., Honda, M., and Hayashino, Y. (2014). Ramelteon for the treatment of insomnia in adults: a systematic review and meta-analysis. Sleep Med *15*, 385-392. 10.1016/j.sleep.2013.11.788.

39. Szabadi, E. (2014). Selective targets for arousal-modifying drugs: implications for the treatment of sleep disorders. Drug Discov Today *19*, 701-708. 10.1016/j.drudis.2014.01.001.
40. Zou, B., Cao, W.S., Guan, Z., Xiao, K., Pascual, C., Xie, J., Zhang, J., Xie, J., Kayser, F., Lindsley, C.W., et al. (2019). Direct activation of G-protein-gated inward rectifying K+ channels promotes nonrapid eye movement sleep. Sleep *42*, 1-16. 10.1093/sleep/zsy244.
41. Tinker, A., Jan, Y.N., and Jan, L.Y. (1996). Regions responsible for the assembly of inwardly rectifying potassium channels. Cell *87*, 857-868. 10.1016/s0092-8674(00)81993-5.
42. Inanobe, A., Yoshimoto, Y., Horio, Y., Morishige, K.I., Hibino, H., Matsumoto, S., Tokunaga, Y., Maeda, T., Hata, Y., Takai, Y., and Kurachi, Y. (1999). Characterization of G-protein-gated K+ channels composed of Kir3.2 subunits in dopaminergic neurons of the substantia nigra. J Neurosci *19*, 1006-1017. 10.1523/JNEUROSCI.19-03-01006.1999.
43. Walsh, K.B. (2011). Targeting GIRK Channels for the Development of New Therapeutic Agents. Front Pharmacol *2*, 64. 10.3389/fphar.2011.00064.
44. Kloukina, V., Herzer, S., Karlsson, N., Perez, M., Daraio, T., and Meister, B. (2012). G-protein-gated inwardly rectifying K+ channel 4 (GIRK4) immunoreactivity in chemically defined neurons of the hypothalamic arcuate nucleus that control body weight. J Chem Neuroanat *44*, 14-23. 10.1016/j.jchemneu.2012.03.003.
45. Carter, S.D., Mifsud, K.R., and Reul, J.M. (2015). Distinct epigenetic and gene expression changes in rat hippocampal neurons after Morris water maze training. Front Behav Neurosci *9*, 156. 10.3389/fnbeh.2015.00156.
46. Logothetis, D.E., Mahajan, R., Adney, S.K., Ha, J., Kawano, T., Meng, X.Y., and Cui, M. (2015). Unifying Mechanism of Controlling Kir3 Channel Activity by G Proteins and Phosphoinositides. Int Rev Neurobiol *123*, 1-26. 10.1016/bs.irn.2015.05.013.
47. Luscher, C., Jan, L.Y., Stoffel, M., Malenka, R.C., and Nicoll, R.A. (1997). G protein-coupled inwardly rectifying K+ channels (GIRKs) mediate postsynaptic but not presynaptic transmitter actions in hippocampal neurons. Neuron *19*, 687-695. 10.1016/s0896-6273(00)80381-5.
48. Signorini, S., Liao, Y.J., Duncan, S.A., Jan, L.Y., and Stoffel, M. (1997). Normal cerebellar development but susceptibility to seizures in mice lacking G protein-coupled, inwardly rectifying K+ channel GIRK2. Proc Natl Acad Sci U S A *94*, 923-927. 10.1073/pnas.94.3.923.
49. Kaufmann, K., Romaine, I., Days, E., Pascual, C., Malik, A., Yang, L., Zou, B., Du, Y., Sliwoski, G., Morrison, R.D., et al. (2013). ML297 (VU0456810), the first potent and selective activator of the GIRK potassium channel, displays antiepileptic properties in mice. ACS Chem Neurosci *4*, 1278-1286. 10.1021/cn400062a.
50. Wydeven, N., Marron Fernandez de Velasco, E., Du, Y., Benneyworth, M.A., Hearing, M.C., Fischer, R.A., Thomas, M.J., Weaver, C.D., and Wickman, K. (2014). Mechanisms underlying the activation of G-protein-gated inwardly

rectifying K+ (GIRK) channels by the novel anxiolytic drug, ML297. Proc Natl Acad Sci U S A *111*, 10755-10760. 10.1073/pnas.1405190111.
51. Djebari, S., Iborra-Lazaro, G., Temprano-Carazo, S., Sanchez-Rodriguez, I., Nava-Mesa, M.O., Munera, A., Gruart, A., Delgado-Garcia, J.M., Jimenez-Diaz, L., and Navarro-Lopez, J.D. (2021). G-Protein-Gated Inwardly Rectifying Potassium (Kir3/GIRK) Channels Govern Synaptic Plasticity That Supports Hippocampal-Dependent Cognitive Functions in Male Mice. J Neurosci *41*, 7086-7102. 10.1523/JNEUROSCI.2849-20.2021.
52. Durkin, J., Suresh, A.K., Colbath, J., Broussard, C., Wu, J., Zochowski, M., and Aton, S.J. (2017). Cortically coordinated NREM thalamocortical oscillations play an essential, instructive role in visual system plasticity. Proc Natl Acad Sci U S A *114*, 10485-10490. 10.1073/pnas.1710613114.
53. Clawson, B.C., Pickup, E.J., Ensing, A., Geneseo, L., Shaver, J., Gonzalez-Amoretti, J., Zhao, M., York, A.K., Kuhn, F.R., Swift, K., et al. (2021). Causal role for sleep-dependent reactivation of learning-activated sensory ensembles for fear memory consolidation. Nat Commun *12*, 1200. 10.1038/s41467-021-21471-2.
54. Pham, J., Cabrera, S.M., Sanchis-Segura, C., and Wood, M.A. (2009). Automated scoring of fear-related behavior using EthoVision software. J Neurosci Methods *178*, 323-326. 10.1016/j.jneumeth.2008.12.021.
55. Hui, G.K., Figueroa, I.R., Poytress, B.S., Roozendaal, B., McGaugh, J.L., and Weinberger, N.M. (2004). Memory enhancement of classical fear conditioning by post-training injections of corticosterone in rats. Neurobiol Learn Mem *81*, 67-74. 10.1016/j.nlm.2003.09.002.
56. Roozendaal, B., Okuda, S., Van der Zee, E.A., and McGaugh, J.L. (2006). Glucocorticoid enhancement of memory requires arousal-induced noradrenergic activation in the basolateral amygdala. Proc Natl Acad Sci U S A *103*, 6741-6746. 10.1073/pnas.0601874103.
57. Raven, F., Heckman, P.R.A., Havekes, R., and Meerlo, P. (2020). Sleep deprivation-induced impairment of memory consolidation is not mediated by glucocorticoid stress hormones. J Sleep Res *29*, e12972. 10.1111/jsr.12972.
58. Fisher, S.P., Godinho, S.I., Pothecary, C.A., Hankins, M.W., Foster, R.G., and Peirson, S.N. (2012). Rapid assessment of sleep-wake behavior in mice. J Biol Rhythms *27*, 48-58. 10.1177/0748730411431550.
59. Pawlyk, A.C., Morrison, A.R., Ross, R.J., and Brennan, F.X. (2008). Stress-induced changes in sleep in rodents: models and mechanisms. Neurosci Biobehav Rev *32*, 99-117. 10.1016/j.neubiorev.2007.06.001.
60. Trachsel, L., Tobler, I., and Borbely, A.A. (1988). Electroencephalogram analysis of non-rapid eye movement sleep in rats. Am J Physiol *255*, R27-37. 10.1152/ajpregu.1988.255.1.R27.
61. Uchida, S., Maloney, T., March, J.D., Azari, R., and Feinberg, I. (1991). Sigma (12-15 Hz) and delta (0.3-3 Hz) EEG oscillate reciprocally within NREM sleep. Brain Res Bull *27*, 93-96. 10.1016/0361-9230(91)90286-s.
62. Sarasso, S., Zubler, F., Pigorini, A., Sartori, I., Castana, L., and Nobili, L. (2021). Thalamic and neocortical differences in the relationship between the time course of delta and sigma power during NREM sleep in humans. J Sleep Res *30*, e13166. 10.1111/jsr.13166.

63. Latchoumane, C.V., Ngo, H.V., Born, J., and Shin, H.S. (2017). Thalamic Spindles Promote Memory Formation during Sleep through Triple Phase-Locking of Cortical, Thalamic, and Hippocampal Rhythms. Neuron *95*, 424-435 e426. 10.1016/j.neuron.2017.06.025.
64. Kim, A., Latchoumane, C., Lee, S., Kim, G.B., Cheong, E., Augustine, G.J., and Shin, H.S. (2012). Optogenetically induced sleep spindle rhythms alter sleep architectures in mice. Proc Natl Acad Sci U S A *109*, 20673-20678. 10.1073/pnas.1217897109.
65. Bandarabadi, M., Herrera, C.G., Gent, T.C., Bassetti, C., Schindler, K., and Adamantidis, A.R. (2020). A role for spindles in the onset of rapid eye movement sleep. Nat Commun *11*, 5247. 10.1038/s41467-020-19076-2.
66. Liu, X., Ramirez, S., Pang, P.T., Puryear, C.B., Govindarajan, A., Deisseroth, K., and Tonegawa, S. (2012). Optogenetic stimulation of a hippocampal engram activates fear memory recall. Nature *484*, 381-385. 10.1038/nature11028.
67. Ribeiro, S., and Nicolelis, M.A. (2004). Reverberation, storage, and postsynaptic propagation of memories during sleep. Learn Mem *11*, 686-696. 10.1101/lm.75604.
68. Stickgold, R., and Walker, M.P. (2007). Sleep-dependent memory consolidation and reconsolidation. Sleep Med *8*, 331-343. 10.1016/j.sleep.2007.03.011.
69. Aton, S.J., Broussard, C., Dumoulin, M., Seibt, J., Watson, A., Coleman, T., and Frank, M.G. (2013). Visual experience and subsequent sleep induce sequential plastic changes in putative inhibitory and excitatory cortical neurons. Proc Natl Acad Sci U S A *110*, 3101-3106. 10.1073/pnas.1208093110.
70. Clawson, B.C., Durkin, J., and Aton, S.J. (2016). Form and Function of Sleep Spindles across the Lifespan. Neural Plast *2016*, 6936381. 10.1155/2016/6936381.
71. Ulloor, J., and Datta, S. (2005). Spatio-temporal activation of cyclic AMP response element-binding protein, activity-regulated cytoskeletal-associated protein and brain-derived nerve growth factor: a mechanism for pontine-wave generator activation-dependent two-way active-avoidance memory processing in the rat. J Neurochem *95*, 418-428. 10.1111/j.1471-4159.2005.03378.x.
72. Datta, S., Li, G., and Auerbach, S. (2008). Activation of phasic pontine-wave generator in the rat: a mechanism for expression of plasticity-related genes and proteins in the dorsal hippocampus and amygdala. Eur J Neurosci *27*, 1876-1892. 10.1111/j.1460-9568.2008.06166.x.
73. Calais, J.B., Ojopi, E.B., Morya, E., Sameshima, K., and Ribeiro, S. (2015). Experience-dependent upregulation of multiple plasticity factors in the hippocampus during early REM sleep. Neurobiol Learn Mem *122*, 19-27. 10.1016/j.nlm.2015.01.002.
74. Yoo, S.S., Hu, P.T., Gujar, N., Jolesz, F.A., and Walker, M.P. (2007). A deficit in the ability to form new human memories without sleep. Nat Neurosci *10*, 385-392. 10.1038/nn1851.
75. Mayfield, J., Blednov, Y.A., and Harris, R.A. (2015). Behavioral and Genetic Evidence for GIRK Channels in the CNS: Role in Physiology, Pathophysiology, and Drug Addiction. Int Rev Neurobiol *123*, 279-313. 10.1016/bs.irn.2015.05.016.

76. Ponce, A., Bueno, E., Kentros, C., Vega-Saenz de Miera, E., Chow, A., Hillman, D., Chen, S., Zhu, L., Wu, M.B., Wu, X., et al. (1996). G-protein-gated inward rectifier K+ channel proteins (GIRK1) are present in the soma and dendrites as well as in nerve terminals of specific neurons in the brain. J Neurosci *16*, 1990-2001. 10.1523/JNEUROSCI.16-06-01990.1996.

3.8 : Chapter 3 Supplementary Information Figures

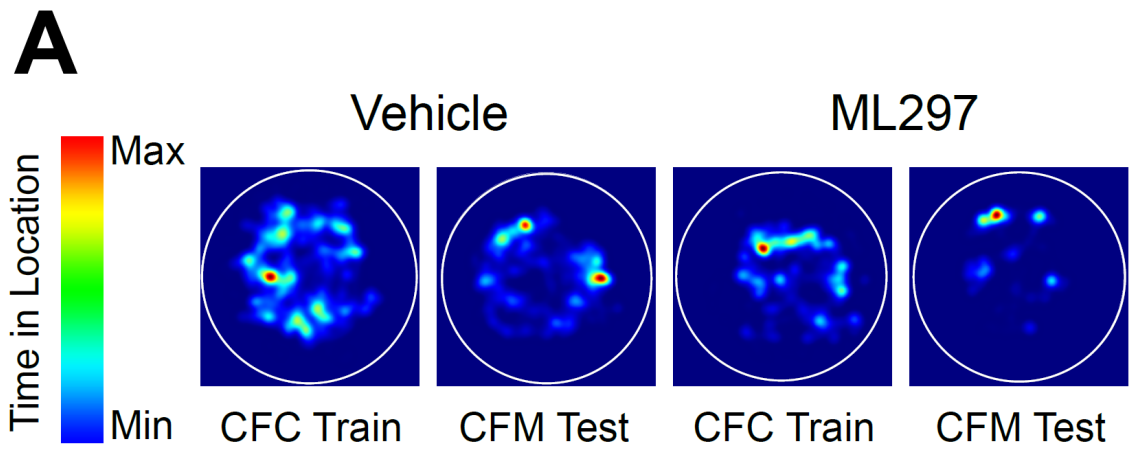

Supplemental Figure 3.1: Representative heat maps of time-in-location for individual EEG-implanted mice during CFC training and CFM testing.

(**A**) Heat maps indicating time spent in various locations within the conditioning chamber, for representative vehicle- and ML297-treated mice during CFC and CFM testing. Red represents locations in the CFC chamber where mice spent the most time, while blue represents locations in the CFC chamber where mice spent the least time.

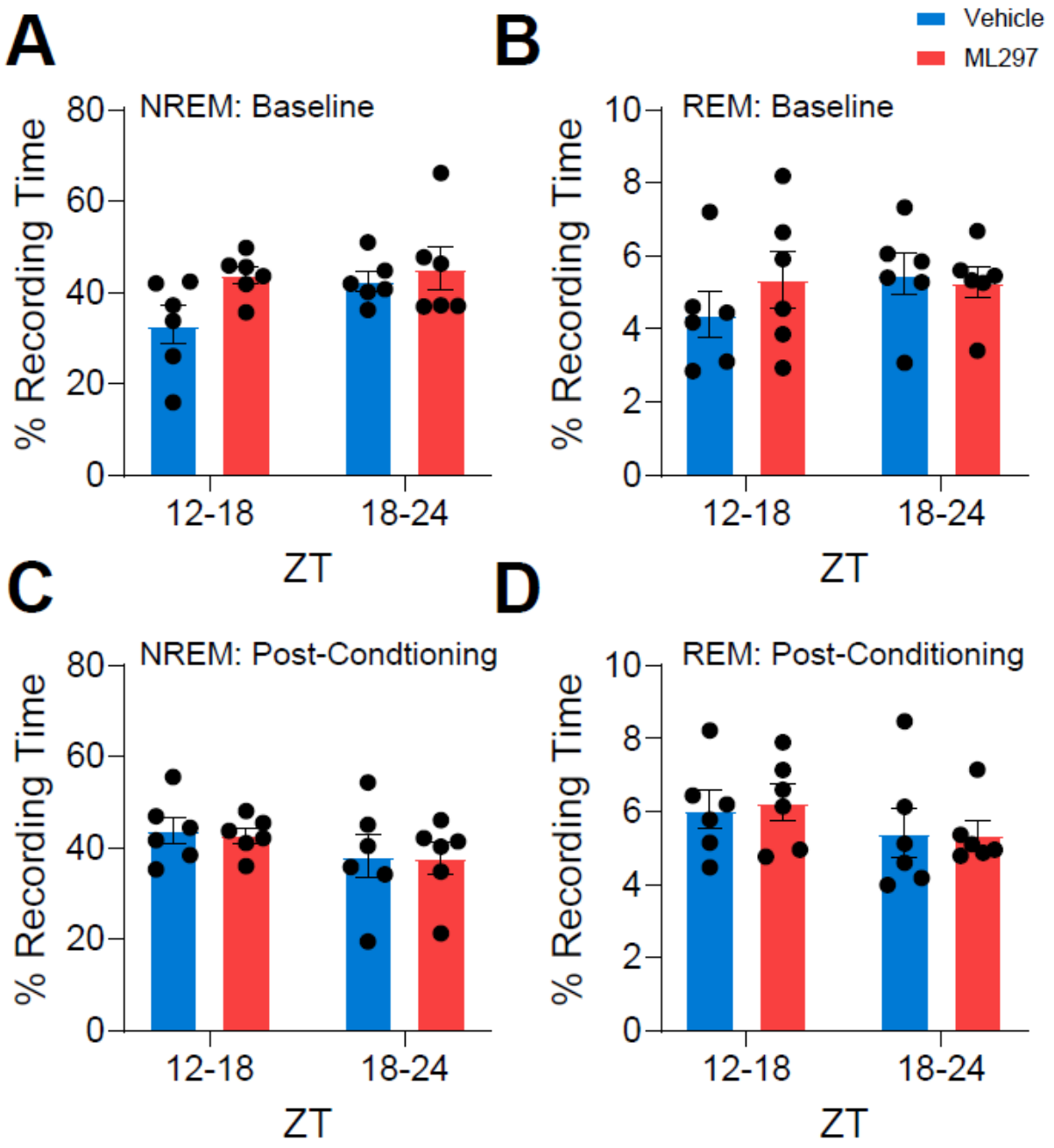

Supplemental Figure 3.2: NREM and REM sleep architecture are similar during the dark phase (ZT12-24) during baseline recording and following CFC.

(**A**) NREM and (**B**) REM total sleep behavior during baseline across 6-h periods of dark phase were similar for vehicle and ML297 groups. (**C**) NREM and (**D**) REM total sleep behavior post-CFC during the dark phase were similar for vehicle and ML297 groups. *n* = 6 mice/group

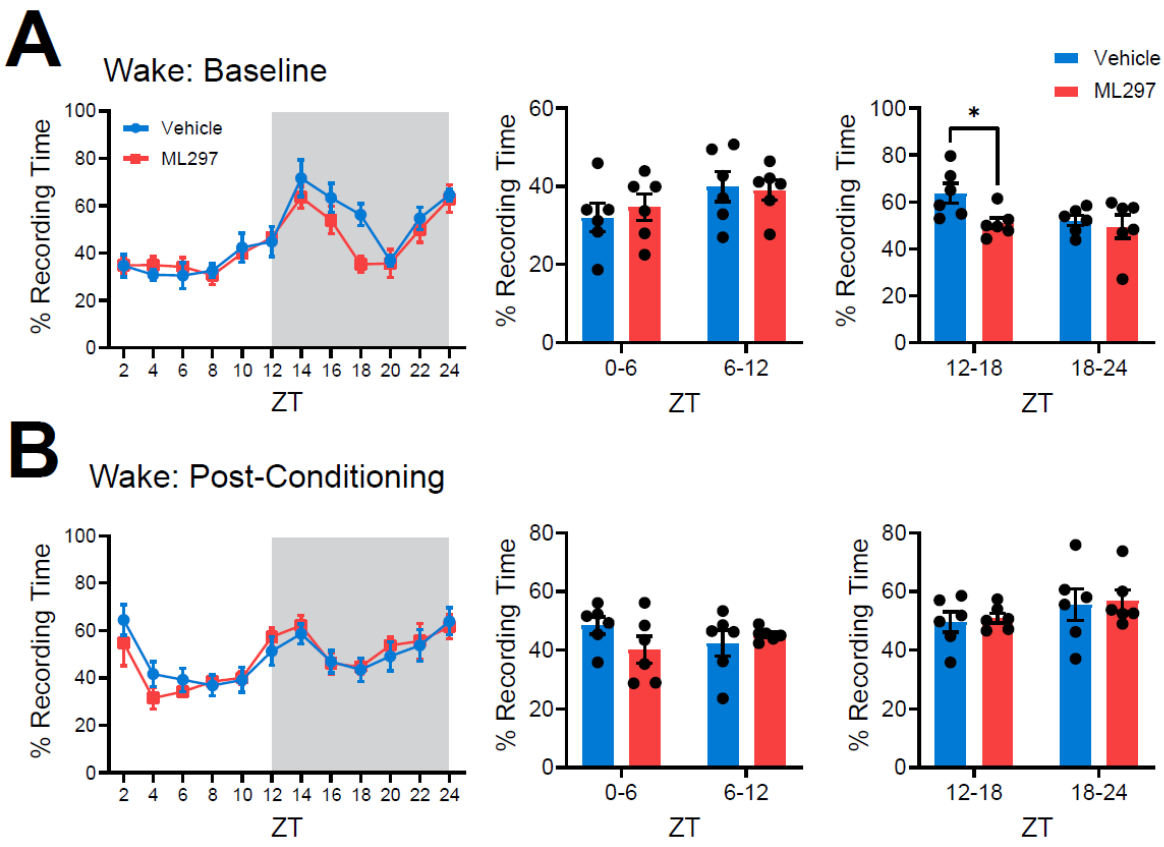

Supplemental Figure 3.3: Wake architecture across the light:dark cycle.

Recording time percentage spent in wake across (**A**) baseline and (**B**) post-CFC periods were generally similar for vehicle and ML297 groups. When percent time in wake was calculated across the first 6 h of the dark phase (ZT12-18), vehicle mice spent more time in wake compared to ML297 mice (* indicates $p < 0.05$, Sidak's *post hoc* test vs. vehicle $n = 6$ mice/group). Gray shaded areas represent lights off.

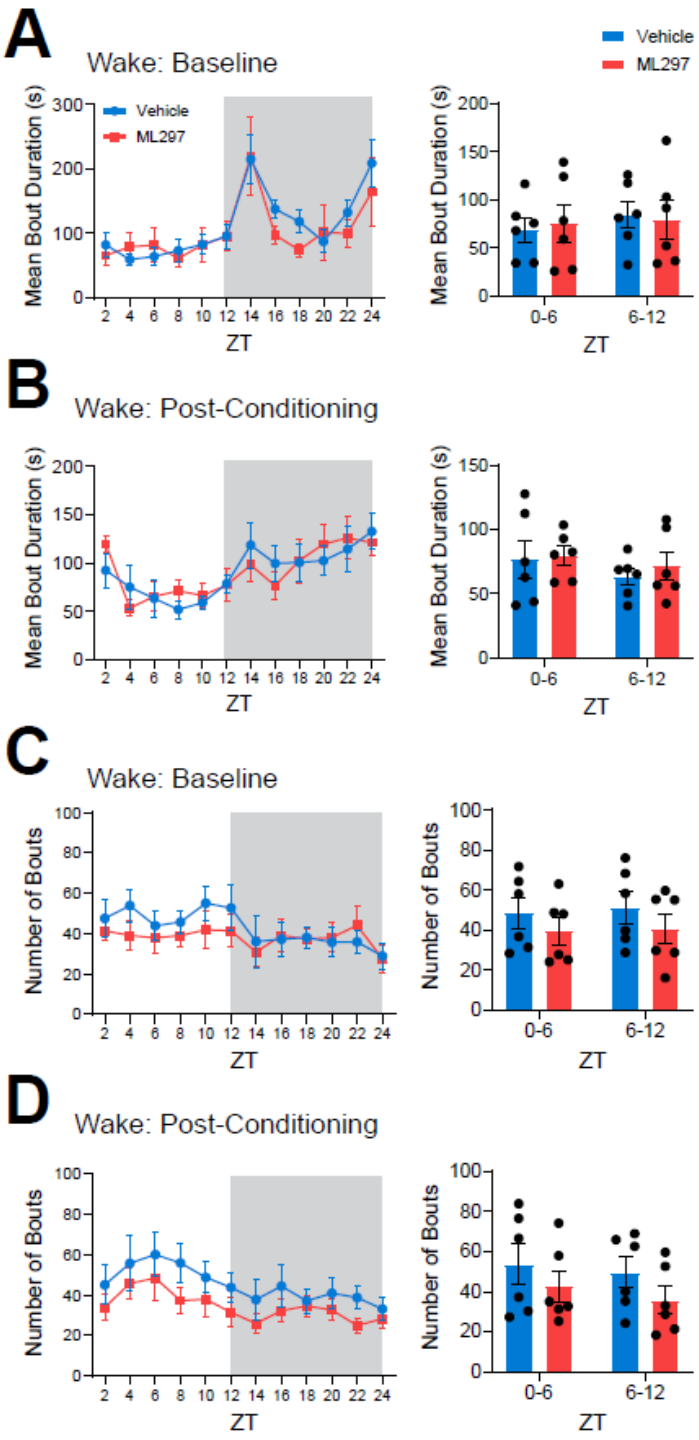

Supplemental Figure 3.4: Wake architecture in vehicle and ML297 groups.

Mean bout duration for wake during (**A**) baseline and (**B**) post-CFC periods in vehicle and ML297 groups were similar. Number of wake bouts during (**C**) baseline and (**D**) post-CFC periods in vehicle- and ML297-treated mice were also similar. Gray shaded areas represent lights off. *n* = 6 mice/group

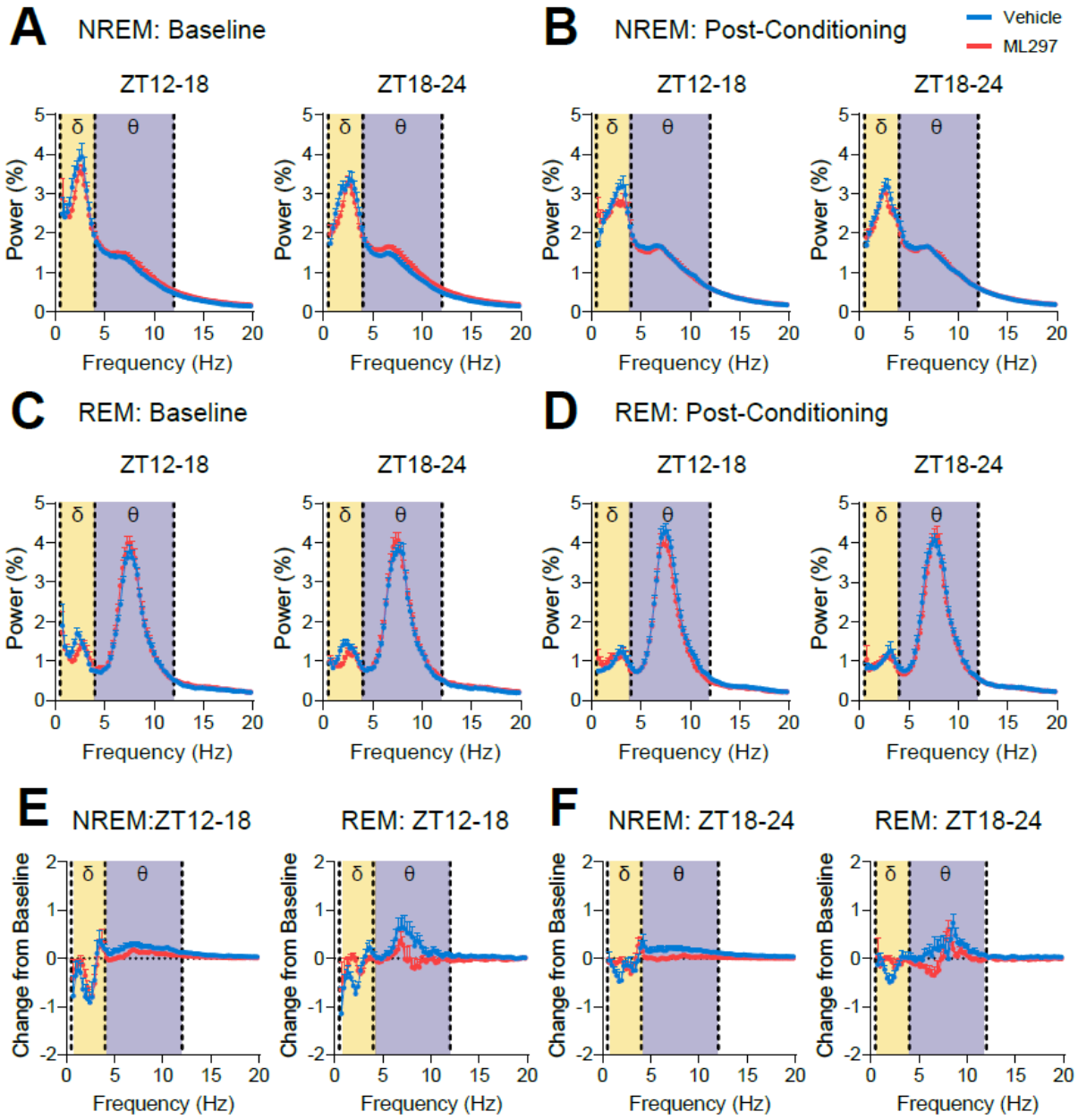

Supplemental Figure 3.5: NREM and REM EEG spectral power across the dark phase (ZT12-24).

EEG power spectra (recorded over visual cortex, bilaterally) for the dark cycle (12-24) are shown for vehicle and ML297 groups during NREM baseline (**A**) and post-CFC (**B**), and during REM baseline (**C**) and post-CFC (**D**). Values indicate % of total spectral power at each frequency band, mean ± SEM; *n* = 6 mice/group. No significant changes between vehicle and ML297 groups were observed during baseline or post-CFC. *n* = 6 mice/group. (**E-F**) Change in spectral power from baseline for NREM and REM sleep. No changes in spectral power from baseline were observed at specific delta or theta frequencies.

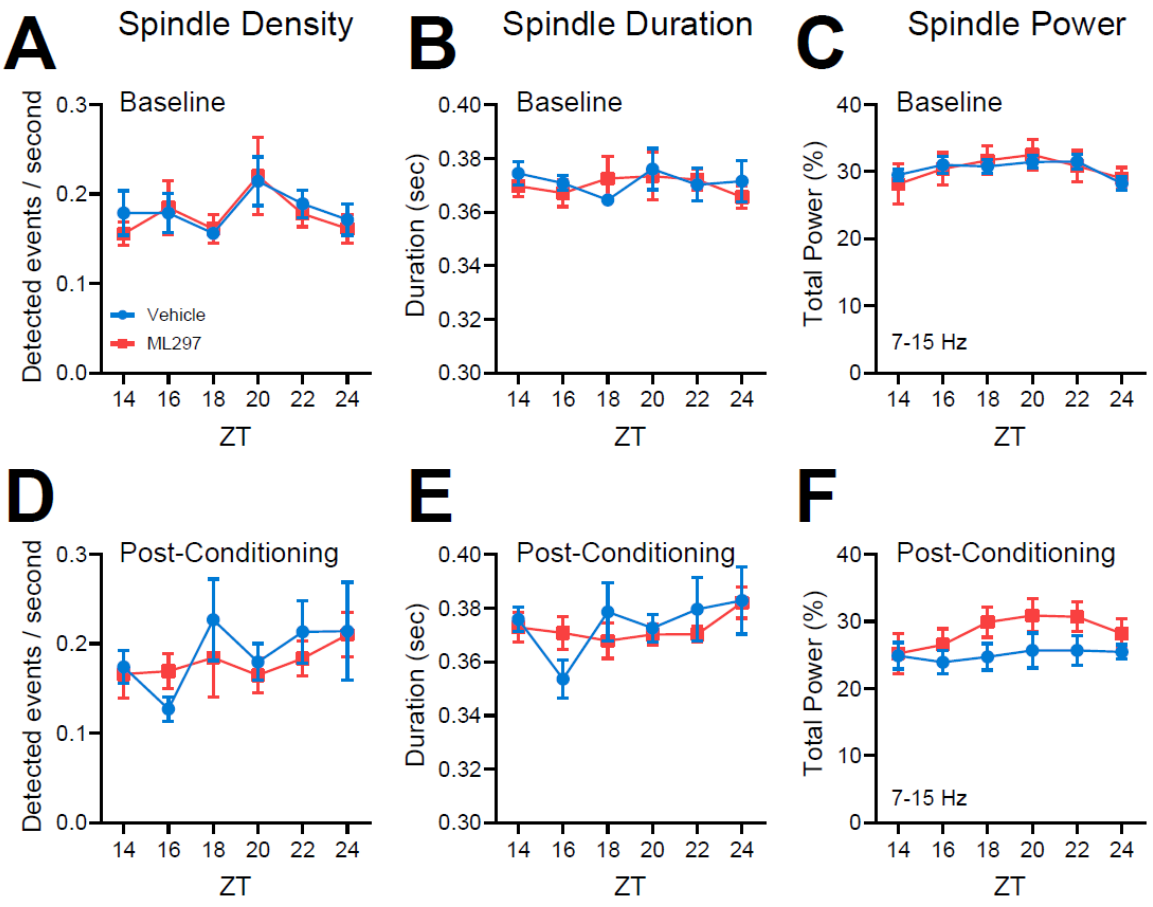

Supplemental Figure 3.6: NREM sleep spindle features in the dark phase (ZT12-24) following CFC.

NREM spindle density (**A**) and spindle duration (**B**) were similar between vehicle and ML297 groups for hours 12-24 during baseline. (**C**) NREM EEG spectral power within the spindle/sigma frequency band (7-15 Hz) was similar between groups at baseline. NREM spindle density (**D**) and mean duration (**E**) were similar between both vehicle- and ML297-treated mice following CFC at ZT12-24. (**F**) Average NREM spindle power was significantly different in vehicle-treated mice relative to ML297-treated mice, over the entire dark phase following CFC (two-way RM ANOVA; p(time of day x treatment) = 0.0300; $F(5, 50 = 2.718)$. Values indicate mean ± SEM; n = 6 mice/group.

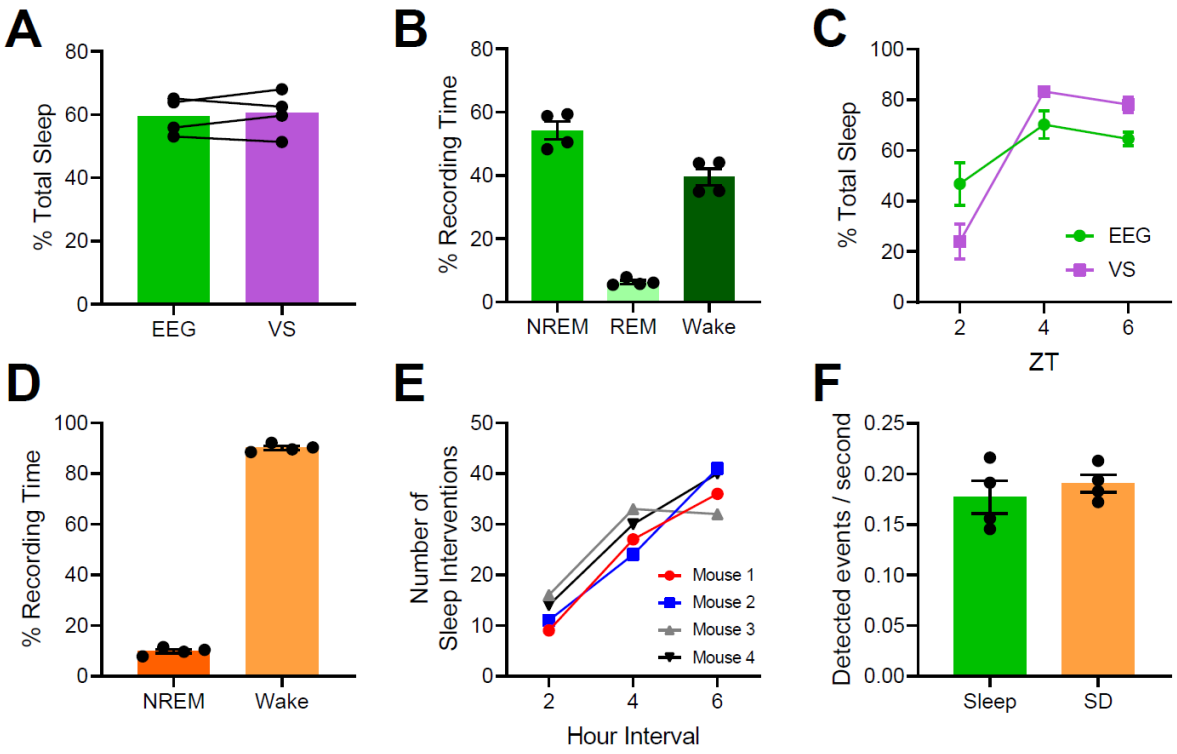

Supplemental Figure 3.7: Validation of visual observation-based sleep scoring and SD methods.

(**A**) Total percentage of time spent in sleep, compared for the same cohort of mice using EEG/EMG and visual scoring (VS) over a 6-h period (ZT0-6), was similar. Values indicate mean ± SEM; n = 4 mice/group. (**B**) Sleep architecture for EEG recorded mice. (**C**) Total sleep across 2-h bins for EEG vs. VS methods. (**D**) Total percentage of recording time spent in wake and NREM sleep in EEG/EMG recorded mice across 6 h SD by gentle handling. As a group, SD mice spent 90% of the SD period awake, and did not enter REM sleep. (**E**) Across SD, an increasing number of experimental interventions (cage tapping, cage shaking, nest disturbances) were required to maintain wakefulness, consistent with increasing sleep pressure. (**F**) Spindle density during brief periods of NREM within SD was similar to that observed during ad lib sleep.

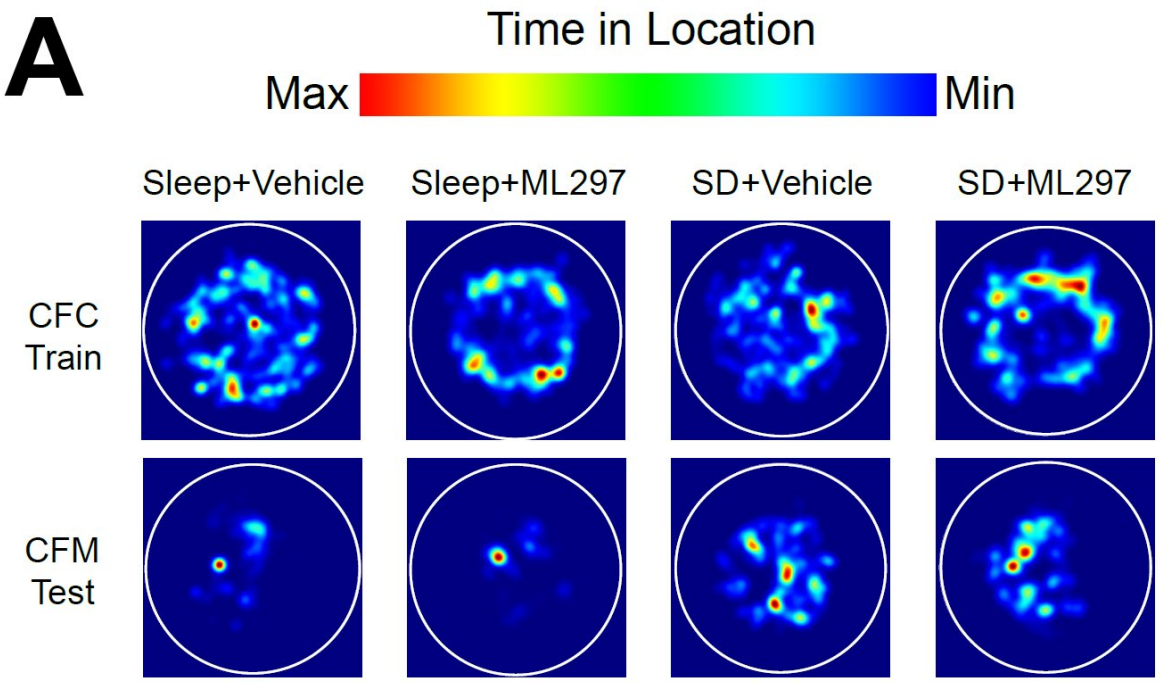

Supplemental Figure 3.8: Representative heat maps of time-in-location for individual non-implanted mice during CFC training and CFM testing.

(**A**) Heat maps indicating time spent in various locations within the CFC chamber for representative vehicle and ML297 mice during CFC and CFM testing. Red represents locations in the CFC chamber where mice spent the most time, while blue represents locations in the CFC chamber where mice spent the least time.

Chapter 4 : Hypnotic Treatment Reverses NREM Sleep Disruption and EEG Desynchronization in a Mouse Model of Fragile X Syndrome to Rescue Memory Consolidation Deficits

This chapter includes the manuscript currently in preparation for submission to Neuron: ***Martinez JD****, Wilson LG, Brancaleone WP, Peterson KP, Popke DS, Caicedo Garzon V, Perez Tremble RE, Donnelly MJ, Torres D, Mendez Ortega SL, Shaver JJ, Clawson BC, Yang Z, Jiang S, & Aton SJ. (2023) Hypnotic treatment reverses NREM sleep disruption and EEG desynchronization in a mouse model of Fragile X syndrome to rescue memory consolidation deficits.*

4.1 : Abstract

Fragile X syndrome (FXS) is a leading cause of genetic-related intellectual disability associated with disrupted cognitive function and profound sleep abnormalities. Sleep loss itself negatively impacts cognitive function, yet the contribution of sleep loss to impaired cognitive function in FXS is understudied. One untested possibility is that disrupted cognition in FXS is exacerbated by abnormal sleep. We hypothesized that disruption of sleep-dependent mechanisms negatively impacts cognitive functions such as memory consolidation. We examined if altering sleep architecture using ML297, a hypnotic treatment acting on G-protein-activated inward-rectifying potassium channels, to promote sleep could improve deficits in memory consolidation in *Fmr1*$^{-/y}$ mice. We

found deficits in NREM sleep architecture, spectral power, and inter-cortical coherence in *Fmr1*$^{-/y}$ mice that were rescued with ML297. Restoration of sleep also showed improved cognition via fear learning and spatial memory tasks. Lastly, we found hippocampal activation patterns associated with memory formation change with ML297 to facilitate improved cognition. These studies provide a comprehensive examination of the impact of sleep on neurophysiological and behavioral phenotypes of FXS, with our data suggesting sleep as a potential therapeutic target for improving health and cognitive outcomes in FXS.

4.2 : Introduction

Fragile X syndrome (FXS) is an X-linked neurodevelopmental disorder (NDD) resulting from silencing of the *FMR1* gene and loss of Fragile X messenger Ribonucleoprotein (FMRP). It is the leading cause of both heritable intellectual disability and syndromic autism spectrum disorder (ASD) in pediatric patients [1,2], and is characterized by altered sensory processing, hyperactivity, and cognitive impairments [3-5]. Available data suggest that FXS patients often experience difficulty falling asleep and frequent nighttime awakenings [6-9], although the relationship between altered sleep and cognitive and behavioral aspects of FXS is unknown. *Fmr1* knockout mice recapitulate behavioral phenotypes seen in FXS patients, and exhibit deficits in sensory-driven synaptic plasticity and hippocampus-mediated learning and memory consolidation [10-15]. However, relatively little is known about their sleep architecture. Limited data using home-cage observational studies show sleep changes across development with juvenile *Fmr1*$^{-/y}$ mice showing no differences in total sleep time during the light phase compared to wild-type (WT) controls, but reaching younger adulthood, *Fmr1*$^{-/y}$ mice begin demonstrating

significantly reduced overall sleep time [16,17]. However, a full characterization of sleep behavior *Fmr1*$^{-/y}$ mice using 24-h polysomnography has not been done. Since sleep loss is known to have detrimental effects on cognitive function and synaptic plasticity in both humans and mice, one untested possibility is that disrupted sensory processing and cognition in FXS could be exacerbated by abnormal sleep.

Sleep has essential roles in plasticity and cognition, specifically hippocampal-dependent memory consolidation [18-26]. This is evident in individuals diagnosed with sleep disorders such as insomnia, who report not only loss of sleep, but associated negative behavioral symptoms such as fatigue and cognitive impairments. In individuals with ASD or another neurodevelopmental disorders, these sleep disturbances are more impactful [27-30]. Successful treatment of sleep disruptions in FXS could prevent sleep loss-mediated negative impacts cognition (i.e., memory processing), but also early brain development and cortical maturation [31-34]. Recent work on new classes of hypnotic drugs including orexin receptor antagonists and activators for G-protein inward rectifying potassium (GIRK) channels have shown promise to promote sleep without affecting other neurobiological functions including cognition [35-37]. Four distinct subunits (GIRK1-4) form homo- and heterotetrametric channels in several brain regions and cardiac tissue with combinations of GIRK1/2 being most common in regions such as the hippocampus, neocortex, and cerebellum [38-40]. GIRK1/2 subunits can be directly activated using the selective and potent compound, ML297, to promote hyperpolarization of the cell and subsequent reduced excitability [41,42]. Recent studies using ML297 in rodents have shown it suppresses seizure activity, acts as an anxiolytic, increases NREM sleep, and improves

memory consolidation via promotion of REM sleep[37,41-44]. Intriguingly, GIRK1/2 channel activity is likely disrupted by loss of FMRP [45,46].

In this study, we characterized sleep architecture and EEG activity in *Fmr1*$^{-/y}$ mice in multiple cortical regions and found deficits that were largely reversed by GIRK1/2 channel agonist, ML297. ML297 administration following training on two hippocampus-mediated, sleep-dependent tasks (object location memory and contextual fear memory) led to a rescue of disrupted consolidation of memory in these tasks. These studies set groundwork for understanding sleep as a therapeutic target for treating patients with FXS.

4.3 : Materials and Methods

4.3.1 : Experimental models and subject details

We generated male *Fmr1*$^{-/y}$ mice and wild-type (WT) littermates in-house by crossing WT male mice with *Fmr1* heterozygous (*Fmr1*$^{+/-}$) both on a C57BL/6 background (The Jackson Laboratory, Stock #. 003025). Genotypes for mice were determined using standard PCR methods and primers set available via the Jackson Laboratory. For all experiments, 4–5-month-old mice were used. Mice were housed under a 12:12 hour light/dark cycle (lights on at 9:00 AM), provided with compressed cotton and “Enviro-dri” paper nesting and bedding material (Shepherd Specialty Papers, TN), and had *ad lib* access to water and food. Mice were housed with littermates until either EEG electrode implantation surgery or behavior, at which point they were single housed in standard cages with extra nesting and bedding material for enrichment. Mice that underwent EEG recording had open tops to ensure no issues with tethering of cables. All mouse husbandry, experimental, and surgical procedures were reviewed and approved by the University of Michigan Internal Animal Care and Use Committee.

4.3.2 : EEG-EMG surgical procedures and neural data acquisition

Mice were anesthetized with 1-2% isoflurane anesthesia in O_2 and administered ketoprofen (0.005 mg/kg; intraperitoneal injection, i.p.). Mice were placed into a stereotaxic frame and maintained under isoflurane. Mice were fitted with two miniature, stainless steel screw electrodes (P1 Technologies, Catalog #: E362/96/1.6/SPC) positioned over primary visual cortex (V1; 2.9 mm anterior/posterior [AP] and 2.7 mm medial/lateral [ML]) and prefrontal cortex (PFC; 1.8 mm ML). A reference screw was placed over cerebellum and a braided stainless steel wire EMG electrode was placed in the nuchal muscle. EMG electrodes were custom made with stranded stainless-steel wire (Cooner Wire, Catalog No: AS636) soldered to miniature stainless steel male pins (P1 Technologies, Catalog No: 363A/PKG). The implant was secured using a pedestal (P1 Technologies, Catalog No: MS7P) bonded with super glue (Loctite) and dental alike solution. Mice were placed in single housed cages and left on a heating pad until fully mobile. After 11 days of postoperative recovery, each mouse was moved to a new cage with an open top and habituated to tethering of flexible cables for 3 days before recorded data collection. Mice were recorded for four consecutive days (96 hours total). Day 1 was a 24-h baseline recording (Baseline A) starting at lights-on (ZT0). After 24 hours (Day 2), mice were injected with vehicle solution at lights-on and recorded. Day 3 was a second baseline recording (Baseline B). Day 4, mice were injected with ML297 (30 mg/kg) at lights-on and recorded for a final 24-hour period.

4.3.3 : Sleep state and power spectra analysis

EEG/EMG signals (0.5-300 Hz) were amplified at 20 ×, digitized, further digitally amplified at 20-100 ×, and continuously recorded (with a 60-Hz notch filter applied to

remove environmental noise) using Plexon Omniplex software and hardware (Plexon Inc., TX) as previously described Baseline and post-treatment recordings were scored manually in 10-second epochs as wake, NREM, or REM sleep using custom MATLAB software and previously published studies [25,26,44,47-49]. Scorers were blind to genotype and recording day. EEG and EMG data were band-pass filtered at 0-90 Hz and 150-250 Hz, respectively, for viewing during scoring. NREM sleep was defined as synchronized, high amplitude, low frequency oscillations within the EEG and low EMG activity. REM sleep was defined as reduced, low frequency oscillations and a theta rhythm pattern (4-12 Hz) with lack of EMG activity. Wakefulness was defined as de-synchronized EEG activity with active EMG activity. For power spectra analysis, raw EEG data (0.5-300 Hz) was first filtered to 0.5-100 Hz using custom MATLAB scripts, Afterwards, using Neuroexplorer 5 software (Nex Technologies), EEG data underwent a fast-Fourier transform (FFT) using a 500 ms window with a Hann taper and window overlap of 50% to display and calculate percentage of power spectral data.

4.3.4 : Sleep spindle identification and spectral coherence analysis

An automated spindle detection algorithm made with custom MATLAB software was used to identify sleep spindles in band-pass filtered EEG data (7-15 Hz), as intervals containing ≥ 6 successive deviations (i.e., peaks or troughs) of signal that surpassed mean signal amplitude by 1.5 standard deviations, lasting between 0.25-1.75 seconds [44,47]. The coherence of raw EEG data at given frequencies was analyzed using Neuroexplorer 5 software (Nex Technologies) using previously published methods [50,51]. Coherence was calculated using a 0.5 s Welch's window with a 50% overlap. Coherence generated values are expressed from 0 to 1.0, with 0 indicating no relationship between

two signals (two brain regions) at a given frequency and 1.0 indicating a perfect, linear relationship. Band coherence for frequency bands of interest was assessed by averaging the coherence values with each designated frequency band.

4.3.5 : Pharmacological preparation and injection

ML297 was purchased from Tocris Bioscience (Catalog #. 5380). For all experiments, ML297 was initially dissolved in DMSO and diluted with 0.5% hydrooxypropyl cellulose aqueous solution. Mice were injected with a 30mg/kg solution of ML297, dosage based on previously published studies in rodent [41,43,44]. Vehicle solutions consisted of 2% DMSO in 0.5% hydroxypropyl cellulose aqueous solution.

4.3.6 : Contextual fear conditioning (CFC)

Mice underwent single-trial CFC as previously described [25,26,44,48,52,53]. Mice were handled by the experimenter for 5 minutes daily for 3 days prior to training. Each mouse was placed in a novel cylindrical conditioning chamber made of clear Plexiglas with a black and white checkerboard pattern and metal grid floor (Med Associates). Before each individual mouse session, the arena was cleaned with a 5% Lysol solution. Mice were allowed to freely explore for 2 min and 28 s, after which they received a 0.75 mA, 2 s foot shock through the grid floor, followed by an additional 30 s in the CFC chamber. Immediately following CFC, mice were returned to their home cage. For studies on ML297, mice were given an i.p. injection of either ML297 (30 mg/kg; Tocris) or vehicle (2% DMSO in 0.5% hydrooxypropyl cellulose aqueous solution). Injections occurred within 2 min of removal from the CFC chamber. Contextual fear memory (CFM) tests were conducted 24 h later by returning mice to the CFC chamber for 5 min. Both CFC training

and CFM testing began at lights-on (ZT0), and mice were video monitored continuously during both sessions.

4.3.7 : Object location memory (OLM) and open field (OF) tests

Mice underwent a single trial OLM task as previously described [23,54,55]. Here, mice are placed in a rectangular arena made of grey PVC walls, transparent PVC bottom, and the following dimensions: length of 40 cm, width of 30 cm, and height of 30 cm. Spatial cues were placed on the opposite sides of the short walls and consisted of one black and white checkerboard pattern and one black and white striping pattern. Mice were handled by the experimenter for 5 minutes daily for 4 days prior to training. Prior to each session, the arena and objects were cleaned with a 10% ethanol solution. Before training, mice were habituated to the arena, which consisted of 5 minutes of free exploration and served as the OF test. The OF test is a rapid assessment of well-defined behaviors such as anxiety-related behaviors, body activity, and locomotion that require little to no prior training to the subject mouse [56]. During training, a pair of identical objects were placed symmetrically across in the middle of the arena. Mice were placed in the arena facing the wall and were allowed to freely explore the arena and objects for 10 mins. Immediately following training, mice were returned to their home cage. For studies on ML297, mice were given an i.p. injection of either ML297 (30 mg/kg; Tocris) or vehicle (2% DMSO in 0.5% hydrooxypropyl cellulose aqueous solution). Injections occurred within 1 min of removal from the OLM arena. OLM tests were conducted 24 h later. During testing, one object was displaced (novel location) along a straight line diagonally from the object in the same position (familiar location). The displacement of the object and its novel location were all counterbalanced to avoid place and object preferences. Mice were again allowed

to freely explore the arena and objects for 10 mins. Both OLM training and OLM testing began at lights-on (ZT0), and mice were video monitored continuously during both sessions and the habituation (OF test) period.

4.3.8 : CFM and OLM behavior quantification

All behavioral measurements were assessed using Ethovision XT 16 (Noldus) software with files coded for blind scoring. For CFC behavior, freezing was measured using in a semi-automated manner. Freezing was first scored based on transient periods of immobility, as described previously [44,57] and was verified offline based on the assessment of characteristic freezing-associated posture [26,49]. CFM-associated freezing behavior was quantified by subtracting each mouse's % freezing time during pre-shock baseline from % freezing time across the entire CFM test, as described previously [26,44,48,52]. For OF test (habituation period), the total ambulatory distance was measured to account for differences in locomotor ability. Thigmotaxis (or wall-hugging behavior), an anxiety-related behavior, was measured by comparing percentage of time spent in the outer (wall) zone vs. the inner (center) zone [56]. Both locomotor ability and thigmotaxis were measured to ensure analyses in OLM were not skewed due to inactivity instead of genotype or treatment effects. For OLM behavior, measurements were based on time mice spent exploring the familiar and displaced object. Engagement with object included directing nose to the object at no more than 1 cm and/or touching the object. A discrimination index was used a relative measure of discrimination corrected for total exploration time [23].

4.3.9 : Sleep monitoring and sleep deprivation (SD)

Following CFC training, mice that were either allowed *ad lib* sleep (Sleep) or were sleep-deprived (SD) via gentle handing over the next 6 h (ZT0-6). This method of SD was chosen based on prior work showing that stress response (e.g. glucocorticoid production) evoked by gentle handling SD is not sufficient to disrupt consolidation of fear memory (and in fact may enhance consolidation) [54,58,59]. For SD, gentle handling procedures included cage tapping or shaking, or nest disturbance and has been previously shown to ensure above 90% wakefulness based on EEG/EMG validation [44]. Following SD, all mice were allowed *ad lib* recovery sleep over the next 18 h prior to CFM testing. For *ad lib* sleep mice, sleep was quantified over the first 6 h post-CFC via visual monitoring. Every 5 min, individual mice were scored as awake or asleep, with sleep identification based on immobility, slow breathing, and presence of stereotyped (crouched) sleep postures, consistent with prior studies [60-62] and has been validated with similar total sleep time in EEG/EMG implanted mice [44].

4.3.10 : Histology and immunohistochemistry

To quantify hippocampal activation patterns associated with recall, 90 min following the conclusion of CFM tests, mice were euthanized with an overdose of sodium pentobarbital and perfused with ice cold PBS, followed by ice cold 4% paraformaldehyde. Brains were dissected, post-fixed, and cryoprotected in a 30% sucrose solution. 50 µm coronal dorsal hippocampal and amygdala sections were cryosectioned. To quantify parvalbumin (PV) interneuron expression in the thalamic reticular nucleus (TRN), brains were dissected, post-fixed, and rinsed in PBS. 100 µm coronal sections containing TRN were collected via a vibratome.

For all tissue, free-floating sections were washed in PBS with 0.2% Triton X-100 (PBST) three times, each for 10 mins,and then incubated in Starting Block™ blocking buffer (Thermo Scientific) for 1 hour. Sections were then incubated overnight in primary antibody at 4°C: rabbit-anti-cFos (1:1000; Abcam, ab190289) in 5% Starting Block blocking solution (hippocampus and amgydala sections) or mouse-anti-PV (1:2000; Millipore, MAB11572) in 5% Starting Block blocking solution (TRN sections). Sections were then washed in PBST, two times for 10 minutes and incubated with secondary antibody: Alexa Fluor 488 (1:200; Invitrogen, A11032) in 5% Starting Block blocking solution (cFos sections) or Alexa Fluor 594 (1:200; Invitrogen, A11034) in 5% Starting Block blocking solution (PV sections). Sections were washed in PBS, two times, mounted on microscope slides (Fisherbrand Superfrost Plus) and coverslipped with Prolong Gold antifade reagent with DAPI (Invitrogen, P36931).

4.3.11 : Microscopy and image analysis

Images were obtained using a Leica SP8 confocal microscope with a 10X objective, to obtain z-stack images (10 µm steps) for maximum projection of fluorescence signals. Identical image acquisition settings (e.g. exposure times, frame average, pixel size) were used for all sections. For analysis of hippocampal and amygdala activation patterns, three images per section of dorsal hippocampus and amygdala were taken per mouse and areas for regions of interest (ROI) were determined using previously established methods [52,60]. cFos+ neuron density was quantified in subregions of these ROIs (i.e., pyramidal or granule cell layers, DG hilus). For analysis of parvalbumin (PV+) interneuron expression within the thalamic reticular nucleus (TRN), cell density was measured using the number of PV+ cells counted within the area made via the ROI

surrounding the TRN. Counts were made by two scorers blinded to genotype and treatment using Fiji image analysis software, with the final number computed using the average of counts made by the two scorers.

4.3.12 : Statistical analysis

Data analyses were carried out in a blind manner; in some cases (e.g., EEG recordings and cell counts), data was consensus scored by two individuals to reduce variability. Exclusion criteria for EEG recordings were based on lack of signal in one cortical region or faulty reference electrode that prevented confirmation of recording signals. For CFC behavior, exclusion criteria consisted of freezing levels above 15% before shock administration during CFC training sessions. For OLM behavior, exclusion criteria included mice that spend less than 10 seconds interacting with objects during 10-minute training sessions or exhibited impaired locomotor ability and/or thigmotaxis. Statistical analyses were carried out using GraphPad Prism software (Version 9.5). For each specific data set, the statistical tests and *p*-values are listed within the appropriate corresponding figure legend.

4.4 : Results

4.4.1 : Fmr1$^{-/y}$ mice have disrupted NREM sleep architecture and altered EEG activity

To fully characterize sleep phenotypes in a FXS mouse model, we used continuous EEG/EMG recording in *Fmr1*$^{-/y}$ mice and male wild-type (WT) littermates. 4-5 month old WT and *Fmr1*$^{-/y}$ mice implanted with bilateral EEG electrodes over primary visual cortex (V1) were recorded in a 12 h: 12 h light:dark cycle, and comparisons of sleep architecture were first made across the 12-h light (i.e., rest) phase (ZT0-12) (**Figure 4.1A-**

B). *Fmr1*$^{-/y}$ mice spent significantly less total time in non-rapid eye movement (NREM) sleep and more time in wake. In contrast, rapid eye movement (REM) sleep amounts were similar between WT and *Fmr1*$^{-/y}$ mice (**Figure 4.1C**). The total number of NREM and wake bouts (but not REM bouts) was significantly greater in *Fmr1*$^{-/y}$ mice compared to WT littermates (**Figure 4.1D**), while the mean duration of NREM bouts (but not wake or REM bouts) was significantly shorter in *Fmr1*$^{-/y}$ mice (**Figure 4.1E**). To test whether other specific features of NREM sleep architecture were disrupted in *Fmr1*$^{-/y}$ mice, we next compared NREM sleep spindles - discrete waxing-and-waning EEG oscillations of 7-15 Hz [i.e., sigma (σ) band]) [63-66] between the two genotypes. Using a semi-automated method to detect spindle events in the EEG [44,47], we found that spindle density in NREM sleep was significantly decreased in *Fmr1*$^{-/y}$ mice compared to WT littermates (**Figure 4.1F**). Mean spindle duration was similar between genotypes (**Supplemental Figure 4.1A**). These changes in spindling were associated with morphological changes in the thalamic reticular nucleus (TRN) – a structure which is known to play an essential role in generation of NREM spindles [67] - in *Fmr1*$^{-/y}$ mice. Using immunohistochemistry (IHC), we found a reduced density of parvalbumin-expressing (PV+) interneurons in the TRN of *Fmr1*$^{-/y}$ mice compared to WT littermates (**Supplemental Figure 4.2**). Together, these findings suggest that NREM sleep is disrupted and fragmented, with alterations to associated thalamocortical oscillations, in this Fragile X mouse model.

Altered EEG patterns in either sleep or wake are widely reported in individuals with ASD and in mouse models of specific neurodevelopmental disorders [68-76]. To better characterize state-specific EEG oscillations in *Fmr1*$^{-/y}$ mice, we next compared power spectral density of EEG activity, across a wide range of frequencies, for each brain state.

Fmr1$^{-/y}$ mice showed significantly increased delta (δ; 0.5-4 Hz), and decreased sigma (σ; 7-15 Hz) power in the EEG during NREM sleep, and significantly reduced theta (θ; 4-12 Hz) activity in the EEG during REM sleep, compared to WT littermates (**Figure 4.1G-H**). Consistent with previous findings from *Fmr1*$^{-/y}$ mice and rats [77-79], gamma (γ; 31-100 Hz) power was increased in the EEG during both NREM and wake in *Fmr1*$^{-/y}$ mice (**Figure 4.1I-J; Supplemental Figure 4.1B-C**). Thus, multiple state-specific cortical, thalamocortical, and hippocampal oscillations [80,81] are disrupted in *Fmr1*$^{-/y}$ mice, in association with disruptions in overall sleep architecture. These changes may be partly due to microcircuit-level differences in brain structures such as the TRN, which are essential for coordinating these oscillations [67].

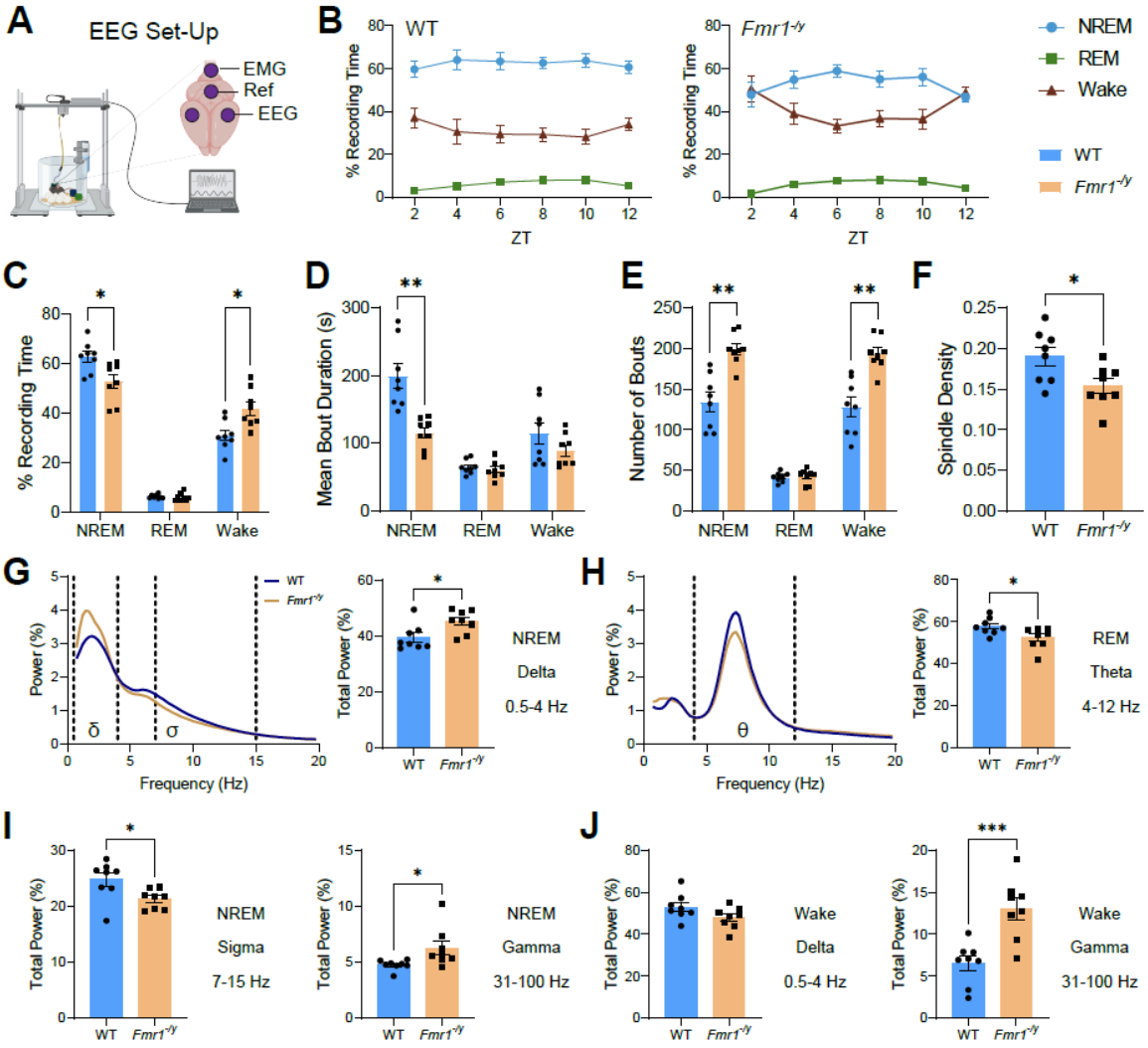
A
EEG Set-Up
EMG
Ref
EEG
B
WT
Fmr1-/y
% Recording Time
ZT
NREM
REM
Wake
WT
Fmr1-/y
C
% Recording Time
NREM
REM
Wake
D
Mean Bout Duration (s)
E
Number of Bouts
F
Spindle Density
G
Power (%)
Frequency (Hz)
δ
σ
Total Power (%)
NREM
Delta
0.5-4 Hz
H
θ
REM
Theta
4-12 Hz
I
NREM
Sigma
7-15 Hz
NREM
Gamma
31-100 Hz
J
Wake
Delta
0.5-4 Hz
Wake
Gamma
31-100 Hz

Figure 4.1: *Fmr1*$^{-/y}$ mice have disrupted NREM sleep architecture and altered EEG activity

(A) Schematic of EEG/EMG recording configuration, with EEG electrodes positioned over bilateral primary visual cortex (V1).

(B) Wild-type (WT) littermates (***left***) and *Fmr1*$^{-/y}$ mutants' (***right***) time spent in sleep and wake states across the 12-h light phase.

(C) Percent recording time (for the entire 12-h light phase) spent in NREM sleep, REM sleep, and wake for WT and *Fmr1*$^{-/y}$ mice. Two-way RM ANOVA, p(state) < 0.0001, p(genotype) = 0.19, p(state x genotype interaction) = 0.0014.

(D) Mean bout durations across the light phase for NREM, REM, and wake. Two-way RM ANOVA, p(state) < 0.0001, p(genotype) = 0.0062, p(state x genotype interaction) = 0.0003.

(E) Number of light-phase bouts of NREM, REM, and wake. Two-way RM ANOVA, p(state) < 0.0001, p(genotype) = 0.0005, p(state x genotype interaction) < 0.0001.

(F) NREM spindle density during the light phase was lower for *Fmr1*$^{-/y}$ mice.

(G) NREM EEG power spectra (***left***), showing increased mean delta (δ; 0.5-4 Hz) power in *Fmr1*$^{-/y}$ mice. Two-way RM ANOVA, p(frequency) < 0.0001, p(genotype) = 0.60, p(frequency x genotype interaction) < 0.0001. Total NREM delta-band power across the 12-h light phase (***right***) was also increased.

(H) REM EEG power spectrum (***left***), showing reduced theta (θ; 4-12 Hz) power in *Fmr1*$^{-/y}$ mice. Two-way RM ANOVA, p(frequency) < 0.0001, p(genotype) = 0.10, p(frequency x genotype interaction) < 0.0001. Total REM theta-band power across the 12-h light phase (***right***) was also reduced.

(I) Total sigma-band for spindles (7-15 Hz; ***left***) and gamma-band (31-100 Hz; ***right***) power were reduced and increased, respectively, in *Fmr1*$^{-/y}$ mice during NREM sleep.

(J) Total delta-band (***left***) and gamma-band (***right***) power were reduced and increased, respectively, in *Fmr1*$^{-/y}$ mice during wake.

n = 8 mice/genotype. *, **, and *** indicate p < 0.05, p < 0.01, and p < 0.001, Sidak's *post hoc* test (**C-E**) or two-tailed, unpaired t-test (**F-J**). Data points and error bars indicate mean ± SEM.

4.4.2 : Administration of novel hypnotic compound ML297 renormalizes NREM sleep architecture in Fmr1$^{-/y}$ mice

After finding evidence of sleep disruption and altered EEG activity in *Fmr1*$^{-/y}$ mice, we sought to restore normal sleep architecture via hypnotic treatment. Recent studies have characterized hypnotic actions of the G protein-coupled potassium channel (GIRK)1/2 activator ML297, which promotes physiologically normal sleep without cognitive side effects [43,82]. Because activation of GIRK channels (via coupling to $GABA_B$ receptors) is thought to be disrupted in FXS due to loss of FMRP [45,46], ML297 may have an ideal mechanism of action for restoring sleep in this mouse model. To explore this possibility, we characterized sleep/wake architecture after administration of ML297 or vehicle in *Fmr1*$^{-/y}$ mice. 4–5-month-old *Fmr1*$^{-/y}$ mice and WT littermates were implanted with EEG recording electrodes over V1 and prefrontal cortex (PFC) to characterize state-specific EEG activity across brain regions. Implanted mice then underwent a 4-day recording paradigm, consisting of baseline and treatment conditions. (**Figure 4.2A**).

Baseline recording days (baselines A and B) were characterized by significantly decreased NREM sleep, increased wake, and comparable REM sleep across the 12-h light phase (ZT0-12) in *Fmr1*$^{-/y}$ mice compared to WT mice, but minimal significant changes across the dark phase (ZT12-24; **Supplemental Figure 4.3A-B**). Disrupted NREM sleep architecture (increased NREM and wake bout numbers, decreased NREM bout durations) was also present in *Fmr1*$^{-/y}$ mice across both baseline days' light phase (**Supplemental Figure 4.3C-F**). While vehicle treatment did not correct disruptions to NREM sleep in *Fmr1*$^{-/y}$ mice (**Figure 4.2B**), recordings following ML297 administration showed restoration of NREM sleep time, bout duration, and bout number to levels seen

in WT littermates (**Figure 4.2C**). Quantification of changes to sleep architecture due to vehicle or ML297 was done by comparing sleep state variables with those in corresponding baseline recordings (i.e., baseline A [day 1] vs. vehicle [day 2]; baseline B [day 3] vs. ML297 [day4]). ML297, but not vehicle, significantly increased NREM sleep amounts across the light phase (i.e., in the 12 h following administration) (**Figure 4.2D**), increased NREM bout duration, and reduced NREM bout numbers in *Fmr1*$^{-/y}$ mice (**Figure 4.2E-F**). No changes in REM were noted after ML297 administration (**Figure 4.2G-K**), and WT littermates administered ML297 showed no changes to either NREM or REM sleep (**Figure 4.2**). Furthermore, latency to NREM and REM sleep was similar between both genotypes and treatments (**Supplemental Figure 4.4**). Wake bouts were also normalized in *Fmr1*$^{-/y}$ mice, leading to decreased wake time and bout numbers (**Supplemental Figure 4.4**). Together, these data suggest that disrupted sleep phenotypes in *Fmr1*$^{-/y}$ mice were renormalized by ML297 to match WT littermates. This indicates that acute ML297 treatment, which restores GIRK1/2 channel activation thought to be disrupted in FXS [45,46], can rescue NREM sleep deficits present in *Fmr1*$^{-/y}$ mice.

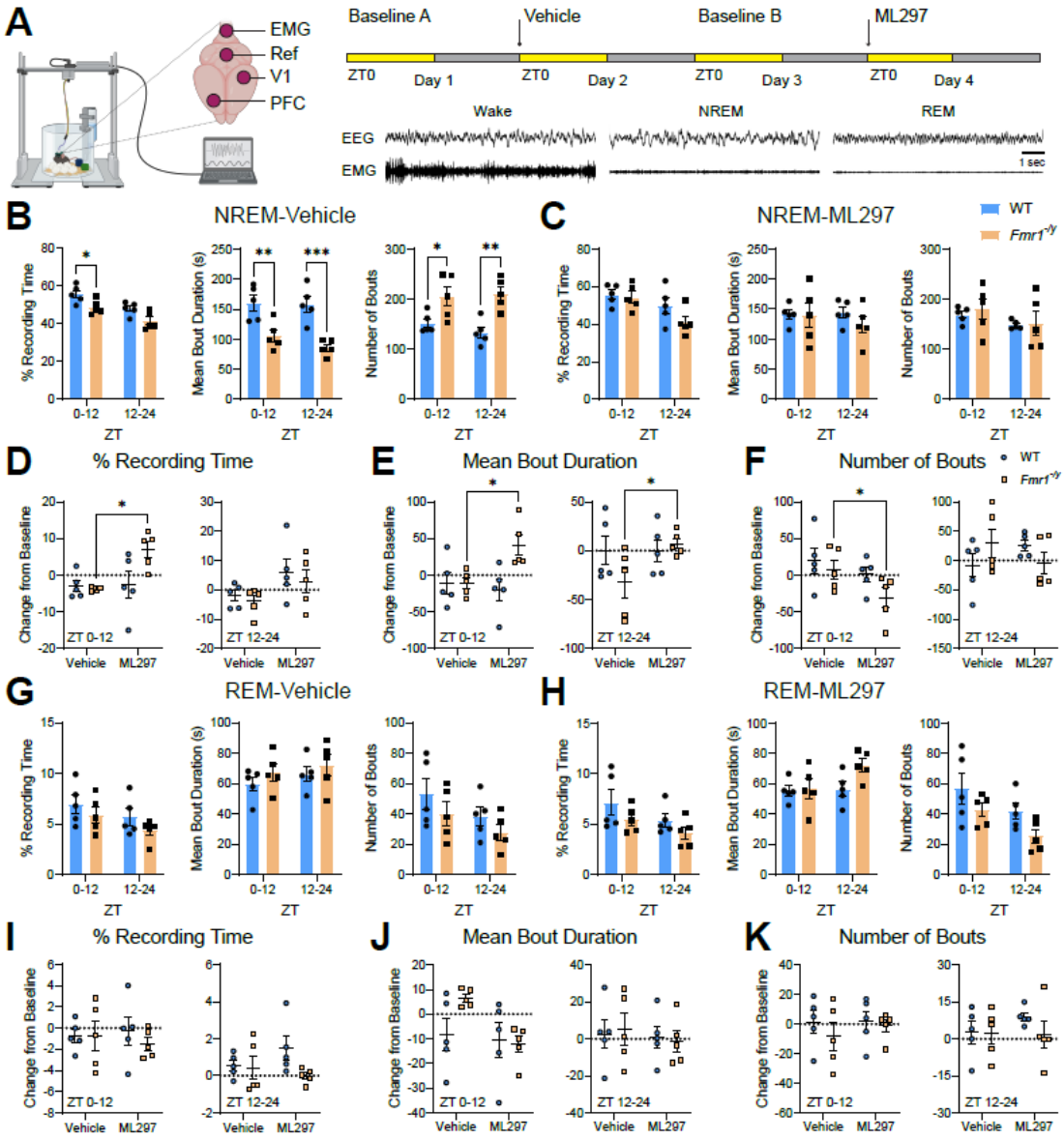
A
EMG
Ref
V1
PFC
Baseline A
Vehicle
Baseline B
ML297
ZT0
Day 1
ZT0
Day 2
ZT0
Day 3
ZT0
Day 4
Wake
NREM
REM
EEG
EMG
1 sec
B
NREM-Vehicle
C
NREM-ML297
WT
Fmr1-/y
% Recording Time
Mean Bout Duration (s)
Number of Bouts
0-12
12-24
ZT
D
% Recording Time
E
Mean Bout Duration
F
Number of Bouts
Change from Baseline
ZT 0-12
ZT 12-24
Vehicle
ML297
G
REM-Vehicle
H
REM-ML297
I
% Recording Time
J
Mean Bout Duration
K
Number of Bouts

Figure 4.2: ML297administration renormalizes light-phase NREM sleep architecture in *Fmr1*$^{-/y}$ mice

(A) Schematic of EEG/EMG recording configuration, with EEG electrodes positioned over primary visual (V1) and prefrontal (PFC) cortical regions (***left***). Experimental timeline of 4-day continuous recording in a 12:12 light-dark cycle (***right***). Baseline recordings were carried out on days 1 and 3; vehicle and ML297 i.p. injections were given at lights-on (ZT0) on days 2 and 4, respectively. Representative 10-sec epochs are shown for wake, NREM sleep, and REM sleep EEG and EMG activity.

(B) NREM percent recording time (***left***), mean bout duration (***middle***), and bout numbers (***right***) are shown post-vehicle injection for WT and *Fmr1*$^{-/y}$ mice. Two-way RM ANOVA for recording time: p(time of day) = 0.001, p(genotype) = 0.015, p(time x genotype interaction) = 0.87. For NREM bout duration: p(time of day) = 0.13, p(genotype) = 0.0017, p(time x genotype interaction) = 0.21. For NREM bout numbers: p(time of day) = 0.52, p(genotype) = 0.0054, p(time x genotype interaction) = 0.23.

(C) NREM percent recording time (***left***), mean bout duration (***middle***), and bout numbers (***right***) are shown post-ML297 injection for WT and *Fmr1*$^{-/y}$ mice. Two-way RM ANOVA for recording time: p(time of day) = 0.016, p(genotype) = 0.16, p(time x genotype interaction) = 0.26. For NREM bout duration: p(time of day) = 0.40, p(genotype) = 0.57, p(time x genotype interaction) = 0.21. For NREM bout numbers: p(time of day) = 0.0092, p(genotype) = 0.73, p(time x genotype interaction) = 0.60.

(D) Changes in percent recording time spent in NREM after vehicle or ML297, vs. time-matched baseline values (i.e., vehicle – baseline A, ML297 – baseline B). Two-way RM ANOVA for ZT0-12: p(treatment) = 0.03, p(genotype) = 0.10, p(treatment x genotype interaction) = 0.04. For ZT13-24: p(treatment) = 0.052, p(genotype) = 0.45, p(treatment x genotype interaction) = 0.83.

(E) Changes in mean NREM bout duration after vehicle or ML297, vs. time-matched baseline values. Two-way RM ANOVA for ZT0-12: p(treatment) = 0.12, p(genotype) = 0.04, p(treatment x genotype interaction) = 0.04. For ZT13-24: p(treatment) = 0.08, p(genotype) = 0.40, p(treatment x genotype interaction) = 0.07.

(F) Changes in numbers of NREM bouts after vehicle or ML297, vs. time-matched baseline values. Two-way RM ANOVA for ZT0-12: p(treatment) = 0.02, p(genotype) = 0.22, p(treatment x genotype interaction) = 0.32. For ZT13-24: p(treatment) = 0.98, p(genotype) = 0.81, p(treatment x genotype interaction) = 0.17.

(G) REM percent recording time (***left***), mean bout duration (***middle***), and bout numbers (***right***) are shown post-vehicle injection for WT and *Fmr1*$^{-/y}$ mice. Two-way RM ANOVA for recording time: p(time of day) = 0.005, p(genotype) = 0.27, p(time x genotype interaction) = 0.69. For REM bout duration: p(time of day) = 0.059, p(genotype) = 0.39, p(time x genotype interaction) = 0.73. For REM bout numbers: p(time of day) = 0.007, p(genotype) = 0.27, p(time x genotype interaction) = 0.76.

(H) REM percent recording time (***left***), mean bout duration (***middle***), and bout numbers (***right***) are shown post-ML297 injection for WT and *Fmr1*$^{-/y}$ mice. Two-way RM ANOVA for recording time: p(time of day) = 0.03, p(genotype) = 0.17, p(time x genotype interaction) = 0.73. For REM bout duration: p(time of day) = 0.07, p(genotype) = 0.15, p(time x genotype interaction) = 0.12. For REM bout numbers: p(time of day) = 0.004, p(genotype) = 0.10, p(time x genotype interaction) = 0.77.

(I) Changes in percent recording time spent in REM after vehicle or ML297, vs. time-matched baseline values (i.e., vehicle – baseline A, ML297 – baseline B). Two-way RM ANOVA for ZT0-12: p(treatment) = 0.87, p(genotype) = 0.63, p(treatment x genotype interaction) = 0.48. For ZT13-24: p(treatment) = 0.65, p(genotype) = 0.09, p(treatment x genotype interaction) = 0.24.

(J) Changes in mean REM bout duration after vehicle or ML297, vs. time-matched baseline values. Two-way RM ANOVA for ZT0-12: p(treatment) = 0.12, p(genotype) = 0.15, p(treatment x genotype interaction) = 0.22. For ZT13-24: p(treatment) = 0.54, p(genotype) = 0.99, p(treatment x genotype interaction) = 0.72.

(K) Changes in numbers of REM bouts after vehicle or ML297, vs. time-matched baseline values. Two-way RM ANOVA for ZT0-12: p(treatment) = 0.66, p(genotype) = 0.34, p(treatment x genotype interaction) = 0.68. For ZT13-24: p(treatment) = 0.39, p(genotype) = 0.48, p(treatment x genotype interaction) = 0.27.

n = 5 mice/genotype. *, **, and *** indicate $p < 0.05$, $p < 0.01$, and $p < 0.001$, Sidak's *post hoc* test. Data points and error bars indicate mean ± SEM.

4.4.3 : Cortical subregion-specific NREM EEG changes, and intracortical desynchrony of NREM oscillations, are partially renormalized by ML297 administration in Fmr1$^{-/y}$ mice

Because we noted changes in state-specific spectral power in *Fmr1*$^{-/y}$ mice, we next assessed how ML297 impacted EEG activity and synchronization across V1 and PFC cortical regions. Across both baseline recordings (baseline A and B) in V1, we again observed increased NREM delta (δ) and gamma (γ) power, and reduced sigma (σ) power, in *Fmr1*$^{-/y}$ mice – changes which were present across both the light and dark phase (**Supplemental Figure 4.5A-D**). In contrast, while gamma power in PFC was similarly elevated in *Fmr1*$^{-/y}$ mice, NREM delta and sigma power were comparable between WT and *Fmr1*$^{-/y}$ mice in PFC (**Supplemental Figure 4.5E-H**). These regional differences in NREM delta power are consistent with reported anteroposterior axis differences in NREM slow wave activity in children and adults with ASD [69,70]. Similarly, baseline recordings in V1 again showed decreased REM theta (θ) power in V1 of *Fmr1*$^{-/y}$ mice (**Supplemental Figure 4.6A-D**), but these changes were not present in PFC (**Supplemental Figure 4.6E-H**). Interestingly, a similar brain region-specific change in the distribution of REM theta has been reported in adult ASD patients[83]. Wake gamma power remained elevated across both cortical areas in *Fmr1*$^{-/y}$ mice in baseline recordings (**Supplemental Figure 4.8**).

Vehicle treatment did not alter NREM-, REM-, or wake-specific EEG features in *Fmr1*$^{-/y}$ mice, in either region (**Figure 4.3A, C, E, G; Supplemental Figure 4.7A, C, E, G; Supplemental Figure 4.9A, C, E, G**). In contrast, ML297 administration normalized NREM delta, sigma, and gamma power to WT levels in V1 of *Fmr1*$^{-/y}$ mice (**Figure 4.3B, D**), and modestly reduced delta power in PFC (**Figure 4.3F, H**). ML297 also normalized

wake gamma activity in V1, but did not reverse elevated gamma in PFC (**Supplemental Figure 4.9B, D, F, H)** or REM theta decreases in *Fmr1*$^{-/y}$ mice (**Supplemental Figure 4.7B, D, F, H**). These findings show that *Fmr1*$^{-/y}$ mice exhibit brain region-specific differences in NREM and REM EEG spectral power that are reminiscent of those in ASD patients, and that ML297 administration can reverse these changes in a brain region-and state-specific manner.

Our observations of both region-specific changes in NREM sigma power (associated with sleep spindles) and altered PV+ interneuron density in the TRN of *Fmr1*$^{-/y}$ mice suggest that coordination of these thalamocortical oscillations might be disrupted by loss of FMRP. Because synchronization of brain activity during sleep spindles is thought to be essential for brain development and cognitive function [67,71,75,81,84-88], we tested whether NREM spindle density or coordination of spindles between brain regions could be altered by administration of ML297. In baseline recordings of V1 EEG activity, we again observed that spindle density was reduced in *Fmr1*$^{-/y}$ mice compared to WT littermates, but spindle density in PFC recordings did not differ significantly between the groups (**Figure 4.4A-B**). Vehicle administration did not affect the reduced spindle density seen in V1 of *Fmr1*$^{-/y}$ mice, but ML297 eliminated the differences in V1 spindles between *Fmr1*$^{-/y}$ mice and WT littermates. Because these changes were brain region-specific (similar to other changes in NREM oscillations in *Fmr1*$^{-/y}$ mice), we compared NREM spindle densities recorded in V1 vs. PFC for individual mice. This comparison revealed that at baseline, spindle densities in the two regions were consistently correlated in WT littermates, but not in *Fmr1*$^{-/y}$ mice (**Figure 4.4C-D**). When mice were treated with either vehicle or ML297, WT littermates continued to show a consistent positive relationship

between V1 and PFC spindle densities. *Fmr1*$^{-/y}$ mice showed no change in response to vehicle treatment (i.e., V1 and PFC spindle densities were not correlated). However, after ML297 treatment, spindle densities became significantly correlated between the V1 and PFC EEG sites of individual mice, suggesting better coordination of these oscillations during NREM sleep. These findings are consistent with our finding of structural alterations to the TRN in *Fmr1*$^{-/y}$ mice, which may lead to desynchrony of spindle oscillations [67], and prior reports that GIRK1/2 channels are well expressed in (and modulate the physiology of) GABAergic TRN neurons [89].

To further quantify state-specific EEG oscillatory synchrony, we compared light-phase V1-PFC spectral coherence for *Fmr1*$^{-/y}$ mice and WT littermates across all four days of recording (**Figure 4.5**). For WT mice, V1-PFC coherence in NREM was similarly affected by vehicle and ML297, leading to decreases in the gamma band and increases in the sigma band (**Figure 4.5A**). Coherence between the brain structures during REM was also similarly affected by vehicle and ML297, leading to decreases in both the theta and gamma bands. Wake gamma-band coherence was increased by both vehicle and ML297 treatment in WT littermates, while wake delta and sigma activity were differentially affected by the two treatments (with ML297 increasing both). *Fmr1*$^{-/y}$ mice displayed baseline patterns of V1-PFC coherence that were distinct from wild-type littermates, with lower NREM and wake coherence in the delta and sigma bands, lower REM coherence in the theta band, and distinct patterns of gamma coherence across all three states (**Figure 4.5B**). ML297, but not vehicle, significantly increased NREM sigma, REM theta, and wake gamma coherence (**Figure 4.5B**). Increases in NREM sigma and REM theta coherence persisted into the dark phase in *Fmr1*$^{-/y}$ mice administered ML297

(**Supplemental Figure 4.10B**). These data suggest that NREM sigma and REM theta coherence, which are generally reduced in *Fmr1*$^{-/y}$ mice, are partially rescued by administration of ML297.

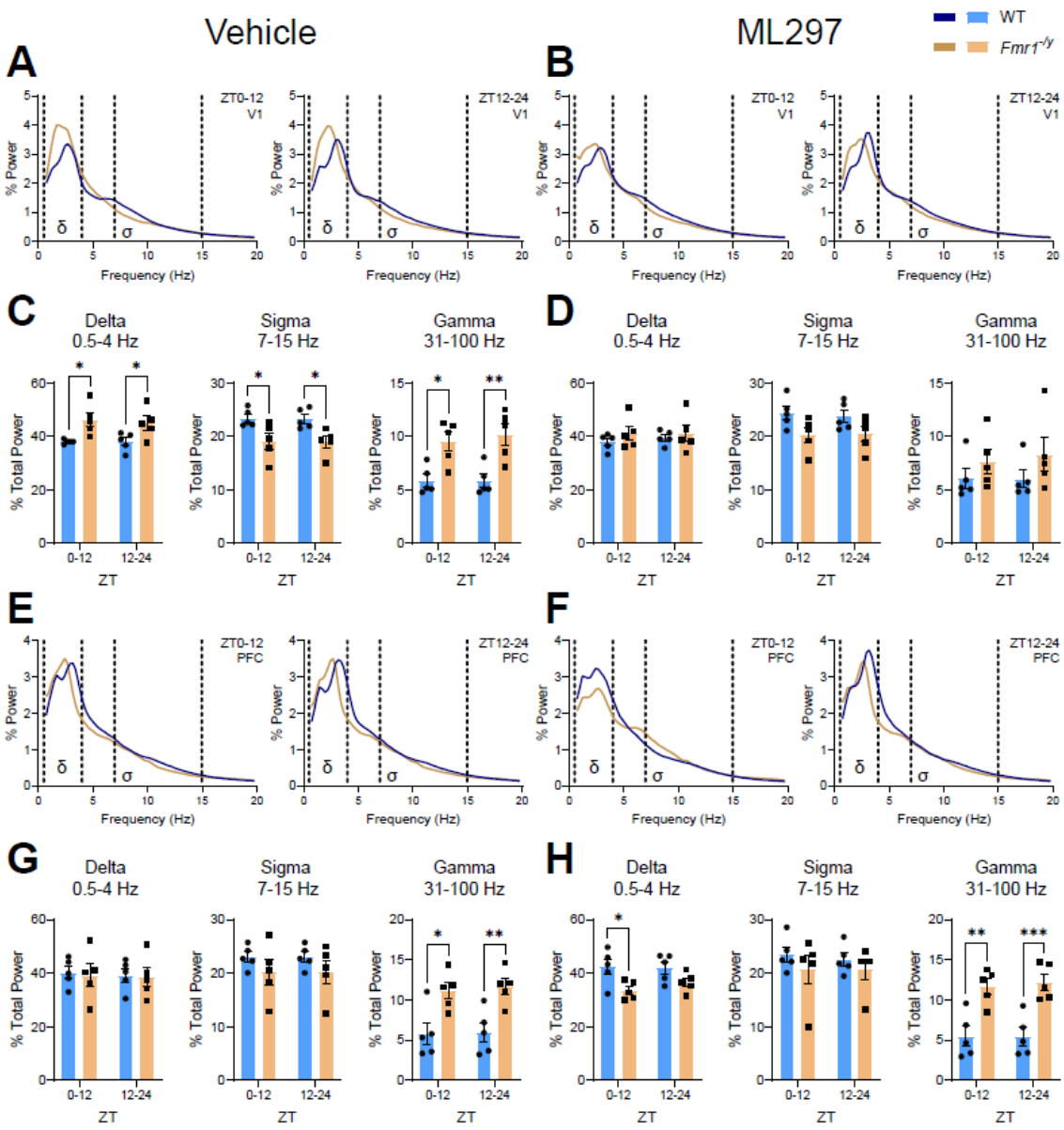
Vehicle
ML297
WT
Fmr1-/y
A
B
C
D
E
F
G
H
ZT0-12 V1
ZT12-24 V1
ZT0-12 PFC
ZT12-24 PFC
% Power
Frequency (Hz)
δ
σ
Delta 0.5-4 Hz
Sigma 7-15 Hz
Gamma 31-100 Hz
% Total Power
ZT
0-12
12-24

Figure 4.3: ML297 renormalizes NREM V1 spectral power in *Fmr1*$^{-/y}$ mice, but minimally affects PFC spectral power

(A) Post-vehicle comparisons of NREM V1 EEG power spectra across ZT0-12 (***left***) and ZT13-24 (***right***) for WT and *Fmr1*$^{-/y}$ mice. Two-way RM ANOVA for ZT0-12: p(frequency) < 0.0001, p(genotype) = 0.0068, p(frequency x genotype interaction) < 0.0001. For ZT13-24: p(frequency) < 0.0001, p(genotype) = 0.83, p(frequency x genotype interaction) < 0.0001.

(B) Post-ML297 comparisons of NREM V1 EEG power spectra across ZT0-12 (***left***) and ZT13-24 (***right***) for WT and *Fmr1*$^{-/y}$ mice. Two-way RM ANOVA for ZT0-12: p(frequency) < 0.0001, p(genotype) = 0.42, p(frequency x genotype interaction) < 0.0001. For ZT13-24: p(frequency) < 0.0001, p(genotype) = 0.36, p(frequency x genotype interaction) < 0.0001.

(C) Total V1 EEG spectral power in the delta (0.5-4 Hz; ***left***), sigma for spindles (7-15 Hz; ***middle***), and gamma (31-100 Hz; ***right***) bands are shown for vehicle-treated WT and *Fmr1*$^{-/y}$ mice. Similar to untreated mice (**Figure 1**), total delta and gamma power were increased, and sigma power was decreased, in V1 of *Fmr1*$^{-/y}$ mice treated with vehicle.

(D) In ML297-treated *Fmr1*$^{-/y}$ mice, V1 EEG power in all three bands was normalized relative to WT littermates.

(E) Post-vehicle comparisons of NREM PFC EEG power spectra across ZT0-12 (***left***) and ZT13-24 (***right***) for WT and *Fmr1*$^{-/y}$ mice. Two-way RM ANOVA for ZT0-12: p(frequency) < 0.0001, p(genotype) = 0.037, p(frequency x genotype interaction) = 0.042. For ZT13-24: p(frequency) < 0.0001, p(genotype) = 0.064, p(frequency x genotype interaction) = 0.0002.

(F) Post-ML297 comparisons of NREM PFC EEG power spectra across ZT0-12 (***left***) and ZT13-24 (***right***) for WT and *Fmr1*$^{-/y}$ mice. Two-way RM ANOVA for ZT0-12: p(frequency) < 0.0001, p(genotype) = 0.429, p(frequency x genotype interaction) < 0.0001. For ZT13-24: p(frequency) < 0.0001, p(genotype) = 0.0033, p(frequency x genotype interaction) < 0.0001.

(G) Total V1 EEG spectral power in the delta (0.5-4 Hz; ***left***), sigma (7-15 Hz; ***middle***), and gamma (31-100 Hz; ***right***) bands are shown for vehicle-treated WT and *Fmr1*$^{-/y}$ mice. While total delta and sigma power remained unaffected in PFC of *Fmr1*$^{-/y}$ mice treated with vehicle, gamma power was significantly increased, similar to V1.

(H) In ML297-treated *Fmr1*$^{-/y}$ mice, PFC EEG power in the delta band was reduced compared to WT littermates, while sigma power was unaffected and gamma power remained significantly elevated.

n = 5 mice/genotype. *, **, and *** indicate p < 0.05, p < 0.01, and p < 0.001, Sidak's *post hoc* test. Data points and error bars indicate mean ± SEM.

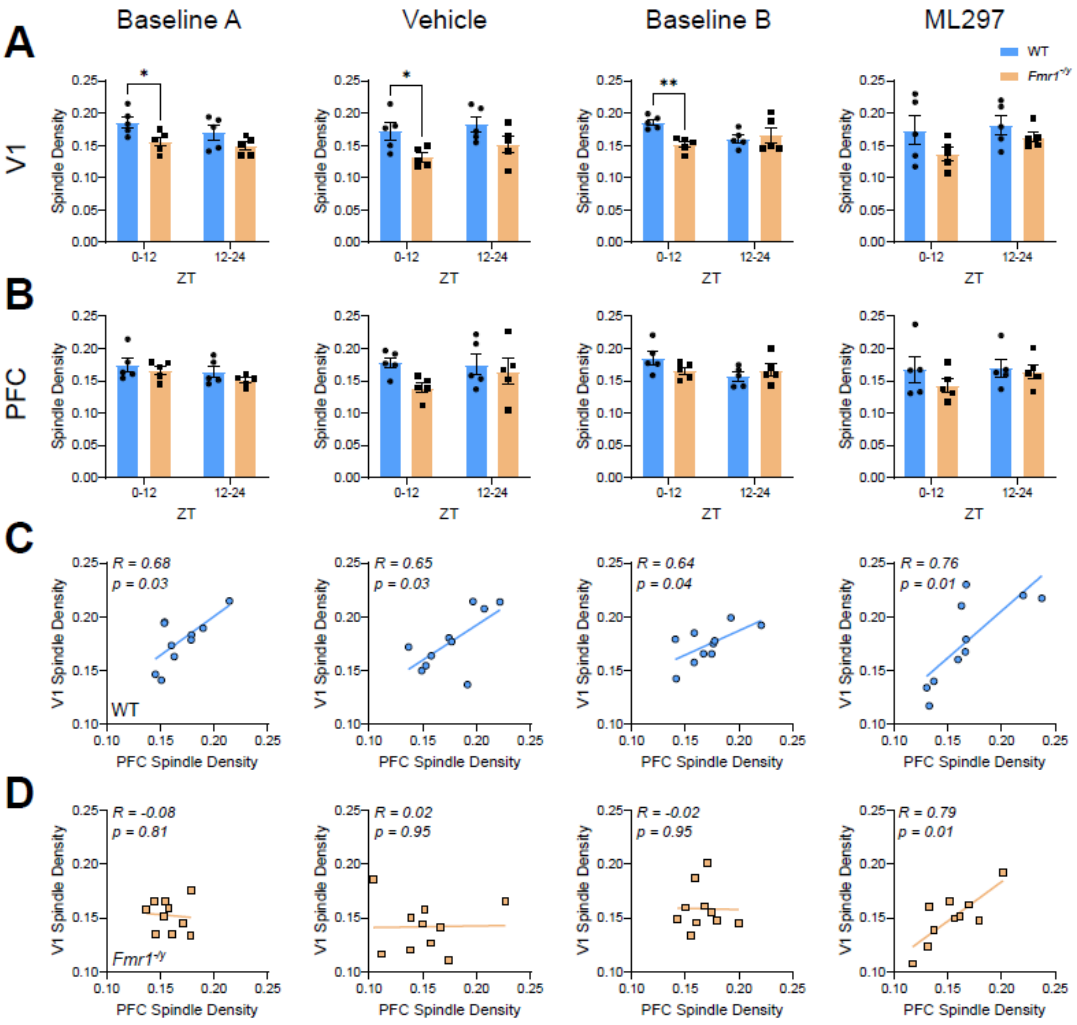

Figure 4.4: *Fmr1*$^{-/y}$ mice show discrepant NREM spindle densities between V1 and PFC due to reduced V1 spindling that is rescued by ML297 administration

(A) V1 NREM sleep spindle density (in Hz) across 4 days of continuous EEG/EMG recording for WT and *Fmr1*$^{-/y}$ mice. Two way RM ANOVA for Baseline A: p(time of day) = 0.018, p(genotype) = 0.056, p(time x genotype interaction) = 0.28. For Vehicle: p(time of day) = 0.22, p(genotype) = 0.013, p(time x genotype interaction) = 0.68. For Baseline B: p(time of day) = 0.43, p(genotype) = 0.11, p(time x genotype interaction) = 0.019. For ML297: p(time of day) = 0.10, p(genotype) = 0.17, p(time x genotype interaction) = 0.38.

(B) PFC NREM sleep spindle density (in Hz) for WT and *Fmr1*$^{-/y}$ mice. Two way RM ANOVA for Baseline A: p(time of day) = 0.0076, p(genotype) = 0.33, p(time x genotype interaction) = 0.48. For Vehicle: p(time of day) = 0.37, p(genotype) = 0.15, p(time x genotype interaction) = 0.28. For Baseline B: p(time of day) = 0.018, p(genotype) = 0.66, p(time x genotype interaction) = 0.012. For ML297: p(time of day) = 0.24, p(genotype) = 0.44, p(time x genotype interaction) = 0.35. n = 5 mice/genotype. * and ** indicate $p < 0.05$ and $p < 0.01$, Sidak's *post hoc* test. Data points and error bars indicate mean ± SEM.

(C) In WT mice, V1 and PFC spindle densities were positively correlated across the 4 days of EEG recording.

(D) In *Fmr1*$^{-/y}$ mice, V1 and PFC spindle densities were not correlated across the first 3 days of EEG recording (Baseline A, Vehicle, and Baseline B), but became correlated after administration of ML297.

n = 5 mice/genotype. Data points in **(C)** and **(D)** represent NREM spindle density across either the light or dark phase (ZT0-12 or ZT12-24) for each mouse. R and p values for Pearson correlation of each data set.

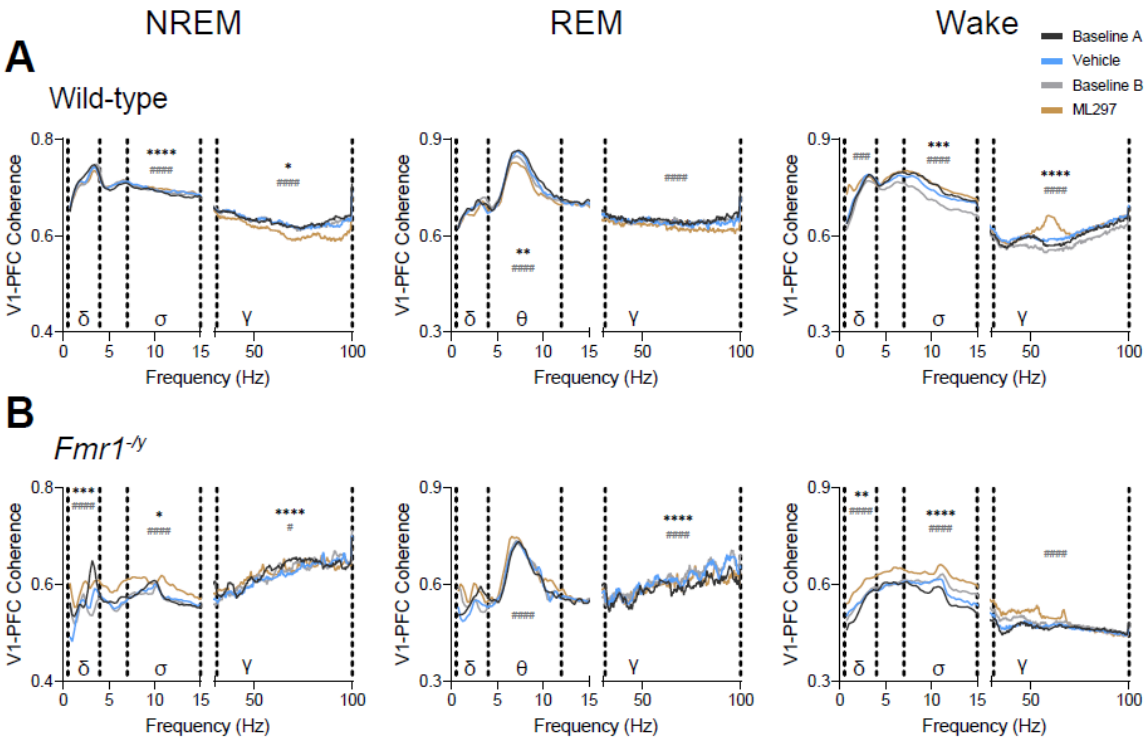

Figure 4.5: V1-PFC EEG coherence during sleep is reduced in *Fmr1*$^{-/y}$ mice, and partially rescued by ML297 administration

(A) State-associated V1-PFC spectral coherence for WT mice, measured during the light phase (ZT0-12). Two-way RM ANOVA for NREM, REM, and wake: p(frequency) > 0.99, p(recording day) < 0.0001, p(frequency x day interaction) > 0.99.

(B) V1-PFC spectral coherence for *Fmr1*$^{-/y}$ mice during the light phase (ZT0-12). Two-way RM ANOVA for NREM, REM, and wake: p(frequency) > 0.99, p(recording day) < 0.0001, p(frequency x day interaction) > 0.99. n = 5 mice/genotype.

n = 5 mice/genotype. *, **, ***, and **** indicate $p < 0.05$, $p < 0.01$, $p < 0.001$, and $p < 0.0001$, Tukey's *post hoc* test for Baseline A vs. Vehicle. #, ##, ###, and #### indicate $p < 0.05$, $p < 0.01$, $p < 0.01$, and $p < 0.0001$, Tukey's *post hoc* test for Baseline B vs. ML297. Different frequency bands are denoted with their symbol and divided by dashed lines: δ = 0.5-4 Hz, θ = 4-12 Hz, σ = 7-15 Hz, γ = 31-100 Hz.

4.4.4 : Post-learning ML297 administration rescues deficits in sleep-dependent memory consolidation in Fmr1$^{-/y}$ mice

In mice, consolidation of hippocampally-mediated contextual fear memory (CFM) and object location memory (OLM), are disrupted by brief sleep deprivation (SD) in the hours immediately following training [21,23,25,44,52,90-92]. *Fmr1*$^{-/y}$ mice have known deficits in CFM [11,93,94] and OLM [95], but it is unclear whether the sleep deficiencies we observe in *Fmr1*$^{-/y}$ mice are related to these deficits. We tested whether promoting sleep using ML297 could rescue sleep-dependent memory consolidation in *Fmr1*$^{-/y}$ mice. We first carried out single-trial conditioning (CFC) in *Fmr1*$^{-/y}$ mice and WT littermates. While the two groups showed a similar very low level of freezing prior to receiving an aversive foot shock during CFC, *Fmr1*$^{-/y}$ mice showed reduced freezing during CFM recall in the shock context 24 h later (**Figure 4.6A-B**). To test whether hypnotic administration could improve CFM consolidation in *Fmr1*$^{-/y}$ mice, mutant and WT mice were administered either vehicle or ML297 immediately following CFC (**Figure 4.6C**). Mice were allowed *ad lib* sleep, but were visually monitored for sleep behavior for 6 h post-CFC. These observations showed *Fmr1*$^{-/y}$ mice given vehicle had significantly reduced total sleep time after CFC compared to those given ML297, and to WT littermates with either treatment (**Supplemental Figure 4.11A**). *Fmr1*$^{-/y}$ mice administered vehicle showed significantly reduced freezing during CFM testing compared with those receiving ML297, and with WT littermates in either condition. Freezing in *Fmr1*$^{-/y}$ mice treated with ML297 was similar to that of WT mice, indicating functional rescue of CFM consolidation (**Figure 4.6C-E**).

We had previously observed that post-CFC ML297 administration improves CFM consolidation in C57BL/6J mice, and that this effect is sleep-dependent [44]. We next tested

whether ML297-mediated improvements in CFM consolidation were also sleep-dependent in *Fmr1*$^{-/y}$ mice. An additional cohort of *Fmr1*$^{-/y}$ mice and WT littermates underwent single-trail CFC followed immediately by ML297 administration, after which they underwent 6 h of SD via gentle handling in their home cage (**Figure 4.6F**). Consistent with the fact that *Fmr1*$^{-/y}$ mice have reduced overall sleep, the number of physical interventions required to prevent sleep during the 6-h SD period was significantly lower in *Fmr1*$^{-/y}$ mice compared to WT littermates, regardless of treatment (**Supplemental Figure 4.11B).** *Fmr1*$^{-/y}$ mice and WT littermates administered ML297 in the context of post-CFC SD showed disruption of CFM, consistent with previous reports [44,90,96] (**Figure 4.6F-H**). This suggests that rescue of CFM consolidation in *Fmr1*$^{-/y}$ mice is sleep-dependent. In a separate cohort of vehicle-treated, SD *Fmr1*$^{-/y}$ or WT mice, we found again that the two SD groups have a similar degree of disruption of CFM consolidation, to one another, and to freely-sleeping *Fmr1*$^{-/y}$ mice (**Supplemental Figure 4.11C-E**). Together, our findings show that rescue of sleep in *Fmr1*$^{-/y}$ mice by ML297 is associated with improved CFM consolidation, and suggest that the loss of sleep in FXS could be a contributing factor to cognitive impairments.

We next tested whether other hippocampus-mediated, sleep-dependent forms of memory consolidation could be rescued in *Fmr1*$^{-/y}$ mice by administering ML297 post-learning. We chose to test OLM (a form of spatial memory known to be disrupted in *Fmr1*$^{-/y}$ mice [95]). Our OLM paradigm consisted of a 5 min period of habituation to the OLM arena on day 1, which also served as an open field (OF) test to measure locomotive ability. Mice were trained for 10 min at ZT0 of day 2, during which they explored two identical objects placed inside the arena. 24 h later, on day 3, mice were returned to the arena where one

object had been moved (displaced) and one object kept in the same location (familiar) (**Figure 4.7A**). During the OF test (habituation period), *Fmr1*$^{-/y}$ mice and WT littermates showed similar locomotion (total travel distance) and relative time spent in outer and inner zones of the arena (**Figure 4.7B**). A discrimination index, used to measure differences in interaction between the displaced object and familiar object, was significantly lower for OLM tests in *Fmr1*$^{-/y}$ mice compared to WT mice (**Figure 4.7C**). To test whether ML297 can rescue OLM consolidation in *Fmr1*$^{-/y}$ mice, a second cohort of mutant mice and littermates were administered vehicle of ML297 immediately after OLM training (**Figure 4.7D**). While locomotion and thigmotaxis were again comparable during habituation between genotypes (**Figure 4.7E**), performance during OLM testing varied by both genotype and treatment. *Fmr1*$^{-/y}$ mice treated with ML297 after training showed a significant improvement in discrimination between displaced and familiar object locations compared to *Fmr1*$^{-/y}$ mice treated with vehicle, suggesting at least a partial rescue of OLM consolidation. However, WT mice treated with ML297 showed no improvement in OLM consolidation, and in fact performed worse than vehicle-treated counterparts (**Figure 4.7F**). Nonetheless, our data suggest that both CFM and OLM consolidation, which are normally disrupted in *Fmr1*$^{-/y}$ mice, can be rescued with ML297 administration.

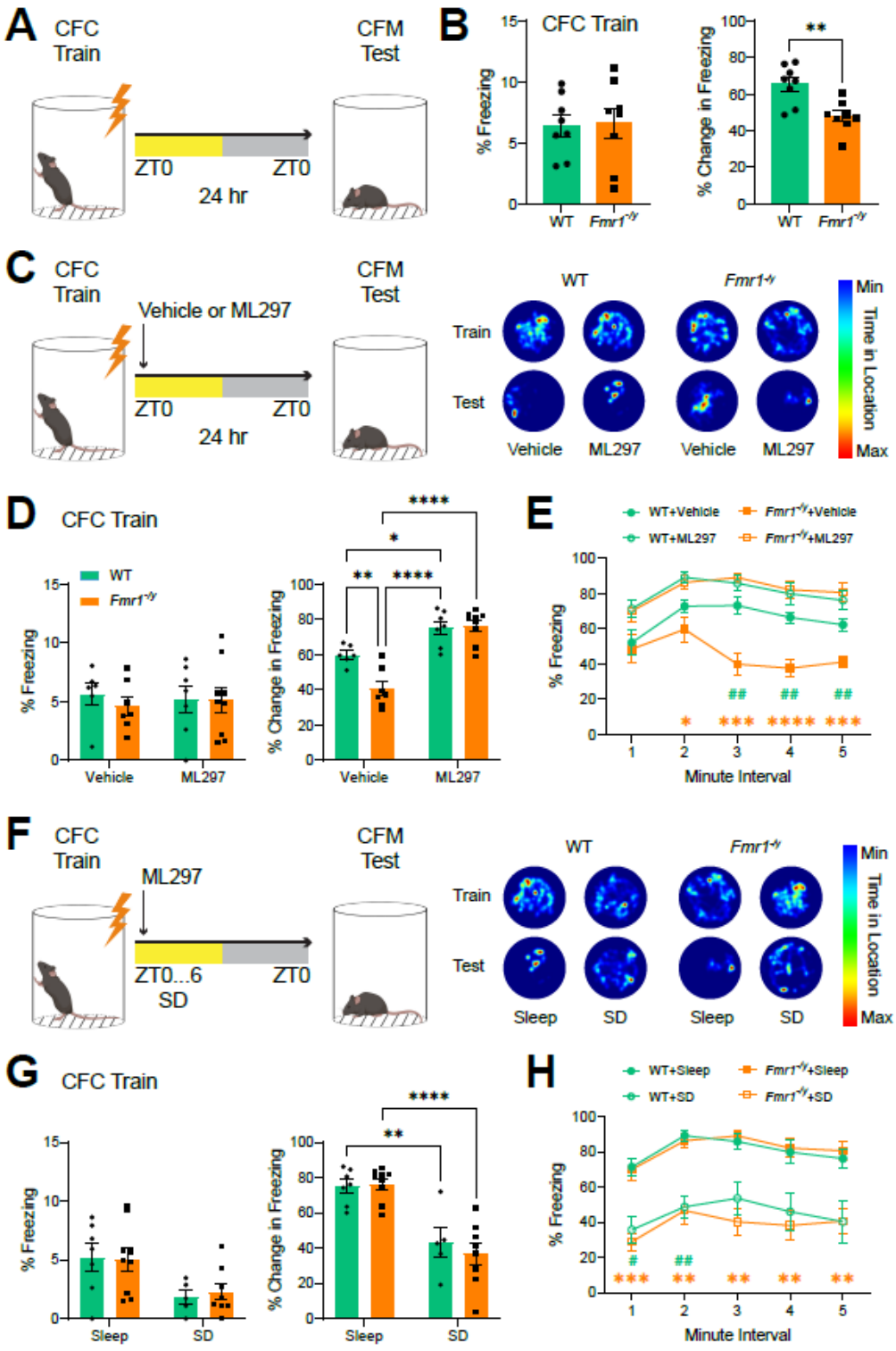
A
CFC Train
CFM Test
ZT0
ZT0
24 hr
B
CFC Train
% Freezing
WT
Fmr1-/y
% Change in Freezing
**
C
CFC Train
Vehicle or ML297
CFM Test
ZT0
ZT0
24 hr
WT
Fmr1-/y
Train
Test
Vehicle
ML297
Vehicle
ML297
Min
Time in Location
Max
D
CFC Train
WT
Fmr1-/y
% Freezing
Vehicle
ML297
% Change in Freezing
****
*
**
****
Vehicle
ML297
E
WT+Vehicle
Fmr1-/y+Vehicle
WT+ML297
Fmr1-/y+ML297
% Freezing
Minute Interval
F
CFC Train
ML297
CFM Test
ZT0...6
SD
ZT0
WT
Fmr1-/y
Train
Test
Sleep
SD
Sleep
SD
Min
Time in Location
Max
G
CFC Train
% Freezing
Sleep
SD
% Change in Freezing
****
**
Sleep
SD
H
WT+Sleep
Fmr1-/y+Sleep
WT+SD
Fmr1-/y+SD
% Freezing
Minute Interval

Figure 4.6: Contextual fear memory (CFM) consolidation is rescued in a sleep-dependent manner by post-CFC ML297 administration in *Fmr1*$^{-/y}$ mice

(A) WT and *Fmr1*$^{-/y}$ mice underwent single-trial CFC at ZT0, and CFM testing 24 h later.

(B) Pre-shock freezing behavior during CFC (***left***) was similar between WT and *Fmr1*$^{-/y}$ mice. CFM (measured as increased freezing from pre-shock baseline during testing; ***right***) was reduced *Fmr1*$^{-/y}$ mice. ** indicates $p < 0.01$, two-tailed, unpaired t-test. $n = 8$ mice/genotype.

(C) WT and *Fmr1*$^{-/y}$ mice underwent single-trial CFC at ZT0, followed immediately by vehicle or ML297 administration, and CFM testing 24 h later (***left***). Representative heat maps (***right***) showing total time-in-location for mice in the conditioning chamber during CFC (pre-shock) and CFM testing.

(D) Pre-shock freezing behavior during CFC (***left***) was similar across treatments, and between WT and *Fmr1*$^{-/y}$ mice. Two-way ANOVA, p(treatment) = 0.96, p(genotype) = 0.60, p(treatment x genotype interaction) = 0.64. Post-CFC ML297 administration rescued CFM (***right***) in *Fmr1*$^{-/y}$ mice. Two-way ANOVA, p(treatment) < 0.0001, p(genotype) = 0.017, p(treatment x genotype interaction) = 0.007. $n = 6$ (WT + vehicle), = 7 (WT + ML297), = 7 (*Fmr1*$^{-/y}$ + vehicle), = 9 (*Fmr1*$^{-/y}$ + ML297). *, **, and **** indicate $p < 0.05$, $p < 0.01$, and $p < 0.0001$, Tukey's *post hoc* test.

(E) Proportion of time spent in freezing (in 1-min bins) across the 5-min CFM testing period for the four treatment groups. Two-way ANOVA, p(time) < 0.0001, p(group) < 0.0001, p(time x group interaction) = 0.04. *, ***, and **** indicate $p < 0.05$, $p < 0.001$, and $p < 0.0001$, *Fmr1*$^{-/y}$ + vehicle vs. *Fmr1*$^{-/y}$ + ML297; ## indicates $p < 0.01$, *Fmr1*$^{-/y}$ + vehicle vs. WT + vehicle, Tukey's *post hoc* test.

(F) WT and *Fmr1*$^{-/y}$ mice underwent single-trial CFC at ZT0, followed immediately by ML297 administration and either *ad lib* sleep or 6-hour sleep deprivation (SD), and CFM testing 24 h later (***left***). Representative heat maps (***right***) showing total time-in-location for mice in the conditioning chamber during CFC (pre-shock) and CFM testing.

(G) Pre-shock freezing behavior during CFC (***left***) was similar between WT and *Fmr1*$^{-/y}$ mice. Two-way ANOVA, p(sleep condition) = 0.004, p(genotype) = 0.88, p(sleep condition x genotype interaction) = 0.74. Post-CFC SD prevented enhancements in CFM consolidation due to ML297 administration (***right***) in all mice. Two-way ANOVA, p(sleep condition) < 0.0001, p(genotype) = 0.64, p(sleep condition x genotype interaction) = 0.47. $n = 7$ (WT + sleep), = 5 (WT + SD), = 9 (*Fmr1*$^{-/y}$ + sleep), = 8 (*Fmr1*$^{-/y}$ + SD). ** and **** indicate $p < 0.01$ and $p < 0.0001$, Tukey's *post hoc* test.

(H) Proportion of time spent in freezing (in 1-min bins) across the 5-min CFM testing period for the four treatment groups. Two-way ANOVA, p(time) < 0.0001, p(sleep condition) < 0.0001, p(time x sleep condition interaction) = 0.93. ** and *** indicate $p < 0.01$ and $p < 0.001$, *Fmr1*$^{-/y}$ + sleep vs. *Fmr1*$^{-/y}$ + SD; # and ## indicate $p < 0.05$ and $p < 0.01$, WT + sleep vs. WT + SD, Tukey's *post hoc* test.

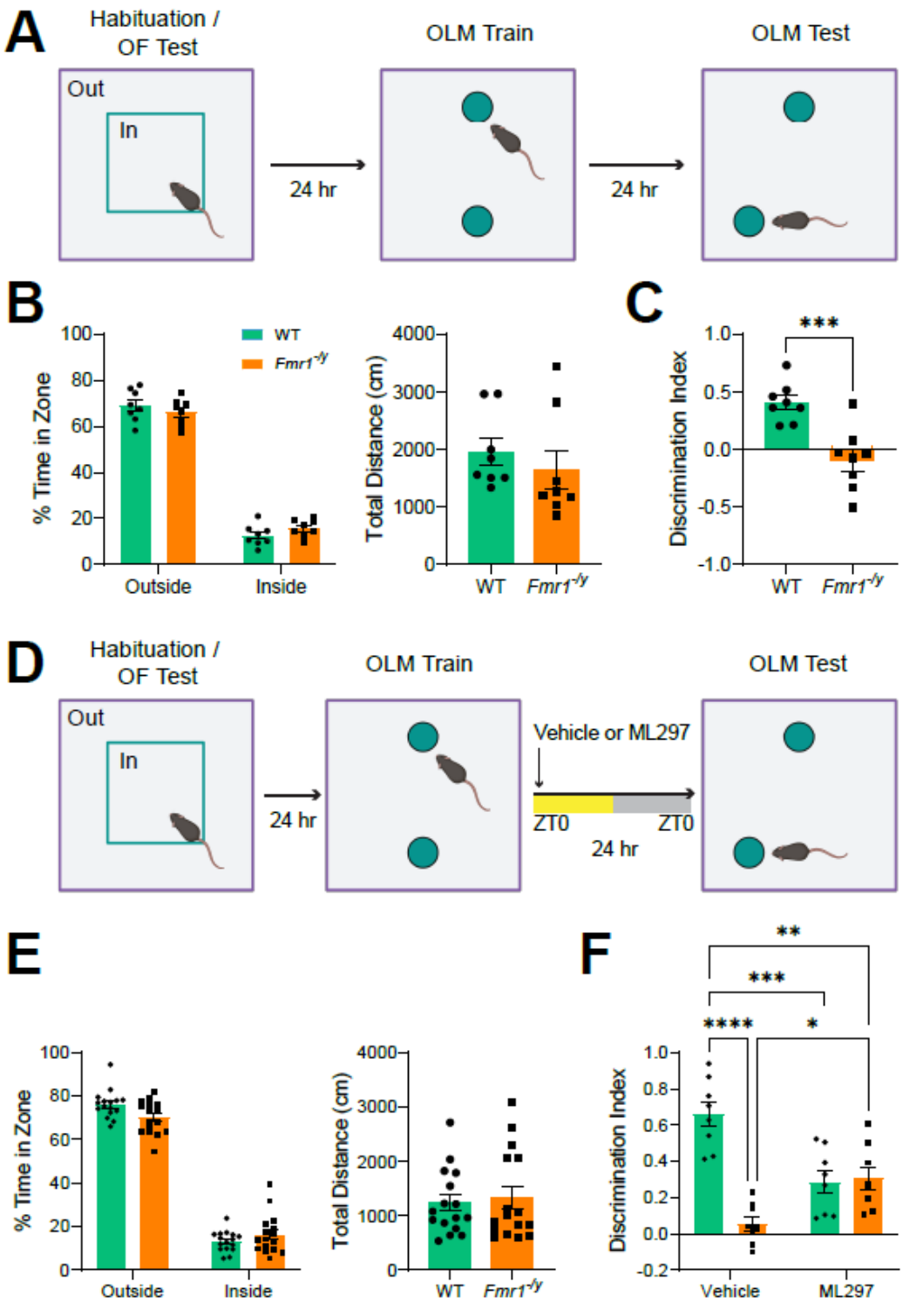
A
Habituation / OF Test
OLM Train
OLM Test
Out
In
24 hr
24 hr
B
% Time in Zone
WT
Fmr1-/y
Outside
Inside
Total Distance (cm)
WT
Fmr1-/y
C
Discrimination Index
***
WT
Fmr1-/y
D
Habituation / OF Test
OLM Train
OLM Test
Out
In
24 hr
Vehicle or ML297
ZT0
ZT0
24 hr
E
% Time in Zone
Outside
Inside
Total Distance (cm)
WT
Fmr1-/y
F
**
***
****
*
Discrimination Index
Vehicle
ML297

Figure 4.7: Sleep-dependent consolidation of object location memory (OLM) is partially rescued by ML297 administration in *Fmr1*$^{-/y}$ mice

(A) WT and *Fmr1*$^{-/y}$ mice (*n* = 8/genotype) underwent habituation to the OLM arena (combined with open field [OF] behavioral measurement) at ZT0. 24 h later, mice underwent OLM training with two identical objects in the arena. After an additional 24 h, mice were tested for OLM in the same arena with one object moved to a new location.

(B) Proportion of time spent in inner and outer zones of the arena (***left***) was similar between WT and *Fmr1*$^{-/y}$ mice during habituation. Two-way ANOVA, p(zone) < 0.0001, p(genotype) = 0.94, p(sleep condition x genotype interaction) = 0.11. Total distance traveled during habituation (***right***) was also similar between genotypes. Two-tailed, unpaired t-test.

(C) *Fmr1*$^{-/y}$ mice failed to discriminate between displaced and non-displaced objects during OLM testing. *** indicates p < 0.001, two-tailed, unpaired t-test.

(D) WT and *Fmr1*$^{-/y}$ mice underwent habituation to the OLM arena and OLM training as described above, followed immediately by ML297 or vehicle administration. After an additional 24 h, mice were tested for OLM in the same arena with one object moved to a new location.

(E) Open field activity (***left***) was similar between WT and *Fmr1*$^{-/y}$ mice during habituation. Two-way ANOVA, p(zone) < 0.0001, p(genotype) = 0.43, p(zone x genotype interaction) = 0.013. Total distance traveled (***right***) was also similar between genotypes. Two-tailed, unpaired t-test.

(F) Vehicle-treated *Fmr1*$^{-/y}$ mice showed impairments in OLM, which were ameliorated by administration of ML297. *n* = 8 mice/experimental condition. Two-way ANOVA, p(treatment) = 0.31, p(genotype) < 0.0001, p(treatment x genotype interaction) < 0.0001. *, **, ***, and **** indicate p < 0.05, p < 0.01, p < 0.001, and p < 0.0001, Tukey's *post hoc* test.

4.4.5 : CFM consolidation improvements with ML297 treatment in Fmr1-/y mice are associated with normalization of dentate gyrus (DG) activation patterns during recall

During both learning and subsequent memory retrieval, neuronal immediate early gene (IEG) expression among hippocampal DG granule cells and granule cell "engram neuron" re-activation plays a causal role in memory recall [97]. We tested whether changes in DG activity during CFM recall accompanied ML297-mediated improvements in CFM consolidation. *Fmr1*$^{-/y}$ mice and WT littermates underwent CFC followed by ML297 or vehicle administration. After CFM recall 24 h later, mice were returned to their home cages and perfused 90 min later to quantify cFos+ neuron density across dorsal hippocampus (**Figure 4.8A**). Across the entire DG region, *Fmr1*$^{-/y}$ mice given vehicle had significantly greater cFos+ neuron density after recall compared to WT-vehicle counterparts. In contrast, *Fmr1*$^{-/y}$ mice given ML297 showed significant reduction of cFos+ neuron density compared to *Fmr1*$^{-/y}$ vehicle counterparts, with density being normalized to levels observed in WT-vehicle mice. In contrast, WT mice given ML297 showed significant increase in DG cFos+ neuron density compared to WT-vehicle mice (**Figure 4.8B**). These same trends in cFos+ neuron density between WT and *Fmr1*$^{-/y}$ mice were also found separately when quantifying the granule cell layers of the superior and inferior blades of the DG, as well as the hilus (**Figure 4.8B**). Overall density of cFos+ neurons in DG predicted successful CFM, although the direction of this relationship differed between *Fmr1*$^{-/y}$ mice and WT littermates. In WT mice, higher density of cFos+ neurons corresponded to increased freezing behavior. In contrast, *Fmr1*$^{-/y}$ mice showed the opposite relationship, where lower density of cFos+ neurons corresponded to increased freezing behavior (**Figure 4.8C**). Our data suggests that overactivation of the

DG network in *Fmr1*$^{-/y}$ mice during CFM recall could be normalized to WT levels by ML297 administration during the consolidation phase.

To understand the impact of ML297 treatment on recall-associated neuronal activation across the rest of the dorsal hippocampus-amygdala circuit, we measured cFos expression within the pyramidal layers of CA1 and CA3, and in lateral and basolateral amygdala, after recall. Within CA1, ML297-treated mice of both genotypes showed significantly increased cFos+ neuron density compared to WT mice with vehicle treatment. However, the density of cFos+ neurons was correlated with successful CFM recall only in WT mice (**Figure 4.8D-E**). Density of cFos+ neurons in CA3 was comparable between genotypes regardless of treatment. Similar to CA1, cFos+ neuron density was predictive of successful CFM recall only in WT mice, not *Fmr1*$^{-/y}$ counterparts (**Figure 4.8F-G**). cFos+ neuron density within the amygdala (**Supplemental Figure 4.12**) also differed in vehicle treatment conditions between WT and *Fmr1*$^{-/y}$ mice – with higher density in lateral and reduced density in basolateral amygdala in *Fmr1*$^{-/y}$ mice after recall. But these differences were relatively unaffected as a function of ML297 administration (**Supplemental Figure 4.12B-D**). Overall, these findings suggest that post-CFC administration of ML297 alters network activity with the hippocampus (primarily within the DG) in *Fmr1*$^{-/y}$ mice, renormalizing activity levels in subsequent recall, and that this is linked to improvement of CFM consolidation. Imbalanced excitation vs. inhibition in brain circuits is a hallmark of FXS [2,15,98-101], our data suggest that reducing neuronal excitability via sleep, and sleep-associated GIRK channel activity, could be a mechanism to help with memory consolidation disruption in FXS. While the amygdala is also a major part of the fear recall circuit, the lack of effects of ML297 on this structure suggest that improvements

in CFM stem from the hippocampus. Lastly, it suggests that freezing behavior seen in *Fmr1*$^{-/y}$ mice with ML297 is tied to learning and memory circuits rather than ones related to aspects which could affect CFM, such as anxiety.

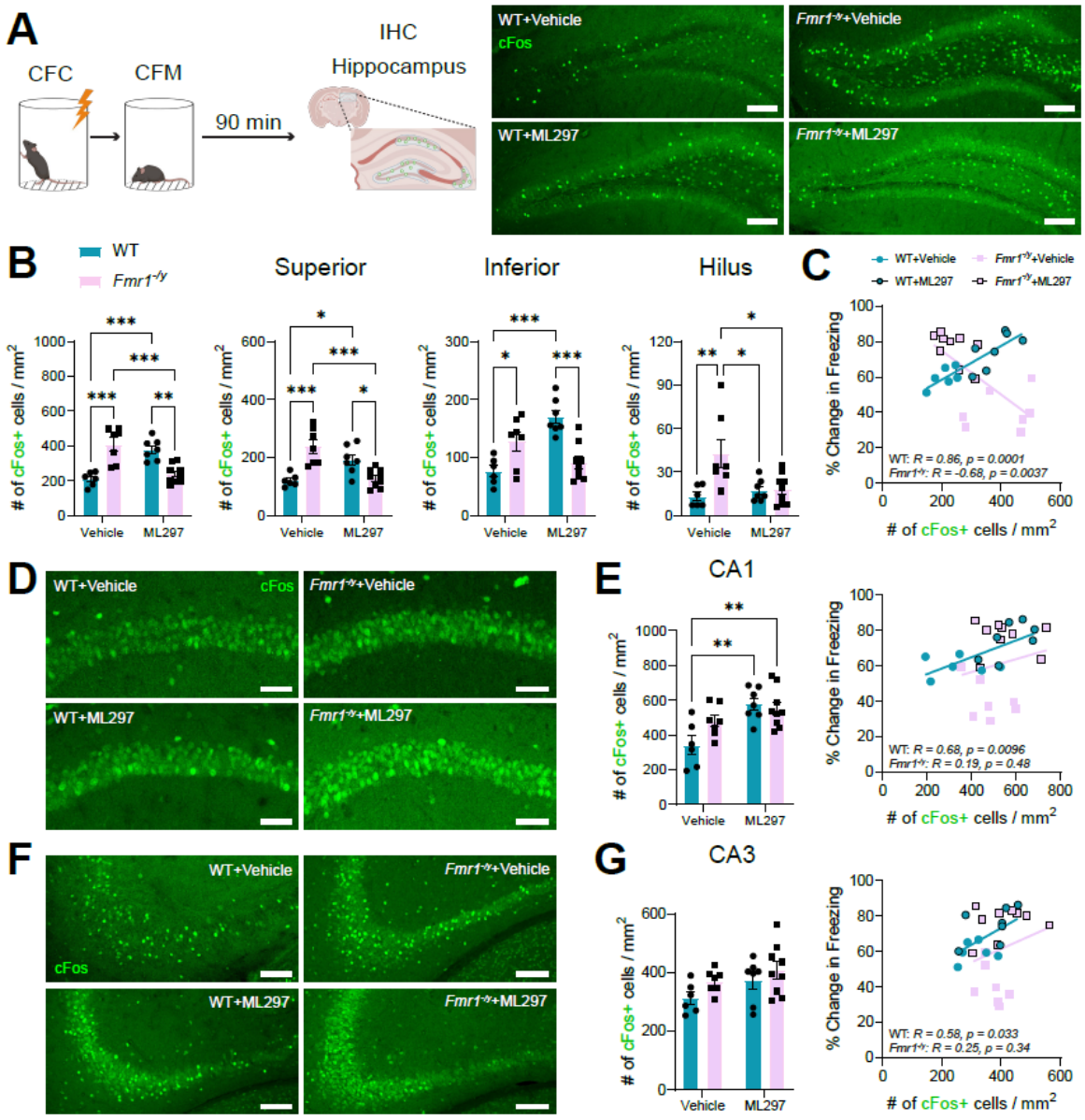
A
CFC
CFM
90 min
IHC
Hippocampus
WT+Vehicle
cFos
Fmr1-/y+Vehicle
WT+ML297
Fmr1-/y+ML297
B
WT
Fmr1-/y
Superior
Inferior
Hilus
# of cFos+ cells / mm2
Vehicle
ML297
C
WT+Vehicle
Fmr1-/y+Vehicle
WT+ML297
Fmr1-/y+ML297
% Change in Freezing
# of cFos+ cells / mm2
WT: R = 0.86, p = 0.0001
Fmr1-/y: R = -0.68, p = 0.0037
D
WT+Vehicle
cFos
Fmr1-/y+Vehicle
WT+ML297
Fmr1-/y+ML297
E
CA1
# of cFos+ cells / mm2
Vehicle
ML297
% Change in Freezing
# of cFos+ cells / mm2
WT: R = 0.68, p = 0.0096
Fmr1-/y: R = 0.19, p = 0.48
F
WT+Vehicle
cFos
Fmr1-/y+Vehicle
WT+ML297
Fmr1-/y+ML297
G
CA3
# of cFos+ cells / mm2
Vehicle
ML297
% Change in Freezing
# of cFos+ cells / mm2
WT: R = 0.58, p = 0.033
Fmr1-/y: R = 0.25, p = 0.34

Figure 4.8: *Fmr1*$^{-/y}$ mice show increased DG network activity during memory recall, which is normalized by ML297 administration during consolidation

(A) Vehicle- and ML297-treated WT and *Fmr1*$^{-/y}$ mice were perfused 90 min following CFM recall to assess hippocampal cFos expression (***left***). Representative recall-associated cFos expression in DG for the four treatment groups (***right***). Scale bar = 100 μm.

(B) Quantification of DG cFos+ neuron density. Two-way ANOVA, for entire DG (***left***): p(treatment) = 0.99, p(genotype) = 0.26, p(treatment x genotype interaction) < 0.0001. For superior granule cell blade: p(treatment) = 0.28, p(genotype) = 0.11, p(treatment x genotype interaction) < 0.0001. For inferior granule cell blade: p(treatment) = 0.03, p(genotype) = 0.28, p(treatment x genotype interaction) < 0.0001. For hilus (***right***): p(treatment) = 0.078, p(genotype) = 0.011, p(treatment x genotype interaction) = 0.016.

(C) Pearson correlation for relationship between DG cFos+ neuron density and freezing during CFM recall.

(D) Representative recall-associated cFos expression in CA1 for the four treatment groups. Scale bar = 200 μm.

(E) Quantification of CA1 cFos+ neuron density (***left***). Two-way ANOVA, p(treatment) = 0.0009, p(genotype) = 0.17, p(treatment x genotype interaction) = 0.054. Pearson correlation for relationship between CA1 cFos+ neuron density and freezing during CFM recall (***right***).

(F) Representative recall-associated cFos expression in CA3 for the four treatment groups. Scale bar = 100 μm.

(G) Quantification of CA3 cFos+ neuron density (***left***). Two-way ANOVA, p(treatment) = 0.064, p(genotype) = 0.077, p(treatment x genotype interaction) = 0.64. Pearson correlation for relationship between CA3 cFos+ neuron density and freezing during CFM recall (***right***).

n = 6 (WT + vehicle), 7 (WT + ML297), 7 (*Fmr1*$^{-/y}$ + vehicle), and 9 (*Fmr1*$^{-/y}$ + ML297). *, **, and *** indicate p < 0.05, p < 0.01 and p < 0.001, Tukey's *post hoc* test.

4.5 : Discussion

To examine the relationship between sleep and cognition in the context of FXS, we first fully characterized sleep parameters in the *Fmr1*$^{-/y}$ (FXS) mouse model. While other studies have suggested that *Fmr1*$^{-/y}$ mice could have similar sleep loss phenotypes comparable to FXS individuals [16,17,102], our study is one of the first to examine sleep architecture across multiple contiguous 24 h periods in *Fmr1*$^{-/y}$ mice using EEG recording techniques. We demonstrate that *Fmr1*$^{-/y}$ mice have deficits in NREM sleep architecture and spectral power primarily during the light phase of the day. The deficits in NREM sleep are analogous to findings seen in polysomnography recordings of FXS patients such as reduced NREM sleep and frequent nighttime awakenings (sleep fragmentation) [6-8]. In contrast, we did not find reduced REM sleep time in *Fmr1*$^{-/y}$ mice, although EEG power spectral density – particularly in the theta band – is altered during REM. The findings not only validate the *Fmr1*$^{-/y}$ mouse model for studying sleep phenotypes related to FXS, but also reinforce the idea that *Fmr1* expression could also play a role in sleep regulation.

In addition to NREM sleep architectural deficits, we also found altered spectral power across NREM sleep, including increased delta and gamma power and reduced sleep spindle density and power. While increased gamma power in *Fmr1*$^{-/y}$ mice during brief intervals of wake has been previously reported [78,79], we show these increases in gamma power also occur during NREM. Many of the changes in EEG spectra recapitulate phenotypes observed in patients with ASD. Here we report increased NREM delta power and decreased spindle density and power during NREM in *Fmr1*$^{-/y}$ mice, which until now was only reported in patients with ASD and/or FXS [30,72,75,103-106] [69,75]. Notably these EEG alterations during NREM (together with reduced theta power in REM) only occur in the

posterior V1 region, not the PFC – where spectral power and spindle density were generally comparable to WT littermates. EEG recordings of ASD children and adults showed similar spatial (i.e., anteroposterior) differences[69,75,83]. We find that this results in widespread changes in spectral coherence between anterior and posterior recording sites in *Fmr1*$^{-/y}$ mice, together with dissimilarities in inter-regional spindle density between these sites during NREM sleep

It is well-established that loss of *Fmr1* leads to reduced excitatory drive onto PV+ interneurons and other GABAergic interneuron subtypes, together with and morphological changes such as increased density of immature dendritic spines in neocortical and hippocampal pyramidal neurons [10,13,15,98,101,107-110]. These alterations are thought to lead to aberrant network excitability, which could underline some of the EEG changes we observe in *Fmr1*$^{-/y}$ mice during sleep. Our data suggest that the TRN, which is essential for generation of NREM spindles [67,81,111], and which is populated by PV+ interneurons, is likely affected by the general disruption of PV+ interneuron function in FXS, leading to spindle alterations. We found a significant reduction of PV interneurons in the TRN of *Fmr1*$^{-/y}$ mice. Further investigation is needed to understand the contribution of specific microcircuit-level alterations in *Fmr1*$^{-/y}$ mice to changes in spectral power and coherence during NREM sleep. Given their role in altering neuronal excitability in FXS and contributing to spindle dysfunction in rodent models of schizophrenia [112], further characterization of the TRN and PV projections to other circuits in the sleep/wake system are needed. Moreover, the specific pharmacological actions of ML297 on GIRK1/2 channels (leading to membrane hyperpolarization) may play a role in the restoration of normal EEG activity after ML297 is administered.

GIRK1/2 function is thought to be selectively disrupted in the absence of FMRP [45,46]. ML297, which activates GIRK1/2 current, has been found to promote NREM sleep without adverse effects to cognition seen in other hypotonic treatments [41,43]. We found that acute administration of ML297 to *Fmr1*$^{-/y}$ mice was enough to renormalize NREM sleep architecture and spectral power (in V1) to parameters observed in WT littermates. In addition, we found that spindle density correlations between V1 and PFC regions were improved. The region-selectivity of these effects further reinforces the region-specificity of EEG differences in *Fmr1*$^{-/y}$ mice. In addition, the fact that oscillatory coherence between structures was only partially rescued by ML297 also emphasizes that future therapeutic studies targeting sleep phenotypes such as epilepsy in *Fmr1*$^{-/y}$ mice, and FXS patients, should take into account that some brain regions are differentially affected by loss of FMRP, and may be differentially altered by treatment.

Sleep has been shown to be critical for numerous functions, including cognition and memory [113,114]. Given the relationship between sleep deficits and cognitive impairment in not only FXS, but other neurodevelopmental disorders, we tested whether restoration of WT sleep phenotypes could improve memory consolidation deficits in *Fmr1*$^{-/y}$ mice. We found ML297-mediated improvements in consolidation of both CFM and OLM – two dorsal hippocampus-dependent, sleep-dependent forms of memory – which are normally disrupted in *Fmr1*$^{-/y}$ mice. We found that this rescue was associated with ML297-mediated reversal of changes to DG cFos+ neuron density at the time of recall in *Fmr1*$^{-/y}$ mice, but was not predicted by changes in neuron activation in other brain structures, such as CA1, CA3, and amygdala.

Our findings suggest that direct GIRK1/2 channel activation via ML297 in *Fmr1*$^{-/y}$ mice could be beneficial for cognition via sleep-promoting effects and highly reinforce the notion of sleep as potential therapeutic target for not only FXS, but other NDD and psychiatric disorders as well. However, any positive effects on cognition may be limited to emotionally valanced memories as spatial memory was negatively affected. Further studies into the role of GIRK channel signaling in sleep-dependent hippocampal memory function would be needed, particularly how different subunit combinations are expressed within regions of spatial and fear memory circuits. Taken together, this suggests that ML297 following learning leads to either immediate changes in the activation level of the DG "engram neurons" – perhaps suppressing noisy activity that would lead to aberrant plasticity – or long-lasting changes that prevent noisy activation 24 h later, during recall. While our present data do not discriminate between these two possibilities, it is worth noting that changes in total sleep amounts following CFC are linked to the subsequent activation of the DG during CFM recall [82]. Because most (but not all) of the EEG and sleep architecture changes caused by ML297 administration are present only in the first 12 h, it is plausible that many of the longer-term outcomes we observe (i.e., during CFM and OLM recall) reflect plastic changes occurring during the first few hours of post-learning sleep [80,81,115-118]. Because these first few hours correspond to a sensitive window for disruption of long-term memory [21,23,25,44,52,90-92,117], this seems like a plausible mechanism by which ML297 is impacting hippocampal plasticity and subsequently, memory recall.

There are a few limitations to our present studies. Previous work has shown that the neocortex and hippocampus can exhibit different sleep states simultaneously [119], so

additional studies using hippocampal LFP or single neuron recording in *Fmr1*$^{-/y}$ mice could clarify how the EEG changes measured here relate to state-dependent network activity in the hippocampus[25,26,48]. In addition, our findings do not discriminate between changes in the hippocampal network due to sleep architecture changes (or oscillatory changes) and those due to other pharmacological effects of ML297 on hippocampal neurons themselves. Future studies using additional hypnotic agents with different mechanisms of action may be needed to disentangle these effects with regard to phenotypic rescue in *Fmr1*$^{-/y}$ mice. Lastly, based on the age of the mice used in this study, our data may be more relevant to treatment of FXS individuals of a slightly older age (i.e., non-pediatric patients). Given the role of sleep has in the shaping of synaptic circuits early in life [24,34,120,121], it warrants further examination whether treating sleep phenotypes in *Fmr1*$^{-/y}$ mice, with ML297 or other hypnotics, earlier in development is beneficial for cognition. On the other hand, young adults with autism are often overlooked in clinical studies and could possibly benefit from therapeutic intervention to restore sleep. Overall, our findings establish NREM sleep phenotypes in *Fmr1*$^{-/y}$ mice and provide proof-of-concept for targeting these phenotypes in the context of treating other aspects of FXS.

4.5.1 : Acknowledgements

We thank the members of the Aton lab for useful feedback on these studies, Abbey Roelofs for coding support, and Gregg Sobocinski for microscopy support. Images in the following figures: Fig. 1A, 2A, 6A, 6C, 6F, 7A, 8A, S11C, S12A, and S12D were created with Biorender.com. This work was supported by a University of Michigan Graduate School Predoctoral Fellowship, Graduate Student Research Grant, and Merit Fellowship to JDM, a University of Michigan Kavli Neuroscience Innovators Magnificent Summer

Fellowship to LGW and WPB, a Neuroscience Undergraduate Research Opportunity Summer Fellowship to REPT, and National Institutes of Health research grants R01 NS104776 and RF1 NS118440 to SJA.

JDM and SJA conceived and designed the study. JDM, LGW, WPB, KGP, VCG, REPT, DSP, MJD, SLMO, DT, SJ, and ZY performed the research. JDM, LGW, WPB, KGP, VCG, REPT, DSP, MJD, JJS, and BCC analyzed data. JDM and SJA wrote the manuscript. SJA supervised the study.

4.6 : References

1. Rogers, S.J., Wehner, D.E., and Hagerman, R. (2001). The behavioral phenotype in fragile X: symptoms of autism in very young children with fragile X syndrome, idiopathic autism, and other developmental disorders. J Dev Behav Pediatr *22*, 409-417. 10.1097/00004703-200112000-00008.
2. Dahlhaus, R. (2018). Of men and mice: modeling the fragile X syndrome. Frontiers in Molecular Neuroscience. Frontiers Media S.A.
3. Baumgardner, T.L., Reiss, A.L., Freund, L.S., and Abrams, M.T. (1995). Specification of the neurobehavioral phenotype in males with fragile X syndrome. Pediatrics *95*, 744-752.
4. Garber, K.B., Visootsak, J., and Warren, S.T. (2008). Fragile X syndrome. Eur J Hum Genet *16*, 666-672. 10.1038/ejhg.2008.61.
5. Hartley, S.L., Seltzer, M.M., Raspa, M., Olmstead, M., Bishop, E., and Bailey, D.B. (2011). Exploring the adult life of men and women with fragile X syndrome: results from a national survey. Am J Intellect Dev Disabil *116*, 16-35. 10.1352/1944-7558-116.1.16.
6. Kronk, R., Bishop, E.E., Raspa, M., Bickel, J.O., Mandel, D.A., and Bailey, D.B., Jr. (2010). Prevalence, nature, and correlates of sleep problems among children with fragile X syndrome based on a large scale parent survey. Sleep *33*, 679-687. 10.1093/sleep/33.5.679.
7. Kronk, R., Dahl, R., and Noll, R. (2009). Caregiver reports of sleep problems on a convenience sample of children with fragile X syndrome. Am J Intellect Dev Disabil *114*, 383-392. 10.1352/1944-7588-114.6.383.
8. Kidd, S.A., Lachiewicz, A., Barbouth, D., Blitz, R.K., Delahunty, C., McBrien, D., Visootsak, J., and Berry-Kravis, E. (2014). Fragile X syndrome: a review of associated medical problems. Pediatrics *134*, 995-1005. 10.1542/peds.2013-4301.
9. Weiskop, S., Richdale, A., and Matthews, J. (2005). Behavioural treatment to reduce sleep problems in children with autism or fragile X syndrome. Dev Med Child Neurol *47*, 94-104. 10.1017/s0012162205000186.
10. Hays, S.A., Huber, K.M., and Gibson, J.R. (2011). Altered neocortical rhythmic activity states in Fmr1 KO mice are due to enhanced mGluR5 signaling and involve changes in excitatory circuitry. J Neurosci *31*, 14223-14234. 10.1523/JNEUROSCI.3157-11.2011.
11. Ding, Q., Sethna, F., and Wang, H. (2014). Behavioral analysis of male and female Fmr1 knockout mice on C57BL/6 background. Behav Brain Res *271*, 72-78. 10.1016/j.bbr.2014.05.046.
12. van der Molen, M.J., Stam, C.J., and van der Molen, M.W. (2014). Resting-state EEG oscillatory dynamics in fragile X syndrome: abnormal functional connectivity and brain network organization. PLoS One *9*, e88451. 10.1371/journal.pone.0088451.
13. Dolen, G., Osterweil, E., Rao, B.S., Smith, G.B., Auerbach, B.D., Chattarji, S., and Bear, M.F. (2007). Correction of fragile X syndrome in mice. Neuron *56*, 955-962. 10.1016/j.neuron.2007.12.001.

14. Dölen, G., and Bear, M.F. (2008). Role for metabotropic glutamate receptor 5 (mGluR5) in the pathogenesis of fragile X syndrome. The Journal of Physiology *586*, 1503-1508. 10.1113/jphysiol.2008.150722.
15. Pan, F., Aldridge, G.M., Greenough, W.T., and Gan, W.B. (2010). Dendritic spine instability and insensitivity to modulation by sensory experience in a mouse model of fragile X syndrome. Proc Natl Acad Sci U S A *107*, 17768-17773. 10.1073/pnas.1012496107.
16. Sare, R.M., Harkless, L., Levine, M., Torossian, A., Sheeler, C.A., and Smith, C.B. (2017). Deficient Sleep in Mouse Models of Fragile X Syndrome. Front Mol Neurosci *10*, 280. 10.3389/fnmol.2017.00280.
17. Sare, R.M., Lemons, A., and Smith, C.B. (2022). Effects of Treatment With Hypnotics on Reduced Sleep Duration and Behavior Abnormalities in a Mouse Model of Fragile X Syndrome. Front Neurosci *16*, 811528. 10.3389/fnins.2022.811528.
18. Walker, M.P., Brakefield, T., Hobson, J.A., and Stickgold, R. (2003). Dissociable stages of human memory consolidation and reconsolidation. Nature *425*, 616-620. 10.1038/nature01930.
19. Stickgold, R., and Walker, M.P. (2005). Memory consolidation and reconsolidation: what is the role of sleep? Trends Neurosci *28*, 408-415. 10.1016/j.tins.2005.06.004.
20. Stickgold, R., and Walker, M.P. (2007). Sleep-dependent memory consolidation and reconsolidation. Sleep Med *8*, 331-343. 10.1016/j.sleep.2007.03.011.
21. Graves, L.A., Heller, E.A., Pack, A.I., and Abel, T. (2003). Sleep deprivation selectively impairs memory consolidation for contextual fear conditioning. Learn Mem *10*, 168-176. 10.1101/lm.48803.
22. Havekes, R., and Abel, T. (2017). The tired hippocampus: the molecular impact of sleep deprivation on hippocampal function. Curr Opin Neurobiol *44*, 13-19. 10.1016/j.conb.2017.02.005.
23. Heckman, P.R.A., Roig Kuhn, F., Meerlo, P., and Havekes, R. (2020). A brief period of sleep deprivation negatively impacts the acquisition, consolidation, and retrieval of object-location memories. Neurobiol Learn Mem *175*, 107326. 10.1016/j.nlm.2020.107326.
24. Aton, S.J., Seibt, J., Dumoulin, M., Jha, S.K., Steinmetz, N., Coleman, T., Naidoo, N., and Frank, M.G. (2009). Mechanisms of sleep-dependent consolidation of cortical plasticity. Neuron *61*, 454-466. 10.1016/j.neuron.2009.01.007.
25. Ognjanovski, N., Maruyama, D., Lashner, N., Zochowski, M., and Aton, S.J. (2014). CA1 hippocampal network activity changes during sleep-dependent memory consolidation. Front Syst Neurosci *8*, 61. 10.3389/fnsys.2014.00061.
26. Ognjanovski, N., Broussard, C., Zochowski, M., and Aton, S.J. (2018). Hippocampal Network Oscillations Rescue Memory Consolidation Deficits Caused by Sleep Loss. Cereb Cortex *28*, 3711-3723. 10.1093/cercor/bhy174.
27. Colten, H.R., and Altevogt, B.M. (2006). Sleep disorders and sleep deprivation: An unmet public health problem (National Academies Press). 10.17226/11617.

28. Liu, X., Hubbard, J.A., Fabes, R.A., and Adam, J.B. (2006). Sleep disturbances and correlates of children with autism spectrum disorders. Child Psychiatry Hum Dev *37*, 179-191. 10.1007/s10578-006-0028-3.
29. Sateia, M.J. (2014). International classification of sleep disorders-third edition: highlights and modifications. Chest *146*, 1387-1394. 10.1378/chest.14-0970.
30. Blackmer, A.B., and Feinstein, J.A. (2016). Management of Sleep Disorders in Children With Neurodevelopmental Disorders: A Review. Pharmacotherapy *36*, 84-98. 10.1002/phar.1686.
31. Basta, M., Chrousos, G.P., Vela-Bueno, A., and Vgontzas, A.N. (2007). Chronic Insomnia and Stress System. Sleep Med Clin *2*, 279-291. 10.1016/j.jsmc.2007.04.002.
32. Owens, J., Adolescent Sleep Working, G., and Committee on, A. (2014). Insufficient sleep in adolescents and young adults: an update on causes and consequences. Pediatrics *134*, e921-932. 10.1542/peds.2014-1696.
33. Kotagal, S., and Broomall, E. (2012). Sleep in children with autism spectrum disorder. Pediatr Neurol *47*, 242-251. 10.1016/j.pediatrneurol.2012.05.007.
34. Wintler, T., Schoch, H., Frank, M.G., and Peixoto, L. (2020). Sleep, brain development, and autism spectrum disorders: Insights from animal models. J Neurosci Res *98*, 1137-1149. 10.1002/jnr.24619.
35. Szabadi, E. (2014). Selective targets for arousal-modifying drugs: implications for the treatment of sleep disorders. Drug Discov Today *19*, 701-708. 10.1016/j.drudis.2014.01.001.
36. Inanobe, A., Yoshimoto, Y., Horio, Y., Morishige, K.I., Hibino, H., Matsumoto, S., Tokunaga, Y., Maeda, T., Hata, Y., Takai, Y., and Kurachi, Y. (1999). Characterization of G-protein-gated K+ channels composed of Kir3.2 subunits in dopaminergic neurons of the substantia nigra. J Neurosci *19*, 1006-1017. 10.1523/JNEUROSCI.19-03-01006.1999.
37. Walsh, K.B. (2011). Targeting GIRK Channels for the Development of New Therapeutic Agents. Front Pharmacol *2*, 64. 10.3389/fphar.2011.00064.
38. Hibino, H., Inanobe, A., Furutani, K., Murakami, S., Findlay, I., and Kurachi, Y. (2010). Inwardly rectifying potassium channels: Their structure, function, and physiological roles. Physiological Reviews. American Physiological Society Bethesda, MD.
39. Luscher, C., Jan, L.Y., Stoffel, M., Malenka, R.C., and Nicoll, R.A. (1997). G protein-coupled inwardly rectifying K+ channels (GIRKs) mediate postsynaptic but not presynaptic transmitter actions in hippocampal neurons. Neuron *19*, 687-695. 10.1016/s0896-6273(00)80381-5.
40. Lüscher, C., and Slesinger, P.A. (2010). Emerging roles for G protein-gated inwardly rectifying potassium (GIRK) channels in health and disease. Nature Reviews Neuroscience. Nature Publishing Group.
41. Kaufmann, K., Romaine, I., Days, E., Pascual, C., Malik, A., Yang, L., Zou, B., Du, Y., Sliwoski, G., Morrison, R.D., et al. (2013). ML297 (VU0456810), the first potent and selective activator of the GIRK potassium channel, displays antiepileptic properties in mice. ACS Chem Neurosci *4*, 1278-1286. 10.1021/cn400062a.

42. Wydeven, N., Marron Fernandez de Velasco, E., Du, Y., Benneyworth, M.A., Hearing, M.C., Fischer, R.A., Thomas, M.J., Weaver, C.D., and Wickman, K. (2014). Mechanisms underlying the activation of G-protein-gated inwardly rectifying K+ (GIRK) channels by the novel anxiolytic drug, ML297. Proc Natl Acad Sci U S A *111*, 10755-10760. 10.1073/pnas.1405190111.
43. Zou, B., Cao, W.S., Guan, Z., Xiao, K., Pascual, C., Xie, J., Zhang, J., Xie, J., Kayser, F., Lindsley, C.W., et al. (2019). Direct activation of G-protein-gated inward rectifying K+ channels promotes nonrapid eye movement sleep. Sleep *42*, 1-16. 10.1093/sleep/zsy244.
44. Martinez, J.D., Brancaleone, W.P., Peterson, K.G., Wilson, L.G., and Aton, S.J. (2022). Atypical hypnotic compound ML297 restores sleep architecture immediately following emotionally-valenced learning, to promote memory consolidation and hippocampal network activation during recall. Sleep. 10.1093/sleep/zsac301.
45. Wolfe, S.A., Workman, E.R., Heaney, C.F., Niere, F., Namjoshi, S., Cacheaux, L.P., Farris, S.P., Drew, M.R., Zemelman, B.V., Harris, R.A., and Raab-Graham, K.F. (2016). FMRP regulates an ethanol-dependent shift in GABABR function and expression with rapid antidepressant properties. Nat Communications *7*, 12867.
46. Pacey, L.K.K., Doss, L., Cifelli, C., van der Kooy, D., Heximer, S.P., and Hampson, D.R. (2011). Genetic deletion of regulator of G-protein signaling 4 (RGS4) rescues a subset of fragile X related phenotypes in the FMR1 knockout mouse. Mol Cell Neurosci *46*, 563-572.
47. Durkin, J., Suresh, A.K., Colbath, J., Broussard, C., Wu, J., Zochowski, M., and Aton, S.J. (2017). Cortically coordinated NREM thalamocortical oscillations play an essential, instructive role in visual system plasticity. Proc Natl Acad Sci U S A *114*, 10485-10490. 10.1073/pnas.1710613114.
48. Ognjanovski, N., Schaeffer, S., Wu, J., Mofakham, S., Maruyama, D., Zochowski, M., and Aton, S.J. (2017). Parvalbumin-expressing interneurons coordinate hippocampal network dynamics required for memory consolidation. Nat Commun *8*, 15039. 10.1038/ncomms15039.
49. Clawson, B.C., Pickup, E.J., Ensing, A., Geneseo, L., Shaver, J., Gonzalez-Amoretti, J., Zhao, M., York, A.K., Kuhn, F.R., Swift, K., et al. (2021). Causal role for sleep-dependent reactivation of learning-activated sensory ensembles for fear memory consolidation. Nat Commun *12*, 1200. 10.1038/s41467-021-21471-2.
50. Kattla, S., and Lowery, M.M. (2010). Fatigue related changes in electromyographic coherence between synergistic hand muscles. Exp Brain Res *202*, 89-99. 10.1007/s00221-009-2110-0.
51. Swift, K.M., Keus, K., Echeverria, C.G., Cabrera, Y., Jimenez, J., Holloway, J., Clawson, B.C., and Poe, G.R. (2020). Sex differences within sleep in gonadally intact rats. Sleep *43*, 1-14. 10.1093/sleep/zsz289.
52. Delorme, J., Wang, L., Kuhn, F.R., Kodoth, V., Ma, J., Martinez, J.D., Raven, F., Toth, B.A., Balendran, V., Vega Medina, A., et al. (2021). Sleep loss drives acetylcholine- and somatostatin interneuron-mediated gating of hippocampal activity to inhibit memory consolidation. Proc Natl Acad Sci U S A *118*. 10.1073/pnas.2019318118.

53. Delorme, J., Wang, L., Kodoth, V., Wang, Y., Ma, J., Jiang, S., and Aton, S.J. (2021). Hippocampal neurons' cytosolic and membrane-bound ribosomal transcript profiles are differentially regulated by learning and subsequent sleep. Proc Natl Acad Sci U S A *118*. 10.1073/pnas.2108534118.
54. Raven, F., Heckman, P.R.A., Havekes, R., and Meerlo, P. (2020). Sleep deprivation-induced impairment of memory consolidation is not mediated by glucocorticoid stress hormones. J Sleep Res *29*, e12972. 10.1111/jsr.12972.
55. Havekes, R., Park, A.J., Tudor, J.C., Luczak, V.G., Hansen, R.T., Ferri, S.L., Bruinenberg, V.M., Poplawski, S.G., Day, J.P., Aton, S.J., et al. (2016). Sleep deprivation causes memory deficits by negatively impacting neuronal connectivity in hippocampal area CA1. Elife *5*, e13424-e13424. 10.7554/eLife.13424.
56. Seibenhener, M.L., and Wooten, M.C. (2015). Use of the Open Field Maze to measure locomotor and anxiety-like behavior in mice. J Vis Exp, e52434. 10.3791/52434.
57. Pham, J., Cabrera, S.M., Sanchis-Segura, C., and Wood, M.A. (2009). Automated scoring of fear-related behavior using EthoVision software. J Neurosci Methods *178*, 323-326. 10.1016/j.jneumeth.2008.12.021.
58. Hui, G.K., Figueroa, I.R., Poytress, B.S., Roozendaal, B., McGaugh, J.L., and Weinberger, N.M. (2004). Memory enhancement of classical fear conditioning by post-training injections of corticosterone in rats. Neurobiol Learn Mem *81*, 67-74. 10.1016/j.nlm.2003.09.002.
59. Roozendaal, B., Okuda, S., Van der Zee, E.A., and McGaugh, J.L. (2006). Glucocorticoid enhancement of memory requires arousal-induced noradrenergic activation in the basolateral amygdala. Proc Natl Acad Sci U S A *103*, 6741-6746. 10.1073/pnas.0601874103.
60. Delorme, J.E., Kodoth, V., and Aton, S.J. (2019). Sleep loss disrupts Arc expression in dentate gyrus neurons. Neurobiol Learn Mem *160*, 73-82. 10.1016/j.nlm.2018.04.006.
61. Puentes-Mestril, C., Delorme, J., Wang, L., Donnelly, M., Popke, D., Jiang, S., and Aton, S.J. (2021). Sleep Loss Drives Brain Region-Specific and Cell Type-Specific Alterations in Ribosome-Associated Transcripts Involved in Synaptic Plasticity and Cellular Timekeeping. J Neurosci *41*, 5386-5398. 10.1523/JNEUROSCI.1883-20.2021.
62. Fisher, S.P., Godinho, S.I., Pothecary, C.A., Hankins, M.W., Foster, R.G., and Peirson, S.N. (2012). Rapid assessment of sleep-wake behavior in mice. J Biol Rhythms *27*, 48-58. 10.1177/0748730411431550.
63. Trachsel, L., Tobler, I., and Borbely, A.A. (1988). Electroencephalogram analysis of non-rapid eye movement sleep in rats. Am J Physiol *255*, R27-37. 10.1152/ajpregu.1988.255.1.R27.
64. Bandarabadi, M., Herrera, C.G., Gent, T.C., Bassetti, C., Schindler, K., and Adamantidis, A.R. (2020). A role for spindles in the onset of rapid eye movement sleep. Nat Commun *11*, 5247. 10.1038/s41467-020-19076-2.
65. Andrillon, T., Nir, Y., Staba, R.J., Ferrarelli, F., Cirelli, C., Tononi, G., and Fried, I. (2011). Sleep spindles in humans: insights from intracranial EEG and unit recordings. J Neurosci *31*, 17821-17834. 10.1523/JNEUROSCI.2604-11.2011.

66. Kim, A., Latchoumane, C., Lee, S., Kim, G.B., Cheong, E., Augustine, G.J., and Shin, H.S. (2012). Optogenetically induced sleep spindle rhythms alter sleep architectures in mice. Proc Natl Acad Sci U S A *109*, 20673-20678. 10.1073/pnas.1217897109.
67. Clawson, B.C., Durkin, J., and Aton, S.J. (2016). Form and function of sleep spindles across the lifespan. Neural Plast. *2016*, 6936381.
68. Souders, M.C., Zavodny, S., Eriksen, W., Sinko, R., Connell, J., Kerns, C., Schaaf, R., and Pinto-Martin, J. (2017). Sleep in Children with Autism Spectrum Disorder. Curr Psychiatry Rep *19*, 34. 10.1007/s11920-017-0782-x.
69. Rochette, A.C., Soulieres, I., Berthiaume, C., and Godbout, R. (2018). NREM sleep EEG activity and procedural memory: A comparison between young neurotypical and autistic adults without sleep complaints. Autism Research *11*, 613-623. 10.1002/aur.1933.
70. Lehoux, T., Carrier, J., and Godbout, R. (2019). NREM sleep EEG slow waves in autistic and typically developing children: Morphological characteristics and scalp distribution. J Sleep Res *28*, e12775. 10.1111/jsr.12775.
71. Tessier, S., Lambert, A., Chicoine, M., Scherzer, P., Soulieres, I., and Godbout, R. (2015). Intelligence measures and stage 2 sleep in typically-developing and autistic children. Int J Psychophysiol *97*, 58-65. 10.1016/j.ijpsycho.2015.05.003.
72. Limoges, E., Mottron, L., Bolduc, C., Berthiaume, C., and Godbout, R. (2005). Atypical sleep architecture and the autism phenotype. Brain *128*, 1049-1061. 10.1093/brain/awh425.
73. Ehlen, J.C., Jones, K.A., Pinckney, L., Gray, C.L., Burette, S., Weinberg, R.J., Evans, J.A., Brager, A.J., Zylka, M.J., Paul, K.N., et al. (2015). Maternal Ube3a Loss Disrupts Sleep Homeostasis But Leaves Circadian Rhythmicity Largely Intact. J Neurosci *35*, 13587-13598. 10.1523/JNEUROSCI.2194-15.2015.
74. Copping, N.A., and Silverman, J.L. (2021). Abnormal electrophysiological phenotypes and sleep deficits in a mouse model of Angelman Syndrome. Mol Autism *12*, 9. 10.1186/s13229-021-00416-y.
75. Lambert, A., Tessier, S., Rochette, A., Scherzer, P.B., Mottron, L., and Godbout, R. (2016). Poor sleep affects daytime functioning in typically developing and autistic children not complaining of sleep problems: A questionnaire-based and polysomnographic study. Research in Autism Spectrum Disorders *23*, 94-106.
76. Liang, S., and Mody, M. (2022). Abnormal Brain Oscillations in Developmental Disorders: Application of Resting State EEG and MEG in Autism Spectrum Disorder and Fragile X Syndrome. Frontiers in Neuroimaging *1*. 10.3389/fnimg.2022.903191.
77. Kozono, N., Okamura, A., Honda, S., Matsumoto, M., and Mihara, T. (2020). Gamma power abnormalities in a Fmr1-targeted transgenic rat model of fragile X syndrome. Sci Rep *10*, 18799. 10.1038/s41598-020-75893-x.
78. Lovelace, J.W., Ethell, I.M., Binder, D.K., and Razak, K.A. (2018). Translation-relevant EEG phenotypes in a mouse model of Fragile X Syndrome. Neurobiol Dis *115*, 39-48. 10.1016/j.nbd.2018.03.012.
79. Jonak, C.R., Lovelace, J.W., Ethell, I.M., Razak, K.A., and Binder, D.K. (2020). Multielectrode array analysis of EEG biomarkers in a mouse model of Fragile X Syndrome. Neurobiol Dis *138*, 104794. 10.1016/j.nbd.2020.104794.

80. Puentes-Mestril, C., and Aton, S.J. (2017). Linking network activity to synaptic plasticity during sleep: hypotheses and recent data. Frontiers in Neural Circuits *11*, doi: 10.3389/fncir.2017.00061.
81. Puentes-Mestril, C., Roach, J., Niethard, N., Zochowski, M., and Aton, S.J. (2019). How rhythms of the sleeping brain tune memory and synaptic plasticity. Sleep *42*, pii: zsz095. 10.1093/sleep/zsz095.
82. Martinez, J.D., Brancaleone, W.P., Peterson, K.G., Wilson, L.G., and Aton, S.J. (2022). Atypical hypnotic compound ML297 restores sleep architecture immediately following emotionally-valenced learning, to promote memory consolidation and hippocampal network activation during recall. Sleep *zsac301*. 10.1101/2022.07.15.500268
83. Gagnon, K., Bolduc, C., Bastien, L., and Godbout, R. (2021). REM Sleep EEG Activity and Clinical Correlates in Adults With Autism. Front Psychiatry *12*. 10.3389/fpsyt.2021.659006.
84. Durkin, J., Suresh, A.K., Colbath, J., Broussard, C., Wu, J., Zochowski, M., and Aton, S.J. (2017). Cortically coordinated NREM thalamocortical oscillations play an essential, instructive role in visual system plasticity. Proceedings National Academy of Sciences *114*, 10485-10490.
85. Durkin, J.M., and Aton, S.J. (2019). How Sleep Shapes Thalamocortical Circuit Function in the Visual System. Annu Rev Vis Sci *5*, 295-315.
86. Aton, S.J., Broussard, C., Dumoulin, M., Seibt, J., Watson, A., Coleman, T., and Frank , M.G. (2013). Visual experience and subsequent sleep induce sequential plastic changes in putative inhibitory and excitatory cortical neurons. Proc Natl Acad Sci U S A *110*, 3101-3106.
87. Wamsley, E.J., Shinn, A.K., Tucker, M.A., Ono, K.E., McKinley, S.K., Ely, A.V., Goff, D.C., Stickgold, R., and Manoach, D.S. (2013). The effects of eszopiclone on sleep spindles and memory consolidation in schizophrenia: a randomized placebo-controlled trial. Sleep *36*, 1369-1376.
88. Blumberg, M.S., Dooley, J.C., and Sokoloff, G. (2020). The developing brain revealed during sleep. Curr Opin Physiol *15*, 14-22.
89. Sun, Q.-Q., Huguenard, J.R., and Prince, D.A. (2002). Somatostatin Inhibits Thalamic Network Oscillations In Vitro: Actions on the GABAergic Neurons of the Reticular Nucleus. J.Neurosci. *22*, 5374-5386.
90. Ognjanovski, N., Broussard, C., Zochowski, M., and Aton, S.J. (2018). Hippocampal Network Oscillations Rescue Memory Consolidation Deficits Caused by Sleep Loss. Cereb. Cortex *28*, 3711-3723. 10.1093/cercor/bhy174.
91. Vecsey, C.G., Baillie, G.S., Jaganath, D., Havekes, R., Daniels, A., Wimmer, M., Huang, T., Brown, K.M., Li, X.Y., Descalzi, G., et al. (2009). Sleep deprivation impairs cAMP signalling in the hippocampus. Nature *461*, 1122-1125.
92. Havekes, R., Park, A.J., Tudor, J.C., Luczak, V.G., Hansen, R.T., Ferri, S.L., Bruinenberg, V.M., Poplawski, S.G., Day, J.P., Aton, S.J., et al. (2016). Sleep deprivation causes memory deficits by negatively impacting neuronal connectivity in hippocampal area CA1. eLife *5*, pii: e13424.
93. Dam, D.V., D 'hooge, R., Hauben, E., Reyniers, E., Gantois, I., Bakker, C.E., Oostra, B.A., Kooy, R.F., De Deyn, P.P., D'Hooge, R., et al. (2000). Spatial

learning, contextual fear conditioning and conditioned emotional response in Fmr1 knockout mice. Behavioural Brain Research.
94. Li, J., Jiang, R.Y., Arendt, K.L., Hsu, Y.T., Zhai, S.R., and Chen, L. (2020). Defective memory engram reactivation underlies impaired fear memory recall in Fragile X syndrome. Elife *9*. 10.7554/eLife.61882.
95. Seese, R.R., Wang, K., Yao, Y.Q., Lynch, G., and Gall, C.M. (2014). Spaced training rescues memory and ERK1/2 signaling in fragile X syndrome model mice. Proc Natl Acad Sci U S A *111*, 16907-16912. 10.1073/pnas.1413335111.
96. Graves, L.A., Heller, E.A., Pack, A.I., and Abel, T. (2003). Sleep deprivation selectively impairs memory consolidation for contextual fear conditioning. Learn. Mem. *10*, 168-176.
97. Liu, X., Ramirez, S., Pang, P.T., Puryear, C.B., Govindarajan, A., Deisseroth, K., and Tonegawa, S. (2012). Optogenetic stimulation of a hippocampal engram activates fear memory recall. Nature *484*, 381-385. 10.1038/nature11028.
98. Contractor, A., Klyachko, V.A., and Portera-Cailliau, C. (2015). Altered Neuronal and Circuit Excitability in Fragile X Syndrome. Neuron *87*, 699-715. 10.1016/j.neuron.2015.06.017.
99. Goncalves, J.T., Anstey, J.E., Golshani, P., and Portera-Cailliau, C. (2013). Circuit level defects in the developing neocortex of Fragile X mice. Nat Neurosci *16*, 903-909. 10.1038/nn.3415.
100. Gibson, J.R., Bartley, A.F., Hays, S.A., and Huber, K.M. (2008). Imbalance of neocortical excitation and inhibition and altered UP states reflect network hyperexcitability in the mouse model of fragile X syndrome. J Neurophysiol *100*, 2615-2626. 10.1152/jn.90752.2008.
101. Sabanov, V., Braat, S., D'Andrea, L., Willemsen, R., Zeidler, S., Rooms, L., Bagni, C., Kooy, R.F., and Balschun, D. (2017). Impaired GABAergic inhibition in the hippocampus of Fmr1 knockout mice. Neuropharmacology *116*, 71-81. 10.1016/j.neuropharm.2016.12.010.
102. Boone, C.E., Davoudi, H., Harrold, J.B., and Foster, D.J. (2018). Abnormal Sleep Architecture and Hippocampal Circuit Dysfunction in a Mouse Model of Fragile X Syndrome. Neuroscience *384*, 275-289. 10.1016/j.neuroscience.2018.05.012.
103. Elia, M., Ferri, R., Musumeci, S.A., Del Gracco, S., Bottitta, M., Scuderi, C., Miano, G., Panerai, S., Bertrand, T., and Grubar, J.C. (2000). Sleep in subjects with autistic disorder: a neurophysiological and psychological study. Brain Dev *22*, 88-92. 10.1016/s0387-7604(99)00119-9.
104. Johnson, K.P., Giannotti, F., and Cortesi, F. (2009). Sleep patterns in autism spectrum disorders. Child Adolesc Psychiatr Clin N Am *18*, 917-928. 10.1016/j.chc.2009.04.001.
105. Picchioni, D., Reith, R.M., Nadel, J.L., and Smith, C.B. (2014). Sleep, plasticity and the pathophysiology of neurodevelopmental disorders: the potential roles of protein synthesis and other cellular processes. Brain Sci *4*, 150-201. 10.3390/brainsci4010150.
106. Accardo, J.A., and Malow, B.A. (2015). Sleep, epilepsy, and autism. Epilepsy Behav *47*, 202-206. 10.1016/j.yebeh.2014.09.081.
107. Goel, A., Cantu, D.A., Guilfoyle, J., Chaudhari, G.R., Newadkar, A., Todisco, B., de Alba, D., Kourdougli, N., Schmitt, L.M., Pedapati, E., et al. (2018). Impaired

perceptual learning in a mouse model of Fragile X syndrome is mediated by parvalbumin neuron dysfunction and is reversible. Nat Neurosci *21*, 1404-1411. 10.1038/s41593-018-0231-0.
108. Angriman, M., Caravale, B., Novelli, L., Ferri, R., and Bruni, O. (2015). Sleep in children with neurodevelopmental disabilities. Neuropediatrics *46*, 199-210. 10.1055/s-0035-1550151.
109. Paluszkiewicz, S.M., Martin, B.S., and Huntsman, M.M. (2011). Fragile X syndrome: the GABAergic system and circuit dysfunction. Dev Neurosci *33*, 349-364. 10.1159/000329420.
110. Contractor, A., Ethell, I.M., and Portera-Cailliau, C. (2021). Cortical interneurons in autism. Nat Neurosci *24*, 1648-1659. 10.1038/s41593-021-00967-6.
111. Vantomme, G., Osorio-Forero, A., Luthi, A., and Fernandez, L.M.J. (2019). Regulation of Local Sleep by the Thalamic Reticular Nucleus. Front Neurosci *13*, 576. 10.3389/fnins.2019.00576.
112. Thankachan, S., Katsuki, F., McKenna, J.T., Yang, C., Shukla, C., Deisseroth, K., Uygun, D.S., Strecker, R.E., Brown, R.E., McNally, J.M., and Basheer, R. (2019). Thalamic Reticular Nucleus Parvalbumin Neurons Regulate Sleep Spindles and Electrophysiological Aspects of Schizophrenia in Mice. Sci Rep *9*, 3607. 10.1038/s41598-019-40398-9.
113. Diekelmann, S., and Born, J. (2010). The memory function of sleep. Nature Reviews Neuroscience.
114. Rasch, B., and Born, J. (2013). About sleep's role in memory. Physiol Rev *93*, 681-766. 10.1152/physrev.00032.2012.
115. Delorme, J., Kodoth, V., and Aton, S.J. (2018). Sleep loss disrupts Arc expression in dentate gyrus neurons. Neurobiol Learn Mem *pii: S1074-7427*, 30091-30091.
116. Puentes-Mestril, C., Delorme, J., Wang, L., Donnelly, M., Popke, D., Jiang, S., and Aton, S.J. (2021). Sleep loss drives brain region- and cell type-specific alterations in ribosome-associated transcripts involved in synaptic plasticity and cellular timekeeping. J Neurosci *41*, 5386-5398.
117. Delorme, J., Wang, L., Roig Kuhn, F., Kodoth, V., Ma, J., Martinez, J.D., Raven, F., Toth, B.A., Balendran, V., Vega Medina, A., et al. (2021). Sleep loss drives acetylcholine- and somatostatin interneuron-mediated gating of hippocampal activity, to inhibit memory consolidation. Proc Natl Acad Sci USA *118*.
118. Delorme, J., Wang, L., Kodoth, V., Wang, Y., Ma, J., Jiang, S., and Aton, S.J. (2021). Hippocampal neurons' cytosolic and membrane-bound ribosomal transcript profiles are differentially regulated by learning and subsequent sleep. Proc Natl Acad Sci USA *118*.
119. Emrick, J.J., Gross, B.A., Riley, B.T., and Poe, G.R. (2016). Different Simultaneous Sleep States in the Hippocampus and Neocortex. Sleep *39*, 2201-2209. 10.5665/sleep.6326.
120. Frank, M.G. (2011). Sleep and developmental plasticity not just for kids. Prog Brain Res *193*, 221-232. 10.1016/B978-0-444-53839-0.00014-4.
121. Frank, M.G., Issa, N.P., and Stryker, M.P. (2001). Sleep enhances plasticity in the developing visual cortex. Neuron *30*, 275-287. 10.1016/s0896-6273(01)00279-3.

4.7 : Chapter 4 Supplementary Information Figures

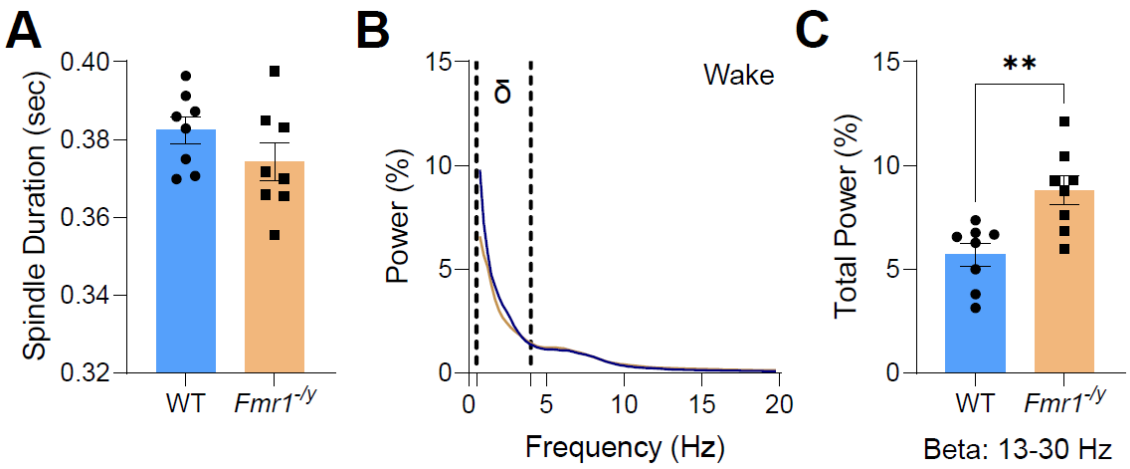

Supplemental Figure 4.1: *Fmr1*$^{-/y}$ mice spindle duration and waking spectral power during the light phase

(A) Comparison of NREM spindle duration during the light phase between WT and *Fmr1*$^{-/y}$ mice. Two-tailed, unpaired t-test.

(B) Left, EEG power spectrum during waking, δ = 0.5-4 Hz. Two-way RM ANOVA, p(Frequency x Genotype) < 0.0001, p(Frequency) < 0.0001, p(Genotype) = 0.0010. Right, average beta power (13-30 Hz) during waking. Two-tailed, unpaired t-test. Asterisks over data points were obtained via two-tailed, unpaired t-test. **p < 0.01. Data shown as mean ± SEM (except EEG spectrum in panel B, data shown as mean). Sample size: n = 8 mice/genotype.

(Related to Fig. 1)

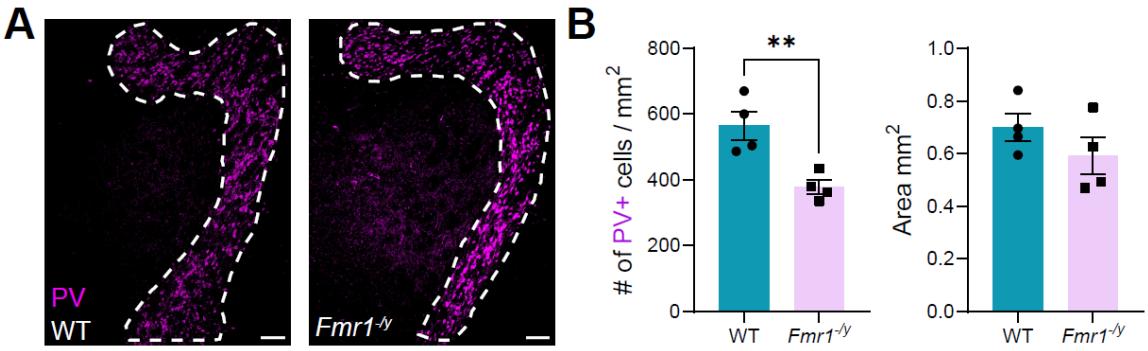

Supplemental Figure 4.2: Parvalbumin (PV+) interneuron expression in the thalamic reticular nucleus (TRN) is reduced in *Fmr1*$^{-/y}$ mice

(A) Representative images of PV+ expressing interneurons in the TRN outlined by dashed lines in WT and *Fmr1*$^{-/y}$ mice. Scale bar = 250 µm.

(B) PV+ interneuron density of the TRN (left) and area of TRN measured (right). Two-tailed, unpaired t-tests. **p < 0.01. Data shown as mean ± SEM. Sample size: n = 4/genotype.

(Related to Fig. 1 and Fig. 4)

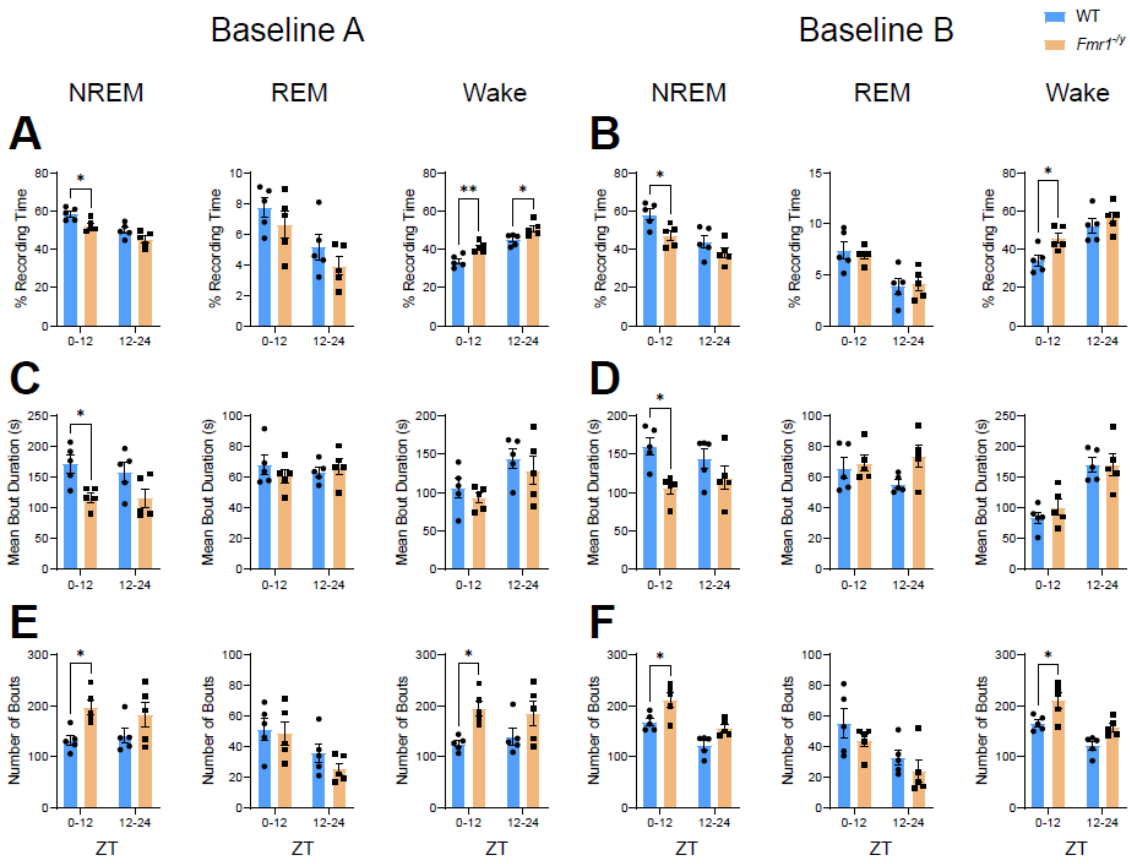
Baseline A
Baseline B
WT
Fmr1-/y
NREM
REM
Wake
NREM
REM
Wake
A
B
C
D
E
F
% Recording Time
Mean Bout Duration (s)
Number of Bouts
0-12
12-24
ZT

Supplemental Figure 4.3: Baseline recordings show deficits in NREM sleep architecture in *Fmr1*$^{-/y}$ mice

(A) Left, percent recording time spent in NREM sleep during baseline A. Two-way RM ANOVA, p(Time of Day x Genotype) = 0.61, p(Time of Day) = 0.0002, p(Genotype) = 0.0044. Middle, percent recording time in REM sleep during baseline A. Two-way RM ANOVA, p(Time of Day x Genotype) = 0.85, p(Time of Day) = 0.0003, p(Genotype) = 0.26. Right, percent recording time in waking during baseline A. Two-way RM ANOVA, p(Time of Day x Genotype) = 0.61, p(Time of Day) < 0.0001, p(Genotype) = 0.0003.

(B) Left, percent recording time spent in NREM sleep during baseline B. Two-way RM ANOVA, p(Time of Day x Genotype) = 0.37, p(Time of Day) = 0.0009, p(Genotype) = 0.011. Middle, percent recording time in REM sleep during baseline B. Two-way RM ANOVA, p(Time of Day x Genotype) = 0.65, p(Time of Day) = 0.0028, p(Genotype) = 0.86. Right, percent recording time in waking during baseline B. Two-way RM ANOVA, p(Time of Day x Genotype) = 0.22, p(Time of Day) = 0.0007, p(Genotype) = 0.056.

(C) Left, mean NREM bout duration during baseline A. Two-way RM ANOVA, p(Time of Day x Genotype) = 0.44, p(Time of Day) = 0.34, p(Genotype) = 0.02. Middle, mean REM bout duration during baseline A. Two-way RM ANOVA, p(Time of Day x Genotype) = 0.24, p(Time of Day) = 0.84, p(Genotype) = 0.74. Right, mean waking bout duration during baseline A. Two-way RM ANOVA, p(Time of Day x Genotype) = 0.87, p(Time of Day) = 0.0012, p(Genotype) = 0.43.

(D) Left, mean NREM bout duration during baseline B. Two-way RM ANOVA, p(Time of Day x Genotype) = 0.23, p(Time of Day) = 0.89, p(Genotype) = 0.0045. Middle, mean REM bout duration during baseline B. Two-way RM ANOVA, p(Time of Day x Genotype) = 0.21, p(Time of Day) = 0.62, p(Genotype) = 0.076. Right, mean waking bout duration during baseline B. Two-way RM ANOVA, p(Time of Day x Genotype) = 0.53, p(Time of Day) < 0.0001, p(Genotype) = 0.52.

(E) Left, number of NREM bouts during baseline A. Two-way RM ANOVA, p(Time of Day x Genotype) = 0.35, p(Time of Day) = 0.81, p(Genotype) = 0.031. Middle, number of REM bouts during baseline A. Two-way RM ANOVA, p(Time of Day x Genotype) = 0.47, p(Time of Day) = 0.0031, p(Genotype) = 0.41. Right, number of waking bouts during baseline A. Two-way RM ANOVA, p(Time of Day x Genotype) = 0.30, p(Time of Day) = 0.89, p(Genotype) = 0.023.

(F) Left, number of NREM bouts during baseline B. Two-way RM ANOVA, p(Time of Day x Genotype) = 0.64, p(Time of Day) = 0.0001, p(Genotype) = 0.0014. Middle, number of REM bouts during baseline B. Two-way RM ANOVA, p(Time of Day x Genotype) = 0.86, p(Time of Day) = 0.0062, p(Genotype) = 0.14. Right, number of waking bouts during baseline B. Two-way RM ANOVA, p(Time of Day x Genotype) = 0.63, p(Time of Day) = 0.0002, p(Genotype) = 0.0011. **(**Asterisks over data points were obtained via Sidak's *post hoc* test. *p < 0.05, **p < 0.01.

Data shown as mean ± SEM. Sample size: n = 5 mice/genotype.

(Related to Fig. 2)

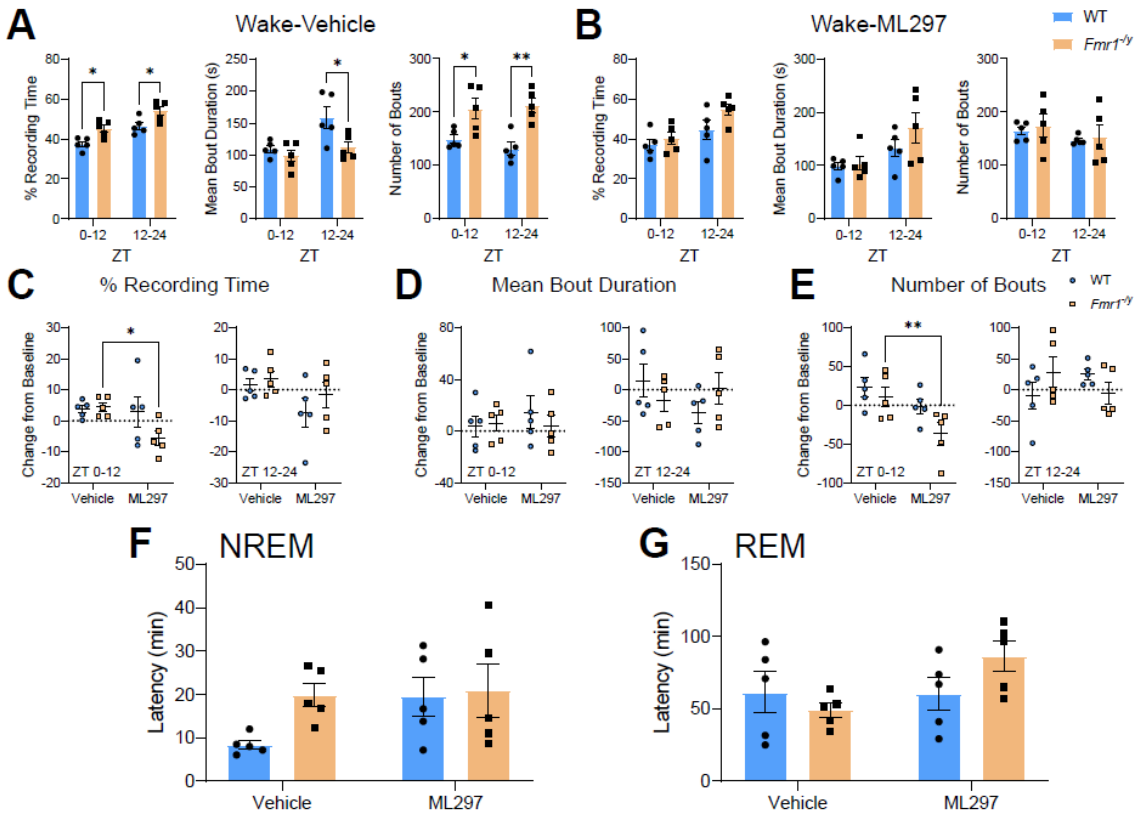
A
Wake-Vehicle
B
Wake-ML297
WT
Fmr1-/y
% Recording Time
Mean Bout Duration (s)
Number of Bouts
ZT
0-12
12-24
C
% Recording Time
D
Mean Bout Duration
E
Number of Bouts
Change from Baseline
ZT 0-12
ZT 12-24
Vehicle
ML297
F
NREM
G
REM
Latency (min)

Supplemental Figure 4.4: GIRK channel activation via ML297 normalizes waking architectural differences in *Fmr1*$^{-/y}$ mice

(A) Left, percent recording time spent in waking post-vehicle injection between WT and *Fmr1*$^{-/y}$ mice. Two-way RM ANOVA, p(Time of Day x Genotype) = 0.95, p(Time of Day) = 0.0002, p(Genotype) = 0.0005. Middle, mean waking bout duration. Two-way RM ANOVA, p(Time of Day x Genotype) = 0.12, p(Time of Day) = 0.017, p(Genotype) = 0.035. Right, total waking bouts. Two-way RM ANOVA, p(Time of Day x Genotype) = 0.20, p(Time of Day) = 0.51, p(Genotype) = 0.0036.

(B) Left, percent recording time spent in waking post-ML297 injection between WT and *Fmr1*$^{-/y}$ mice. Two-way RM ANOVA, p(Time of Day x Genotype) = 0.26, p(Time of Day) = 0.0062, p(Genotype) = 0.12. Middle, mean waking bout duration. Two-way RM ANOVA, p(Time of Day x Genotype) = 0.28, p(Time of Day) = 0.0075, p(Genotype) = 0.31. Right, total waking bouts. Two-way RM ANOVA, p(Time of Day x Genotype) = 0.89, p(Time of Day) = 0.24, p(Genotype) = 0.64.

(C) Vehicle and ML297 changes in waking percent recording time during the light (ZT0-12, left) and dark (ZT13-24, right) phases from time-matched baseline values (baseline A-vehicle and baseline B-ML297). ZT0-12: two-way RM ANOVA, p(Treatment x Genotype) = 0.12, p(Treatment) = 0.071, p(Genotype) = 0.18. ZT13-24: two-way RM ANOVA, p(Treatment x Genotype) = 0.58, p(Treatment) = 0.061, p(Genotype) = 0.27.

(D) Vehicle and ML297 changes in mean waking bout duration during the light (ZT0-12, left) and dark (ZT13-24, right) phases from time-matched baseline values (baseline A-vehicle and baseline B-ML297). ZT0-12: two-way RM ANOVA, p(Treatment x Genotype) = 0.37, p(Treatment) = 0.57, p(Genotype) = 0.71. ZT13-24: two-way RM ANOVA, p(Treatment x Genotype) = 0.13, p(Treatment) = 0.45, p(Genotype) = 0.86.

(E) Vehicle and ML297 changes in number of waking bouts during the light (ZT0-12, left) and dark (ZT13-24, right) phases from time-matched baseline values (baseline A-vehicle and baseline B-ML297). ZT0-12: two-way RM ANOVA, p(Treatment x Genotype) = 0.37, p(Treatment) = 0.010, p(Genotype) = 0.069. ZT13-24: two-way RM ANOVA, p(Treatment x Genotype) = 0.17, p(Treatment) = 0.99, p(Genotype) = 0.79.

(F) Latency to NREM sleep after vehicle or ML297 treatment in wild-type (WT) and *Fmr1*$^{-/y}$ mice. Two-way RM ANOVA, p(Treatment x Genotype) = 0.23, p(Treatment) = 0.15, p(Genotype) = 0.13.

(G) Latency to REM sleep after vehicle or ML297 treatment. Two-way RM ANOVA, p(Treatment x Genotype) = 0.09, p(Treatment) = 0.11, p(Genotype) = 0.54. Asterisks over data points were obtained via Sidak's *post hoc* test. *$p < 0.05$, **$p < 0.01$. Data shown as mean ± SEM. Sample size: n = 5 mice/genotype.

(Related to Fig 2)

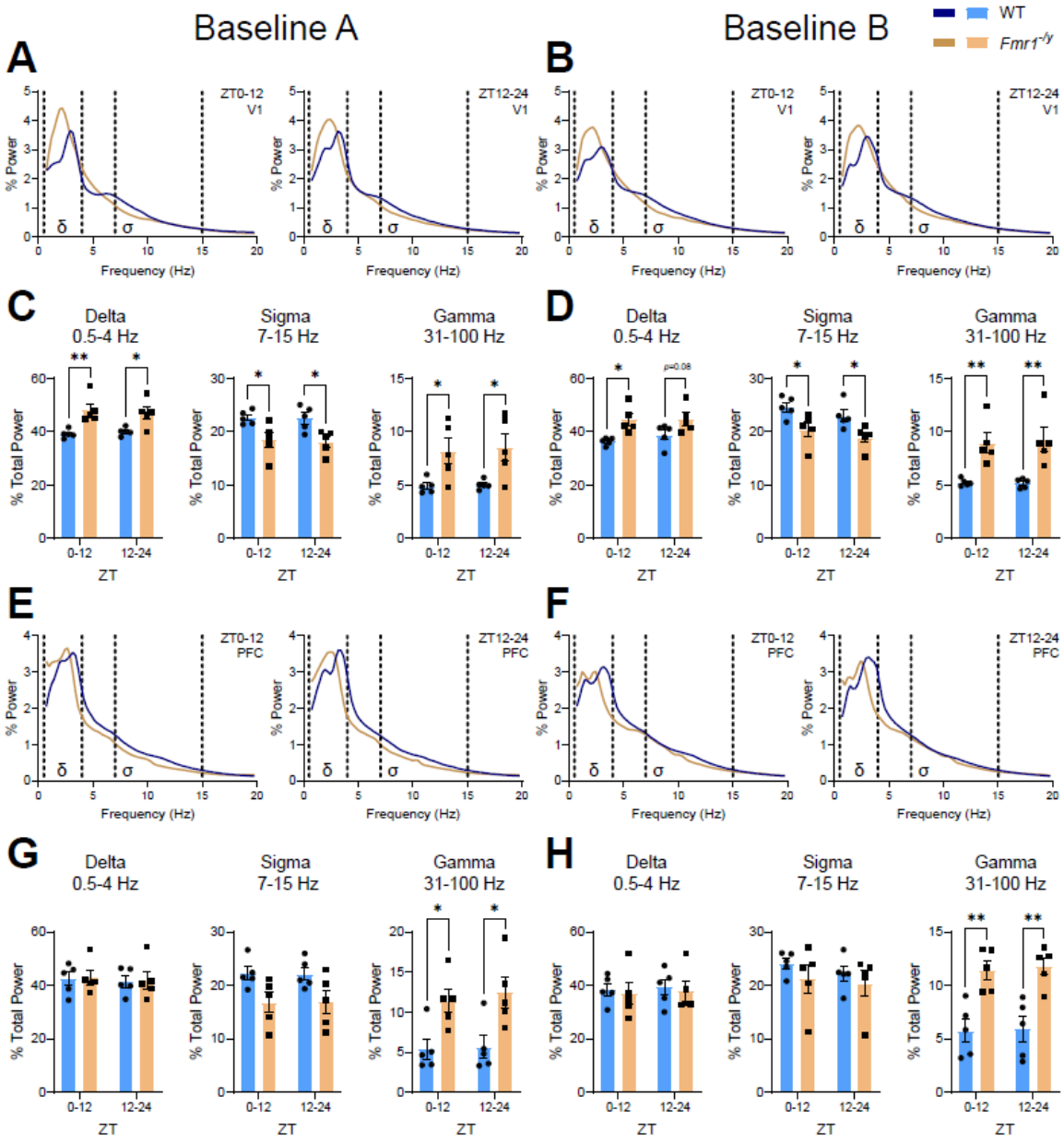
Baseline A
Baseline B
WT
Fmr1-/y
A
B
C
D
E
F
G
H
ZT0-12 V1
ZT12-24 V1
ZT0-12 PFC
ZT12-24 PFC
% Power
Frequency (Hz)
δ
σ
Delta 0.5-4 Hz
Sigma 7-15 Hz
Gamma 31-100 Hz
% Total Power
ZT
0-12
12-24
p=0.08

Supplemental Figure 4.5: Baseline NREM spectral power in V1 and PFC in WT and *Fmr1*$^{-/y}$ mice

(A) NREM EEG power spectrum in V1 for baseline A during ZT0-12 (left) and ZT13-24 (right). ZT0-12: two-way RM ANOVA, p(Frequency x Genotype) < 0.0001, p(Frequency) < 0.0001, p(Genotype) = 0.015. ZT13-24: two-way RM ANOVA, p(Frequency x Genotype) < 0.0001, p(Frequency) < 0.0001, p(Genotype) = 0.81.

(B) NREM EEG power spectrum in V1 for baseline B during ZT0-12 (left) and ZT13-24 (right). ZT0-12: two-way RM ANOVA, p(Frequency x Genotype) < 0.0001, p(Frequency) < 0.0001, p(Genotype) = 0.33. ZT13-24: two-way RM ANOVA, p(Frequency x Genotype) < 0.0001, p(Frequency) < 0.0001, p(Genotype) = 0.35.

(C) Left, average NREM delta (0.5-4 Hz) power in V1 during baseline A. Two-way RM ANOVA, p(Time of Day x Genotype) = 0.23, p(Time of Day) = 0.90, p(Genotype) = 0.008. Middle, average NREM sigma for spindle (7-15 Hz) power. Two-way RM ANOVA, p(Time of Day x Genotype) = 0.84, p(Time of Day) = 0.68, p(Genotype) = 0.015. Right, average NREM gamma power. Two-way RM ANOVA, p(Time of Day X Genotype) = 0.24, p(Time of Day) = 0.033, p(Genotype) = 0.0027.

(D) Left, average NREM delta (0.5-4 Hz) power in V1 during baseline B. Two-way RM ANOVA, p(Time of Day x Genotype) = 0.16, p(Time of Day) = 0.10, p(Genotype) = 0.025. Middle, average NREM sigma (7-15 Hz) power. Two-way RM ANOVA, p(Time of Day x Genotype) = 0.88, p(Time of Day) = 0.012, p(Genotype) = 0.218. Right, average NREM gamma power. Two-way RM ANOVA, p(Time of Day X Genotype) = 0.26, p(Time of Day) = 0.46, p(Genotype) = 0.0052.

(E) NREM EEG power spectrum in PFC for baseline A during ZT0-12 (left) and ZT13-24 (right). ZT0-12: two-way RM ANOVA, p(Frequency x Genotype) = 0.042, p(Frequency) < 0.0001, p(Genotype) = 0.0207. ZT13-24: two-way RM ANOVA, p(Frequency x Genotype) = 0.0002, p(Frequency) < 0.0001, p(Genotype) = 0.0279.

(F) NREM EEG power spectrum in PFC for baseline B during ZT0-12 (left) and ZT13-24 (right). ZT0-12: two-way RM ANOVA, p(Frequency x Genotype) = 0.0073, p(Frequency) < 0.0001, p(Genotype) = 0.025. ZT13-24: two-way RM ANOVA, p(Frequency x Genotype) = 0.0003, p(Frequency) < 0.0001, p(Genotype) = 0.081.

(G) Left, average NREM delta (0.5-4 Hz) power in PFC during baseline A. Two-way RM ANOVA, p(Time of Day x Genotype) = 0.95, p(Time of Day) = 0.18, p(Genotype) = 0.88. Middle, average NREM sigma (7-15 Hz) power. Two-way RM ANOVA, p(Time of Day x Genotype) = 0.80, p(Time of Day) = 0.91, p(Genotype) = 0.054. Right, average NREM gamma power. Two-way RM ANOVA, p(Time of Day X Genotype) = 0.24, p(Time of Day) = 0.068, p(Genotype) = 0.018.

(H) Left, average NREM delta (0.5-4 Hz) power in PFC during baseline B. Two-way RM ANOVA, p(Time of Day x Genotype) = 0.92, p(Time of Day) = 0.28, p(Genotype) = 0.75. Middle, average NREM sigma (7-15 Hz) power. Two-way RM ANOVA, p(Time of Day x Genotype) = 0.38, p(Time of Day) = 0.043, p(Genotype) = 0.42. Right, average NREM gamma power. Two-way RM ANOVA, p(Time of Day X Genotype) = 0.19, p(Time of Day) = 0.27, p(Genotype) = 0.035.

Asterisks over data points were obtained via Sidak's *post hoc* test. *p < 0.05, **p < 0.01. Data shown as mean ± SEM (except EEG spectrum in panels A-B and E-F, data shown as mean). Panels A-B and E-F show frequency bands denoted by their symbol and divided by dashed lines: δ = 0.5-4 Hz; σ = 7-15 Hz. Sample size: n = 5 mice/genotype.

(Related to Fig. 3)

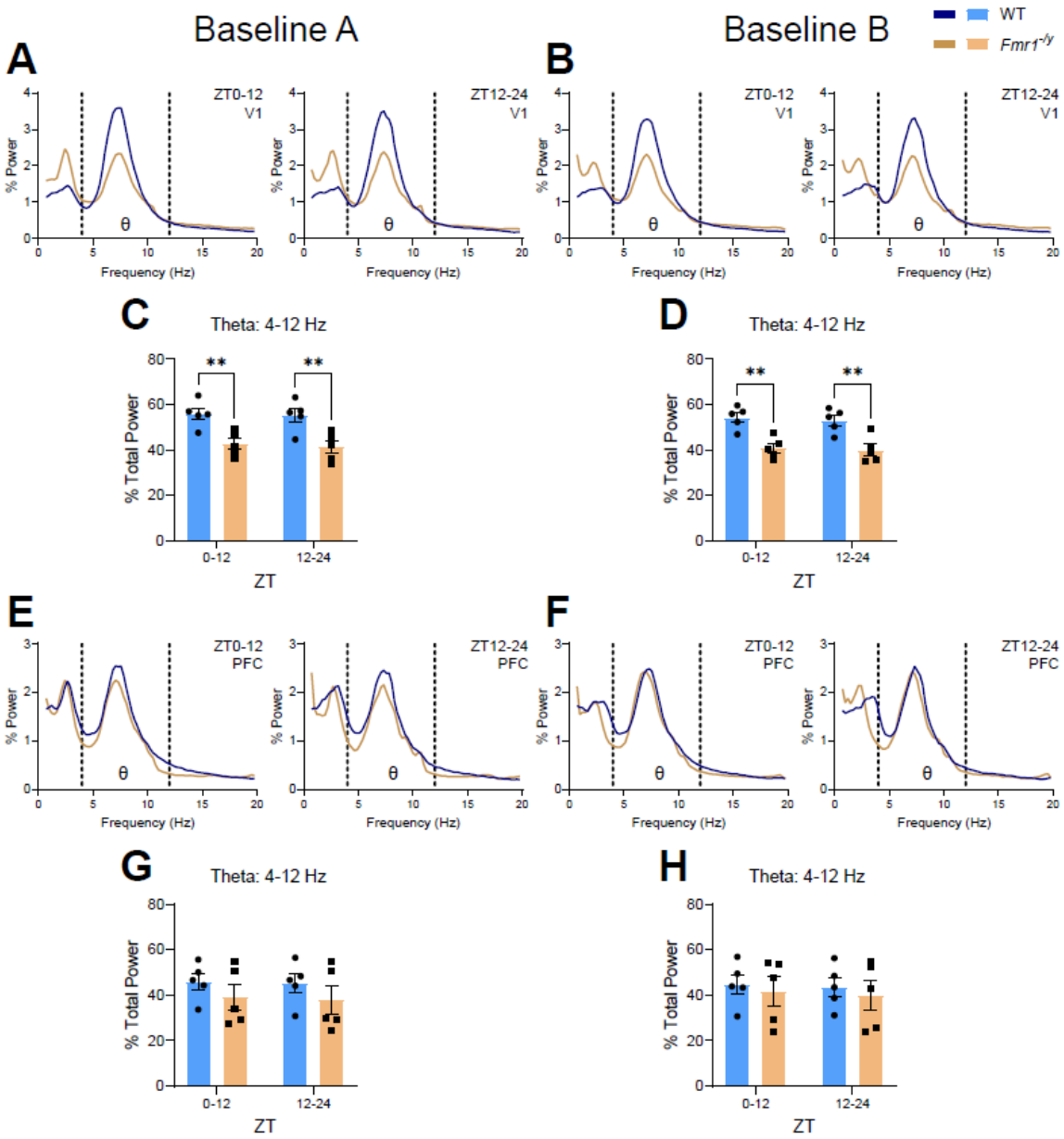
Baseline A
Baseline B
WT
Fmr1-/y
A
B
ZT0-12
V1
ZT12-24
V1
% Power
Frequency (Hz)
θ
C
D
Theta: 4-12 Hz
% Total Power
**
0-12
12-24
ZT
E
F
ZT0-12
PFC
ZT12-24
PFC
G
H

Supplemental Figure 4.6: Baseline REM spectral power in V1 and PFC in WT and *Fmr1*$^{-/y}$ mice

(A) REM EEG power spectrum in V1 for baseline A during ZT0-12 (left) and ZT13-24 (right). ZT0-12: two-way RM ANOVA, p(Frequency x Genotype) < 0.0001, p(Frequency) < 0.0001, p(Genotype) = 0.11. ZT13-24: two-way RM ANOVA, p(Frequency x Genotype) < 0.0001, p(Frequency) < 0.0001, p(Genotype) = 0.072.

(B) REM EEG power spectrum in V1 for baseline B during ZT0-12 (left) and ZT13-24 (right). ZT0-12: two-way RM ANOVA, p(Frequency x Genotype) < 0.0001, p(Frequency) < 0.0001, p(Genotype) = 0.089. ZT13-24: two-way RM ANOVA, p(Frequency x Genotype) < 0.0001, p(Frequency) < 0.0001, p(Genotype) = 0.23.

(C) Average theta (4-12 Hz) power in V1 during baseline A. Two-way RM ANOVA, p(Time of Day x Genotype) = 0.49, p(Time of Day) = 0.067, p(Genotype) = 0.0073.

(D) Average REM theta (4-12 Hz) power in V1 during baseline B. Two-way RM ANOVA, p(Time of Day x Genotype) = 0.50, p(Time of Day) = 0.034, p(Genotype) = 0.0033.

(E) REM EEG power spectrum in PFC for baseline A during ZT0-12 (left) and ZT13-24 (right). ZT0-12: two-way RM ANOVA, p(Frequency x Genotype) > 0.99, p(Frequency) < 0.0001, p(Genotype) = 0.051. ZT13-24: two-way RM ANOVA, p(Frequency x Genotype) > 0.99, p(Frequency) < 0.0001, p(Genotype) = 0.048.
(F) REM EEG power spectrum in PFC for baseline B during ZT0-12 (left) and ZT13-24 (right). ZT0-12: two-way RM ANOVA, p(Frequency x Genotype) > 0.99, p(Frequency) < 0.0001, p(Genotype) = 0.21. ZT13-24: two-way RM ANOVA, p(Frequency x Genotype) = 0.99, p(Frequency) < 0.0001, p(Genotype) = 0.41.

(G) Average REM theta (4-12 Hz) power in PFC during baseline A. Two-way RM ANOVA, p(Time of Day x Genotype) = 0.68, p(Time of Day) = 0.19, p(Genotype) = 0.34.

(H) Average REM theta (4-12 Hz) power in PFC during baseline B. Two-way RM ANOVA, p(Time of Day x Genotype) = 0.69, p(Time of Day) = 0.059, p(Genotype) = 0.67. Asterisks over data points were obtained via Sidak's *post hoc* test. **p < 0.01.

Data shown as mean ± SEM (except EEG spectrum in panels A-B and E-F, data shown as mean). Panels A-B and E-F show frequency bands denoted by their symbol and divided by dashed lines: θ = 4-12 Hz. Sample size: n = 5 mice/genotype.

(Related to Fig. 3)

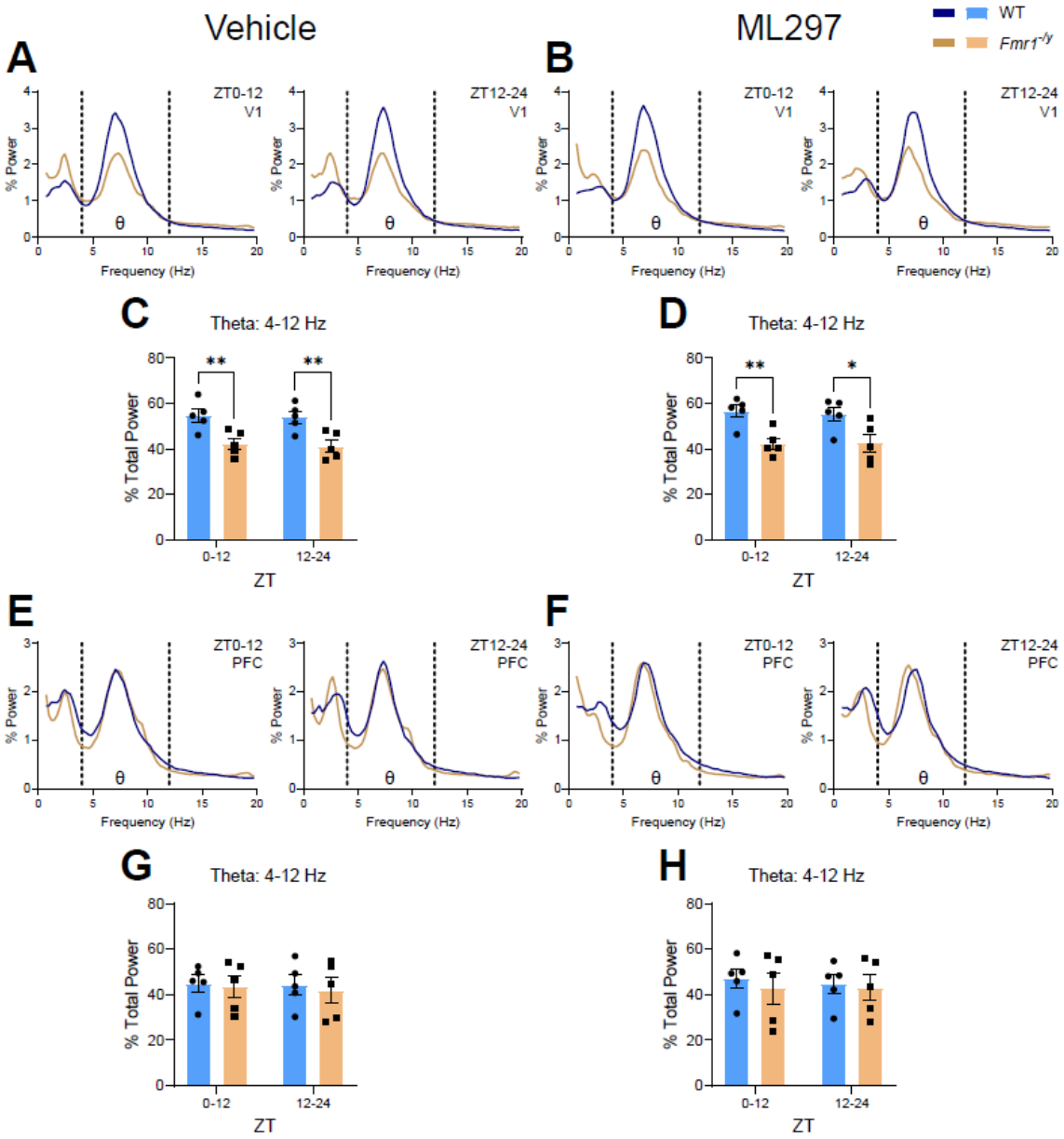
Vehicle
ML297
WT
Fmr1-/y
A
B
ZT0-12
V1
ZT12-24
V1
% Power
Frequency (Hz)
θ
C
D
Theta: 4-12 Hz
% Total Power
**
*
0-12
12-24
ZT
E
F
ZT0-12
PFC
ZT12-24
PFC
G
H

Supplemental Figure 4.7: REM spectral power in V1 and PFC unaffected by GIRK channel activation in WT and *Fmr1*$^{-/y}$ mice

(A) REM EEG power spectrum in V1 for vehicle-treated mice during ZT0-12 (left) and ZT13-24 (right). ZT0-12: two-way RM ANOVA, p(Frequency x Genotype) < 0.0001, p(Frequency) < 0.0001, p(Genotype) = 0.064. ZT13-24: two-way RM ANOVA, p(Frequency x Genotype) < 0.0001, p(Frequency) < 0.0001, p(Genotype) = 0.15.

(B) REM EEG power spectrum in V1 for ML297-treated mice during ZT0-12 (left) and ZT13-24 (right). ZT0-12: two-way RM ANOVA, p(Frequency x Genotype) < 0.0001, p(Frequency) < 0.0001, p(Genotype) = 0.024. ZT13-24: two-way RM ANOVA, p(Frequency x Genotype) < 0.0001, p(Frequency) < 0.0001, p(Genotype) = 0.031.

(C) Average theta (4-12 Hz) power in V1 for vehicle-treated mice. Two-way RM ANOVA, p(Time of Day x Genotype) = 0.83, p(Time of Day) = 0.28, p(Genotype) = 0.0093.

(D) Average REM theta (4-12 Hz) power in V1 for ML297-treated mice. Two-way RM ANOVA, p(Time of Day x Genotype) = 0.45, p(Time of Day) = 0.50, p(Genotype) = 0.012.

(E) REM EEG power spectrum in PFC for vehicle-treated mice during ZT0-12 (left) and ZT13-24 (right). ZT0-12: two-way RM ANOVA, p(Frequency x Genotype) > 0.99, p(Frequency) < 0.0001, p(Genotype) = 0.18. ZT13-24: two-way RM ANOVA, p(Frequency x Genotype) > 0.99, p(Frequency) < 0.0001, p(Genotype) = 0.36.

(F) REM EEG power spectrum in PFC for ML297-treated during ZT0-12 (left) and ZT13-24 (right). ZT0-12: two-way RM ANOVA, p(Frequency x Genotype) > 0.99, p(Frequency) < 0.0001, p(Genotype) = 0.15. ZT13-24: two-way RM ANOVA, p(Frequency x Genotype) = 0.99, p(Frequency) < 0.0001, p(Genotype) = 0.27.

(G) Average REM theta (4-12 Hz) power in PFC for vehicle-treated mice. Two-way RM ANOVA, p(Time of Day x Genotype) = 0.62, p(Time of Day) = 0.21, p(Genotype) = 0.77.

(H) Average REM theta (4-12 Hz) power in PFC for ML297-treated mice. Two-way RM ANOVA, p(Time of Day x Genotype) = 0.30, p(Time of Day) = 0.42, p(Genotype) = 0.70.

Asterisks over data points were obtained via Sidak's *post hoc* test. *p < 0.05, **p < 0.01. Data shown as mean ± SEM (except EEG spectrum in panels A-B and E-F, data shown as mean). Panels A-B and E-F show frequency bands denoted by their symbol and divided by dashed lines: θ = 4-12 Hz. Sample size: n = 5 mice/genotype.

(Related to Fig. 3)

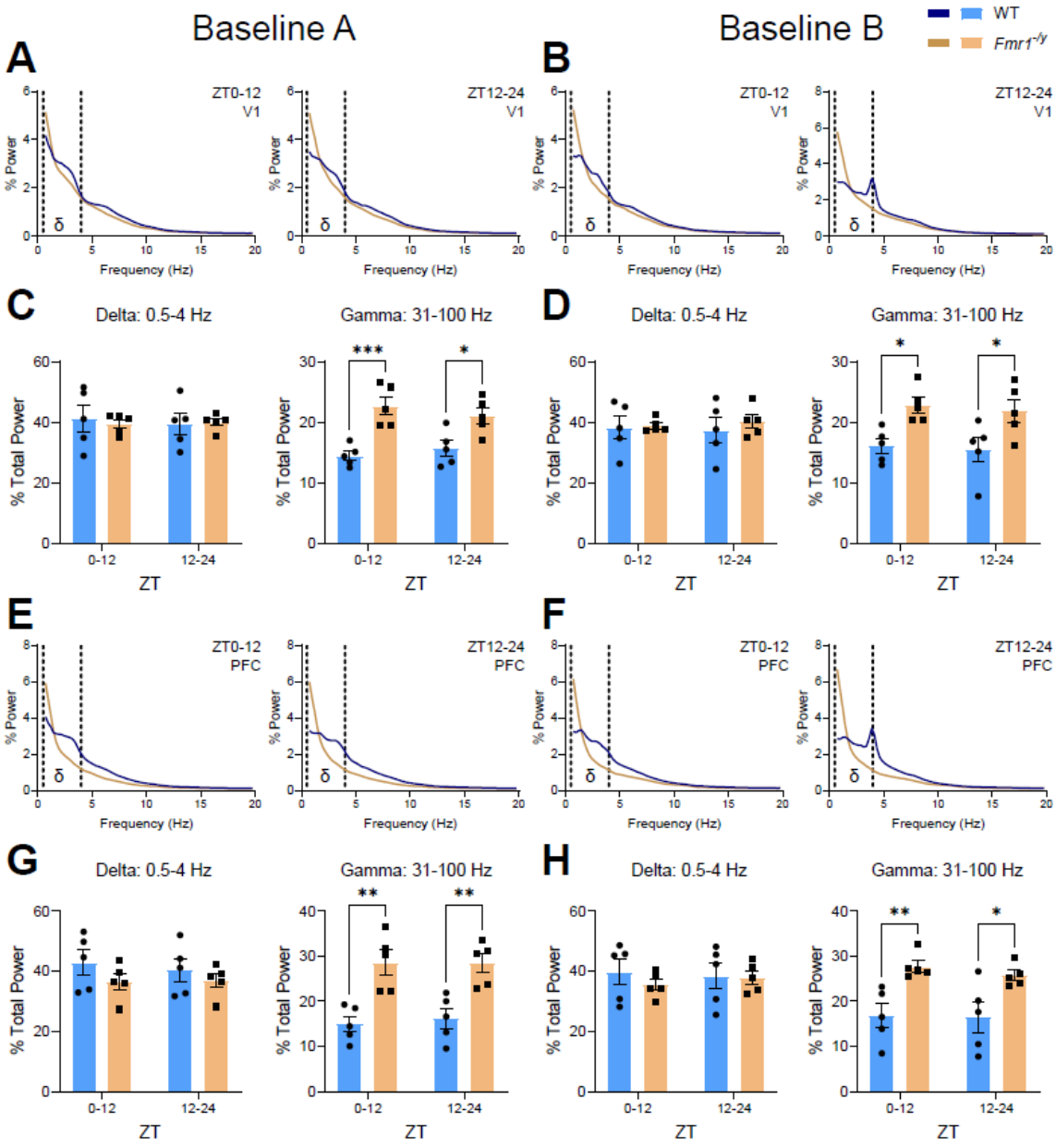
Baseline A
Baseline B
WT
Fmr1-/y
A
B
ZT0-12
V1
ZT12-24
V1
% Power
Frequency (Hz)
δ
C
D
Delta: 0.5-4 Hz
Gamma: 31-100 Hz
% Total Power
ZT
0-12
12-24
***
*
E
F
ZT0-12
PFC
ZT12-24
PFC
G
H
**

Supplemental Figure 4.8: Baseline waking spectral power in V1 and PFC in WT and *Fmr1*$^{-/y}$ mice

(A) Wake EEG power spectrum in V1 for baseline A during ZT0-12 (left) and ZT13-24 (right). ZT0-12: two-way RM ANOVA, p(Frequency x Genotype) = 0.99, p(Frequency) < 0.0001, p(Genotype) = 0.15. ZT13-24: two-way RM ANOVA, p(Frequency x Genotype) = 0.0001, p(Frequency) < 0.0001, p(Genotype) = 0.24.

(B) Wake EEG power spectrum in V1 for baseline B during ZT0-12 (left) and ZT13-24 (right). ZT0-12: two-way RM ANOVA, p(Frequency x Genotype) < 0.0001, p(Frequency) < 0.0001, p(Genotype) = 0.41. ZT13-24: two-way RM ANOVA, p(Frequency x Genotype) < 0.0001, p(Frequency) < 0.0001, p(Genotype) = 0.50.

(C) Left, average wake delta (0.5-4 Hz) power in V1 during baseline A. Two-way RM ANOVA, p(Time of Day x Genotype) = 0.26, p(Time of Day) = 0.50, p(Genotype) = 0.90. Right, average wake gamma power. Two-way RM ANOVA, p(Time of Day X Genotype) = 0.13, p(Time of Day) = 0.79, p(Genotype) = 0.0024.

(D) Left, average wake delta (0.5-4 Hz) power in V1 during baseline B. Two-way RM ANOVA, p(Time of Day x Genotype) = 0.23, p(Time of Day) = 0.75, p(Genotype) = 0.68. Right, average wake gamma power. Two-way RM ANOVA, p(Time of Day X Genotype) = 0.88, p(Time of Day) = 0.49, p(Genotype) = 0.013.

(E) Wake EEG power spectrum in PFC for baseline A during ZT0-12 (left) and ZT13-24 (right). ZT0-12: two-way RM ANOVA, p(Frequency x Genotype) < 0.0001, p(Frequency) < 0.0001, p(Genotype) = 0.0072. ZT13-24: two-way RM ANOVA, p(Frequency x Genotype) < 0.0001, p(Frequency) < 0.0001, p(Genotype) = 0.0095.

(F) Wake EEG power spectrum in PFC for baseline B during ZT0-12 (left) and ZT13-24 (right). ZT0-12: two-way RM ANOVA, p(Frequency x Genotype) < 0.0001, p(Frequency) < 0.0001, p(Genotype) = 0.016. ZT13-24: two-way RM ANOVA, p(Frequency x Genotype) < 0.0001, p(Frequency) < 0.0001, p(Genotype) = 0.051.

(G) Left, average wake delta (0.5-4 Hz) power in PFC during baseline A. Two-way RM ANOVA, p(Time of Day x Genotype) = 0.13, p(Time of Day) = 0.20, p(Genotype) = 0.31. Right, average wake gamma power. Two-way RM ANOVA, p(Time of Day X Genotype) = 0.35, p(Time of Day) = 0.53, p(Genotype) = 0.0032.

(H) Left, average wake delta (0.5-4 Hz) power in PFC during baseline B. Two-way RM ANOVA, p(Time of Day x Genotype) = 0.035, p(Time of Day) = 0.44, p(Genotype) = 0.64. Right, average wake gamma power. Two-way RM ANOVA, p(Time of Day X Genotype) = 0.42, p(Time of Day) = 0.32, p(Genotype) = 0.011.

Asterisks over data points were obtained via Sidak's *post hoc* test. *p < 0.05, **p < 0.01, ***p < 0.001. Data shown as mean ± SEM (except EEG spectrum in panels A-B and E-F, data shown as mean). Panels A-B and E-F show frequency bands denoted by their symbol and divided by dashed lines: δ = 0.5-4 Hz. Sample size: n = 5 mice/genotype.

(Related to Fig. 3)

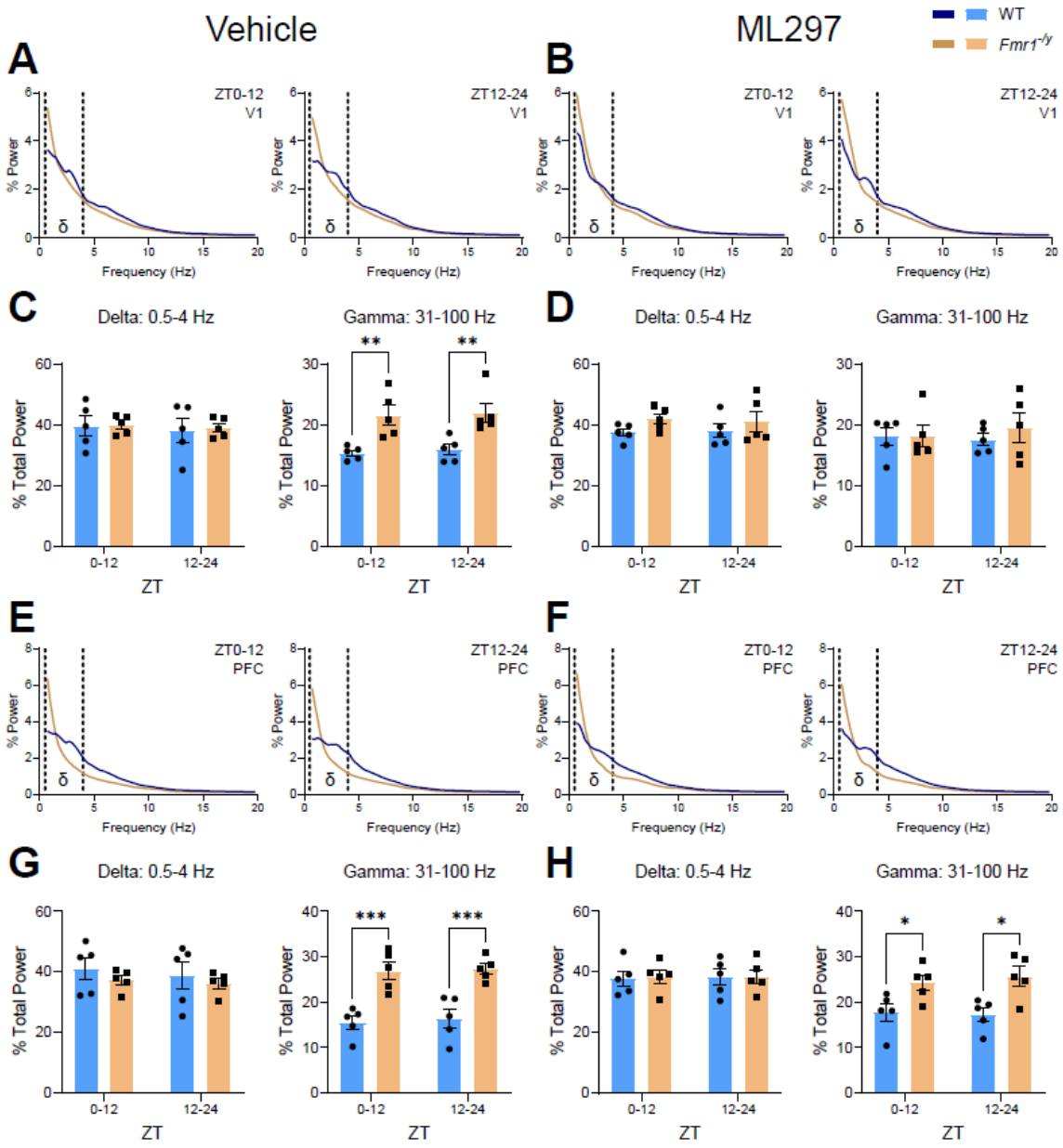
Vehicle
ML297
WT
Fmr1-/y
A
B
C
D
E
F
G
H
ZT0-12
V1
ZT12-24
V1
ZT0-12
PFC
ZT12-24
PFC
% Power
Frequency (Hz)
δ
Delta: 0.5-4 Hz
Gamma: 31-100 Hz
% Total Power
ZT
0-12
12-24
**
***
*

Supplemental Figure 4.9: Gamma power in V1, but not PFC during wakefulness is reduced with GIRK channel activation in WT and *Fmr1*$^{-/y}$ mice

(A) Wake EEG power spectrum in V1 for vehicle-treated mice during ZT0-12 (left) and ZT13-24 (right). ZT0-12: two-way RM ANOVA, p(Frequency x Genotype) < 0.0001, p(Frequency) < 0.0001, p(Genotype) = 0.14. ZT13-24: two-way RM ANOVA, p(Frequency x Genotype) < 0.0001, p(Frequency) < 0.0001, p(Genotype) = 0.31.

(B) Wake EEG power spectrum in V1 for ML297-treated mice during ZT0-12 (left) and ZT13-24 (right). ZT0-12: two-way RM ANOVA, p(Frequency x Genotype) < 0.0001, p(Frequency) < 0.0001, p(Genotype) = 0.83. ZT13-24: two-way RM ANOVA, p(Frequency x Genotype) < 0.0001, p(Frequency) < 0.0001, p(Genotype) = 0.44.

(C) Left, average wake delta (0.5-4 Hz) power in V1 for vehicle-treated mice. Two-way RM ANOVA, p(Time of Day x Genotype) = 0.68, p(Time of Day) = 0.11, p(Genotype) = 0.85. Right, average wake gamma power. Two-way RM ANOVA, p(Time of Day X Genotype) = 0.90, p(Time of Day) = 0.55, p(Genotype) = 0.0054.

(D) Left, average wake delta (0.5-4 Hz) power in V1 for ML297-treated mice. Two-way RM ANOVA, p(Time of Day x Genotype) = 0.68, p(Time of Day) = 0.92, p(Genotype) = 0.21. Right, average wake gamma power. Two-way RM ANOVA, p(Time of Day X Genotype) = 0.36, p(Time of Day) = 0.66, p(Genotype) = 0.64.

(E) Wake EEG power spectrum in PFC for vehicle-treated mice during ZT0-12 (left) and ZT13-24 (right). ZT0-12: two-way RM ANOVA, p(Frequency x Genotype) < 0.0001, p(Frequency) < 0.0001, p(Genotype) = 0.0034. ZT13-24: two-way RM ANOVA, p(Frequency x Genotype) < 0.0001, p(Frequency) < 0.0001, p(Genotype) = 0.011.

(F) Wake EEG power spectrum in PFC for ML297-treated mice during ZT0-12 (left) and ZT13-24 (right). ZT0-12: two-way RM ANOVA, p(Frequency x Genotype) < 0.0001, p(Frequency) < 0.0001, p(Genotype) = 0.031. ZT13-24: two-way RM ANOVA, p(Frequency x Genotype) < 0.0001, p(Frequency) < 0.0001, p(Genotype) = 0.010.

(G) Left, average wake delta (0.5-4 Hz) power in PFC for vehicle-treated mice. Two-way RM ANOVA, p(Time of Day x Genotype) = 0.46, p(Time of Day) = 0.071, p(Genotype) = 0.48. Right, average wake gamma power. Two-way RM ANOVA, p(Time of Day X Genotype) = 0.76, p(Time of Day) = 0.41, p(Genotype) = 0.0013.

(H) Left, average wake delta (0.5-4 Hz) power in PFC for ML297-treated mice. Two-way RM ANOVA, p(Time of Day x Genotype) = 0.86, p(Time of Day) = 0.91, p(Genotype) = 0.89. Right, average wake gamma power. Two-way RM ANOVA, p(Time of Day X Genotype) = 0.44, p(Time of Day) = 0.70, p(Genotype) = 0.012. Asterisks over data points were obtained via Sidak's *post hoc* test. *p < 0.05, **p < 0.01, ***p < 0.001. Data shown as mean ± SEM (except EEG spectrum in panels A-B and E-F, data shown as mean). Panels A-B and E-F show frequency bands denoted by their symbol and divided by dashed lines: δ = 0.5-4 Hz. Sample size: n = 5 mice/genotype.

(Related to Fig. 3)

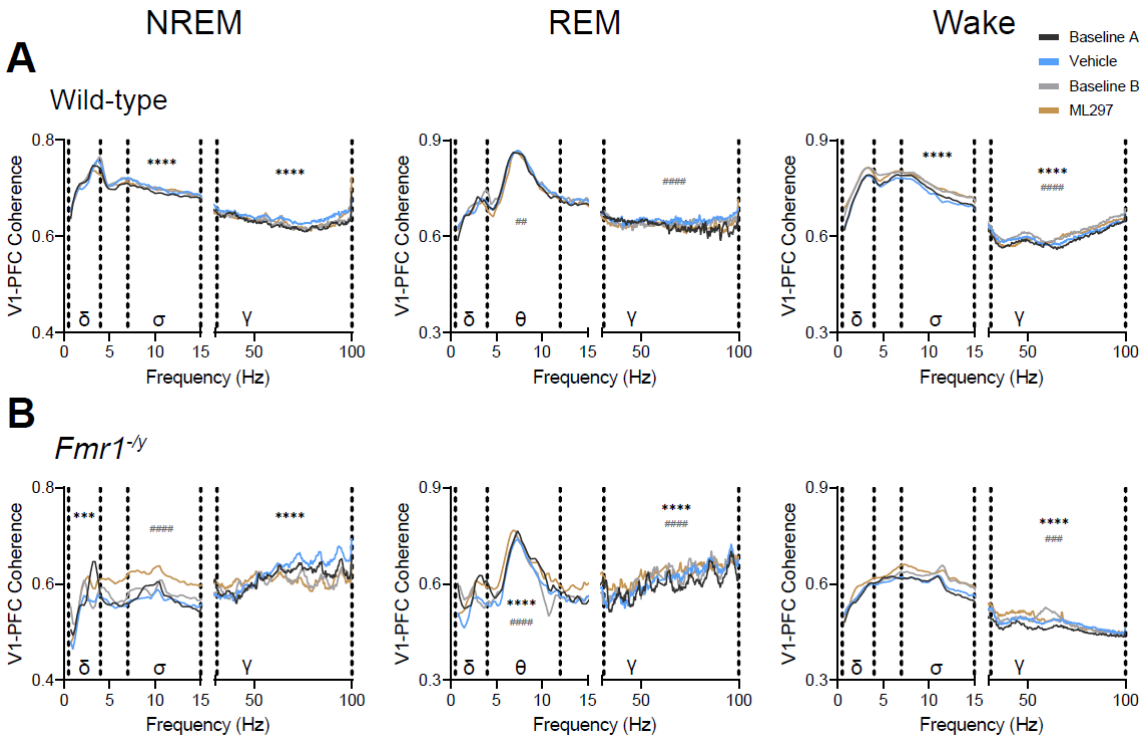

Supplemental Figure 4.10: Interregional field coherence between WT and *Fmr1*$^{-/y}$ mice during sleep and wakefulness differs in various frequency bands across the dark phase

(A) Primary visual cortex (V1)-prefrontal cortex (PFC) spectral coherence during the dark phase (ZT13-24) for wild-type mice across continuous recording days for NREM sleep, REM sleep, and waking. NREM sleep, two-way RM ANOVA, p(Frequency x Recording Day) > 0.99, p(Frequency) > 0.99, p(Recording Day) < 0.0001. REM sleep, two-way RM ANOVA, p(Frequency x Recording Day) > 0.99, p(Frequency) > 0.99, p(Recording Day) < 0.0001. Waking, two-way RM ANOVA, p(Frequency x Recording Day) > 0.99, p(Frequency) > 0.99, p(Recording Day) < 0.0001.

(B) V1-PFC spectral coherence for *Fmr1*$^{-/y}$ mice during the dark phase (ZT0-12). NREM sleep, two-way RM ANOVA, p(Frequency x Recording Day) = 0.0064, p(Frequency) > 0.99, p(Recording Day) < 0.0001. REM sleep, two-way RM ANOVA, p(Frequency x Recording Day) = 0.86, p(Frequency) > 0.99, p(Recording Day) < 0.0001. Waking, two-way RM ANOVA, p(Frequency x Recording Day) > 0.99, p(Frequency) > 0.99, p(Recording Day) < 0.0001.

Each panel shows coherence values for 0.5-15 and 31-100 Hz. Different frequency bands are denoted with their symbol and divided by dashed lines: δ = 0.5-4 Hz, θ = 4-12 Hz, σ = 7-15 Hz, γ = 31-100 Hz. Symbols (*baseline A vs. vehicle; #baseline B vs. ML297) over data points were obtained via Tukey's *post hoc* test. **p < 0.01, ***p < 0.001, ****p < 0.0001. ##p < 0.01, ###p < 0.001, ####p < 0.0001. Data shown as mean. Sample size: n = 5 mice/genotype.

(Related to Fig. 5)

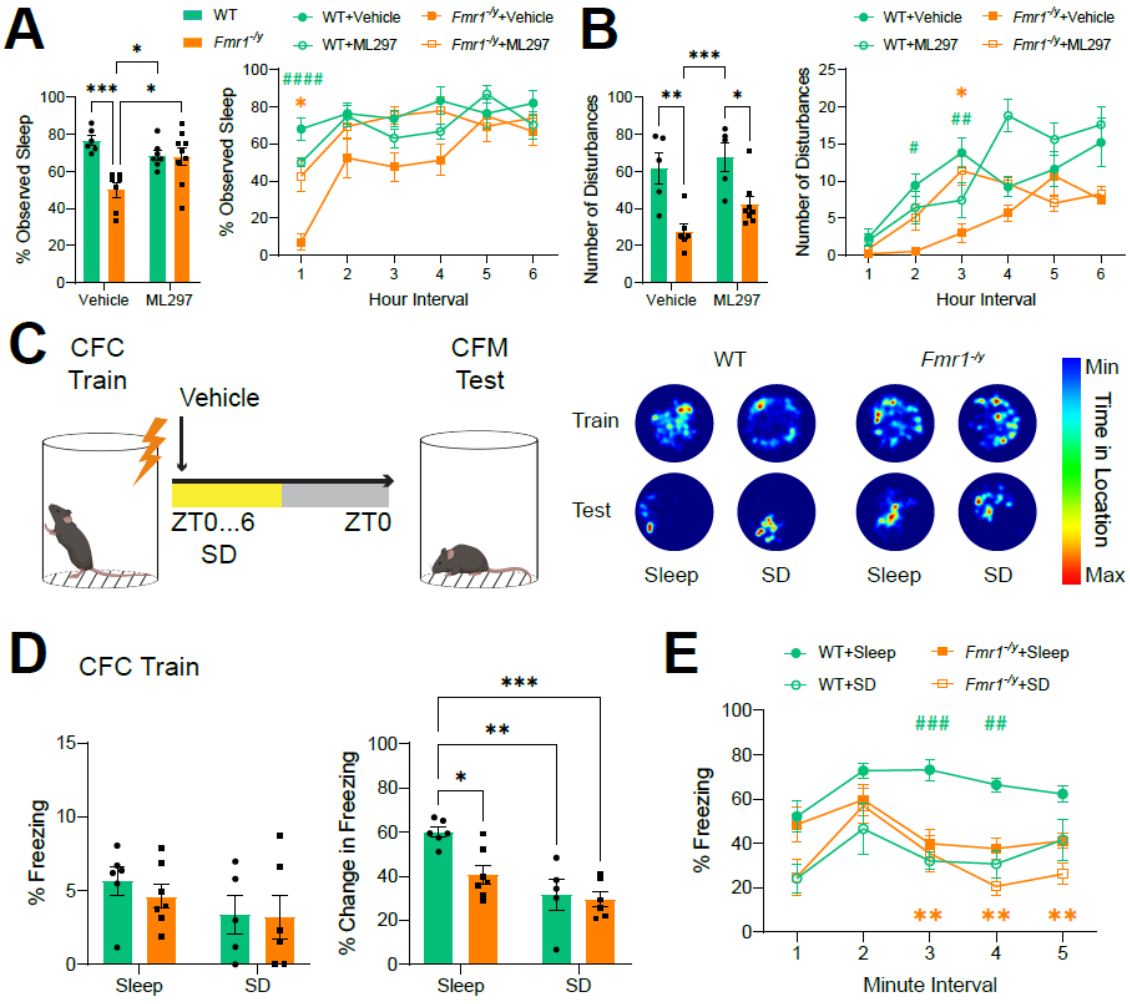
A
WT
Fmr1-/y
% Observed Sleep
Vehicle
ML297
WT+Vehicle
WT+ML297
Fmr1-/y+Vehicle
Fmr1-/y+ML297
Hour Interval
B
Number of Disturbances
C
CFC Train
Vehicle
ZT0...6 SD
ZT0
CFM Test
Train
Test
Sleep
SD
Min
Time in Location
Max
D
CFC Train
% Freezing
% Change in Freezing
E
WT+Sleep
WT+SD
Fmr1-/y+Sleep
Fmr1-/y+SD
Minute Interval

Supplemental Figure 4.11: Sleep behavior and sleep-dependent contextual fear memory vehicle controls in WT and *Fmr1*$^{-/y}$ mice

(A) Left, total amounts of visually observed sleep during the first 6 hours following contextual fear conditioning (CFC). Two-way ANOVA, p(Treatment x Genotype) = 0.0028, p(Treatment) = 0.21, p(Genotype) = 0.0019. Right, visually observed sleep behavior in 1 hour intervals across the first 6 hours post-CFC. Two-way RM ANOVA, p(Hour x Genotype + Treatment) = 0.0092, p(Hour) <0.0001, p(Genotype + Treatment) = 0.0008.

(B) Left, total number of sleep disturbances via gentle handling during the 6-hour sleep deprivation (SD) period. Two-way ANOVA, p(Treatment x Genotype) = 0.48, p(Treatment) = 0.098, p(Genotype) < 0.0001. Right, number of sleep disturbances in 1-hour intervals across the 6-hour SD period. Two-way RM ANOVA, p(Hour x Genotype + Treatment) <0.0001, p(Hour) <0.0001, p(Genotype + Treatment) = 0.0006.

(C) Left, schematic of CFC paradigm with 24-hour contextual fear memory (CFM) recall testing with vehicle administration with either *ad lib* sleep or 6-hour SD. Right, representative heat maps of time-in-location for mice during CFC training and CFM testing.

(D) Left, freezing behavior between WT and *Fmr1*$^{-/y}$ mice during CFC training. Two-way ANOVA, p(Genotype x Treatment) = 0.71, p(Treatment) = 0.12, p(Genotype) = 0.60. Right, change in freezing behavior during CFM testing. Two-way ANOVA, p(Genotype x Treatment) = 0.061, p(Treatment) = 0.0002, p(Genotype) = 0.023. (E) Freezing behavior in 1-minute intervals across the 5-minute CFM testing period between WT and *Fmr1*$^{-/y}$ mice after vehicle treatment with either sleep or SD. Two-way RM ANOVA, p(Minute x Genotype + Sleep Condition) = 0.044, p(Minute) < 0.0001, p(Genotype + Sleep Condition) = 0.0001.

Data shown as mean ± SEM. *Asterisks over data points in panels A(left), B(left) D, G were obtained via Tukey's *post hoc* test. *p < 0.05, **p < 0.01, ***p < 0.001. Sample sizes (panel A): n = 6 (WT + vehicle), = 7 (WT + ML297), = 7 (*Fmr1*$^{-/y}$ + vehicle), = 9 (*Fmr1*$^{-/y}$ + ML297). Sample sizes (panel B): n = 5 (WT + vehicle), = 5 (WT + ML297), = 6 (*Fmr1*$^{-/y}$ + vehicle), = 8 (*Fmr1*$^{-/y}$ + ML297). Sample sizes (panel D-E): n = 6 (WT + sleep), = 5 (WT + SD), = 7 (*Fmr1*$^{-/y}$ + sleep), = 6 (*Fmr1*$^{-/y}$ + SD). Symbols over data points (***Fmr1*$^{-/y}$ + vehicle vs. *Fmr1*$^{-/y}$ + ML297; $^{\#}$*Fmr1*$^{-/y}$ + vehicle vs. WT + vehicle (panels A-B) and *WT + sleep + sleep vs. *Fmr1*$^{-/y}$ + sleep; $^{\#}$WT + sleep vs. WT + SD (panel E)) were obtained via Tukey's *post hoc* test. *p < 0.05, **p < 0.01. $^{\#}$p < 0.05, $^{\#\#}$p < 0.01, $^{\#\#\#}$p <0.001, $^{\#\#\#\#}$p < 0.0001.

(Related to Fig 6)

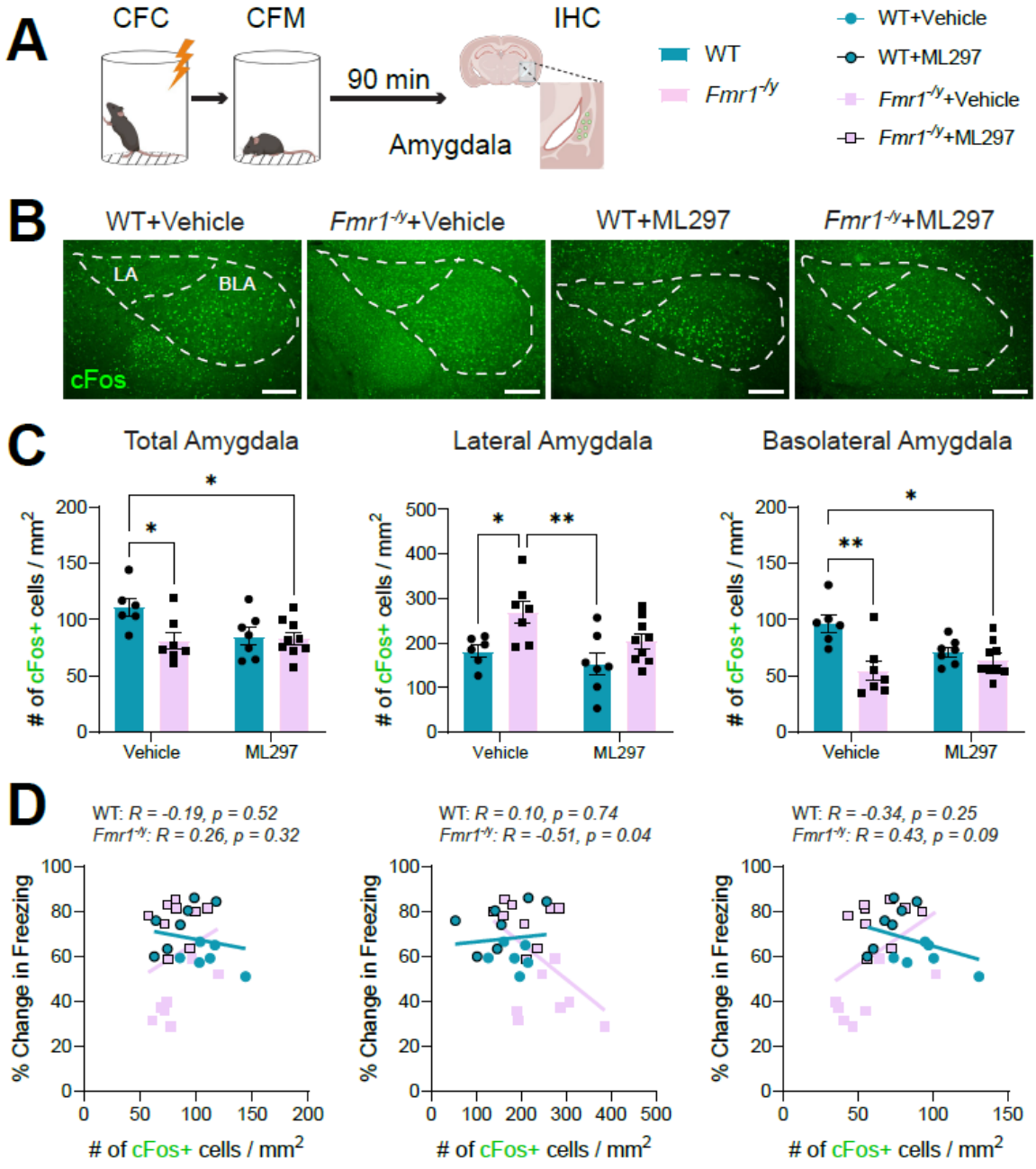
A
CFC
CFM
90 min
IHC
Amygdala
WT
Fmr1-/y
WT+Vehicle
WT+ML297
Fmr1-/y+Vehicle
Fmr1-/y+ML297
B
WT+Vehicle
Fmr1-/y+Vehicle
WT+ML297
Fmr1-/y+ML297
LA
BLA
cFos
C
Total Amygdala
Lateral Amygdala
Basolateral Amygdala
# of cFos+ cells / mm2
Vehicle
ML297
D
WT: R = -0.19, p = 0.52
Fmr1-/y: R = 0.26, p = 0.32
WT: R = 0.10, p = 0.74
Fmr1-/y: R = -0.51, p = 0.04
WT: R = -0.34, p = 0.25
Fmr1-/y: R = 0.43, p = 0.09
% Change in Freezing
# of cFos+ cells / mm2

Supplemental Figure 4.12: cFos expression after fear memory recall is relatively unaffected in the amygdala of both WT and *Fmr1*$^{-/y}$ mice

(A) Schematic of experimental paradigm. Brains were perfused 90 minutes following contextual fear memory (CFM) recall and cFos expression was measured in the amygdala using immunohistochemistry.

(B) Representative images of cFos+ neurons in the amygdala following CFM recall in both WT and *Fmr1*$^{-/y}$ mice with vehicle or ML297 treatment. Dashed outlines define the lateral amygdala (LA) and basolateral amygdala subregions. Scale bar = 200 μm.

(C) Left, cFos+ neuron density in the total amygdala region. Two-way ANOVA, p(Genotype x Treatment) = 0.06, p(Treatment) = 0.10, p(Genotype) = 0.032. Middle, cFos+ neurons in the LA subregion. Two-way ANOVA, p(Genotype x Treatment) = 0.41, p(Treatment) = 0.037, p(Genotype) = 0.0033. Right, cFos+ neurons in the BLA subregion. Two-way ANOVA, p(Genotype x Treatment) = 0.013, p(Treatment) = 0.27, p(Genotype) = 0.0011.

(D) Pearson correlations of change in freezing behavior during CFM recall vs. associated number of cFos+ neurons in the total amygdala (left), LA (middle), and BLA (right) subregions. *Asterisks over data points were obtained via Tukey's *post hoc* test. *$p < 0.05$, **$p < 0.01$. Data shown as mean ± SEM. Sample sizes: n = 6 (WT + vehicle), = 7 (WT + ML297), = 7 (*Fmr1*$^{-/y}$ + vehicle), = 9 (*Fmr1*$^{-/y}$ + ML297).

(Related to Fig. 8)

Chapter 5 : Discussion

5.1 : Conclusions and Future Directions

Across an average lifetime, a person spends about 25 years of that time sleeping. That is roughly 9,125 days or 219,000 hours spent in what is described as a natural and reversible state that is defined by a decreased responsiveness to the environment, relative inactivity, and loss of consciousness [1-3]. The time invested in this one, dynamic behavior suggests that sleep is critical for an orchestra of functions. Studies across decades have demonstrated that sleep is necessary for numerous functions, including - but not limited to - energy conservation, restoration of cellular components (i.e., macromolecules), waste clearance of metabolic products, innate and adaptive immunity (i.e. regulation of inflammatory processes) and lastly, neural plasticity during early neurodevelopment [4,5]. Sleep's role in neurodevelopment is unsurprising, as human infants can spend up to 16-17 hours asleep per day, which decreases gradually as the brain slowly matures into adulthood [6,7]. During this time, sleep has been shown to be essential in the shaping of a diverse number of neural circuits for proper behavioral function, especially those linked to cortical plasticity and memory consolidation, [6,8]. However, one question remains is how atypical neurodevelopment is affected by sleep or lack thereof. This dissertation aims to elucidate on that question by examining the role of sleep as important therapeutic target for recovery of visual plasticity during critical period

development and improvement of cognitive function in Fragile X syndrome, a prevalent neurodevelopment disorder (NDD).

The shaping of neural circuits involved in sensory processing takes place during a biologically determined stage of development known as the critical period [9,10]. A prime example of this phenomenon is ocular dominance plasticity (ODP). Here, loss of binocular visual input leads to depression of synaptic responses in the primary visual cortex (V1) and results in loss of binocular vision, a condition known as amblyopia in humans [9,11-14]. While it is known that sleep regulates many of the network and molecular mechanisms that facilitate this plasticity and subsequent amblyopia [15-18], less is known about sleep function in recovery from amblyopia. In **Chapter 2**, we provided one of the first side-by-side comparisons of how binocular vs. monocular visual experience and subsequent sleep affect recovery of deprived eye (DE) responses to restore binocularity in the visual cortex. We found that binocular recovery experience (opening of both eyes) facilitates faster recovery of DE responses than monocular experience (opening of DE only and closing of spared eye). We showed that at both the physiological level with single-unit recordings of firing rates **(Figure 2.1, Figure 2.2**) and molecular level with activity-dependent cFos staining (**Figure 2.3**). We also demonstrated that recovery of DE responses via binocular experience was dependent on subsequent sleep (**Figure 2.4, Figure 2.5, and Figure 2.6**). These findings imply that sleep not only has roles in the typical developmental plasticity, but also plays vital roles in normalizing circuits when altered by outside experience. Furthermore, as amblyopia is a common form of vision loss in children that has mixed recovery results from clinical intervention [19-23], our results suggest that the relative timing of sleep following treatment could be an important factor

in promoting full recovery. Nevertheless, further insight into neurobiological mechanisms on how sleep impacts recovery of visual responses in amblyopia remains to be studied.

There are many directions one could take in interpreting these findings for follow-up work, with one focusing on the function of sleep in recovery in adult amblyopia patients. Given that treatments during early childhood are mixed, many individuals are affected with amblyopia well into adulthood [19]. This has prompted numerous studies focused on the re-opening of the critical period and associated plasticity mechanisms in adult mice to help promote recovery visual responses made during ODP. However, the long-lasting effects of this recovery are mixed in rodent models [24-26]. Given that we know sleep is needed for these recovery changes in early development, studies can focus on how timing of sleep is needed for recovery of visual, cellular responses in the adult cortex using electrophysiology techniques. One direction that extends into both juvenile and adult recovery, is a further examination of the molecular mechanisms that underlie binocular experience and sleep-mediated recovery of visual responses. Our findings showed cFos activation patterns after binocular recovery experience to be comparable to normally-reared mice. One could extend these findings at a greater resolution by studying the biosynthetic changes in cell types within the binocular visual cortex using a combination of genetic tools such as single-cell RNA sequencing and bioinformatics. Lastly, other biological components such as perineuronal nets (PNN), which are extracellular matrix structures that surrounding parvalbumin (PV) interneurons, regulate the closure of the critical period [27]. While their role in mediating changes in ODP are well-studied, little is known about how they can be measured and used to alter critical period plasticity and promote recovery [28]. They are also known to change composition in a

circadian manner that is influenced by sleep loss [29], so their possible role in facilitating recovery relative to sleep timing during binocular recovery is also of relevant interest.

Sleep loss and cognitive deficits are common phenotypes seen in a variety of NDDs including Fragile X syndrome (FXS) [30-32]. A wealth of literature exists showing the need for sleep for cognitive processes such as memory consolidation [8,33,34], yet little is known about how these phenomena are affected in the context FXS, or any other NDD. In **Chapter 3 and 4**, we set out to understand if restoring sleep via a novel hypnotic treatment could have any benefits in rescuing sleep-dependent hippocampal memory function in a mouse model for FXS (*Fmr1*$^{-/y}$ mice). **Chapter 3** served as a control study examining the effects of our proposed hypnotic treatment, ML297, which acts via G-protein-coupled inward rectifying potassium (GIRK) channels. While a past study demonstrated its effectiveness in promoting non-rapid eye movement (NREM) sleep without disrupting recall of hippocampal-dependent memory [35], its effects on sleep during memory consolidation were unknown. We measured how administration of ML297 affected sleep-dependent contextual fear memory (CFM). We found that GIRK1/2 channel activation via ML297 improved CFM recall through a reorganization and promotion of REM sleep immediately following the hours of contextual fear conditioning (CFC) training (**Figure 3.1, Figure 3.2**). Furthermore, spectral power in various frequency bands were normalized to baseline sleep conditions (**Figure 3.3, Figure 3.4**). Lastly, the improvements in CFM recall were found to be sleep-dependent and driven by changes in hippocampal activity (**Figure 3.5, Figure 3.6**). Our findings show that ML297 (GIRK1/2 activation) has promise as a potential hypnotic, but further studies are needed to fully understand the implications of GIRK channel signaling in sleep and memory function.

ML297 targets the GIRK1 subunit directly to reduce neuronal excitability, but GIRK1 primarily exists as heteromer with other GIRK subunits (GIRK2-4) [36,37]. Future studies understanding if a specific combination of GIRK1 heteromers (i.e. GIRK1/2 vs GIRK1/4) induce the sleep promoting effects will allow for better specificity of the drug and brain regional targets. Since ML297 does not yield any specific preference for GIRK1/2 or GIRK1/4, small molecules such as GAT1508 have been recently developed to target GIRK1/2 specifically [38]. One can perform similar studies using EEG/EMG recordings and behavioral learning assays to compare if these sleep-dependent learning improvements area based specifically on actions via GIRK1/2 signaling.

After establishing ML297 as a promising hypnotic in **Chapter 3**, we set out to measure if improving sleep deficits in *Fmr1*$^{-/y}$ mice could also help improve cognition in **Chapter 4**. We first characterized the sleep/wake cycle of *Fmr1*$^{-/y}$ mice, which has not been done before at the resolution of measuring both architecture and oscillatory activity using EEG/EMG measurements. We found that *Fmr1*$^{-/y}$ mice exhibited NREM sleep architectural and spectral power deficits (**Figure 4.1, Figure 4.2, Figure 4.3**) analogous to human polysomnography studies in children with FXS and autism spectrum disorder (ASD) [30,39-44]. This not only validated the *Fmr1*$^{-/y}$ mouse model for our studies and implicated that the loss of *Fmr1* expression alters sleep behavior, but also for future studies in sleep and the pathophysiology of FXS. The baseline studies also showed that *Fmr1*$^{-/y}$ mice have dissimilarities in spectral power between anterior and posterior cortical regions (**Figure 4.4, Figure 4.5**), mirroring reports of polysomnography recordings of children with ASD suggesting that *Fmr1*$^{-/y}$ mouse model can also be used to study the neurobiological mechanisms underlying asynchronous oscillation patterns. Our

assessment of ML297 showed that we can not only rescue NREM sleep deficits (**Figure 4.2, Figure 4.3**), but also rescue CFM recall in a sleep-dependent manner as well that is associated with alteration of hippocampal activation patterns during CFM recall (**Figure 4.6, Figure 4.8**). Our findings not only showcase the use of sleep as a therapeutic target for promoting cognition in FXS, but also implicate that GIRK1/2 channel signaling may also be affected in FXS as well. Many directions could be taken to fully investigate the neural circuitry underlying the deficits in NREM sleep in FXS at both the basic and translational levels. From a basic science perspective, studies could use other approaches such optogenetics to induce NREM oscillations patterns in *Fmr1*$^{-/y}$ mice and see if NREM sleep is truly sufficient to promote cognitive learning. One of our findings was that sleep spindle density and power was reduced in *Fmr1*$^{-/y}$ mice (**Figure 4.4**). Sleep spindle activity is generated within the thalamic reticular nucleus (TRN), driven by activation of GABAergic interneuron activity such as PV activity [45-48]. One could use opto- or chemo-genetic approaches to activate PV interneurons and measure if sleep spindles are generated to promote NREM sleep and REM sleep transitions which in turn help promote memory consolidation and other beneficial impacts.

On the behavioral side, we found improvement in CFM recall, but is unknown how hippocampal firing dynamics are affected in *Fmr1*$^{-/y}$ mice in relation to sleep and memory. One could combine single-unit recordings and ML297 administration to measure neuronal firing activity related to CFC learning at baseline and after GIRK channel activation. One can also take it a step further and use optogenetics to stimulate critical hippocampal oscillation rhythms found during CFM consolidation [49-51] and assess if those are sufficient to promote learning in *Fmr1*$^{-/y}$ mice. Furthermore, we only tested hippocampal-dependent

learning in our assays, but other behaviors related to anxiety, hyperactivity, and social learning could also be impacted by sleep loss phenotypes in FXS [31,52-54]. The use of ML297 to test if promotion of sleep could improve these and other behavioral domains can also be assessed. In addition, a look into GIRK channel dysfunction can be further assessed by using *in situ* hybridization to obtain a clear characterization of GIRK expression throughout several brain regions, followed by *in vitro* recordings on possible channel dysfunction dynamics. Lastly, from a biomedical and translational science level, given that ML297 as a hypnotic still requires much characterization, other hypnotics currently exist for sleep-related disorders such as insomnia [55-60]. One can test how these treatments promote sleep and subsequent improvement in cognition for current individuals with FXS and other related disorders.

In sum, as the function of sleep continues to be assessed in all aspects of science, its role as a potential therapeutic target for treating neurological dysfunction should be emphasized. Given that sleep is a universal behavior in humans, its effects on facilitating recovery in domains such as synaptic plasticity and cognition could have an extensive impact on treatment for many clinical populations. Lastly, sleep is a critical behavior that we need to do daily from the moment we are born, long into adulthood for proper neural function. From helping us learn to see and speak our first words as infants to remembering that funny line from a Bob's Burger episode (S4, E14, 14:07), sleep will have a role facilitating these processes to come to fruition. I know this was a long dissertation, so if you want to remember a few things from what you may have learned, go get some rest and enjoy some sleep. Sleep will only help you in the short and long run.

5.2 : References

1. Scullin, M.K., and Bliwise, D.L. (2015). Sleep, cognition, and normal aging: integrating a half century of multidisciplinary research. Perspect Psychol Sci *10*, 97-137. 10.1177/1745691614556680.
2. Siegel, J.M. (2005). Clues to the functions of mammalian sleep. Nature. Nature Publishing Group.
3. Vorster, A.P., and Born, J. (2015). Sleep and memory in mammals, birds and invertebrates. Neurosci Biobehav Rev *50*, 103-119. 10.1016/j.neubiorev.2014.09.020.
4. Zielinski, M.R., McKenna, J.T., and McCarley, R.W. (2016). Functions and Mechanisms of Sleep. AIMS Neurosci *3*, 67-104. 10.3934/Neuroscience.2016.1.67.
5. Sulaman, B.A., Wang, S., Tyan, J., and Eban-Rothschild, A. (2023). Neuro-orchestration of sleep and wakefulness. Nat Neurosci *26*, 196-212. 10.1038/s41593-022-01236-w.
6. Wintler, T., Schoch, H., Frank, M.G., and Peixoto, L. (2020). Sleep, brain development, and autism spectrum disorders: Insights from animal models. J Neurosci Res *98*, 1137-1149. 10.1002/jnr.24619.
7. Roffwarg, H.P., Muzio, J.N., and Dement, W.C. (1966). Ontogenetic development of the human sleep-dream cycle. Science *152*, 604-619. 10.1126/science.152.3722.604.
8. Rasch, B., and Born, J. (2013). About sleep's role in memory. Physiol Rev *93*, 681-766. 10.1152/physrev.00032.2012.
9. Berardi, N., Pizzorusso, T., and Maffei, L. (2000). Critical periods during sensory development. Curr Opin Neurobiol *10*, 138-145. 10.1016/s0959-4388(99)00047-1.
10. Hensch, T.K. (2004). Critical period regulation. Annu Rev Neurosci *27*, 549-579. 10.1146/annurev.neuro.27.070203.144327.
11. Knudsen, E.I. (2004). Sensitive periods in the development of the brain and behavior. J Cogn Neurosci *16*, 1412-1425. 10.1162/0898929042304796.
12. Hensch, T.K. (2005). Critical period mechanisms in developing visual cortex. Curr Top Dev Biol *69*, 215-237. 10.1016/S0070-2153(05)69008-4.
13. Birch, E.E. (2013). Amblyopia and binocular vision. Progress in Retinal and Eye Research. Pergamon.
14. Hensch, T.K., and Quinlan, E.M. (2018). Critical periods in amblyopia. Vis Neurosci *35*, E014. 10.1017/S0952523817000219.
15. Frank, M.G., Issa, N.P., and Stryker, M.P. (2001). Sleep enhances plasticity in the developing visual cortex. Neuron *30*, 275-287. 10.1016/s0896-6273(01)00279-3.
16. Aton, S.J., Seibt, J., Dumoulin, M., Jha, S.K., Steinmetz, N., Coleman, T., Naidoo, N., and Frank, M.G. (2009). Mechanisms of sleep-dependent consolidation of cortical plasticity. Neuron *61*, 454-466. 10.1016/j.neuron.2009.01.007.
17. Frank, M.G. (2011). Sleep and developmental plasticity not just for kids. Prog Brain Res *193*, 221-232. 10.1016/B978-0-444-53839-0.00014-4.

18. Aton, S.J., Broussard, C., Dumoulin, M., Seibt, J., Watson, A., Coleman, T., and Frank, M.G. (2013). Visual experience and subsequent sleep induce sequential plastic changes in putative inhibitory and excitatory cortical neurons. Proc Natl Acad Sci U S A *110*, 3101-3106. 10.1073/pnas.1208093110.
19. Attebo, K., Mitchell, P., Cumming, R., Smith, W., Jolly, N., and Sparkes, R. (1998). Prevalence and causes of amblyopia in an adult population. Ophthalmology *105*, 154-159. 10.1016/s0161-6420(98)91862-0.
20. Pediatric Eye Disease Investigator, G. (2002). The clinical profile of moderate amblyopia in children younger than 7 years. Archives of ophthalmology (Chicago, Ill. : 1960) *120*, 281-287.
21. Holmes, J.M., Beck, R.W., Kraker, R.T., Cole, S.R., Repka, M.X., Birch, E.E., Felius, J., Christiansen, S.P., Coats, D.K., Kulp, M.T., and Pediatric Eye Disease Investigator, G. (2003). Impact of patching and atropine treatment on the child and family in the amblyopia treatment study. Arch Ophthalmol *121*, 1625-1632. 10.1001/archopht.121.11.1625.
22. Webber, A.L., and Wood, J. (2005). Amblyopia: prevalence, natural history, functional effects and treatment. Clin Exp Optom *88*, 365-375. 10.1111/j.1444-0938.2005.tb05102.x.
23. Pineles, S.L., Aakalu, V.K., Hutchinson, A.K., Galvin, J.A., Heidary, G., Binenbaum, G., VanderVeen, D.K., and Lambert, S.R. (2020). Binocular Treatment of Amblyopia: A Report by the American Academy of Ophthalmology. Ophthalmology *127*, 261-272. 10.1016/j.ophtha.2019.08.024.
24. Prusky, G.T., Alam, N.M., and Douglas, R.M. (2006). Enhancement of vision by monocular deprivation in adult mice. J Neurosci *26*, 11554-11561. 10.1523/JNEUROSCI.3396-06.2006.
25. Baroncelli, L., Bonaccorsi, J., Milanese, M., Bonifacino, T., Giribaldi, F., Manno, I., Cenni, M.C., Berardi, N., Bonanno, G., Maffei, L., and Sale, A. (2012). Enriched experience and recovery from amblyopia in adult rats: impact of motor, social and sensory components. Neuropharmacology *62*, 2388-2397. 10.1016/j.neuropharm.2012.02.010.
26. Kaneko, M., and Stryker, M.P. (2014). Sensory experience during locomotion promotes recovery of function in adult visual cortex. Elife *3*, e02798. 10.7554/eLife.02798.
27. Reichelt, A.C., Hare, D.J., Bussey, T.J., and Saksida, L.M. (2019). Perineuronal Nets: Plasticity, Protection, and Therapeutic Potential. Trends Neurosci *42*, 458-470. 10.1016/j.tins.2019.04.003.
28. Heimel, J.A., van Versendaal, D., and Levelt, C.N. (2011). The role of GABAergic inhibition in ocular dominance plasticity. Neural Plast *2011*, 391763. 10.1155/2011/391763.
29. Pantazopoulos, H., Gisabella, B., Rexrode, L., Benefield, D., Yildiz, E., Seltzer, P., Valeri, J., Chelini, G., Reich, A., Ardelt, M., and Berretta, S. (2020). Circadian Rhythms of Perineuronal Net Composition. eNeuro *7*. 10.1523/ENEURO.0034-19.2020.
30. Musumeci, S.A., Ferri, R., Elia, M., DalGracco, S., Scuderi, C., Stefanini, M.C., Castano, A., and Azan, G. (1995). Sleep neurophysiology in fragile X patients. Developmental Brain Dysfunction *8*, 218-222.

31. Rogers, S.J., Wehner, D.E., and Hagerman, R. (2001). The behavioral phenotype in fragile X: symptoms of autism in very young children with fragile X syndrome, idiopathic autism, and other developmental disorders. J Dev Behav Pediatr *22*, 409-417. 10.1097/00004703-200112000-00008.
32. Penagarikano, O., Mulle, J.G., and Warren, S.T. (2007). The pathophysiology of fragile x syndrome. Annu Rev Genomics Hum Genet *8*, 109-129. 10.1146/annurev.genom.8.080706.092249.
33. Diekelmann, S., and Born, J. (2010). The memory function of sleep. Nature Reviews Neuroscience.
34. Klinzing, J.G., Niethard, N., and Born, J. (2019). Mechanisms of systems memory consolidation during sleep. Nat Neurosci *22*, 1598-1610. 10.1038/s41593-019-0467-3.
35. Zou, B., Cao, W.S., Guan, Z., Xiao, K., Pascual, C., Xie, J., Zhang, J., Xie, J., Kayser, F., Lindsley, C.W., et al. (2019). Direct activation of G-protein-gated inward rectifying K+ channels promotes nonrapid eye movement sleep. Sleep *42*, 1-16. 10.1093/sleep/zsy244.
36. Kaufmann, K., Romaine, I., Days, E., Pascual, C., Malik, A., Yang, L., Zou, B., Du, Y., Sliwoski, G., Morrison, R.D., et al. (2013). ML297 (VU0456810), the first potent and selective activator of the GIRK potassium channel, displays antiepileptic properties in mice. ACS Chem Neurosci *4*, 1278-1286. 10.1021/cn400062a.
37. Zhao, Y., Gameiro-Ros, I., Glaaser, I.W., and Slesinger, P.A. (2021). Advances in Targeting GIRK Channels in Disease. Trends Pharmacol Sci *42*, 203-215. 10.1016/j.tips.2020.12.002.
38. Xu, Y., Cantwell, L., Molosh, A.I., Plant, L.D., Gazgalis, D., Fitz, S.D., Dustrude, E.T., Yang, Y., Kawano, T., Garai, S., et al. (2020). The small molecule GAT1508 activates brain-specific GIRK1/2 channel heteromers and facilitates conditioned fear extinction in rodents. J Biol Chem *295*, 3614-3634. 10.1074/jbc.RA119.011527.
39. Angriman, M., Caravale, B., Novelli, L., Ferri, R., and Bruni, O. (2015). Sleep in children with neurodevelopmental disabilities. Neuropediatrics *46*, 199-210. 10.1055/s-0035-1550151.
40. Liang, S., and Mody, M. (2022). Abnormal Brain Oscillations in Developmental Disorders: Application of Resting State EEG and MEG in Autism Spectrum Disorder and Fragile X Syndrome. Frontiers in Neuroimaging *1*. 10.3389/fnimg.2022.903191.
41. Cohen, S., Conduit, R., Lockley, S.W., Rajaratnam, S.M., and Cornish, K.M. (2014). The relationship between sleep and behavior in autism spectrum disorder (ASD): a review. J Neurodev Disord *6*, 44. 10.1186/1866-1955-6-44.
42. Picchioni, D., Reith, R.M., Nadel, J.L., and Smith, C.B. (2014). Sleep, plasticity and the pathophysiology of neurodevelopmental disorders: the potential roles of protein synthesis and other cellular processes. Brain Sci *4*, 150-201. 10.3390/brainsci4010150.
43. Veatch, O.J., Maxwell-Horn, A.C., and Malow, B.A. (2015). Sleep in Autism Spectrum Disorders. Curr Sleep Med Rep *1*, 131-140. 10.1007/s40675-015-0012-1.

44. Blackmer, A.B., and Feinstein, J.A. (2016). Management of Sleep Disorders in Children With Neurodevelopmental Disorders: A Review. Pharmacotherapy *36*, 84-98. 10.1002/phar.1686.
45. Steriade, M., and Timofeev, I. (2003). Neuronal plasticity in thalamocortical networks during sleep and waking oscillations. Neuron *37*, 563-576. 10.1016/s0896-6273(03)00065-5.
46. Kim, A., Latchoumane, C., Lee, S., Kim, G.B., Cheong, E., Augustine, G.J., and Shin, H.S. (2012). Optogenetically induced sleep spindle rhythms alter sleep architectures in mice. Proc Natl Acad Sci U S A *109*, 20673-20678. 10.1073/pnas.1217897109.
47. Latchoumane, C.V., Ngo, H.V., Born, J., and Shin, H.S. (2017). Thalamic Spindles Promote Memory Formation during Sleep through Triple Phase-Locking of Cortical, Thalamic, and Hippocampal Rhythms. Neuron *95*, 424-435 e426. 10.1016/j.neuron.2017.06.025.
48. Thankachan, S., Katsuki, F., McKenna, J.T., Yang, C., Shukla, C., Deisseroth, K., Uygun, D.S., Strecker, R.E., Brown, R.E., McNally, J.M., and Basheer, R. (2019). Thalamic Reticular Nucleus Parvalbumin Neurons Regulate Sleep Spindles and Electrophysiological Aspects of Schizophrenia in Mice. Sci Rep *9*, 3607. 10.1038/s41598-019-40398-9.
49. Ognjanovski, N., Maruyama, D., Lashner, N., Zochowski, M., and Aton, S.J. (2014). CA1 hippocampal network activity changes during sleep-dependent memory consolidation. Front Syst Neurosci *8*, 61. 10.3389/fnsys.2014.00061.
50. Ognjanovski, N., Schaeffer, S., Wu, J., Mofakham, S., Maruyama, D., Zochowski, M., and Aton, S.J. (2017). Parvalbumin-expressing interneurons coordinate hippocampal network dynamics required for memory consolidation. Nat Commun *8*, 15039. 10.1038/ncomms15039.
51. Ognjanovski, N., Broussard, C., Zochowski, M., and Aton, S.J. (2018). Hippocampal Network Oscillations Rescue Memory Consolidation Deficits Caused by Sleep Loss. Cereb Cortex *28*, 3711-3723. 10.1093/cercor/bhy174.
52. Elia, M., Ferri, R., Musumeci, S.A., Del Gracco, S., Bottitta, M., Scuderi, C., Miano, G., Panerai, S., Bertrand, T., and Grubar, J.C. (2000). Sleep in subjects with autistic disorder: a neurophysiological and psychological study. Brain Dev *22*, 88-92. 10.1016/s0387-7604(99)00119-9.
53. Heulens, I., D'Hulst, C., Van Dam, D., De Deyn, P.P., and Kooy, R.F. (2012). Pharmacological treatment of fragile X syndrome with GABAergic drugs in a knockout mouse model. Behav Brain Res *229*, 244-249. 10.1016/j.bbr.2012.01.031.
54. Dahlhaus, R. (2018). Of men and mice: modeling the fragile X syndrome. Frontiers in Molecular Neuroscience. Frontiers Media S.A.
55. Mednick, S.C., McDevitt, E.A., Walsh, J.K., Wamsley, E., Paulus, M., Kanady, J.C., and Drummond, S.P. (2013). The critical role of sleep spindles in hippocampal-dependent memory: a pharmacology study. J Neurosci *33*, 4494-4504. 10.1523/JNEUROSCI.3127-12.2013.
56. Vienne, J., Lecciso, G., Constantinescu, I., Schwartz, S., Franken, P., Heinzer, R., and Tafti, M. (2012). Differential effects of sodium oxybate and baclofen on

EEG, sleep, neurobehavioral performance, and memory. Sleep *35*, 1071-1083. 10.5665/sleep.1992.
57. Hall-Porter, J.M., Schweitzer, P.K., Eisenstein, R.D., Ahmed, H.A., and Walsh, J.K. (2014). The effect of two benzodiazepine receptor agonist hypnotics on sleep-dependent memory consolidation. J Clin Sleep Med *10*, 27-34. 10.5664/jcsm.3352.
58. Watson, C.J., Baghdoyan, H.A., and Lydic, R. (2010). Neuropharmacology of Sleep and Wakefulness. Sleep Med Clin *5*, 513-528. 10.1016/j.jsmc.2010.08.003.
59. Monti, J.M., Spence, D.W., Buttoo, K., and Pandi-Perumal, S.R. (2017). Zolpidem's use for insomnia. Asian J Psychiatr *25*, 79-90. 10.1016/j.ajp.2016.10.006.
60. Gobbi, G., and Comai, S. (2019). Sleep well. Untangling the role of melatonin MT1 and MT2 receptors in sleep. J Pineal Res *66*, e12544. 10.1111/jpi.12544.